

*S100 Proteins Control Cytoskeletal Dynamics in Cancer*

Thesis submitted for the Degree of Doctor of Philosophy at the

University of Leicester

By

Ban Hussein Alwash

Cancer Studies and Molecular Medicine

College of Medicine and Psychology

December 2017

# ***S100 Proteins Control Cytoskeletal Dynamics in Cancer***

Ban Hussein Alwash

## **Abstract**

The S100 family of calcium binding proteins exhibits a unique pattern of cell type specific expression. These proteins are found in the cytoplasm and/or nucleus of a variety of cells, and involved in the control of a wide range of cellular processes such as cell cycle progression and differentiation. S100A4 and S100A6 are members of the S100 protein family that interact with several molecular targets including the heavy chain of non-muscle myosin IIA (NM IIA) and annexin II, respectively. NM IIA is a major actin-associated motor protein, which is involved in cell motility and cytokinesis.

Assembly/disassembly of myosin filaments is primarily controlled by myosin light chain phosphorylation. However, small calcium-binding proteins of the S100 family also play an active role in the dynamics of actin-myosin filaments, leading to an increase in the dissemination of tumour cells. Accordingly, the main aim of this work was to study the molecular mechanism underlying S100A4/A6 function in epithelial mesenchymal transition (EMT) and provide *in vivo* data highlighting their role in the regulation of myosin dynamics. Intriguingly, we employed a novel transition electron microscopy approach to study the function of non-muscle IIA isoforms and their interactions with S100A4/A6 in A431/ZEB2 cells undergoing an EMT. Our data confirmed that both 6S and 10S myosin isoforms do exist in cells and directly interact with S100A4/A6 *in vivo*.

Depletion of S100A4 resulted in the disappearance of the peaks corresponding to monomeric myosin indicating that S100A4 is required for balancing monomer-polymer equilibrium in cells. In blot overlay, both S100A4 and S100A6 showed similar binding site on myosin fragment 4 (C-terminus). However, a new S100A6 binding site was mapped on myosin heavy chain represented in M53 fragment which is a part of rod domain. In addition to the solubility of myosin in high ionic buffer, S100A4 and S100A6 are able to solubilise the myosin which was measured by the turbidity assay. Moreover, a decrease in ATPase activity of actomyosin complex in cells undergoing EMT was observed in the presence of S100A4/A6.

In conclusion: This study shows that S100A4/A6 protein interacts with NM IIA. There is no redundancy and both proteins promote myosin dynamics, cell migration and invasion. S100A4 and S100A6 are up-regulated by ZEB2 and is implicated in the dynamic regulation of myosin filaments by switching the balance towards monomeric myosin.

## **Acknowledgements**

First and foremost, I would especially like to express a lot of gratitude to thank my supervisors Dr Marina Kriajevska and Dr Mohammed El-Mezgueldi for immense knowledge, their guidance in all the time of research and writing of this thesis. They helped with both laboratory techniques as well as understanding the results of my experiments. Their enthusiasm and passion for the subject has been truly inspiring and provided me with the best scientific foundation. I would like thank Professor Clive Bagshaw for his advice during my study. I am highly thankful to Professor Martyn Mahaut-Smith for sharing his broad knowledge, experiences.

Massive thanks Dr Eugene Tulchinsky who provided unlimited advice, answered all my questions and pointed me in the right direction. Also, many thanks to all the other students of EMT without whom, my PhD would have been a very lonely place! for all their friendship and encouragement during my journey. A special thanks to Dr Andrew Irvine for sharing unpublished data and reagents, I hope I did your previous work justice!

I would also like to thank Khawla Kasar for her unlimited support and her wiliness to contribute to this work.

I am also indebted to the support of Natalie Allcock and for her vast technical expertise and patience in answering my lab-related queries. I would like to thank all the biochemistry lab members and other master students I have meet during my time here for valuable input and help, as well as sharing of frustration.

My warmest thanks go to my family: my parents, brothers; Ahmed and Ameer and my children; Rawan, Ali and Jaber who have always encouraged me to achieve my dreams and been keen listeners to my progress. They have supported me throughout my working in this thesis and my life in general. The end of the PhD is the start of our new chapter.

# Table of Contents

<b>Chapter 1 : Introduction .....</b>	<b>1</b>
1.1 Cancer and metastasis .....	2
1.1.1 Cancer .....	2
1.2 S100 protein family.....	15
1.2.1 S100 proteins genes .....	17
1.2.2 Structure of S100 proteins.....	18
1.2.3 S100 proteins expression and function. ....	24
1.2.4 S100A4 and S100A6 expressions correlate with poor of cancer prognosis.....	26
1.2.5 S100 protein interact with target proteins .....	30
1.3 Myosin II.....	31
1.4 Aims and objectives .....	42
<b>Chapter 2 : Materials and Methods .....</b>	<b>44</b>
2.1 Materials .....	45
2.2 Chemicals.....	45
2.2.1 Cell Culture .....	45
2.2.2 Protein analysis .....	48
2.2.3 Immunofluorescence Materials.....	49
2.2.4 Immunogold Labelling.....	49
2.2.5 Cloning and DNA analysis .....	49
2.2.6 Antibodies .....	50
2.2.7 Oligonucleotides .....	53
2.2.8 Constructs .....	56
2.2.9 Plasmid map of M53/S100A6 for PQE30 cloning vector.....	57
2.2.10 Equipments .....	59
2.2.11 Buffers and solutions preparations.....	60
2.3 Mammalian cell Culture methods .....	62
2.3.1 Cell culture technique .....	62
2.3.2 Cell passaging and seeding .....	62
2.3.3 Cell counting.....	63
2.3.4 Long-term storage of cells .....	63
2.3.5 Established integration of plasmid DNA .....	63

2.4	Transfection with Ingenio® Electroporation solution .....	64
2.5	Transient transfection and creation of stable cell lines .....	64
2.6	Chemical treatment .....	65
2.7	Protein Analysis methods.....	65
2.7.1	Preparation of protein lysates.....	65
2.7.2	Protein quantification.....	66
2.7.3	Sodium Dodecyl Sulphate-Polyacrylamide Gel Electrophoresis (SDS-PAGE) .....	66
2.7.4	ATPase assay .....	71
2.7.5	Immunocytochemistry .....	72
2.8	Technique of molecular biology .....	76
2.8.1	DNA manipulation.....	76
2.8.2	Small-scale protein expression trials.....	81
2.8.3	Large scale protein expression and purification.....	81
2.9	Blot overlay.....	84
2.10	Turbidity assay.....	85
2.11	Analysis and statistics .....	85
2.11.1	Sequence alignment .....	85
2.11.2	Statistics .....	85
<b>Chapter 3 S100A4 regulates the equilibrium between 10S and 6S forms of non-muscle myosin IIA .....</b>		<b>87</b>
3.1	Introduction.....	88
3.2	Aims.....	89
3.3	Results.....	90
3.3.1	Investigation of S100A4-myosin IIA complexes during EMT .....	90
3.3.2	Effect of RLC phosphorylation on S100A4-myosin IIA interaction. ....	121
3.3.3	Effect of MHC phosphorylation on S100A4-myosin IIA interaction.....	138
3.4	Discussion .....	149
3.4.1	Evaluation of S100A4-myosin IIA complexes in A431/ZEB2 cells .....	150
3.4.2	Effect of phosphorylation of MHC and MLC on S100A4-myosin IIA interaction in A431/ZEB2 cells. ....	153
3.4	Conclusion .....	155
<b>Chapter 4 Study of S100A4-myosin IIA complexes by negative staining.....</b>		<b>157</b>
4.1	Introduction.....	158

4.2	Results.....	159
4.2.1	Analysis of the myosin immunoprecipitated from A431/ZEB2-WT cells by negative-staining electron microscopy .....	159
4.2.2	Analysis of S100A4-GFP-myosin IIA complexes by negative staining electron microscopy. 160	
4.3	Discussion .....	164
<b>Chapter 5 : S100A6 is a new regulator of myosin dynamics .....</b>		<b>165</b>
5.1	Introduction.....	166
5.2	Aims .....	167
5.3	Results.....	168
5.3.1	Assessment of ATPase activity of myosin IIA extracted during EMT.....	168
5.3.2	Study of NMHC IIA half-life by cycloheximide chase assay.....	171
5.3.3	S100A6 co-localises with myosin IIA .....	175
5.3.4	Mapping of the S100A6 binding site. ....	184
5.3.5	Expression and purification of the myosin recombinant proteins.....	184
5.3.6	Analysis of non-muscle myosin heavy chain IIA interaction with S100A6 by blot overlay 187	
5.3.7	S100A4 and S100A6 are new regulators of myosin dynamics.....	198
5.4	Discussion .....	203
5.4.1	Co-localisation of S100A6 and NM IIA in cells.....	203
5.4.2	S100A4 and S100A6 inhibit the actin - activated ATPase activity of NMC IIA .....	204
5.4.3	S100A6 interacts with M53 fragment.....	204
5.4.4	S100A4/A6 dissociates NM IIA in turbidity assay.....	205
5.5	Conclusion .....	206
<b>Chapter 6 : General Discussion .....</b>		<b>207</b>
6.1	Discussion .....	208
6.2	Conclusions and future work .....	213
<b>Chapter 7 Appendix.....</b>		<b>221</b>

## List of Figures

Figure 1-1: The Hallmarks of Cancer recognized in 2000.....	2
Figure 1-2: Emerging Hallmarks and Enabling Traits of cancer .....	3
Figure 1-3: Scheme of the metastatic cascade. ....	5
Figure 1-4: Schematic illustration of alteration in the cellular morphology and protein expression during EMT.....	7
Figure 1-5: Structures of the human ZEB1 and ZEB2 proteins.....	9
Figure 1-6: Schematic representative of the Rho GTPase cycle.....	12
Figure 1-7: Features of cell polarity, Rho GTPases and cell movement.....	14
Figure 1-8: Signalling of S100 A4, A6 and A2 in cancer cells.....	16
Figure 1-9: S100 genes are located on chromosome 1 .....	18
Figure 1-10: Multiple sequence alignment of human S100proteins .....	19
Figure 1-11: Dimer Structure of S100A4 in the presence of calcium.....	21
Figure 1-12: Effect of calcium on the S100A4. ....	23
Figure 1-13: Scheme of a monomer of non-muscle myosin II. ....	32
Figure 1-14: Diagram of the compact 10 S conformation of NM II.....	36
Figure 1-15: Schematic representative of NM IIA filament assembly regulation. ....	40
Figure 2-1: Plasmid map of S100A6 and M53 proteins .....	58
Figure 2-2: Schematic illustration of Western blot apparatus.....	68
Figure 2-3: Scheme of immunogold labelling .....	74
Figure 2-4: Statistical evaluation of co-localisation of random particles.....	75
Figure 2-5: Scheme of protein purification system with Ni-NTA .....	84
Figure 3-1: EMT induction in A431/ ZEB2-WT cells.....	90
Figure 3-2: Activation of S100A4 expression during EMT.....	91
Figure 3-3: Immunoprecipitation of S100A4 and GFP from A431/ZEB2-WT .....	93
Figure 3-4: Localisation of S100A4 and GFP-myosin IIA in A431/ ZEB2-WT cells .....	94
Figure 3-5: Localisation of $\alpha$ -Tubulin in A431/ZEB2 cells.....	95
Figure 3-6: Schematic representing the possible distances of the two forms of myosin molecule 10S and 6S. ....	97
Figure 3-7: Electron micrographs of single immunogold labeling of A431/ZEB2-WT cells for GFP or S100A4. ....	100

Figure 3-8: Electron micrographs of single immunogold labeling of A431/ZEB2-WT cells for myosin heavy chain IIA or GFP. ....	101
Figure 3-9: Electron micrograph of immunogold labelling of A431/ ZEB2-WT cells for secondary antibody only. ....	102
Figure 3-10: Electron micrographs of double immunogold labelling of S100A4 and GFP in A431/ ZEB2-WT cells.....	104
Figure 3-11: Electron micrographs of immunogold labelling of A431/ZEB2 cells expressing GFP- $\alpha$ -Tubulin stained for S100A4 and GFP antibodies. ....	106
Figure 3-12: Co-localisation of S100A4 and GFP-myosin IIA in A431/ ZEB2-WT and A431/ ZEB2 - $\alpha$ -Tubulin cells.....	107
Figure 3-13: Characterisation of S100A4 Knockdown in A431/ZEB2-WT cells .....	109
Figure 3-14: Electron micrographs of immunogold labelling of siControl and siS100A4 cells for MHC IIA and GFP.....	111
Figure 3-15: Knockdown S100A4 leads to assembly of myosin IIA into filaments .....	112
Figure 3-16: Inhibition of the MRLC phosphorylation by the ROCK inhibitor Y27632 .....	114
Figure 3-17: GFP and S100A4 co-localised at distances consistent with 10S conformation as a result of inhibition of RLC phosphorylation.....	115
Figure 3-18: Inhibition of RLC phosphorylation results in co-localisation between S100A4 and myosin IIA at one significant peak consistent with 10S myosin monomer.....	117
Figure 3-19: ROCK inhibition blocked RLC phosphorylation on Thr18/Ser19.....	118
Figure 3-20: Coupling S100A4 knockdown and ROCK inhibition alter myosin IIA confirmation.....	120
Figure 3-21: Characterization of cells expressing GFP-tagged mutants of the RLC.....	123
Figure 3-22: Immunoprecipitation of S100A4 and GFP-myosin IIA from cells expressing RLC-WT and mutants.....	125
Figure 3-23: Localisation of S100A4 and GFP-myosin IIA in cells expressing RLC-WT and mutants during EMT.....	127
Figure 3-24: Electron micrographs of double immunogold labelling of cells expressing RLC-WT for MHC IIA and GFP.....	129
Figure 3-25: S100A4 interacts with 10S and 6S myosin IIA monomers in RLC-WT cells .....	130
Figure 3-26: S100A4 interacts only with 10S myosin monomer in T18A/S19A cells.....	132
Figure 3-27: RNAi-mediated knockdown of S100A4 in RLC-T18A/S19A cells. ....	134
Figure 3-28: Knockdown of S100A4 promotes assembly of myosin IIA into filaments in RLC-T18A/S19A mutants .....	137
Figure 3-29: Western blot analysis of lysates of A431/ZEB2 cells expressing MHC phosphodeficient and phosphomimetic cells.....	139

Figure 3-30: S100A4-myosin IIA complexes were detected in A431/ZEB2 cells expressing phosphodeficient and phosphomimetic MHC IIA mutants. ....	141
Figure 3-31: Localisation of S100A4 and GFP-myosin IIA in cells expressing MHC IIA mutants. ....	143
Figure 3-32: Dephosphorylation of MHC IIA promotes formation of 6S assembly-competent conformation. ....	145
Figure 3-33: Knockdown of S100A4 in MHC-S1943D cells leads to a dramatic shift of myosin IIA monomer from 10S toward 6S form. ....	148
Figure 3-34: A regulatory mechanism of S100A4 and myosin phosphorylation in controlling myosin IIA dynamics. ....	156
Figure 4-1: Myosin IIA forms filament bundles in 100 mM salt buffer. ....	160
Figure 4-2: S100A4 supports 10S form of myosin IIA as an alternative role of RLC phosphorylation. .	163
Figure 4-3: ROCK inhibitor (Y27632) blocks MLC phosphorylation. ....	163
Figure 5-1: Measurement of ATPase activity of the isolated GFP-tagged myosin IIA from A431/ZEB2-WT cells grown in the absence and presence of Dox. ....	169
Figure 5-2: S100A4/A6 inhibits the actin-activated ATPase activity of GFP-tagged myosin IIA during EMT. ....	170
<b>Figure 5-3: Measurement of proteins half-life in A431/ZEB2-WT cells. ....</b>	<b>172</b>
Figure 5-4: The effect of S100A4/S100A6 on the MHC IIA half-life. ....	174
Figure 5-5: Co-immunoprecipitation of GFP and S100A6 from A431/ZEB2-WT cells. ....	176
Figure 5-6: Immunofluorescence staining of A431/ZEB2 cells expressing WT and mutants of the MHC IIA. ....	178
Figure 5-7: Immunofluorescence staining of A431/ZEB2 cells expressing GFP-tagged myosin light chains mutants. ....	179
Figure 5-8: Electron micrograph of A431/ZEB2-WT cells immunogold labelled for S100A6. ....	180
Figure 5-9: S100A6 expression is increased in A431/ZEB2-WT untreated and treated cells with Y27632 during EMT. ....	181
Figure 5-10: Electron micrographs of immunogold labelled A431/ZEB2-WT and A431/ZEB2-WT +Y27632 cells for S100A6 and GFP. ....	182
Figure 5-11: Co-localisation of S100A6 with-myosin IIA in control cells and after treatment with Y27632. ....	183
Figure 5-12: A schematic map of the recombinant NMHC IIA protein fragments. ....	184
Figure 5-13: Coomassie blue staining of the purified NMHC IIA fragments under denaturing condition. ....	186
Figure 5-14: Detection of a new site of interaction of S100A6 with myosin heavy chain IIA by blot overlay. ....	188

Figure 5-15: Mapping of S100A6 binding sites on the MHC IIA. ....	190
Figure 5-16: Schematic represents mapping of new S100A6 binding site on rod domain of NMHC IIA. .....	191
Figure 5-17: Schematics of cloning of M53 and S100A6 DNA into pQE30 plasmid. ....	193
Figure 5-18: M53 fragment is a part of rod coiled coil domain of NMHC IIA. ....	194
Figure 5-19: Isolation of M53 and S100A6 proteins purified under native condition. ....	195
Figure 5-20: Localisation of S100A6 and S100A4 binding sites on NMHC IIA by blot overlay analysis .....	197
Figure 5-21: Alteration of the Hmyo3B turbidity is controlled by NaCl concentration. ....	199
Figure 5-22: Dissociation of Hmyo 3B filaments by S100A6. ....	201
Figure 5-23: Dissociation of M200 filaments by S100A4/S100A6. ....	202
Figure 6-1: Schematic representative assembly/disassembly of non-muscle myosin II in the presence of calcium. ....	210
Figure 6-2: Interaction of S100A6 with M53 peptide by NMR titration. ....	212
Figure 7-1: The nucleotides and amino acids sequences of the Hmyo3B fragment designed with stop codons. ....	224
<b>Figure 7-2: Sequence of M53 fragment of NM IIA</b> .....	226
Figure 7-3: Sequence of M53 fragment of NM IIA. ....	229
Figure 7-4: Schematic representative of pQE-30 Sequence: .....	230
Figure 7-5: Analysis of M53 plasmid DNA by gel agarose electrophoresis. ....	231
Figure 7-6: Isolation of S100A4 proteins purified under native condition. ....	232
Figure 7-7: Myosin IIA exists in monomers in high salt buffer. ....	233
Figure 7-8: S100A4 interacts only with 10S myosin monomer in S1943E cells. ....	234

## List of Tables

Table 1-1: Expression of S100A4 or S100A6 in different human cancers .....	28
Table 2-1: Description of cells and plasmids that used in this study .....	46
Table 2-2: Description of primary antibodies used during this study. All antibodies were prepared in 5% milk/TBST .....	50
Table 2-3: Description of secondary antibodies used during this study. All antibodies were prepared in 5% milk/TBS or BSA.....	52
Table 2-4: Description of oligonucleotide primers used during this study .....	53
Table 2-5: Description of plasmids used during this work .....	56
Table 2-6: General equipments used during this study .....	59
Table 2-7: Description of chemicals that used for preparation of buffers. ....	60
Table 2-8: Volumes of PBS, TE and DMEM essential for Cells Passaging.....	62
Table 2-9: Volume (ml) of components required to prepare 10 ml of resolving gel with different concentration. This table was adapted from (Maly and Nitsch, 2007). ....	67
Table 2-10: PCR cycles for site-directed mutagenesis .....	78
Table 2-11: PCR cycles for cloning.....	79
Table 2-12: Digestion of the DNA and the plasmid vector with the restriction enzymes .....	80

## List of Abbreviations

ABC	ATP binding cassette
APS	Ammonium persulfate
ADP	Adenosine diphosphate
ALS	Amyotrophic Lateral Sclerosis
AMP	Ampicillin
ATP	Adenosine triphosphate
ACD	Assembly Competence Domain
$\alpha$ -SMA	$\alpha$ -smooth muscle actin
BCA	Bicinchoninic acid
BGP	$\beta$ -glycerophosphate
BMP	Bone Morphogenetic Protein
BSA	Bovine Serum Albumin
CaCl <sub>2</sub>	Calcium Chloride
CDK1	Cyclin-dependent kinase 1
CID	CtBP interacting domain
CTLs	CD8 <sup>+</sup> cytotoxic T lymphocytes
CK2	Casein kinase 2
CSCs	Cancer stem cells
CRC	Colorectal carcinoma
CI	Confidence Interval
CTCs	Circulating Tumor Cells
CSR	Complete Spatial Randomness
CHX	Cycloheximide
GAPs	GTPase-activating proteins
GEFs	guanine nucleotide exchange factors
DAPI	4',6-diamidino-2-phenylindol
DMEM	Dulbecco's Modified Eagle Medium

DMSO	Dimethyl Sulfoxide
S100s	S100 proteins
ECM	Extracellular matrix
E.coli	Escherichia coli
EDTA	Ethylenediaminetetraacetic acid
EDC	Epidermal differentiation complex
EGF	Epidermal Growth Factor
EGTA	Ethylene glycol tetraacetic acid
ELC	Essential light chain
EMT	Epithelial mesenchymal transition
EM	Electron microscopy
EndMT	Endothelial-mesenchymal transition
ES	Embryonic stem
FBS	Foetal bovine serum
FRAP	Fluorescence Recovery After Photobleaching
FGF	Fibroblast Growth factor
FT	Flow through
FSP1	Fibroblast-specific protein 1
GEFs	Guanine nucleotide exchange factors
GAPs	GTPase-activating proteins
GFP-MHC-WT	GFP-myosin heavy chain IIA wild-type
GDI	Guanine nucleotide dissociation inhibitors
GuHCl	Guanidine Hydrochloride
HGF/SF	Hepatocyte Growth Factor/Scatter Factor
Hrs	Hours
HMM	Heavy meromyosin
HRP	Horseshoe peroxidase
HIF-1	Hypoxia –inducible factor 1
IF	Immunofluorescence
ICQ	Intensity correlation quotient

IL	Interleukin
IP	Immunoprecipitation
KLC	Kinesin light chain
LAR	Leukocyte common antigen-related
LB	Luria broth
Lgl	Lethal Giant Larvae (Lgl2)
LMM	Light meromyosin
μl	Microliter
M	Molar
MET	Mesenchymal to epithelial transition
MHC	Myosin heavy chain
MHC	Myosin heavy chain IIA
Mins	minutes
MLC	Myosin Light Chain
MLCK	Myosin light chain kinase
MLCP	Myosin Light Chain Phosphatase
MRLC	Myosin regulatory light chain
MRCK	Myotonic dystrophy kinase-related Cdc42-binding kinase
MP	myosin phosphatase
MYPT 1	Myosin phosphatase target subunit 1
mRNA	Messenger RNA
MMPs	Matrix metalloproteinases
NETs	Neutrophil extracellular traps
Ni <sup>2+</sup> -NTA	Nitrilotriacetic acid
Ni <sup>2+</sup>	Nickel
NM II	Non-muscle myosin II
NSCLC	Non-small cell lung cancer
PAGE	Polyacrylamide gel electrophoresis
PCR	Polymerase Chain Reaction
PAK	p21-associated kinase
PBS	Phosphate Buffer Saline

PCC	Pearson's Correlation Coefficient
PDAC	Pancreatic Ductal Adenocarcinoma
PDM	Products Differences from the Mean
PFA	Paraformaldehyde
PKA	Protein kinase A
P-gp	P-glycoprotein
PKC	Protein Kinase C
PMSF	PhenylMethylSulfonyl Fluoride
PP1	Protein Phosphatase 1
PVDF	Poly vinylidene fluoride
RLC	Regulatory light chain
R-Smads	Receptor Regulated Smads
pMLC	Phosphorylated Myosin Light Chain
RNA	Ribonucleic Acid
RNAi	RNA Interference
ROCK	Rho-Associated Coiled-coil Kinase
RAGE	Receptor for Advanced Glycation End-Products
RT	Room Temperature
RA	Rheumatoid Arthritis
RTKs	Receptor Tyrosine Kinases
Sc	Scleroderma
SDS	Sodium Dodecyl Sulphate
SFTPs	S100-Fused Type Proteins
SIP1	Smad-interacting protein 1
siRNA	Small interfering ribonucleic acid
siControl	Non-targeting siRNA
siS100A4	S100A4-targeting siRNA
SHH	Sonic Hedgehog
$\alpha$ SMA	Smooth Muscle Actin
SBD	Smad-Binding Domain
TRPM7	Transient Receptor Potential Melastatin 7

TAE	Tris Acetic Acid EDTA
TBS-T	Tris Buffered Saline-Tween
TEM	Transmission Electron Microscopy
TE	Trypsin
PP 1	Type 1 protein phosphatase catalytic subunit
TGF- $\beta$	Transforming Growth Factor- $\beta$
TNF- $\alpha$	Tumour Necrosis factor- $\alpha$
v/v	Volume by volume
w/v	Weight by volume
WASP	Wiskott-Aldrich Syndrome Protein
WT	Wild type
VBA	Visual Basic for Applications
ZIPK	Leucine Zipper Interacting Kinase

## **Chapter 1 : Introduction**

## 1.2 Cancer and metastasis

### 1.2.1 Cancer

Cancer is a disease where cells grow and proliferate in an uncontrolled way invading any tissue of the body. There are many factors that contribute to initiating cancer including, genetic, environmental, clinical, and lifestyle factors (Font-Burgada et al., 2016). Carcinogenesis is a multi-step process caused by genetic alteration resulting from a persistent genetic mutation, such as chromosome number changes. Therefore, continuous modification of tumour cell genomes leads to progressive conversion of a normal cell to transformed, malignant tumour cell (Pikor et al., 2013). The first 6 hallmarks of cancer were proposed in 2000, these consist evading apoptosis, maintaining growth signalling, insensitivity to anti-growth signals, tissue invasion and metastasis, immortality, and sustained angiogenesis (Hanahan and Weinberg, 2000). These six hallmarks capabilities that enable tumor growth and metastatic dissemination for diversity of neoplastic diseases are described in (Figure 1.1).

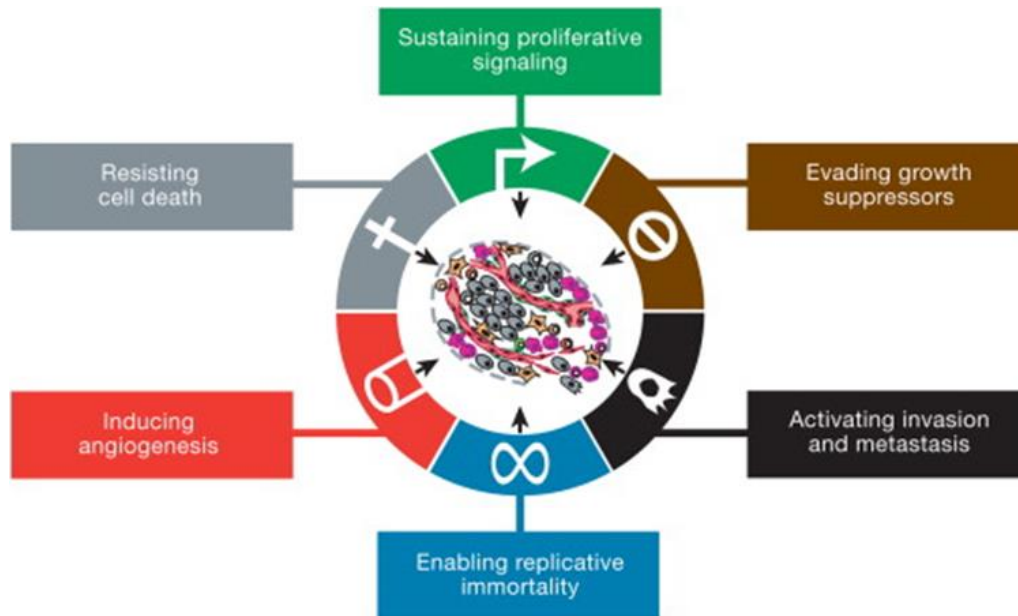


**Figure 1-1: The Hallmarks of Cancer recognized in 2000**

The six hallmarks of cancer and the proposed capabilities of cancer cells to acquire tumourigenic properties. Scheme was taken from (Hanahan and Weinberg, 2011).

The specific hallmarks exhibited by an individual tumor may ultimately contribute to better tumor classification and aid in directing treatment. A decade on, published research reported a further two important emerging hallmarks and enabling characteristics depicted in (Figure 1.2); including genomic instability and tumour promoting inflammation (Hanahan and Weinberg, 2011).

Genomic instability accelerates tumour progression by driving gene mutation (S Datta et al., 2013). An increasing body of research suggest that tumor-associated inflammatory response enhances tumorigenesis and progression by activating proliferative signaling, proangiogenic factors and extracellular matrix-modifying enzymes that facilitate angiogenesis (Valastyan and Weinberg, 2011, DeNardo et al., 2010).

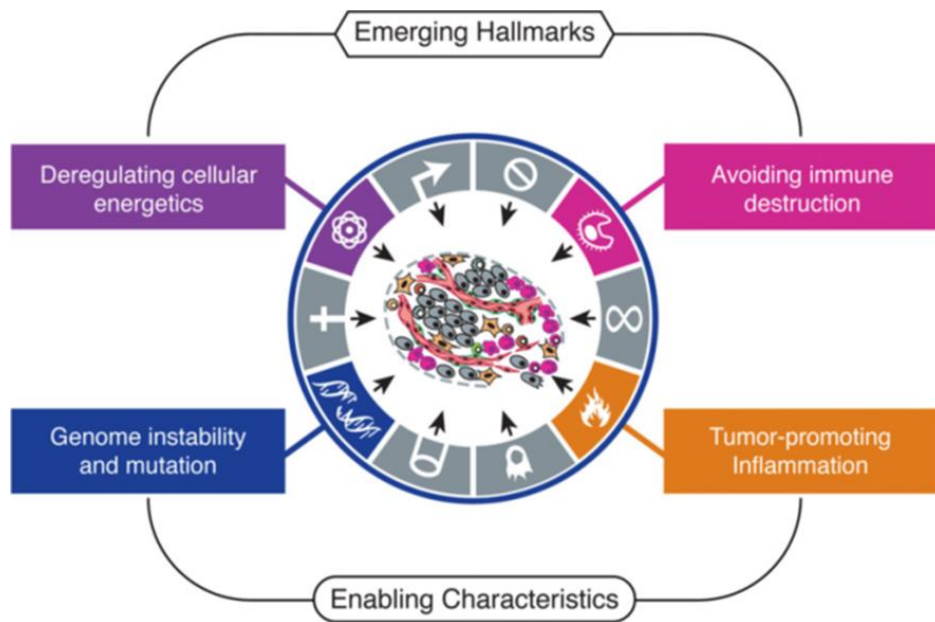


**Figure 1-2: Emerging Hallmarks and Enabling Traits of cancer**

In addition to the six core hallmarks of cancer, two emerging hallmarks and two enabling characteristics have been identified. Emerging hallmarks reprogrammed energy metabolism and evading immune response, and enabling traits to contribute to carcinogenesis by genome mutation, and tumor-promoting inflammation. Diagram taken from (Hanahan and Weinberg, 2011).

In fact, metastasis is the main cause of cancer-related death, with the surgical removal of primary tumors and adjuvant therapy likely to result in curing the disease (Pavlova and Thompson, 2016).

### 1.2.1.1 Metastatic cascade

Metastasis represents a multi-step biological process which is composed of sequential events which must be completed in order for the tumor cells to reside at another site. This new tumour is known as secondary tumour (Valastyan and Weinberg, 2011) (Figure 1.3). Most malignant tumours are incurable due to the resistance of disseminated cancer cells to therapeutic agents (Steeg, 2006). This explains why > 90% of mortality from cancer is a result of metastasis. As such, the effective treatment of cancer depends not only on surgical resection and adjuvant therapy, but also on the ability to inhibit the process of metastasis (Gupta et al., 2006). There are several signaling pathways contribute to initiate tumor metastasis, such as the Hedgehog (Hh), Wnt signaling pathways, TGF- $\beta$ , and Notch signaling pathway (Hanna and Shevde, 2016, Rizzo et al., 2008, Fodde and Brabletz, 2007, Derynck et al., 2001). Overexpression of matrix metalloproteinases (MMPs) in cancer cells is a crucial step for metastasis, as MMPs mediate cell invasion by degrading extracellular matrix (ECM) and controlling angiogenesis.

Progression of metastases arising from dissemination of cancer cells in which benign, macroscopic tumours transform to a malignant state (Klein, 2009). There are seven distinct steps of metastasis known as the 'Invasion-Metastasis Cascade (Valastyan and Weinberg, 2011) summarized as the following:

- i. Local invasion into the surrounding ECM and stromal layers.
- ii. Intravasation into blood vessels or lymphatic system.
- iii. Survival within the circulatory system.
- iv. Arrest at distant organ sites.
- v. Extravasation at secondary site.
- vi. Survival in foreign microenvironment and form micrometastasis
- vii. Reinitiation of proliferative programs at secondary site.

To induce metastasis, tumor cells detaches from each other because of reduced adhesiveness and loss their epithelial phenotype mediated by tight and gap junctions, desmosomes as well as hemidesmosomes and adherens junctions. Tumor cells acquire the ability to degrade the basement membrane by expressing MMPs and pass through the surrounding extracellular matrix to reach the vasculature and intravasating as they penetrate the lymphatic or vascular circulation and

survival in the circulatory system followed by extravasation (Dotan et al., 2009). During cancer progression, a variety of tumor cells show changes in their plasticity by morphological and phenotypical conversions including the epithelial to mesenchymal transition (EMT) (Katsuno et al., 2013, Sleeman and Thiery, 2011, Juanes-García et al., 2016). Ultimately, these cells will attach at a new location and proliferate to produce the secondary tumour (van Zijl et al., 2011).

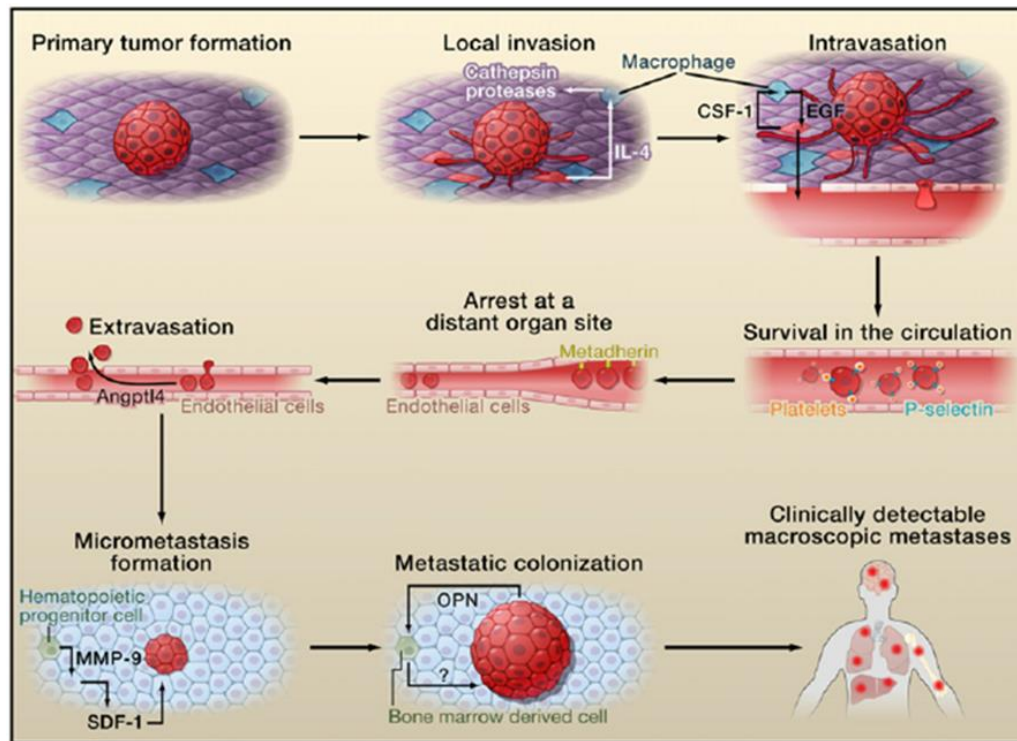


**Figure 1-3: Scheme of the metastatic cascade.**

Cancer Cells (red) lose their epithelial character and gain invasive characteristics. The cells then intravasate into blood or lymphatic vessels and disseminate. Mesenchymal epithelial transition (MET) occurs at sites of distant metastasis. At a secondary site, cells undergo outgrowth and adapt to a new environment. Figure adapted from (Valastyan and Weinberg, 2011).

After successful invasion of cancer cells, they must survive in this new microenvironment. Thus, cells should resist the stress of blood flow, shear forces and turbulence, as well as the attack by NK cells. A main defense for hematogenous survival of cancer cells is forming an emboli through a binding with platelets that protect the tumour cells from immune detection (Khamis et al., 2012, Joyce and Pollard, 2009). Intrinsically, the interactions between tumour cells and the surrounding

stroma influences tumourigenesis, progression and ultimately patient prognosis (Quail and Joyce, 2013).

Moreover, studies observed that mice with combined immunodeficiency in both T cells CD8+ cytotoxic T lymphocytes (CTLs), CD4+ Th1 helper) and NK cells were even more susceptible to cancer development than immunocompetent controls (Hanahan and Weinberg, 2011). A recent study suggests that neutrophils which are considered as the first line of defense during infections, promote cancer progression and neutrophil extracellular traps (NETs) appear to help metastases of cancer cells by enhancing adhesion of circulating tumor cells (CTCs) in distant organs (Cools-Lartigue et al., 2013).

The cellular origin, intrinsic properties of the cancer, tissue affinities and circulation patterns determine not only the sites of tumour spread, but also the severity of metastasis to distant organs (Nguyen et al., 2009). For example, brain cancer incidence is frequent in patients with lung and breast cancer (Schouten et al., 2002), whereas prostate cancer is unique in that bone is often the only clinically detectable site of metastasis (Logothetis and Lin, 2005). In addition, small-cell neuroendocrine carcinomas induces metastasis into the brain (Viswanathan et al., 2004), while colon cancers almost always cause metastasis to the liver. The hepatic portal vein receives all of the blood draining from gastrointestinal tract and directly joins the liver (Nguyen et al., 2009).

#### **1.2.1.2 Epithelial-mesenchymal transition and metastasis**

EMT is a reversible embryonic program that is often activated during cancer progression (Fischer et al., 2015). This biological process allows non-motile, polarized, epithelial cells undergoing changes that enable them to assume features of a mesenchymal phenotype (Figure 1.4) (Serrano-Gomez et al., 2016, Liu et al., 2013b). Mesenchymal cells have a fibroblast-like morphology with the ability to migrate, resist to apoptosis and increase extracellular matrix (ECM) degradation by matrix metalloproteinases (MMPs) enzymes (Chaffer and Weinberg, 2011). EMT stimulates the dynamic remodeling of actomyosin structures facilitating cell locomotion and enabling metastatic dissemination of cancer cells (Thiery et al., 2009).

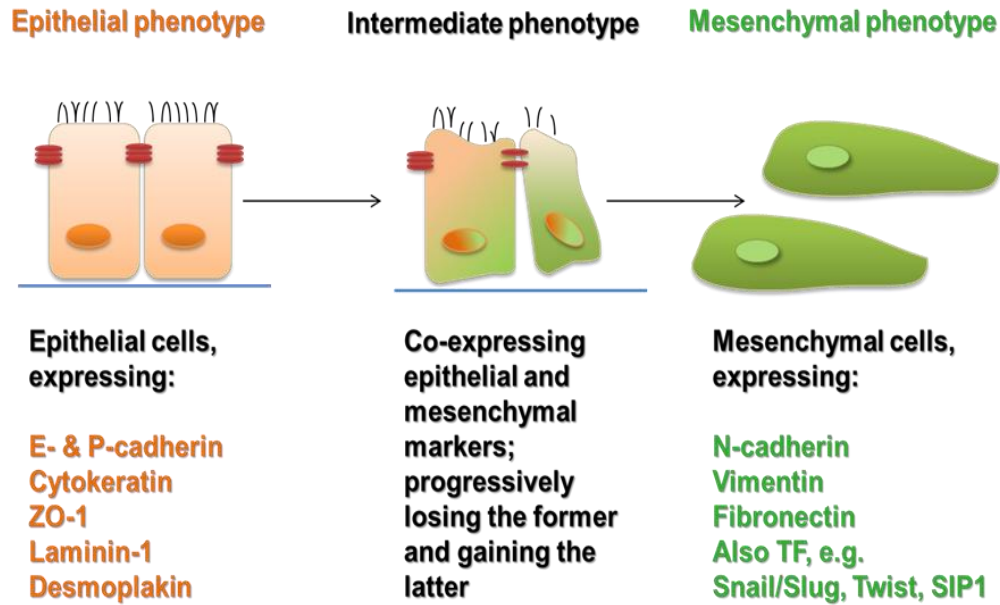


**Figure 1-4: Schematic illustration of alteration in the cellular morphology and protein expression during EMT.**

During EMT, epithelial cells lose cell-cell contacts, polarity and acquire mesenchymal phenotype. This process is initiated by a diverse set of signaling pathways, such as TGF- $\beta$ , FGF, Notch and Wnt that activate the transcriptional repressors of E-cadherin (ZEB, Snail and Twist). (Kalluri and Weinberg, 2009).

It was established that EMT is a vital driver of invasion and metastasis of various solid tumors, including breast, gastric and colon cancers (reviewed in (Son and Moon, 2010)). Many studies have implicated that EMT contributes to various diseases progression such as organ fibrosis and cancer (Kanlaya and Thongboonkerd, 2016). EMT is also an essential mechanism in the developmental process and tissue repair such as wound healing (Heo et al., 2011).

On the other hand, mesenchymal cells undergo the reverse process of EMT, with mesenchymal to epithelial transition (MET) allowing tumour cells to switch back to epithelial phenotype at distant sites highlighting the plastic nature of the cellular phenotype; MET enables cells to contact to other tissues and develop into secondary tumours (Dotan et al., 2009).

Key epithelial markers are lost during EMT, including E-cadherin, cytokeratin, occludin and Desmoplakin. In contrast, mesenchymal markers increase during this process, such as N-cadherin,

vimentin, Smooth Muscle Actin ( $\alpha$ SMA) and fibronectin (reviewed in (Lu et al., 2014)). E-cadherin is a surface protein responsible for establishment and maintenance of cell-cell adhesions, cell polarity and structural integrity (Mejlvang et al., 2007). Intracellularly, E-cadherin binds to p120 catenin and  $\beta$ -catenin which binds to  $\alpha$ -catenin to form the cadherin–catenin complex, thereby mediating intracellular signaling and linking adherence junctions to the actin cytoskeleton.  $\beta$ -catenin dissociates from the cadherin complex and is translocated into the nucleus where it works as a transcription factor which is often associated with loss of E-cadherin expression (Harris and Tepass, 2010).

EMT controlling genes are activated through signalling initiated by transforming growth factor- $\beta$  (TGF- $\beta$ ), notch signalling pathway, Wnt signalling pathways and Fibroblast Growth factor (FGF) (Huang et al., 2013). There are several repressors of E-cadherin which have been identified, including Zinc finger transcription factors Snail (Snail1/2), Twist (Twist1/2) and the ZEB family (ZEB1/2). These proteins play an essential role in regulating gene expression profiles that control cell morphology, invasive behaviour and cell adhesion. Loss of E-cadherin expression in mouse keratinocytes activates the expression of MMP-9 mRNA levels, particularly in the tumour stroma, thereby remodeling the ECM within the tumour environment (Jordà et al., 2005).

#### **1.2.1.2.1 The ZEB family of transcription factors**

##### **1.2.1.2.1.1 The structure of ZEB proteins**

ZEB families of zinc finger transcription factors are proteins which play an essential role in initiating EMT and maintaining a mesenchymal phenotype (Mejlvang et al., 2007).

Vertebrates have two homologous ZEB proteins. Zinc-finger-E-box-binding protein 1 (ZEB1) also known as  $\delta$ EF1, TCF8, AREB6, ZFHEP, NIL-2A, ZFHX1A, and BZP that are encoded by the *ZFHX1A* gene. This protein was first identified as a nuclear factor that specifically binds to the essential element of lens-specific  $\delta$ 1-crystallin enhancer when it was molecularly cloned from the chicken (Funahashi et al., 1993). The second member Zinc-finger-E-box-binding protein 2 (ZEB2) also termed SIP1, which is encoded by an independent gene *ZFHX1B*, was first discovered from a yeast two-hybrid screen through its ability to bind to Smad (Verschueren et al., 1999). The human

ZEB1 gene is mapped to chromosome 10 p11.2 and human ZEB2 gene is located at chromosome 2q22. ZEB proteins exhibit high degree of sequence homology, containing two widely separated zinc finger-binding domains (Beltran et al., 2008). The N-terminal domain consists of four Zn-fingers, whereas the other domain which located in the C-terminal end, contains three zinc fingers. Both ZEB proteins mediate repression of transcription through an interaction with a high affinity sequence CACCT(G) E-boxes located in target gene promoters (Comijn et al., 2001).

ZEB family members have another important functional domain in central regions of the proteins. Those include CtBP interacting domain (CID), and SMAD-binding domain (SBD). The central region contains also the POU-like homeodomain (HD) which does not bind to DNA, but may play a role in protein-protein interactions (Figure 1.5) (Vandewalle et al., 2009, Postigo and Dean, 1999).

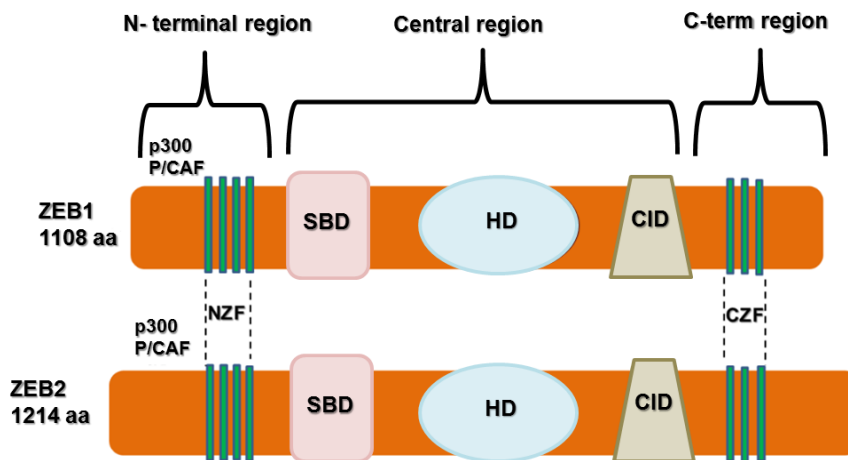


**Figure 1-5: Structures of the human ZEB1 and ZEB2 proteins.**

ZEB proteins composed of N-terminal (NZF) and C-terminal (CZF) zinc-finger clusters, central homeodomain (HD) and CtBP-interacting domain (CID). Protein region implicated in p300/PCAF binding site. This figure is adopted from (Vandewalle et al., 2009).

Both ZEB1 and ZEB2 proteins can bind to activate Receptor Regulated Smads (R-Smads) including R-Smads-1, R-Smads-2 and R-Smads-3 via the SBD (Postigo et al., 2003). It was found that ZEB1-Smad signalling causes transcriptional activation, whereas ZEB2-Smad complex causes transcriptional repression. Both proteins can also act as either transcriptional repressors or activators via diverse recruitment to transcriptional co-activators (p300 and P/CAF) and co-

repressors (CtBP) (Van Grunsven et al., 2006). A comparative expression analysis of ZEB1 and ZEB2 proteins in various cancer cell lines indicated that ZEB1 protein was expressed at much higher level than ZEB2 mostly in mesenchymal carcinoma cells. Interestingly, ZEB proteins and miR-200 family members have opposite functions; both ZEB1 and ZEB2 inhibit the expression of miR-200 to promote metastasis (Brabletz and Brabletz, 2010).

In addition, ZEB1 and SNAIL proteins can down-regulate different epithelial markers including cell polarity proteins such as Crumbs3 and Lethal giant larvae (Lgl2). zZEB1 is important for metastasis by repressing the expression of the stemness-inhibiting microRNAs miR-200 and miR-203. ZEB1 can also confer stemness properties, thereby acquires a migrating cancer stem cell phenotype (Lehmann et al., 2016). Interestingly, ZEB1 interacts directly with YAP, resulting in transcriptional activation of YAP target gene expression. This ZEB1/YAP target gene set is a strong predictor of poor survival in patients with breast cancer (Lehmann et al., 2016). ZEB1 is associated with aggressive behaviour, metastasis, and poor prognosis in several cancers, including breast, pancreatic and lung cancer (Bronsert et al., 2014). Unlike ZEB1 structure, ZEB2 developed a divergent 5'-UTR (untranslated region) which have highly complex organization with multiple splicing products originating from different promoters (Beltran et al., 2008). ZEB proteins play a critical role during embryonic development. For instance, ZEB2 expression was seen in the neuroectoderm and neural crest derivatives in mouse embryos highlighting the importance of ZEB2 in nervous system development (Van de Putte et al., 2003).

#### **1.2.1.2.1.2 ZEB2 in cancer**

ZEB2 is considered one of several regulators of malignant tumour progression. Numerous studies have reported that the expression of ZEB2 protein in the epithelial epidermoid carcinoma cell line A431, led to morphological changes of the cell phenotype from epithelial to fibroblast-like cells associated with a decreased expression of E-cadherin and  $\alpha$ -catenin, and re-localisation of  $\beta$ -catenin from the nucleus to the cytoplasm (Vandewalle et al., 2005). The same study found that the suppression of E-cadherin expression was accompanied by an enhanced loss of cells aggregation as well as the acquisition of invasive properties in A431 cells. Interestingly, exogenous expression of ZEB2 in carcinoma cells, such as in human epidermoid carcinoma A431 cells, initiates EMT and converts epithelial cells into mesenchymal ones (Mejlvang et al., 2007). It has

been reported that TGF $\alpha$ , hypoxia, TNF $\alpha$  and IL-1 signals are involved in ZEB2 up-regulation and initiation of EMT although the precise mechanism of ZEB2 transcription is not well understood (Katoh and Katoh, 2009).

Furthermore, induction of ZEB2 expression in A431 cells resulted in G1 phase cell cycle arrest due to ZEB2-mediated transcriptional repression of cyclin D1, causing an enhancement of the level of hypo-phosphorylated and inactive tumor suppressor protein, thereby preventing progression via the cell cycle (Mejlvang et al., 2007).

ZEB2 was also identified in a large-scale screen for tumour related genes, which detected its potential role in oncogenic transformation. ZEB2 is highly expressed in different human cancers such as breast (Comijn et al., 2001), ovarian (Katoh and Katoh, 2009), gastric (Alves et al., 2007), pancreatic (Imamichi et al., 2007) and liver cancers (Miyoshi et al., 2004). In addition, ZEB2 is overexpressed in transitional cell carcinoma of the bladder and is a strong driver of cancer progression and positively associated with a poor therapeutic outcome (Sayan et al., 2009).

A function of ZEB2 in cancer is not restricted to EMT only, but ZEB2 was also shown to be involved in glioma progression. For instance, ZEB2 repression by siRNA in U251 and U87 glioma cell lines was attributed to the inhibition of cell proliferation and promoted apoptosis in glioma cell lines (Qi et al., 2012). It has also been found that ZEB2 has an essential role in maintaining Epstein-Barr virus (EBV) latency by directly binding its promoter, Zp. EBV promoter correlates with different types of cancer, such as Burkitt's lymphoma and Hodgkin's disease (Ellis et al., 2010).

### **1.2.1.3 The Role of Rho GTPases in cancer**

Rho GTPases have a well-known function in regulating cytoskeleton and cell adhesion dynamics and therefore contribute to a variety of cellular processes, including cell migration, cell polarity and cell cycle progression. Rho-GTPases govern the contractile forces that are crucial for cell polarisation and translocation, and are intricately linked to the overarching regulation of the actomyosin cytoskeleton (Hodge and Ridley, 2016). Rho signaling activity is controlled by guanine nucleotide exchange factors (GEFs) which catalyse the exchange of GDP to GTP. However, to inactivate Rho activity, GTPase-activating proteins (GAPs) facilitating the intrinsic

GTPase activity to re-form the GDP bound state. Ultimately, the guanine nucleotide dissociation inhibitors (GDIs) interact with the inactive GTPase domains and their covalently attached lipid groups. The GDIs prevent the dissociation of GDP from Rho GTPases that might block spontaneous activation (Figure 1.6) (Jaffe and Hall, 2005). Hence, Rho GTPases work as molecular switches to control signal transduction pathways by cycling between a GDP-bound inactive form and a GTP-bound active form (Ridley, 2015).

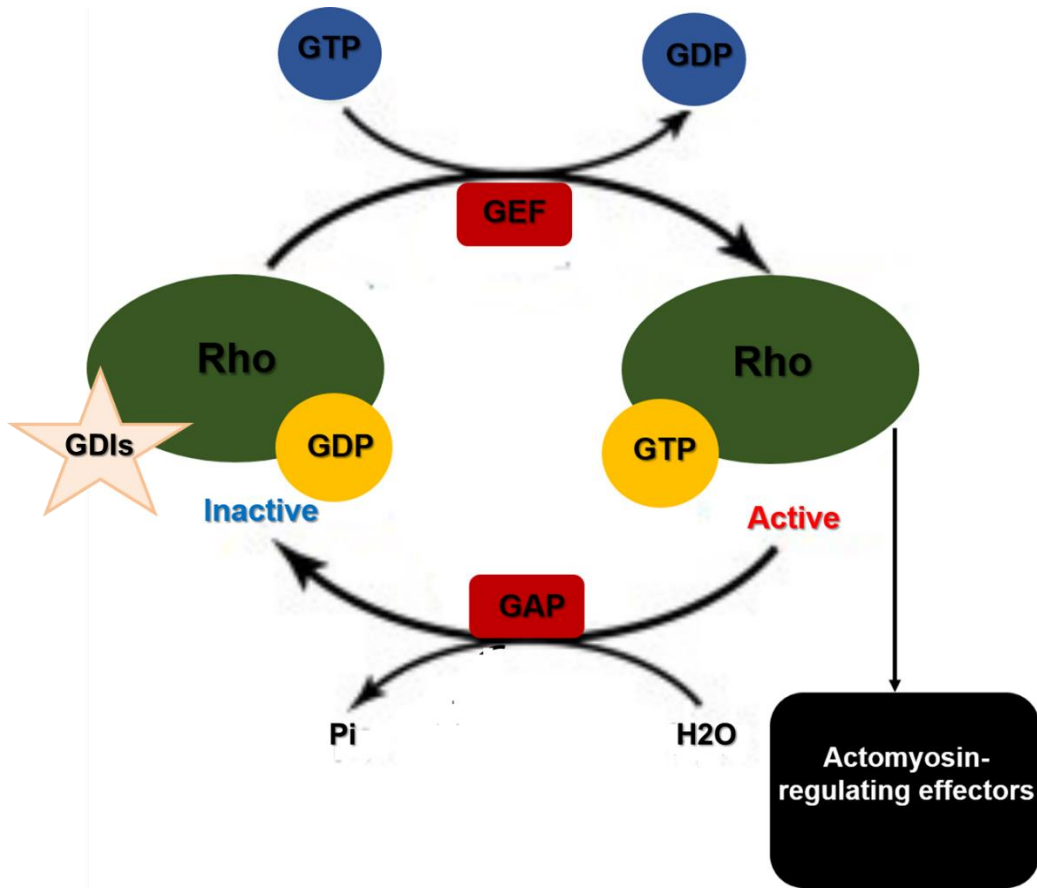


**Figure 1-6: Schematic representative of the Rho GTPase cycle.**

A diagram illustrating of the regulation of Rho GTPase activity in cells by Rho-dependent factors. GEFs are able to activate the exchange of GDP for GTP, thereby stimulating Rho-GTPases for interaction with downstream actomyosin-regulating effectors, whilst GAPs binding to the GTPase enhance the intrinsic GTPase activity in which bound GTP is switched to GDP. GDIs interact with the GDP-bound form of the molecule leading to prevent binding of GTP and thus subsequent activation. This figure is adopted from (Raftopoulou and Hall, 2004).

The typical Rho family members consist of RhoA, Rac1 and Cdc42. The amino acid substitutions that were demonstrated in a typical Rho family members change the ability to interact with GTP/GDP (Hodge and Ridley, 2016).

About 30 potential effectors have been detected for Rho, Rac, and Cdc42, such as serine/threonine kinases, tyrosine kinases, lipid kinases oxidases, scaffold proteins and lipases (Bishop and Alan, 2000). In mammals, it has been shown that abnormal activation of the Rho/ROCK pathway has been detected in brain and spinal cord injury, and inhibition of ROCKs leads to accelerated regeneration and recovery after spinal-cord injury in mammals (Mueller et al., 2005). Mechanistically, it has been shown that Rho GTPases coordinate many cellular responses by controlling formation of different actin assemblies. Indeed, Rac1 activates the WAVE complex, resulting in Arp2/3-mediated actin polymerization at the leading edge to form a lamellipodium, while Cdc42 triggers extension of filopodia; finger-like protrusions formed by parallel arrays of actin filaments. Cdc42 is required for stimulation of the N-WASP/WIP complex which leads to a release in the auto-inhibitory interaction and activation of the C-terminal Arp2/3 binding site (Figure 1.7-A) (Infante and Ridley, 2013, Raftopoulou and Hall, 2004). Rho itself is active at the front of the cell. It also induces formation of stress fibers and activates actin-myosin complex formation (Srinivasan et al., 2003).

During the movement of mesenchymal cells, filopodia and lamellipodia, which are induced by polymerization of actin filaments, contact the extracellular matrix through integrins, forming focal adhesions (extension and attachment). The contraction force of actomyosin interaction moves the nucleus and cell body forward (contraction). This movement is accomplished by tail retraction at the rear of the cell, leading to detachment of focal adhesion (rear release) (Figure 1.7-B) (Infante and Ridley, 2013).

Important evidence from human tumours showed that Rho GTPase signaling has been implicated in dissemination of a wide range of cancers (Porter et al., 2016), such as overexpression of RhoA, ROCK-I, ROCK-II, Rac1, and Cdc42 have been linked to progression in testicular cancer (Kamai et al., 2004). In addition, overexpression of Rho A and Rho C are associated with a poor prognosis in esophageal squamous cell carcinoma (Faried et al., 2007).

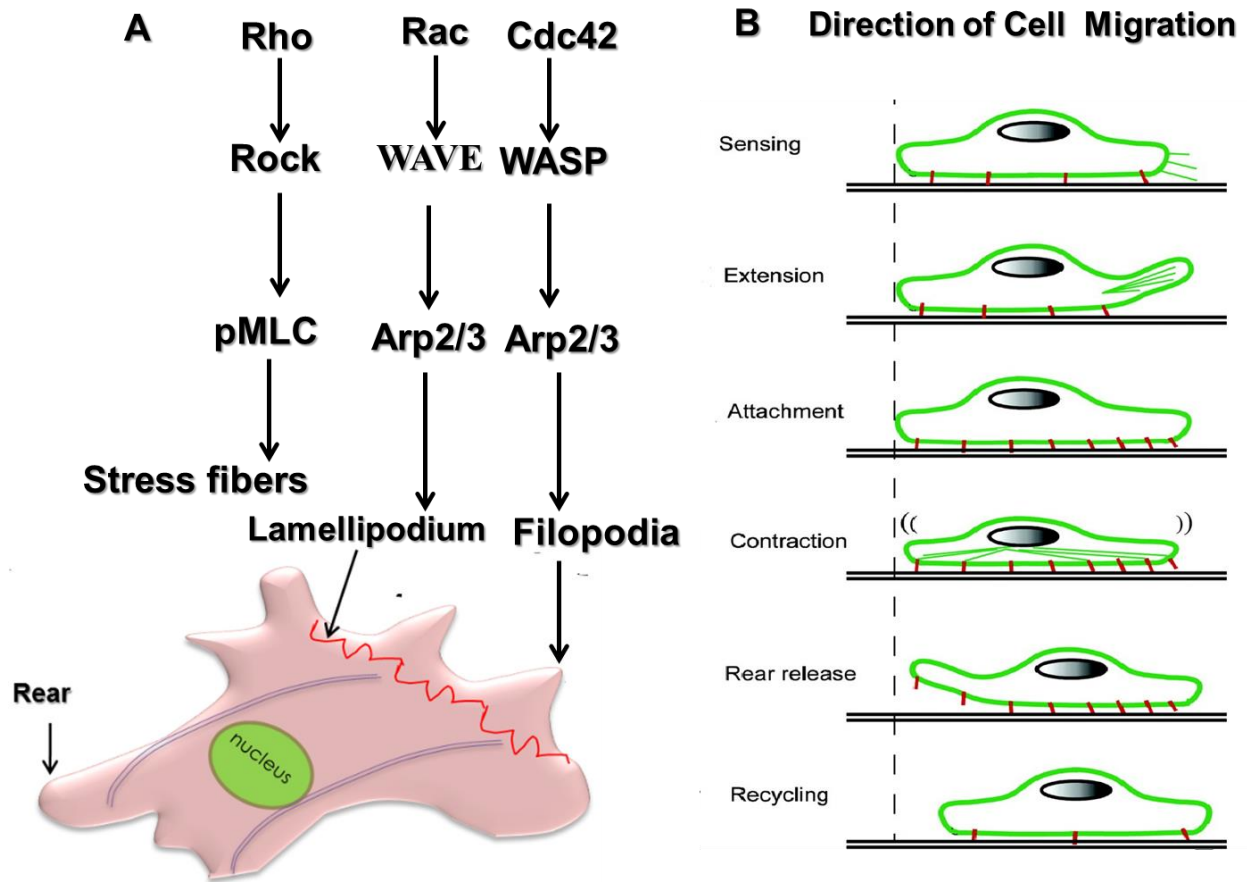


**Figure 1-7: Features of cell polarity, Rho GTPases and cell movement**

A-Rac1 activates the WAVE complex, leading to Arp2/3 mediated actin polymerization at the leading edge to form lamellipodium. Cdc42 can also contribute to membrane extension through WASP which activates the Arp2/3 complex. Rho induces actin polymerisation and membrane retraction. B- Direction of cell migration; filopodia and lamellipodia, which are induced by polymerization of actin filaments promote extension of the cell, the contraction force of actomyosin interaction leads to forward movement of the nucleus and cell body, followed by tail retraction at the rear of the cell, resulting in detachment of focal adhesion. Figure was adapted from Infante and Ridley, (2013).

### 1.3 S100 protein family

The S100 protein family constitutes the largest sub-group of EF-hand-containing calcium binding proteins which are expressed exclusively in vertebrates. EF hand domains are characterised by a helix-loop-helix motif of which the loop is responsible for calcium co-ordination (Moravkova et al., 2016). This family is composed of at least 21 relatively small members which have a low molecular weight of around 10-12 kDa (Bresnick et al., 2015, Leclerc et al., 2009). The first member of the S100 family was purified from bovine brain by (Moore, 1965). S100 proteins are so-called as they are soluble in 100% ammonium sulfate solution at neutral pH (Gaynor et al., 1981).

Within cells, S100 proteins have been implicated in various intercellular processes including cellular proliferation, apoptosis,  $\text{Ca}^{2+}$  homeostasis, cell migration and inflammation via interactions with a variety of target proteins. Additionally, extracellular S100 proteins exert regulatory activities through activation of surface receptors in autocrine and paracrine manner (Donato et al., 2013), such as the receptor for advanced glycation end-products (RAGE) and toll-like receptor 4 (Chen et al., 2014b). When RAGE is engaged by its ligands, different signaling pathways may be activated in a ligand-dependent manner. These signaling pathways include the PI3K/Akt pathway; various mitogen-activated protein kinase (MAPK) pathways involving Erk1/2, p38, and JNK; and other pathways involving small GTPases, such as p21-Ras, Rac-1, or cdc42. RAGE engagement by its results in the activation of numerous transcription factors, such as NF- $\kappa$ B, AP-1, STAT-3 and CREB. Because the RAGE gene is under the control of NF- $\kappa$ B, the engagement of RAGE by its ligands leads to augmented RAGE activation in a positive feedback circle (Figure 1.8) (Leclerc and Vetter, 2015).

The extracellular S100 proteins regulate the activity of different types of blood cells, articular chondrocytes, neurons, astrocytes and myoblasts, thereby contributing to initiation of the innate and adaptive immune responses, chemotaxis tissue repair and tumor cell invasion (Donato et al., 2013). S100B is actively secreted from astrocytes, neurons, microglia (Ellis et al., 2007). S100A8 and S100A9 are aggressively secreted from activated neutrophils and macrophages and can be detected in the body fluids as potential inflammatory marker (Stříž and Trebichavský, 2004). In addition, S100A4 secreted by parietal endoderm triggers cardiomyogenesis in embryonic bodies (Sary et al., 2005), whereas S100A6 can be actively released from human glioblastoma after

calcium activation of the cells (Leclerc et al., 2009). The majority of S100 proteins are expressed in the human epidermis or in cultured keratinocytes (Böni et al., 1997).

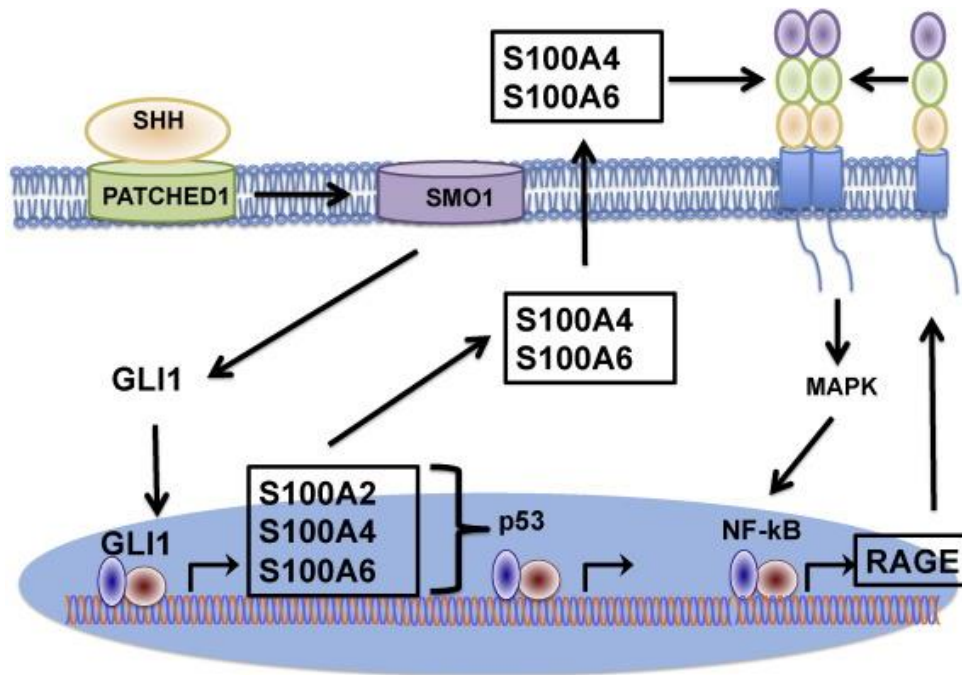


**Figure 1-8: Signalling of S100 A4, A6 and A2 in cancer cells**

RAGE is involved by its ligands, multiple signaling pathways is stimulated in a ligand-dependent manner. These signaling pathways include the PI3K/Akt pathway; various mitogen-activated protein kinase (MAPK) pathways involving Erk1/2, p38, NF-κB, and JNK. Figure was adapted from (Leclerc and Vetter, 2015).

### 1.3.1 S100 proteins genes

Some S100 genes are located on the chromosome 1q21; a locus known as the epidermal differentiation complex (EDC) (Figure 1.9) (Ravasi et al., 2004). Other gene locations include S100B which maps to chromosome 21q22, S100G which maps to chromosome Xp22, S100P, which maps to chromosome 4p16, and S100Z, which maps to chromosome 5q13 (Marenholz et al., 2006). The EDC also contains genes encoding the S100-fused type proteins (SFTPs) which contains a full-length S100 protein domain fused in-frame to multiple tandem repeats consist of one or two sequences, for which the function is not well known (reviewed in (Bresnick et al., 2015). The mammalian S100 genes consist of three exons. The first exon only encode the 5'UTR, whereas the second and third exons code for the open reading frame and 3'UTR (Kraemer et al., 2008).

Calcium is a highly versatile intracellular signal that controls the structure and function of the S100 proteins allowing them to act as calcium sensors which stimulate different cellular processes. The S100 proteins are often binding  $\text{Ca}^{2+}$  ions weakly in the absence of a protein target; upon binding their target proteins,  $\text{Ca}^{2+}$ -binding then increases by as much as 200 to 400-fold (Zimmer and Weber, 2010).

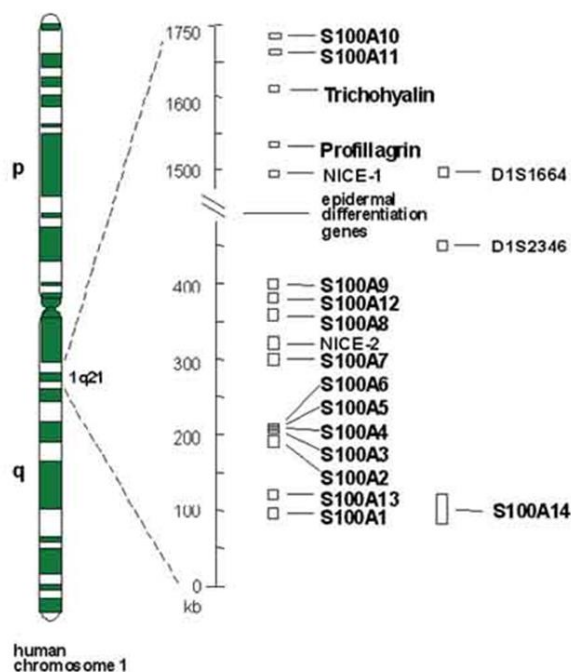


**Figure 1-9: S100 genes are located on chromosome 1**

S100 genes are located on human chromosome 1q21 in region termed the epidermal differentiation complex. Two commonly used genomic markers (D1S1664 and D1S234). p and q indicate the short and the long arm of the chromosome, respectively (Ravasi et al., 2004).

### 1.3.2 Structure of S100 proteins

S100 proteins have a common structure composed of pseudo (N-terminal) and canonical carboxyl (C-terminal) EF-hand, that are separated by a hinge region (Santamaria-Kisiel et al., 2006, Eckert et al., 2004). In canonical (C-terminal) EF-hand, the loop contains 12 amino acids that binds calcium with a 100-fold higher affinity than the pseudo (N-terminal) domain, which contains 14 amino acids ((Eckert et al., 2004, Zimmer et al., 2003). The highest degree of sequence variability is found within the hinge and C-terminal region (Figure 1.10).

## Psuedo EF-Hand

```

S100A1 ..... ..MGSELET AMETLINVFH AHSGKEGDKY KLSKELKEL LQTELSGFLD
S100A2 ..... ..MSSLEQ ALAVLVTFH KYSCQEGDKF KLSKGMKEL LHKELPSFVG
S100A3 ..... ..MARPLEQ AVAAIVTFQ EYAGRCGDKY KIQSSLKEL LQKELPTWTP
S100A4 ..... ..MACPLEK ALDVMVSTFH KYSGKEGDKF KLNKSELKEL LTRRLPSFLG
S100A5 ..... ..METPLEK ALTTMVTFH KYSGREGSKL TLSRKLKEL IKKELGLG..
S100A6 ..... ..MACPLDQ AIGLLVAIFH KYSGREGDKH TLSKELKEL IQKELTIG..
S100A7 ..... ..MSNTQER SIIGMIDMFH KYTRRD...D KIDKPSLLTM M.KENFPNFL
S100A8 ..... ..MLTELEK ALNSIIDVYH KYSLIKGNFH AVYRDLKLL LETECPQYIR
S100A9 ..... ..MTKMSQLER NIETIINTFH QYSVKLGHPD TLNQGFKEL VRKDLQNFLK
S100A10 ..... ..MPSQMEH AMETMPTFH KFAGDKGY...LTKELRVL MEKEFPGFLE
S100A11 ..... ..MAKISSPTETER CIESLIAVFO KYAGKDCYNY TLSKFLSF MNTELAAFTK
S100A12 ..... ..MTKLEE HLEGIVNIFH QYSVRKHGFH TLSKGLKQL LTKELANTIK
S100A13 ..... ..MAAEPLTELEE SIETVVVTFH TPARQGRKD SLSVNFKEL VTQQLPHLLK
S100A14 MGQCRSANAE DAQEFSDVER ALETLIKNFH QYS.VEGGKE TLTPSLRDL VTQQLPHLMP
S100A16 ..... ..MSDCYTELEK AVIVLVENFY KYYSKYSLVK NKISKSSFRE MLQKELNHML
S100B ..... ..M.SELEK AMVALIDVFH QYSGREGDKH KLNKSELKEL INNELSHFLE
S100P ..... ..M.TELEK AMGMIIDVFS RYSGSEGSTQ TLTGKGLKVL MEKELPGFLQ
S100Z ..... ..MPTQLEM AMDTMIRIFH RYSGKARKRF KLSKGLKLL LQRELTEFLS
Calbindin..... ..MSTKK SPEELKRIFE KYAAKEGDPD QLSKDLKLL IQAEFFSLLK
  
```

Helix 1

Helix 2

## Canonical EF-Hand

```

S100A1 ...AQKDVDA VDKVMKELSE KQGEVDFQF YVVLVAALTV ACNFFWENS.....
S100A2 ...EKVDEEG LKKLMGSLDE NSQOQVDFQF YAVFLALITV MCNDFFOGCP DRP.....
S100A3 ...SEFRECD YNKFMVSLDT NKQCEVDFGF YVRSLSLCLL YCHEYFKECP PEPPCPQ...
S100A4 ...KRTDEAA FQKLMNSLDS MRNEVDFQF YCVFLSCIAM MCNEFFEGFP DKQPRKK...
S100A5 ...EMKESS IDDLMKSLK NSQEIIDFKF YSVFLTMLCM AYNDFFLEON K.....
S100A6 ...SKLQDAE IARLMEDLIR NKQCEVNFQF YVTFGLGALAL IYNEALKG...
S100A7 SACDKKGTNY LADVFEKTKK MEKKIDFSE FLSLLGDIAT DYHKSIGAAP CSGGSQ...
S100A8 ..K....KG ADVWFKELSI NTGAVNFQF FLILVIKMGV AAHKSHHEES HKE.....
S100A9 ..KENKNEKV IEHIMEDLIT NAKQLSFEF FIMLMARLITW ASHEKMEEGD EGPGRHHKPG LGEQTP
S100A10 ..N.QKDPLA VDKIMKDLQ CRGKGVGFQS FFSLIAGLTI ACND.YFVVH MKQKQKK...
S100A11 ..N.QKDPGV LDRMMKLLT NSGQLDFS FLNLIGGLAM ACHDSFLKAV PSQKRT...
S100A12 ..N.IKDKAV IDEIFQGLDA KQEQVDFQF FISLVAITALK AAHYHTHKE.....
S100A13 .....DVGS LDEKMKSLIV KQSELKFN YWRLIGELAK EIRK..KKDL KIRKK...
S100A14 .....SNG LEEKIANLGS CNNSKLEFRS FWELIGEAAK SVKL..ER..PVRGH...
S100A16 ..SDTGNRKA ADKLIQNLDA NHGRISFDY YWTLIGGITG PIAKLIHQEQ QQSSS...
S100B ..E.IKEQEV VDKVMETLON KQGECDQFQ FMAFVAVTT ACHE.FFEHE.....
S100P ..S.GKDKDA VDKLLKDLDA KQEAQVDFSE FIVFVAITS ACHK.YFEKA GLK.....
S100Z ..C.QKETQL VDKIVQDLDA NKNEVDFNE FVVMVAALTV ACND.YFVEQ LKKKQK...
Calbindin.....GPNT LDDLEQELSK KQGEVSFEF FQVLVKKISO.....
  
```

Helix 3

Helix 4

**Figure 1-10: Multiple sequence alignment of human S100proteins**

S100 proteins consist of a pseudo (N-terminal) and Canonical (C-terminal) EF-hand. Each EF hand composed of a helix-loop-helix motif. Red shaded-residues indicate identical residues whilst yellow-shaded are biochemically similar residues. Note the lack of sequence homology within the hing and tail region.

The basic quaternary structure of S100 proteins is a homodimer. S100 proteins exist as symmetric homodimers in solution controlled by non-covalent interactions between hydrophobic residues of helices 1 and 4 from each monomer (Gingras et al., 2008). However, these proteins have the ability to form the oligomers which are functionally relevant. In addition to dimerisation, it is well established that bound  $\text{Ca}^{2+}$  ions trigger the formation of tetrameric structures of S100 proteins *in vivo* (Streicher et al., 2010). The quaternary structure of proteins is essential not only for the stability of S100 proteins, but also for the function of the S100 proteins (Ostendorp et al., 2007).

The intracellular roles of S100A4 are associated with the dimeric structure, while the oligomeric form has an extracellular function. The crystal structure of S100A4 in calcium dependent manner illustrated that one of hydrophobic motifs in each dimer binds to the C-terminal end of another. Therefore, tetramerisation disrupts the binding with the target proteins (Gingras et al., 2008). The structure of S100A4 was shown in (Figure 1.11) (Elliott et al., 2012).

The screening of a mouse mammary adenocarcinoma cDNA library by (Tarabykina et al., 2001) showed that S100A4 forms homodimers and heterodimers with S100A1. Moreover, mutational investigation revealed that Cys-76 and Cys-81 of S100A4 are crucial for its interaction with S100A1 but not for the S100A4 homodimerization. The data obtained from (Tarabykina et al., 2001) also revealed that apoS100A4 exists in solution as a mixture of monomers and dimers in a reversible equilibrium. Furthermore, this study also suggested that few residues within helix IV are important for dimerization of S100A4 *in vivo* including Phe-72, Tyr-75, Phe-78, and Leu-79 using the yeast two-hybrid system.

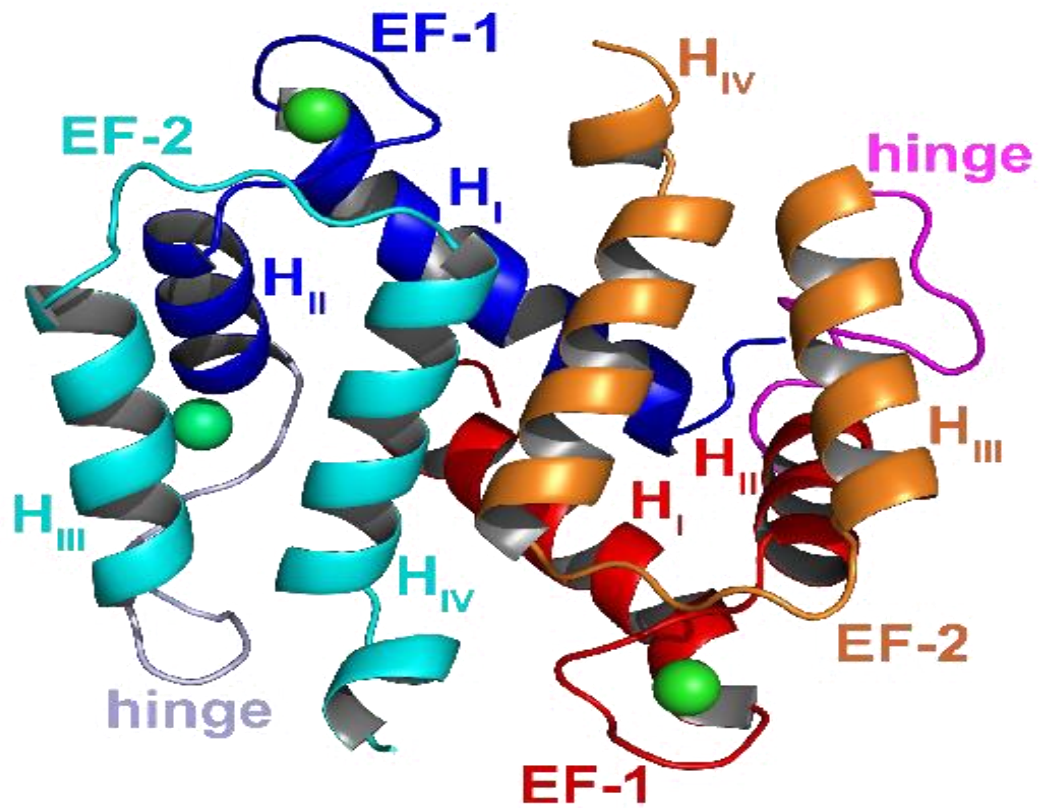


**Figure 1-11: Dimer Structure of S100A4 in the presence of calcium**

The dimer structure of S100A4 that present in  $\text{Ca}^{2+}$  bound form is stabilised by non-covalent hydrophobic residues in helix 1 and helix 4. The figure was adopted from (Elliott et al., 2012).

### 1.3.2.1 Calcium-binding affinity of S100 proteins

Calcium ions regulate cell function and physiology and it is used to regulate protein or enzymatic activities (Bao et al., 2012). Due to their sensitivity to calcium in a manner similar to calmodulin and troponin C, S100 proteins undergo conformational changes and control the biological activity through calcium binding (Sedaghat and Notopoulos, 2008). LPA activates G protein-coupled receptor signal transduction pathways and Ras/MAP kinase (MAPK) cascade leads to generate diacylglycerol (DAG) and inositol triphosphate (IP3) from phosphatidylinositol diphosphate (PIP2). DAG activates protein kinase C (PKC), and IP3 mobilizes  $\text{Ca}^{2+}$  (Contos et al., 2000).

In terms of S100A4 and S100A6, binding of calcium to these proteins initiates a conformational change and leads to re-orientation of helix3 opening a large cleft that is comprised of residues from the hinge region, helix 3, and helix 4 (Figure 1.12-A and B). This leads to an exposure of hydrophobic binding pocket that is necessary for binding to a variety of target proteins. The pseudo EF (non-canonical) hand loop co-ordinates calcium through backbone carbonyls, while the canonical EF hand loop binds calcium mainly through side chain carboxyls or carbonyls (Gingras et al., 2008, Pathuri et al., 2008). Due to varying affinities of the non-canonical and canonical EF hand to calcium, there are a huge differences in calcium-binding properties of S100A4 (Badyal et al., 2011). However, NMR dMelvata revealed that filling of the pseudo EF hand occurs at a lower calcium concentration than does filling of the canonical EF hand (Dutta et al., 2002).

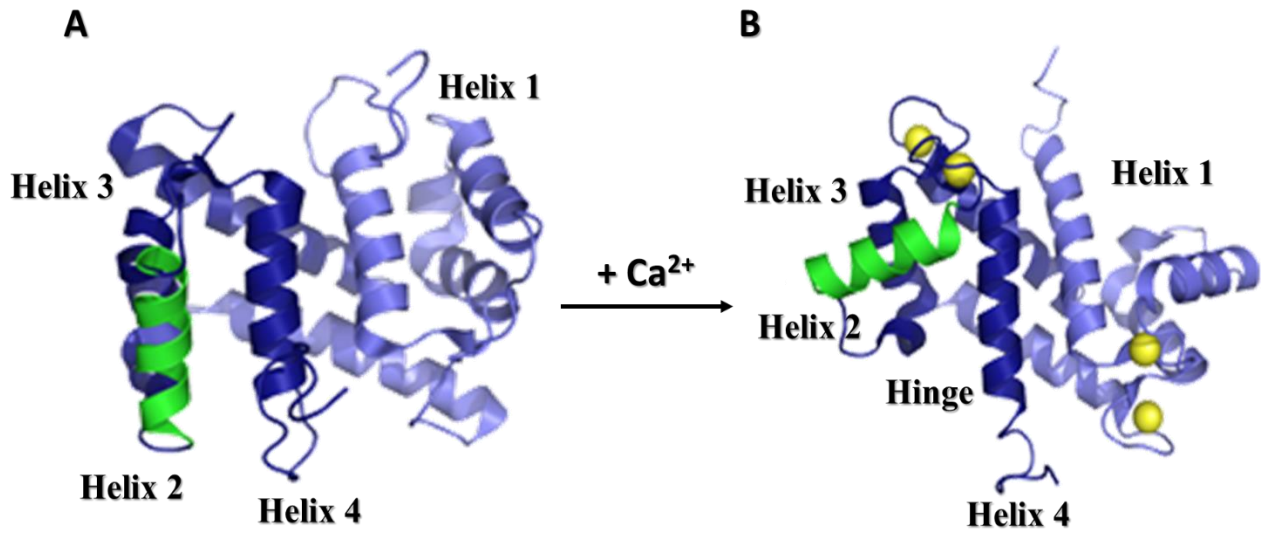


**Figure 1-12: Effect of calcium on the S100A4.**

A-S100A4 in the apo form. B- Conformational changes occur in S100A4 in the presence of calcium causing helix 3 to undergo a 60° reorientation. Exposure of a hydrophobic cleft between helix 3 (green), helix4 (blue) and the hinge region. This cleft serves as an important site for protein-protein interactions. Calcium ions are represented as yellow spheres. The figure is adapted from (Gingras et al., 2008).

### **1.3.3 S100 proteins expression and function.**

S100 proteins are involved in different biological processes, including cell division, differentiation, cytoskeleton organization, and cell migration via interactions with a variety of target proteins (Bresnick et al., 2015). Generally, the role of individual S100 proteins depend on the cell types where they are expressed. S100B is expressed in Langerhans cells and melanocytes and S100P is expressed in Meissner's corpuscles (Del Valle et al, 1994). Intracellular S100B has a role in chemically irritated melanocytes suggesting the increased intracellular S100B expression as a compensatory reaction to reduce cytotoxicity. Therefore, it is considered as a potential biomarker for the detection of cytotoxicity of melanocytes (Cheong et al., 2014). S100P was initially identified from placental tissue, hence its name. S100P is also expressed in high levels in epithelial cells of the stomach and Its expression significantly increases in many solid tumors, such as ovarian, prostate, gastric, colorectal, breast and pancreatic carcinomas. S100P is clinically used as a diagnostic marker of pancreatic ductal adenocarcinoma (Leclerc and Vetter, 2015). In some occasions, a specific S100 protein might be induced in certain pathological conditions in a cell type that does not express it in normal physiological conditions (Donato et al., 2013).

Expression of numerous members of the S100 family is a common feature of human cancers, and thereby they actively contribute to tumorigenic processes such as cell proliferation, metastasis, angiogenesis and immune evasion. Development of inhibitors for melanoma and prostate cancer are in clinical trials that directly targeting two members of S100 proteins, S100B and S100A9, respectively. Human S100A8/S100A9 is chemotactic for neutrophils and they have an effect on migration of tumor cells by facilitating tumor cell invasion S100A8/S100A9 also activate proinflammatory cytokine production by human monocytes and macrophages through the NF- $\kappa$ B and p38 MAPK pathways and thereby promote cancer development through RAGE mediated production of inflammatory mediators (Donato et al., 2013).

S100A1 interacts with protein kinase A (PKA) mediating enhancement in the Ca<sup>2+</sup> influx in embryonic mouse and neonatal rat ventricular cardiomyocytes. Cardiomyocytes secrete S100A1 during ischemia which is taken up by superior cervical ganglion neurons. Therefore S100A1 acts as a signaling molecule which rises the sympathetic output (Hernandez-Ochoa et al., 2009). The S100A10-annexin 2 complex play an important role in controlling and localizing the plasma membrane to

TRP transient receptor potential (TRP) channels and modulate the channel activity. The latter has been shown by using annexin 2 interfering RNA, which inhibited currents through TRP channels (van de Graaf et al., 2003b). S100A4 which is also known as (mts1, CAPL, pEL98, Calvasculin, p9Ka, and FSP1) (Schmidt-Hansen et al., 2004) has been shown to be expressed in different types of cells and tissues including fibroblasts, lymphocytes, macrophages, parietal cells of stomach and smooth muscle cells (Wetting et al., 2011, Schneider et al., 2008, Takenaga et al., 1997). Additionally, S100A4 mRNA and protein have been detected in intestinal fibroblasts and isogenic proximal tubule cells of the kidney (Barraclough, 1998). In fact, S100A4 is a marker of a specific subset of inflammatory macrophages in liver injury, fibrosis, and cancer (Österreicher et al., 2011). It was documented that macrophages derived from S100A4-deficient mice displays a defect in chemotactic motility *in vitro* (Li et al., 2010). S100A4 also activates cytokine production during the allergic inflammatory processes including granulocyte colony-stimulating factor and eotaxin-2 from T lymphocytes (Grum-Schwensen et al., 2010). S100A4 is also involved in the alteration which occurred between keratocytes, fibroblasts and myofibroblasts during corneal wound healing (Ryan and Bernard, 2003). Consequently, the expression of S100A4 is considered as a hallmark of myofibroblast formation by EMT (Le Hir et al., 2005). Moreover, S100A4 has a supportive role in injured myocardium via promoting smooth muscle cell migration, proliferation, and mediating arterial muscularisation (Schneider et al., 2007). Although it is established that S100A4 contributes to tumor cell motility and metastatic progression, the exact underlying mechanisms remain elusive (Tarabykina et al., 2007).

Another EF-hand calcium binding protein of the S100 family is S100A6 which is overexpressed in the brainstem and reactive astrocytes (Hoyaux et al., 2000). It is also known as Calcyclin/2A9/5B10/PRA and is involved in the regulation of different cellular activities such as proliferation, differentiation, as well as apoptosis. However, the precise biological function of S100A6 is not well known (Filipek et al., 2008). S100A6 is expressed in various cell types, such as fibroblasts, epithelial cells, nerve cells and blood cells (Kuźnicki et al., 1992). As such, S100A6 is able to regulate various intracellular functions, including protein phosphorylation, enzyme activities and Ca<sup>2+</sup> homeostasis (Boom et al., 2004). In addition, depletion of S100A6 leads to a reduction in both cyclin-dependent kinase 1 (CDK1) and phospho CDK1 levels, which are crucial for eukaryote cell-cycle progression (Bao et al., 2012).

In mammalian cells, S100A6 and S100A4 are involved in the growing and differentiation of hair follicles, as they contribute to the initial step of skin tissue re-epithelialisation (Ito and Kenji, 2001). Additionally, this protein plays a role in the mucus secretion in the epithelia that lines the gastrointestinal, respiratory, and urinary tracts. S100A6 also activates the process of insulin release from the pancreatic cells. It has been reported that S100A6 expression is elevated under stress conditions (Leśniak et al., 2005). Other research revealed that S100A6 regulates the function of the actin cytoskeleton, cell growth and apoptosis by interacting with p53 (Fernandez-Fernandez et al., 2008). Moreover, S100A6 expression is augmented in many types of cancer and there is association between tumour progression and serum S100A6 level (Leśniak et al., 2005).

#### **1.3.4 S100A4 and S100A6 expressions correlate with poor of cancer prognosis**

S100A4 has a critical role in promoting cancer metastasis. Although S100A4 is not tumorigenic, it triggers migration and invasion of already existing cancer cells, leading to aggressive tumor growth and formation of metastasis (Pachmayr et al., 2017, Dmytriyeva et al., 2012). A direct association has been shown between changes in S100A4 expression and migratory abilities of tumour cells (Salama et al., 2008). In addition, S100A4 activate T-lymphocytes cells leading to the production of cytokines and growth factors which are correlated with poor prognosis in cancer patients (Grum-Schwensen et al., 2010). The collected data from a study by (Huang et al., 2016) study suggested that expression of S100A4 is a strong marker for lymph node metastasis of pancreatic cancer, and therefore, it is considered as an important factor for prognosis and survival of patients with this disease. Another study revealed that a high expression of S100A4 contributes to an aggressive phenotype of endometrioid carcinoma by accelerating the proliferation and invasion of tumour cells (Tahara et al., 2016). In addition, S100A4 enhances the migration and invasion of hepatocellular carcinoma cells through NF-kappa B-dependent matrix metalloproteinase MMP-9 signalling (Zhang et al., 2013). S100A4 gene also activates the invasiveness of human prostate cancer via transcriptional regulation of MMP-9 and might be associated with tumorigenesis (Saleem et al., 2006).

Research confirmed that S100A4 stimulates invasive growth of the mouse adenocarcinoma cells as its involvement in tumor-stroma interplay (Schmidt-Hansen et al., 2004). Such evidence

suggests that S100A4 could also be used as a marker of tumour invasiveness and metastasis in cancer. The evidence came firstly from (Rudland et al., 2000) study which was conducted in breast cancer patients showing that S100A4 expression is a well-established marker of disease progression by analysing a group of 349 patients and it was identified that S100A4 expression is considered to be a significant predictor of patients survival. There are number of pathological factors indicating patient death from metastatic disease including the size of the primary tumor and gene products involved such as erbB-2, erbB-3 and oestrogen receptors e.g., ER4 and p53. In all, eighty percent of the S100A4-negative patients were alive for 19 years follow-up, whereas only 11% of the S100A4-positive cases survived (de Silva Rudland et al., 2011). In contrast to these data, other studies on breast cancer, non- small cell lung cancer (NSCLC) and gastric cancer showed that there is an association between S100A4 expression and an aggressive tumour phenotype. However, these studies did not find a relationship between S100A4 expression and patients survival (Pedersen et al., 2002, Wang et al., 2010b, Kimura et al., 2000). Completely opposite results were obtained from an evaluation of the expression of S100A6 in patients with NSCLC, as it was found that expression of S100A6 protein in a cohort of 130 patients with pathological stage I NSCLC displayed a trend of longer survival compared with S100A6-negative cases. The survival differences in S100A4 positive cases with S100A6 expression indicates that in NSCLC, S100A6 could act antagonistically to S100A4 and modulate its metastatic potential (De Petris et al., 2009). Data from another study confirmed that S100A4 is widely expressed in brain cancer, as S100A4 knockout mice resulted in reduced tumour growth and reduced metastasis to the brain (Bresnick et al., 2015). In addition, 22 out of 27 of a series of breast cancer patients were S100A4 positive and associated with intracranial progression (Zakaria et al., 2016). A research carried out by (Kikuchi et al., 2006) examined the expression of S100A4 in 113 epithelial ovarian neoplasms patients suggested that the nuclear expression of S100A4 represents an aggressive tumour phenotype. Expression data from (Barbazan et al., 2016) showed that nuclear localisation of S100A4 conveyed a significantly worse prognosis in colorectal cancer patients. A cohort of resected specimens from 127 patients with colorectal cancer, found that S100A4 protein was clearly absent in normal colorectal mucosa, while it was detected in 35.4% of the tumor cases, whilst there was no association between the reactivity and E-cadherin or p53 expression. However, positive immunoreactivity of S100A4 protein was shown to be correlated with cancer recurrence and with significantly worse overall survival rate (Kwak et al., 2010). Indeed, the presence of

S100A4 protein in a cohort of 101 tissues from patients with primary bladder cancer were found to be associated with those primary tumours that later advanced with distant metastasis, thereby reducing patient survival (Davies et al., 2002).

In terms of S100A6, published results found that S100A6 expression was reported to be considered as a prognostic marker in osteosarcoma and colorectal cancer, where enhanced S100A6 expression in cancer cells have been coupled with improved patients survival. Furthermore, knockdown of endogenous S100A6 promotes cell migration and invasion. In contrast, (Vimalachandran et al., 2005) revealed that high nuclear S100A6 levels in pancreatic cancer resulted in a decreased patient survival. In addition, S100A6 was overexpressed in gastric cancer compared with matched noncancerous mucosa and it was correlated with a clinically aggressive phenotype and poor survival of patients (Wang et al., 2010a). Additionally, there is association between S100A6 mRNA levels in metastases and the survival time of melanoma patients (Maelandsmo et al., 1997).

Functionally, S100A6 was shown to play a critical role in various molecular processes within tumorigenesis. In an *in vivo* mouse model with renal cell carcinoma, it was shown that knockdown of S100A6 led to a significant decrease in tumour mass due to arrest of the G2/M phase (Bao et al., 2012). Despite a significantly increased expression of S100A6 in resected tumour tissue from human and mouse model with cholangiocarcinoma, serum levels of S100A6 were not significantly changed compared to healthy controls. However, cholangiocarcinoma patients with a high levels of S100A6 exhibit a poor prognosis when compared to patients with lower S100A6 levels (Loosen et al., 2016). Table (1.1) illustrates important cancers associated with S100A4 and S100A6.

**Table 1-1: Expression of S100A4 or S100A6 in different human cancers**

Disease	References (S100A4)	References (S100A6)
<b>Breast cancer</b>	(Platt-Higgins et al., 2000, Lee et al., 2004) ; (Saleem et al., 2006, Ismail et al., 2008, de Silva Rudland et al., 2006).	(McKiernan et al., 2011)

<b>Colorectal carcinoma</b>	(Kwak et al., 2010) (Huang et al., 2011, Kang et al., 2012, Liu et al., 2013c, Hemandas et al., 2006, Lim et al., 2014, Sugai et al., 2017).	(Komatsu et al., 2000); (Melle et al., 2008)
<b>Ovarian carcinoma</b>	(Kikuchi et al., 2006, Mælandsmo et al., 2009).	
<b>Oral squamous cell carcinoma</b>	(Natarajan et al., 2014)	
<b>Gastric cancer</b>	(Ling and Li, 2013, Wang et al., 2010b)	(Wang et al., 2010a)
<b>Pancreatic cancer</b>	(Oida et al., 2006, Tsukamoto et al., 2013, Lee et al., 2014).	(Lokman et al., 2011) (Vimalachandran et al., 2005)
<b>Renal cell carcinoma</b>	(Yang et al., 2012, Matsumoto et al., 2007).	(Nishi et al., 2014)
<b>Bladder cancer</b>	(Davies et al., 2002, Matsumoto et al., 2007, Ismail et al., 2008, Kim and Park, 2014).	(Ismail et al., 2016)
<b>Non-small lung cancer</b>	(Bai et al., 2014, Miyazaki et al., 2006).	(De Petris et al., 2009)
<b>Prostate cancer</b>	(Saleem et al., 2006, Gupta et al., 2003)	(Rehman et al., 2005, Rehman et al., 2004)
<b>Human Melanoma</b>	(Crnogorac-Jurcevic et al., 2003)	(Gonzalez-Martinez et al., 2003, Weterman et al., 1992).
<b>Brain cancer</b>	(Harris et al., 2008, Camby et al., 1999).	(Harris et al., 2008)
<b>Liver cancer</b>	(Fabris et al., 2011, Yan et al., 2013)	(Melle et al., 2008, Li et al., 2014)

### 1.3.5 S100 protein interact with target proteins

S100 proteins exist in cells as anti-parallel hetero- and homodimers and upon calcium binding interact with target proteins in the presence of calcium (Eckert et al., 2004). Accordingly, S100A4 binding to p53 interferes with the DNA binding activity of p53 *in vitro* and reporter gene transactivation *in vivo*. It has been shown that S100A4 is able to inhibit PKC-mediated phosphorylation, and thereby induce p53-dependent apoptosis (Grigorian et al., 2001). Other published study by van Dieck and colleagues found that S100A4 and 100A6 interact with various oligomeric forms of p53 *in vitro*, using analytical ultracentrifugation and multiangle light scattering, but S100A6 bound more tightly to tetrameric than to monomeric p53 (van Dieck et al., 2009). S100A4 also interacts with the C terminus of the liprin  $\beta$ 1 molecule which belongs to the family of leukocyte common antigen-related (LAR) transmembrane tyrosine phosphatase leading to the inhibition of liprin  $\beta$ 1 phosphorylation (Kriajevska et al., 2002). According to the literature, the best characterised target for S100A4 is NM IIA. Indeed, S100A4 interacts selectively with NM IIA leading to filament disassembly or the prevention of filament formation (Kiss, 2014, Irvine, 2012, Kriajevska et al., 2002, Kriajevska et al., 1994); (Kriajevska, 1998). More recently, it was found that S100A4 binds to the N-terminal ERM domain (N-ERMAD) of ezrin which has a role in cell morphology changes, adhesion and migration (Biri-Kovács et al., 2017).

In terms of S100A6 target proteins, the co-localisation between S100A6 and tropomyosin has been documented by a number of studies (Orre et al., 2007, Golitsina et al., 1996). It was also demonstrated that S100A6 specifically interacts with the tetratricopeptide (TPR) domains of kinesin light chain (KLC) in a  $\text{Ca}^{2+}$ -dependent manner, resulting in regulation of the TPR protein-ligand interactions *in vitro*. TPR domain was originally recognized by sequence comparisons among yeast protein. Hop directly associates with Hsp70 and Hsp90 via the TPR domains and regulates Hop-Hsp70 and Hop-Hsp90 complex formation (Shimamoto et al., 2008). Following this, another study determined the binding of S100A6 to annexin 2 in the membrane of pancreatic cancer cells and triggers cancer cell migration (Nedjadi et al., 2009).

S100A1 interacts with protein kinase A mediating an enhancement in the  $\text{Ca}^{2+}$  influx in embryonic mouse and neonatal rat ventricular cardiomyocytes. Chronic deficiency of S100A1 results in impairment of the  $\text{Ca}^{2+}$  release mechanism from intracellular stores (Gusev et al., 2009).

Cardiomyocytes secrete S100A1 during ischemia which is taken up by superior cervical ganglion neurons. Therefore, S100A1 acts as an important regulator of heart function (Hernández-Ochoa et al., 2009). The S100A10-annexin 2 complexes play an essential role in localization transient receptor potential (TRP) channels to the plasma membrane and modulating the channel activity (van de Graaf et al., 2003a). S100A1 and S100B interact with annexin 5 and 6 to activate  $\text{Ca}^{2+}$  flux across artificial membrane (Garbuglia et al., 2000). In addition, S100B is expressed in Islet of Langerhans cells and melanocytes and S100P is expressed in various cell types and also interacts with multiple targets, such as annexin (Eckert et al., 2004, Del Valle et al., 1998).

#### **1.4 Myosin II**

Myosins are described as a large superfamily of actin-based molecular motor proteins, which are present in eukaryotic cells (Wang et al., 2011). Myosins are constituting of at least 25 different classes which play a critical role in several cellular processes that require force generation (Conti and Adelstein, 2008). Non-muscle myosin II (NM II) is a chemo-mechanical protein existing as a monomer that consists of three pairs of polypeptides including two heavy chains (NMHCs), two essential light chains (ELCs), two regulatory light chains (RLCs) termed IQ motifs, and coiled-coil or rod domain composed of two myosin heavy chains (MHC II) with a non-helical C terminal end; allows some myosins to self-assemble into filaments. (Figure 1.13) (Heissler and Manstein, 2013). Generally, myosin and actin slide filaments past each other and assembled into bundles of actomyosin filament which leads to ATP hydrolysis and thereby converting chemical energy into movement (Juanes-García et al., 2016); (Vicente-Manzanares et al., 2009). Class II myosins were discovered in animal cells 60 years ago (Sellers, 2000). Myosin II are divided into skeletal, cardiac and smooth muscle myosin, as well as non-muscle myosin II (NM II) (Dulyaninova and Bresnick, 2013).

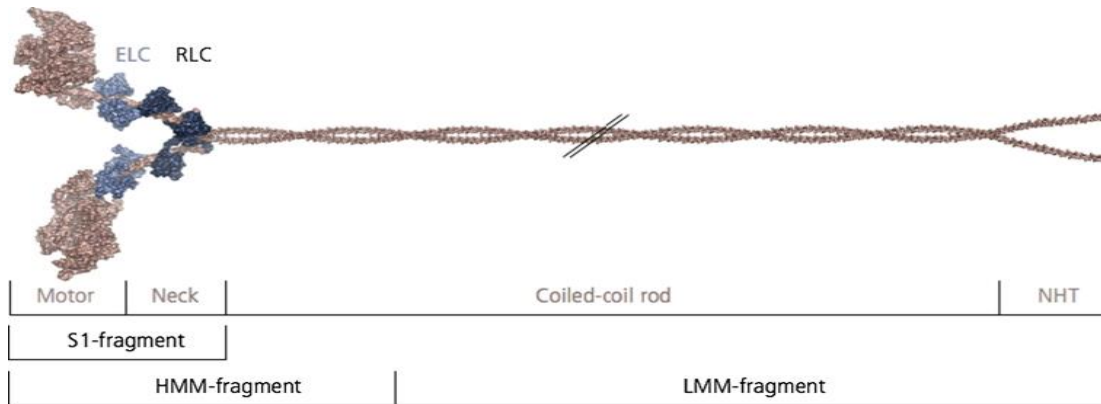


**Figure 1-13: Scheme of a monomer of non-muscle myosin II.**

The myosin molecule consists of a globular head domain followed by an  $\alpha$ -helical coiled-coil rod domain that terminates in a non-helical tail piece. The neck domain consists of two sets of light chains that bind to NMHC. NM II cleaves into three fragments: single-headed subfragment-1 (S1), double-headed heavy meromyosin (HMM) and light meromyosin (LMM) (Heissler and Manstein, 2013a).

NM II isoforms are also expressed in cardiac, smooth and skeletal muscle cells (Heissler and Manstein, 2013b, Dulyaninova et al., 2007). It is obvious that the contractile activity of actomyosin complex is crucial in various muscle tissues, such as the beating of the heart. However, it is also evident that NM II contributes in a variety of cellular processes which require force, such as cell migration, polarity and cytokinesis (Billington et al., 2013a). The globular head of each NM II consist of  $Mg^{2+}$  ATP binding site as well as an actin binding region which allow it to move in antiparallel manner through conformational changes induced by ATP hydrolysis (Vicente-Manzanares et al., 2009); (Sellers, 2000).

#### 1.4.1.1 Non-muscle myosin II isoforms

There are three isoforms of myosin heavy chains; A, B and C (MIIA, MIIB, MIIC) that are encoded by three distinct genes; *Myh9*, *Myh10* and *Myh14*, respectively (Billington et al., 2013a) *Myh9*, *Myh10* are regulated in a tissue-dependent manner and they have been localized on chromosome 22q11.2 for MHC IIA and 17p13 for MHC IIB (Simons et al., 1991). Different cells and tissue expressed at least one or two of all three non-muscle myosin II motor proteins. For instance, myosin IIA and myosin IIB are expressed in endothelial and epithelial cells at similar levels (Betapudi, 2014). The expression of MHC IIA is more abundant in intestinal cells and the spleen, while MHC IIB is highly expressed in the brain and testes (Itoh and Adelstein, 1995). MHC

IIC is expressed abundantly in lung. However, myosin IIA is the only myosin II motor protein which is expressed in the circulating platelets (Betapudi, 2014). These isoforms have been created by the splicing of pre-mRNA by inserting different amino acids near ATP binding site and /or near actin binding site (Itoh and Adelstein, 1995).

Although these isoforms exhibit 60-80% identity at their amino acids, they have specific functions (Dulyaninova and Bresnick, 2013); (Wang et al., 2011). Interestingly, these isoforms are expressed at different levels and they have different roles and intracellular distributions (Billington et al., 2013b). NM IIA was distributed at the periphery of the cells and concentrated at the leading edge, whereas NM IIB was primarily concentrated in the perinuclear area and to a lesser extent in the cell periphery (Cai et al., 2006). NM IIB activates lamellipodia and growth cone extensions, whereas NM IIA drives cell membrane retraction during cell movement. Indeed, the specific functions of NM IIC during cell migration are poorly understood (Betapudi, 2014).

In humans, there are many *Myh9*-related disorders result from *Myh9* mutations, including May-Hegglin anomaly and Fechtner syndrome (Heath et al., 2001). The non-helical sequence of the heavy chain tail is different between the three isoforms. However, there are heterotypical complexes produced between NM II isoforms especially during initial cell spreading (Beach et al., 2014).

#### **1.4.1.2 Regulation of NM IIA assembly**

There are two sets of mechanisms regulating NM IIA filament assembly; phosphorylation of myosin light and heavy chains in parallel with S100A4 protein binding at C-terminal end of myosin IIA heavy chain which is more isoform-specific (Clark et al., 2007).

##### **1.4.1.2.1 Myosin light chain phosphorylation**

Assembly of monomeric myosin into filaments is regulated by reversible phosphorylation of two key residues which were located on the RLC phosphorylation sites; Ser19 and Thr18. This phosphorylation promotes ATPase activity resulting in actin binding and contraction by controlling the conformation of the myosin head (Vicente-Manzanares et al., 2009);(Yuen et al., 2009). It is established that the basis of this regulation depend mainly on the conformation of the myosin molecule, as phosphorylation of RLCs disrupts the head-head and head-tail interactions

and transform folded blocked 10S molecule to an elongated unfolded 6S conformation which forms bipolar filaments (Jung et al., 2011). Several lines of evidence strongly suggest that in the fully dephosphorylated state and in the presence of ATP, the myosin II molecules exist in an assembly-incompetent structure referred to the 10S form based on its sedimentation coefficient. However, phosphorylation of the RLC by myosin light chain kinase (MLCK), Rho-associated coiled-coil kinase (ROCK), results in uniquely polymerised myosin monomeric form into bipolar filaments (Dulyaninova and Bresnick, 2013). It has been shown that blocking of the assembly of myosin into filaments can be promoted using anti-brush border of myosin monoclonal antibodies, such as (BM4) which binds to the tip of the myosin tail *in vitro*, and induces the folded 10S form of myosin, whereas BM1 binding prevents the extended 6S monomer from folding into the 10S state (Citi et al., 1989).

Electron microscopy studies show that the head-tail interaction plays a critical role in regulating the activity of NM IIA molecules through the formation of the compact monomeric state and preventing filament assembly (Jung et al., 2011). Previous electron microscopy research has shown that the interaction of C-terminal parts of myosin non-helical region built up the backbone structure of self-assembled smooth muscle myosin (Cross et al., 1991). *In vitro*, smooth muscle myosin from chicken gizzard and non-muscle myosin molecules have an equilibrium between bending 10S conformation and an extended 6S conformation which can polymerise into filaments (Kendrick-Jones et al., 1987). These two forms of myosin molecules refer to sedimentation coefficient of each molecule as evaluated by ultracentrifugation and electron microscopy polymerization pathway, which can be analysed as a dynamic monomer-polymer equilibrium (Polymer  $\leftrightarrow$  6 S monomer  $\leftrightarrow$  10 S monomer). Since then, a folded pool has been detected for NM IIA and other myosin isoforms (Sellers and Knight, 2007). It was established that the folded 10S conformation of smooth muscle myosin significantly reduced ATPase activity and effectively trapped ADP and Pi products at the active sites (Cross et al., 1988). These studies revealed that 10S monomer is physiologically related to the inert form of myosin that diminish ATP consumption until assembly of myosin into filaments allowing effective contractile activity over a wide range of cell lengths.

The structure of 10S myosin was analysed using negative stain electron microscopy of individual folded 10S molecules from turkey gizzard smooth muscle. This study revealed a symmetrical interaction between both heads of myosin; the actin-binding region of one head contacts the converter region of the other which involved in actin-binding. Therefore, one head is prevented from actin binding, whereas the other blocks ATPase activity (Burgess et al., 2007). Another study by (Jung et al., 2008) showed a similar finding with NM IIA which indicates similar biochemical and structural properties. In addition, it has been shown that the folding of the tail is induced by the ionic interactions between the positively-charged N-terminal sequence of the RLC and a negatively-charged region near the start of tail segment 3 (Jung et al., 2011). Although previous studies reported evidences confirming the presence of 10S state *in vitro*, there was a direct evidence provided by (Milton et al., 2011) suggesting the presence of the 10S conformation in cells by designing a peptide referring to the lever region of airway smooth muscle myosin that mediates links with segment 3 of the tail. Generally, they used smooth muscle cells that were mildly permeabilized with  $\alpha$ -toxin and incubated cells in 10S promoting buffer (EGTA and MgATP). This leads to filament disassembly, but when cells were incubated in the 10S buffer with peptide, it promoted the stress-fibers formation confirming that the existence of 10S myosin molecules in cells. Figure 1.10 illustrates that the segment 3 of the 10S tail has been displaced to the lever region of the blocked head leading to the formation of contacts with the N-terminal end of the RLC (Jung et al., 2011).

Reversible phosphorylation of RLC is regulated by multiple kinases including MLCK, ROCK, leucine zipper interacting kinase (ZIPK), and myotonic dystrophy kinase-related Cdc42-binding. These kinases are most widely implicated in phosphorylation of RLC at Ser19, Thr18 or both and destabilise 10S conformation (Cho et al., 2011); (Le et al., 2013). There are different signaling pathways controlling these kinases. For example, MLCK was activated by  $\text{Ca}^{2+}$ -calmodulin, whereas the small GTPase RhoA activated ROCK (Katoh et al., 2011). On the other hand, dephosphorylation of RLC was catalyzed by ROCK and myosin phosphatase-targeting subunit 1 (MYPT1) (Matsumura and Hartshorne, 2008).

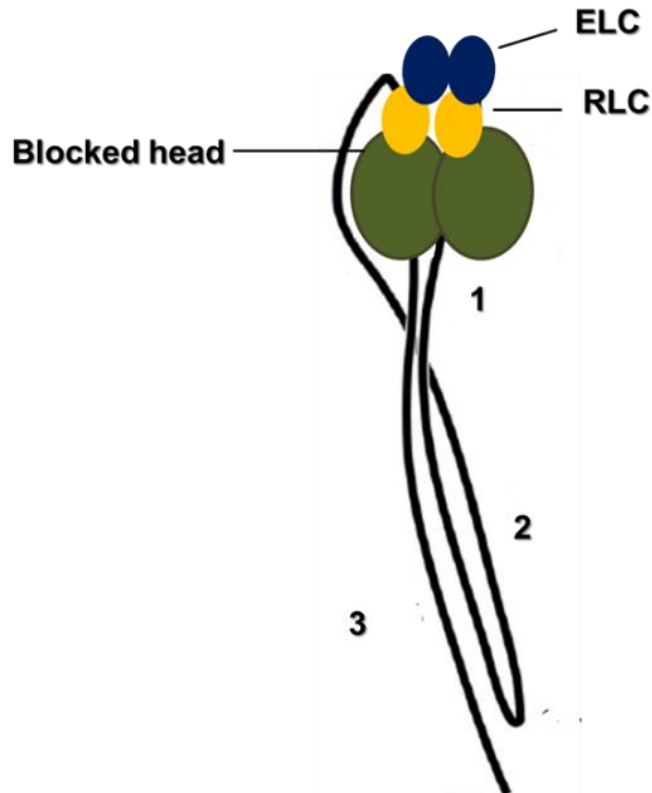


**Figure 1-14: Diagram of the compact 10 S conformation of NM II**

A diagram of 10S myosin molecule. In the rod domain, the three equal length segments are labelled as segment 1, 2 and 3. The two heads interact symmetrically to block the ATPase activity of one and the actin-binding ability of the other. A head-tail interaction also stabilises the structure within the blocked head of 10S and form links with N-terminal domain of the RLC which binds to ELC. Therefore, phosphorylation of either Ser19 or Thr 18 disrupts the 10S conformer. Figure adapted from (Jung et al., 2011).

#### 1.4.1.2.2 Myosin heavy chain phosphorylation

Despite the fact that the heavy chain phosphorylation was detected more than 30 years ago in vertebrates, RLC phosphorylation has been considered the main mechanism for myosin IIA filament assembly *in vivo*. However, heavy chain phosphorylation provides another regulatory mechanism for myosin IIA assembly (Dulyaninova and Bresnick, 2013). The majority of MHC IIA phosphorylation sites are located at the coiled-coil and C-terminal tail regions. There are various kinases that phosphorylate myosin at these sites, including the transient receptor potential

melastatin 7 (TRPM7), protein kinase C (PKC) family and casein kinase 2 (CK2) (Betapudi, 2014); (Dulyaninova et al., 2005). PKC phosphorylates myosin IIA on single site at Ser 1916 near C-terminal end of coiled-coil, myosin IIB on multiple serines in the coiled-coil and tailpiece and myosin IIC on tailpiece only (Dulyaninova et al., 2005). Myosin IIA heavy chain phosphorylation at Ser1916 is intensively enhanced after TGF- $\beta$ -induced EMT in mammary epithelial cells (Beach et al., 2011a). Myosin heavy chain phosphorylation plays a critical role in driving filament assembly in the model organism *Dictyostelium* (Egelhoff et al., 1993). However, regulation of mammalian myosin filament assembly by heavy chain phosphorylation is still not well understood (Beach et al., 2011a). Despite this, (Murakami et al., 1998) reported that Ser 1916/1943 phosphorylation did not have an effect on myosin filament assembly, another study by (Dulyaninova et al., 2005) revealed that myosin heavy chain phosphorylation by PKC and CK2 modulates filaments assembly. Moreover, the biochemical data from (Dulyaninova et al., 2007) research showed that MDA-MB-231 cells expressing NMHC IIA constructs either S1943D or E mutants displayed reduced myosin filamentous level associated with enhanced cell migration. Conversely, cells expressing NMHC IIA S1943A mutant exhibited stable filaments formation and decreased cell motility. In addition to this study, individual mutation or double mutation of S1916 or S1943 to alanine blocks recruitment of GFP-NM IIA filaments to leading edge protrusions and blocks maturation of anterior focal adhesions (Rai et al., 2017). A corresponding study suggested that an increase in the expression of S1943A MHC IIA construct in Hela cells promotes filament assembly (Breckenridge et al., 2009). Based on studies by (Dulyaninova et al., 2007) and Dulyaninova et al., 2005), it was established that CK2 is responsible for MHC IIA phosphorylation at S1943. However, a recent study found that when CK2 activity is reduced, S1943 was phosphorylated indicating other kinases are essential for this phosphorylation (Betapudi et al., 2011).

Additional phosphorylation sites have also been identified at Thr 1800, Ser 1803 and 1808 on the coiled-coil region of NM IIA which is phosphorylated by TRPM6/7 and have been shown to decrease filament assembly *in vitro* and diminish the incorporation of NM IIA into actin *in vivo* (Dulyaninova and Bresnick, 2013). These kinases also phosphorylate myosin IIB and myosin IIC in the tailpiece. In addition, TRPM7 regulates cell polarisation and migration (Clark et al., 2007).

Although the positive and negative charge are characteristic of the NM IIA coiled-coil, tail segments are not able to form filaments. However, a 29 residues sequence near the C-terminus of the tail known as assembly competence domain (ACD) is required for filament assembly (Dulyaninova and Bresnick, 2013). Indeed, the ACD stabilizes the tail–tail interactions by acting as a unique, positively charged interaction surface that can stably contact multiple complementary, negatively charged surfaces in the tail domain, thereby mediating filament assembly (Ricketson et al., 2010). Accordingly, there are many factors that affect ACD either by heavy chain phosphorylation or by protein binding that disturb filament formation (Ronen et al., 2010).

#### **1.4.1.2.3 S100A4-non-muscle myosin IIA interaction regulates filament assembly**

Myosin II was originally identified as a potential interacting binding partner for S100A4 in (Kriajevska et al., 1994) which S100A4 was immunoprecipitated from mouse mammary adenocarcinoma cell line. Binding of both NM IIA and NM IIB to S100A4 has been detected at approximate stoichiometry of 3 moles of S100A4 per mole of NMHC II in a calcium dependent manner (Kriajevska et al., 1994). However, a recent study of high resolution crystallography reported that one dimer of S100A4 is enough to bind to one NM IIA peptide promoting a significant conformational change upon complex formation and actin release. Although NM IIA and NM IIB have 85% of amino acid identity in the globular head domain and 72% in the coiled-coil region, S100A4 binds to NM IIA with a 9-fold higher affinity than for NM IIB (Li et al., 2003a). Numerous research has demonstrated that the NM IIA binding site of S100A4 dimer is located at the C-terminus region of amino acid residues at A1907 – G1938 where the overlapping end of the helical rod and start of the non-helical tail (Li et al., 2003a, Kriajevska et al., 2000). Regarding the functional effect and mechanical details of S100A4 binding, it was shown that S100A4 binding promotes myosin filaments disassembly by promoting monomeric form of activated myosin (Badyal et al., 2011). However, (Li et al., 2003a) concluded that the binding site in a shorter peptide located in 1909 – 1924 residues and (Malashkevich et al., 2010) represented a binding site in a peptide composed of residues A1907-R1923. Biochemical and cellular studies have established that NM IIA assembly is regulated via RLC and MHC phosphorylation and binding of NM IIA to S100A4 provides a mechanism for modulating the assembly of myosin filaments (Betapudi, 2014).

The start of the S100A4 binding site is proximal to the ACD mediating filament disassembly which enhances potential metastasis of cancer cells (Kiss et al., 2012). Studies have been revealed that metastasis associated cellular migration is coupled to S100A4-NM IIA interaction (Li et al., 2003). Thus, mutation of the C-EF hand of S100A4 by deletion of the last 15 amino acids abolished the interaction with NM IIA which was associated with reduced metastasis induction by decreasing migration and invasion of cancer cells (Zhang et al., 2005). Likewise, further work later showed that the mutation of the two C-terminal lysine residues of S100A4 leads to decrease the interaction with NM IIA to levels observed for the truncated protein. Moreover, the rates of migration of the AA mutant-containing cells were significantly reduced compared with wild-type S100A4 using mammary carcinoma cell line; Rama37 (Ismail et al., 2008). However, these biochemical investigations did not characterise how these mutations affected the dimerization of S100A4 and that could indirectly affect its binding with NM IIA.

Although myosin heavy chain phosphorylation contributes in regulating filament assembly, the effect of S100A4 binding on heavy chain phosphorylation and whether S100A4 itself is affected by phosphorylation requires further investigation. *In vitro* studies revealed that the interaction of S100A4 with myosin is presumed to attenuate MHC IIA phosphorylation at Ser 1917 and Ser 1943 by PKC and CK2, respectively (Kriajevska et al., 1998, Kriajevska et al., 2000). Subsequent study by Dulyaninova and colleagues suggested that CK2 phosphorylation protects against S100A4 mediated inhibition of myosin IIA assembly (Dulyaninova et al., 2005).

Indeed, the binding site on NM IIA overlapped PKC phosphorylation site at Ser 1916 and the phosphorylation on this site does not affect S100A4 binding (Dulyaninova et al., 2007). Figure (1.11) summarized the mechanism of NM IIA filaments assembly/disassembly (Irvine, 2012).

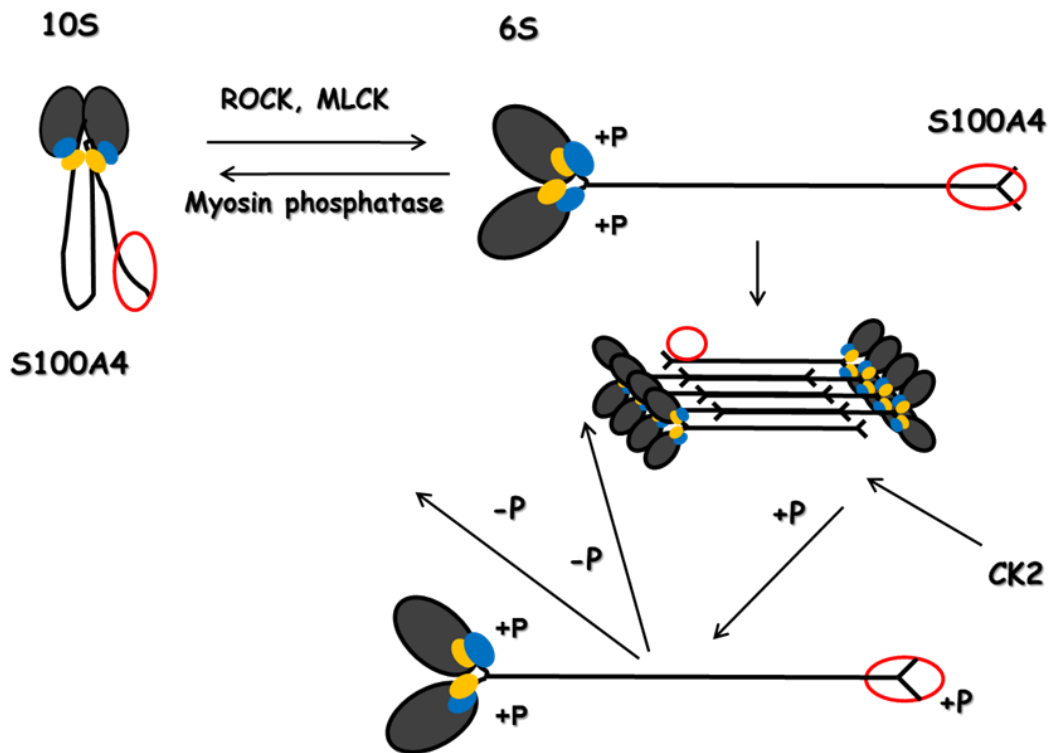


**Figure 1-15: Schematic representative of NM IIA filament assembly regulation.**

Phosphorylation of the RLC at either Ser19 or Thr 18 causes unfolding of the myosin molecule into extended 6S conformation. Phosphorylated 6S form of NM IIA promotes bipolar filaments formation which is mediated by the tail domain of myosin IIA molecule. MHC IIA phosphorylation is regulated by PKC and CK2. S100A4 binds to the C-terminus of myosin IIA promoting filament disassembling. Figure is adopted from (Irvine, 2012).

#### 1.4.1.2.4 Non-muscle IIA associated diseases

Mutation and alternative splicing of MYH9 predispose to the onset and progression of many diseases. These are multiple diseases related to MYH9 disorders (MYH9RD) due to autosomal-dominant disorders. MYH9RD is reported in patients carrying mutations in the motor domain (R702C/H and R1165C/L) of myosin IIA that leads to deafness, cataracts, Döhle-like inclusions, nephritis, and thrombocytopenia (Savoia and Pecci, 2015). Ablation of NM IIA induces metastatic squamous cell carcinoma in the skin (Ma and Adelstein, 2014).

Results from mice showed that familial hypertrophic cardiomyopathy mutations associated with dephosphorylation of RLC leading to impairment of heart function due to a decrease of the ventricle contractility (Davis et al., 2001). In addition, mutations in RLC phosphorylation are linked to cancer and familial aortic dissections that may cause sudden death (Betapudi, 2014).

Some pathogens such as HIV-1 selectively decrease NM IIA expression in kidney, thereby inducing renal disease probably to escape clearance through the urine (Hays et al., 2012) which observed in rapidly progressing proteinuria.

## 1.5 Aims and objectives

**Hypothesis:** S100A4 and S100A6 proteins are involved in regulation of myosin dynamics.

### 1. Aim

Characterise S100A4/A6-myosin IIA complexes in established model of EMT; human epidermoid carcinoma A431 cells with a Tet-On inducible expression of ZEB2 (Mejlvang et al., 2007).

#### Objectives

- Characterise the activation of S100A4/A6 during EMT by Western blotting.  
Confirm the formation of S100A4/A6 complexes with myosin IIA by co-immunoprecipitation.
- Analyse the co-localisation of S100A4/A6 and myosin IIA in cells using confocal and transmission electron microscopy.
- Assess the effect of S100A4 on the formation of folded 10S form of myosin IIA by negative staining transmission electron microscopy.

### 2. Aim

To analyse the role of S100A4 in regulation the NM IIA dynamics.

#### Objectives

- Use of RNA interference to knockdown S100A4 protein in cells to assess the role of S100A4 in maintaining monomeric fraction and regulating 10S/6S equilibrium.
- Detect the effect of phosphorylation of myosin heavy and light chains on S100A4-myosin IIA interaction in cells.

### **3. Aim**

Characterise S100A6-myosin IIA interaction and identify S100A6 binding site.

#### **Objectives**

- To map S100A6-binding site on myosin heavy chain by blot overlay technique.
- To elucidate the potential effect of S100A4/A6 on ATPase activity of actomyosin IIA complex.
- Study the effect of S100A4/A6 on myosin filament assembly by measuring myosin turbidity in low salt solutions.

## **Chapter 2 : Materials and Methods**

## **2.2 Materials**

## **2.3 Chemicals**

All chemicals were of analytical or molecular biology grade quality and purchased from Sigma-Aldrich, Dorset, UK or Fisher Scientific, Loughborough, UK unless otherwise stated.

### **2.3.1 Cell Culture**

#### **2.3.1.1 Eukaryotic cell line**

A431/ZEB2 cell lines were described previously (Mejlvang et al., 2007). The parental cell line, A431 cell line is a human an epidermoid carcinoma which was originally obtained from the American Type Tissue Culture Collection (ATCC, Rockville, MD., USA). Various A431/ZEB2 cells expressing GFP-NM IIA, mutant clones of heavy and light chains, have been used in this study. The plasmid pEGFP-NMHC-IIA-C3 expresses the full-length corrected human non-muscle myosin heavy chain under the control of a constitutive cytomegalovirus (CMV) promoter, with enhanced GFP (EGFP) fused at the amino terminus of the NMHC-IIA coding region. This plasmid was used to express wild type GFP-NMHC-IIA. Heavy chain phosphodeficient mutant was constructed by replacing Ser1943 in NM IIA with alanine, whereas phosphomimetic mutant was constructed by replacing Ser1943 with aspartic acid or glutamic acid. Light chain phosphodeficient mutant was constructed by unphosphorylatable alanine substitutions, and phosphomimetic mutant was constructed by phosphomimetic aspartic acid substitutions. All cell lines were obtained from lab stocks. A431/ZEB2-GFP-NM IIA heavy chain phosphomimetic mutants were generated in this study by phosphomimetic aspartic acid or glutamic acid substitutions; (table 2.1) shows the details of cell lines.

**Table 2-1: Description of cells and plasmids that used in this study**

<b>Cell line</b>	<b>Description</b>	<b>Reference</b>
<b>A431</b>	Human epidermoid carcinoma of the vulva (epidermis) derived from 85-year old female.	(Giard et al., 1973)
<b>A431/ZEB2-GFP-MHC IIA-WT</b>	Stable clone of A431/ZEB2 cells expressing constitutively active N-terminally tagged-GFP-myosin IIA (human) under the CMV promoter.	(Irvine, 2012)
<b>A431/ZEB2-GFP-MHC IIA-S1943A</b>	pEGP-C1 eukaryotic expression vector. Mutants of A431/ZEB2 cells expressing constitutively active N-terminally tagged-GFP-MHC IIA-S1943A (human) under the CMV promoter.	(Dulyaninova et al., 2007).
<b>A431/ZEB2-GFP-MHC IIA-S1943E</b>	pEGP-C1 eukaryotic expression vector. Mutants of A431/ZEB2 cells expressing constitutively active N-terminally tagged-GFP-MHC IIA-S1943E (human) under the CMV promoter.	Generated during this study
<b>A431/ZEB2-GFP-MHC IIA-S1943D</b>	pEGP-C1 eukaryotic expression vector. Mutants of A431/ZEB2 cells expressing constitutively active N-terminally tagged-GFP-MHC IIA-S1943E (human) under the CMV promoter.	Generated during this study
<b>A431/ZEB2-GFP-RLC IIA-T18A/S19A</b>	pEGP-C3 eukaryotic expression vector. Mutants of A431/ZEB2 cells expressing constitutively active N-terminally tagged-GFP-RLC T18A/S19A (human) under the CMV promoter.	(Beach et al., 2011b)
<b>A431/ZEB2-GFP-RLC IIA-T18D/S19D</b>	pEGP-C3 eukaryotic expression vector. Mutants of A431/ZEB2 cells expressing constitutively active N-terminally tagged-GFP-RLC T18D/S19D (human) under the CMV promoter.	(Beach et al., 2011b)

### 2.3.1.2 Cell Culture Reagents and supplements

Dulbecco's Modified Eagle's Media (DMEM) with high glucose (4.5g/l), heat-inactivated Fetal Bovine Serum Gold (FBS) were obtained from Sera lab, UK. 100X-Pencillin/Streptomycin (100µg/ml) and 10X-Trypsin/EDTA were purchased from PAA, Laboratories, Inc., UK. Nu-Serum™ was obtained from BD Bioscience, UK. Doxycycline (Dox) and Dimethyl sulfoxide (DMSO) were bought from Sigma-Aldrich, Dorset, UK. Y27632 was purchased from Calbiochem, UK. Phosphate Buffered Saline (PBS) tablets was obtained from Oxoid Ltd, UK. Plastic tissue culture flasks include 25 cm<sup>2</sup>, 75 cm<sup>2</sup>, 175 cm<sup>2</sup> tissue culture flasks and 6, 12 and 24-well plates were purchased from Fisher Thermo Scientific, UK. Glass pipettes which include 5,10, and 25 ml also were bought from Fisher Thermo Scientific, UK. 15 and 50 ml centrifuge tubes were

purchased from Scientific Laboratory Supplies, UK. Freezing- cryo-tubes were purchased from Fisher Thermo Scientific, UK. Transfection cuvettes were purchased from Geneflow, UK. Disposable Neubauer hemocytometers (C-CHIPs) were bought from NanoEnTEK Inc. Seoul, South Korea.

### **2.3.1.3 Small-interfering RNA oligonucleotides**

RISC-free™ control and Smartpool ON-target Plus™ siRNAs to S100A4 and S100A6 were purchased from Dharmacon, Epsom, UK.

## **2.3.2 Protein analysis**

### **2.3.2.1 SDS-PAGE**

30% acrylamide/bis-acrylamide and Coomassie stain were bought from BioRad, UK. N,N,N',N'-Tetramethylethylenediamine (TEMED), bromophenol blue,  $\beta$ -mercaptoethanol and Ammonium Persulfate (APS) were purchased from Sigma-Aldrich, Dorset, UK. Pierce bicinchoninic acid (BCA) Protein Assay Kit was purchased from Thermo Scientific. UK. Pre-stained protein ladder and Coomassie stain were bought from Biorad. Blocking, SDS-PAGE running, lysis, transfer buffer was prepared from lab stocks.

### **2.3.2.2 Western Blotting Reagents**

Pierce ECL Western Blotting Substrate kit, CL-XPosure film purchased from Thermo Scientific, UK. Ponceau-S and tween-20 were purchased from Sigma-Aldrich, Dorset, UK. Immobilon-P polyvinylidene fluoride (PVDF) membrane was bought from Millipore, Bedford, MA, USA. Methanol and acetic acid was purchased from Fischer Scientific, UK. Super Signal West Dura Chemiluminescent Substrate for HRP and CL-Exposure Film were bought from Thermo Scientific, UK. Primary antibodies used for Western blotting are described in (table 2.2). Goat anti-mouse HRP and Goat-anti rabbit HRP secondary antibodies were purchased from Dako, Ely, UK.

### **2.3.2.3 Immunoprecipitation Reagents**

IGEPAL-40 (NP-40 substitute), phenylmethanesulfonylfluoride (PMSF),  $\beta$ -glycerophosphate (BGP), sodium fluoride, leupeptin, aprotinin, glycine and sodium orthovanadate were purchased from Sigma-Aldrich, Dorset, UK. Protein G agarose was purchased from Thermo Scientific, UK. Coomassie Protein Quantification kit (Bradford Assay) was purchased from Thermo Scientific, UK. Mouse anti-S100A4 monoclonal antibody was purchased from Prolifa, USA. Mouse Anti-S100A6, Mouse anti S100A4, Rabbit anti-GFP polyclonal antibody was bought from Immuno Kontakt. GFP-Trap <sup>®</sup>A bead was purchased from Chromo Tek. Immunoprecipitation buffer was prepared from lab stocks.

### **2.3.2.4 Protein Purification Reagents**

NaH<sub>2</sub>PO<sub>4</sub>, NaCl, DTT, HEPES, Imidazole, Tris-base, Guanidine Hydrochloride (GuHCl), urea and Luria Broth (LB) were bought from Sigma-Aldrich, Dorset, UK, protease inhibitors-Roche

without EDTA was purchased from Roche Diagnostic GmbH, Germany. Isopropyl  $\beta$ -D-1-thiogalactopyranoside- (IPTG), Nickel ( $\text{Ni}^{2+}$ )-Nitrilotriacetic acid ( $\text{Ni}^{2+}$ -NTA) agarose were bought from Qiagen, UK and DNase 1, RNase free were purchased from Mannheim, Germany.

#### **2.3.2.5 Blot Overlay Reagents**

NP-40, DTT, BSA/ $\text{H}_2\text{O}$ , NaCl, Tris-Cl pH7.5, Gelatin,  $\text{CaCl}_2$  and EGTA were purchased from Sigma-Aldrich, Dorset, UK. Pure S100A4 protein (5mg/ml) from lab stocks and pure S100A6 protein (5mg/ml) prepared in the lab were used for the Blot overlay assay.

#### **2.3.3 Immunofluorescence Materials**

TritonX-100, 4', 6-diamidino-2-phenylindole (DAPI) and Triton X-100 were bought from Sigma-Aldrich, Dorset, UK. Paraformaldehyde, glass slides and filter papers were purchased from VWR, UK. Ibidi mounting medium was obtained from Thermo Scientific, UK. Bovine Serum Albumin (BSA) was purchased from Fisher Thermos, UK.

#### **2.3.4 Immunogold Labelling**

Rabbit antibody against GFP antibody (5 $\mu\text{g}/\text{ml}$ ) was bought from Immunokontakt, whereas Mouse anti-GFP antibody was purchased from Amsbio (1mg/ml). Mouse anti-S100A4 monoclonal antibody (75 $\mu\text{g}/\text{ml}$ ) was purchased from Prolifa, USA. Anti-myosin heavy chain (1936-1950) a.a (1mg/ml) was purchased from (BioLegend), UK. Goat anti-rabbit 30 nm gold and goat anti-mouse 15 nm gold secondary antibodies were purchased from British Bio cell Inc., UK. Staining and blocking buffers were made from lab stocks. BSAT/BPS buffer was made up from lab stocks.

#### **2.3.5 Cloning and DNA analysis**

KOD Hot Smart Master Mix was purchased from Novagen, UK. Miller's LB Broth Base, Lennox L agar and ampicillin were bought from Invitrogen, UK. *Dpn* I was purchased from New England Biolabs, USA. Agarose, 100 bp and 1 kbp DNA ladders were bought from Geneflow, UK. Mini prep DNA isolation kits was supplied from Qiagen, UK. Bam H1-HF and Hind III-HF and 10X NEB 2.1 buffer were purchased from New England Biolabs. NucleoSpin Gel and PCR Clean-up was bought from Macherey-Nagel, Germany. Antarctic Phosphatase and 10X Antarctic Phosphatase reaction buffer were purchased from New England Biolabs. UltraPure Agarose was bought from Invitrogen. T4 DNA ligase and 10X T4 DNA ligase buffer were purchased from Invitrogen, UK.

### 2.3.6 Antibodies

**Table 2-2: Description of primary antibodies used during this study. All antibodies were prepared in 5% milk/TBST**

Antibodies	Immunogen	Species	$\mu\text{g}/\mu\text{l}$	Dilution		Antigen MW (kDa)	Company Country
				Western	IF & EM		
Purified myosin heavy chain IIA. (a.a 1936-1950).	Peptide GKADGAEAKPAE corresponding to the C-terminus of human non-muscle myosin heavy chain isoform A	Polyclonal Rabbit	1.0	1:000		250	BioLegend, UK
Non-muscle myosin heavy chain IIA.	Peptide GKADGAEAKPAE corresponding to the C-terminus of human non-muscle myosin heavy chain isoform A	Polyclonal Rabbit	1.0	1:1000	1:1000	250	Covance
$\alpha$ -Tubulin	Raised against a C-terminal section.	Mouse monoclonal IgG1	n/k	1:124000		55	Sigma-Aldrich, UK
GFP	Full length GFP	Polyclonal Rabbit	1.0	1:1000	1:500 (IF) 1:50 (EM)	30	AMB
GFP	Full length GFP	Monoclonal Mouse	1.0	1:1000	1:500 (IF) 1:50 (EM)	30	AMB
S100A6	Full length human S100A6	Monoclonal Mouse	1.5	1:1000		9	Sigma-Aldrich, UK
S100A6	Full length human S100A4	Polyclonal Rabbit	10	1:500	1:50 (EM)		Proteintech, UK

S100A4	Full length human S100A4	Polyclonal Rabbit	10	1:500	1:50 (EM)	10	Proteintech,UK
S100A4	Full length human S100A4	Monoclonal Mouse	10	1:500	1:500 (IF) 1:50 (EM)	10	Prolifia
E-Cadherin	Raised against the cytoplasmic domain of E-cadherin	Monoclonal Mouse	120	1:2000		120	B& D transduction, USA
Vimentin	Purified cow lens vimentin	Monoclonal Mouse	57	1:1000	N/A	57	B&D Pharmingen,
ZEB2	Raised against the N-terminal 380 amino acids of human ZEB2	Mouse	180	1:1000	N/A	180	Home made
HA-probe(Y-11)	Epitope mapping within an internal region of the influenza hemagglutinin (HA) protein, blocking peptide, sc-805 p	Polyclonal Rabbit	n/k	1:5000	N/A	N/A	Santa Cruz, UK
Myosin light chain (Ser19/Thr 18)	Corresponding to residues surrounding Thr18/Ser19 of human myosin light chain 2	Rabbit		1:1000 (BSA)			CST
Di-phospho-myosin light chain (Ser19/Thr18)	corresponding to residues surrounding Thr18/Ser19 of human myosin light chain 2	Rabbit		1:500 (BSA)	N/A	N/A	CST

CST – Cell signalling Technologies, n/k – not known

IF – immunofluorescence – Western blot

**Table 2-3: Description of secondary antibodies used during this study. All antibodies were prepared in 5% milk/TBS or BSA**

<b>Antibodies</b>	<b>Immunogen</b>	<b>Dilution</b>	<b>Country</b>
Anti-Rabbit IgG/HRP	Polyclonal Goat	1:2000 (WB)	Dako Cytomation, Denmark
Anti-Mouse IgG/HRP	Polyclonal Goat	1:2000 (WB)	Dako Cytomation, Denmark
Anti-Goat IgG/HRP	Polyclonal Donkey	1:2000 (WB)	Santa Cruz Biotechnology, Inc, USA
Alexa Fluor® 488 Anti- Rabbit IgG Antibodies	Polyclonal Donkey	1:500 (IF)	Invitrogen
Alexa Fluor® 568 Anti- Mouse IgG Antibodies	Polyclonal Donkey	1:500 (IF)	Invitrogen
Goat anti-Rabbit gold 30 nm	Rabbit	1:100 (EM)	Invitrogen
Goat anti-Mouse 15 nm gold	Mouse	1:100 (EM)	Invitrogen

### 2.3.7 Oligonucleotides

**Table 2-4: Description of oligonucleotide primers used during this study**

<b>Primer</b>	<b>Sequence</b>	<b>Length (nt)</b>	<b>TM (C°)</b>	<b>Notes</b>
<b>MH IIA-3B- stop1 F</b>	GCTTCCAGGAATAAAGCT <u>TAGA</u> AAGCAG AAACGC	<b>33 bp</b>	<b>63.2</b>	Primers set for site-directed mutagenesis of pQE30-3B fragment of myosin IIA heavy chain.
<b>MH IIA-3B- stop1 R</b>	CCGTTTCTGCTTCTAAGCTTTATTCCTG GAAGC	<b>33 bp</b>	<b>63.2</b>	Primers set for site-directed mutagenesis of pQE30-3B fragment of myosin IIA heavy chain.
<b>MH IIA-3B- stop2 F</b>	AAAGGGGACT <u>AG</u> GAGCACAAGCGCAAG	<b>27 bp</b>	<b>62.8</b>	Primers set for site-directed mutagenesis of pQE30-3B fragment of myosin IIA heavy chain.
<b>MH IIA-3B- stop2 R</b>	CTTGCGCTTGTGCTCCTAGTCCCCTTT	<b>27 bp</b>	<b>62.8</b>	Primers set for site-directed mutagenesis of pQE30-3B fragment of myosin IIA heavy chain.
<b>MH IIA-3B- stop3 F</b>	CAGTCCGACAGCT <u>AGT</u> CCAGCAAGCAA GCTC	<b>27 bp</b>	<b>64.3</b>	Primers set for site-directed mutagenesis of pQE30-3B fragment of myosin IIA heavy chain.

Primer	Sequence	Length (nt)	TM (C°)	Notes
<b>MH IIA-3B-stop3 R</b>	GAGCTTGCTGGACTAGCTGTCGGACTG	<b>27 bp</b>	<b>64.3</b>	Primers set for site-directed mutagenesis of pQE30-3B fragment of myosin IIA heavy chain.
<b>MH IIA-3B-stop4 F</b>	CAGCTGGAGGAGT <u>AG</u> GAGGAGGAGGC CAAG	<b>27 bp</b>	<b>64.3</b>	Primers set for site-directed mutagenesis of pQE30-3B fragment of myosin IIA heavy chain.
<b>MH IIA-3B-stop4 R</b>	CTTGGCCTCCTCCTACTCCTCCAGCCTG	<b>27 bp</b>	<b>63</b>	Primers set for site-directed mutagenesis of pQE30-3B fragment of myosin IIA heavy chain.
<b>MH IIA-3B-stop5 F</b>	CTGGAAACTGCTT <u>AG</u> GGAGGAGGTGAA GAGGAAG	<b>30 bp</b>	<b>63</b>	Primers set for site-directed mutagenesis of pQE30-3B fragment of myosin IIA heavy chain.
<b>MH IIA-3B-stop5 R</b>	CTTCCTCTTCACCTCCTAAGCAGTTTCC AG	<b>30 bp</b>	<b>63</b>	Primers set for site-directed mutagenesis of pQE30-3B fragment of myosin IIA heavy chain.
<b>MH IIA-M53-F</b>	GTGT GGATCC TCC AGC AAG CTC ACC AAG GAC TTC	<b>24 bp</b>	<b>64.4</b>	Forward sequencing primer for MH IIA-M53 open reading

				frame (Full-length M53).
<b>MH IIA-M53-R</b>	GTGT AAGCTT CTA CTC CTC CAG CTG CTC CCG	<b>21 bp</b>	<b>65.6</b>	Reverse sequencing primer for MH IIA-M53 open reading frame (Full-length M53).
<b>S100A6.ORF-F</b>	ATGGCAAAAATCTCCAGCCCTAC	<b>23 bp</b>	<b>60.5</b>	Forward sequencing primer for S100A6 open reading frame (Full-length S100A6).
<b>S100A6.ORF-R</b>	GGTCCGCTTCTGGGAAGG	<b>18 bp</b>	<b>60.5</b>	Reverse sequencing primer for S100A6 open reading frame (Full-length S100A6).

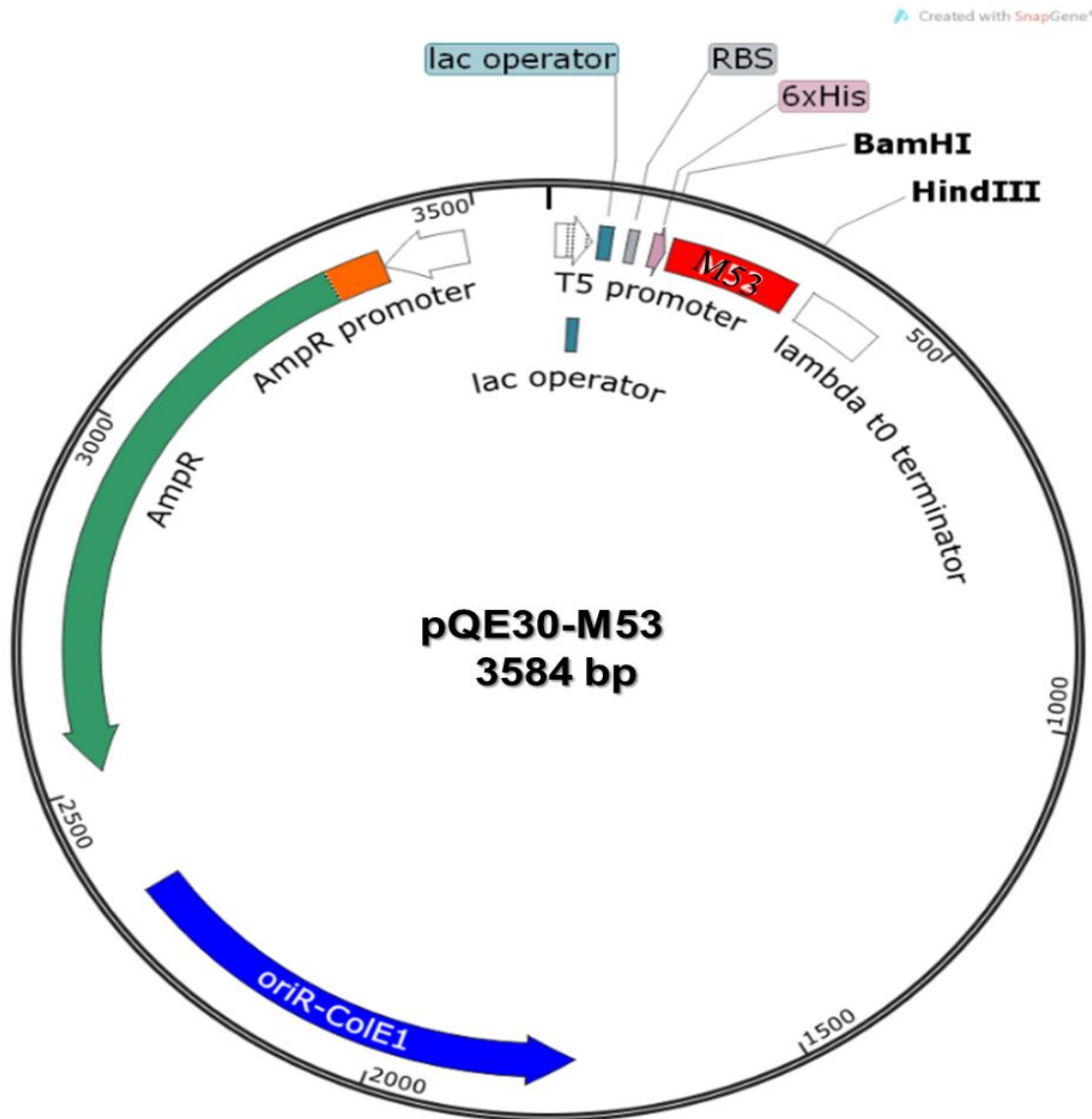
### 2.3.8 Constructs

**Table 2-5: Description of plasmids used during this work**

<b>Plasmid</b>	<b>Vector</b>	<b>Insert</b>	<b>Notes</b>	<b>Sources</b>
<b>pQE30-S100A6 WT</b>	pQE30; prokaryotic expression vector	Full length human S100A6	S100A6 cloned between Bam HI and Hind III. Downstream of tetracycline response element (TRE) and CMV promoter lacking enhancers ( $P_{min}CMV$ ). Gene is only transcribed in the presence of rtTA and Doxycycline.	Dr M. Kriajevska (CSMM, University of Leicester)
<b>pQE30 M53-myosin IIA</b>	pQE30 prokaryotic expression vector	Coiled-coil region of non-muscle myosin IIA	M53-cloned between Bam HI and Hind III. Downstream of T5 promoter and <i>lac</i> operator. Transcription only in the presence of lactose analogs such as IPTG and T5 RNA promoter.	Dr M. Kriajevska (CSMM, University of Leicester)

### 2.3.9 Plasmid map of M53/S100A6 for PQE30 cloning vector.

Map of the pQE30-M53/S100A6 cloning vector, the M53/S100A6 cloning site for insertion of the PCR product occurs within the multiple cloning site (MCS). Selection of successfully transformed M15-*E.coli* cells occurs via the ampicillin (Amp) resistance gene (Figure 2.1). Plasmid map produced using Snap Gene Viewer 283 and APE version 2.0.45.



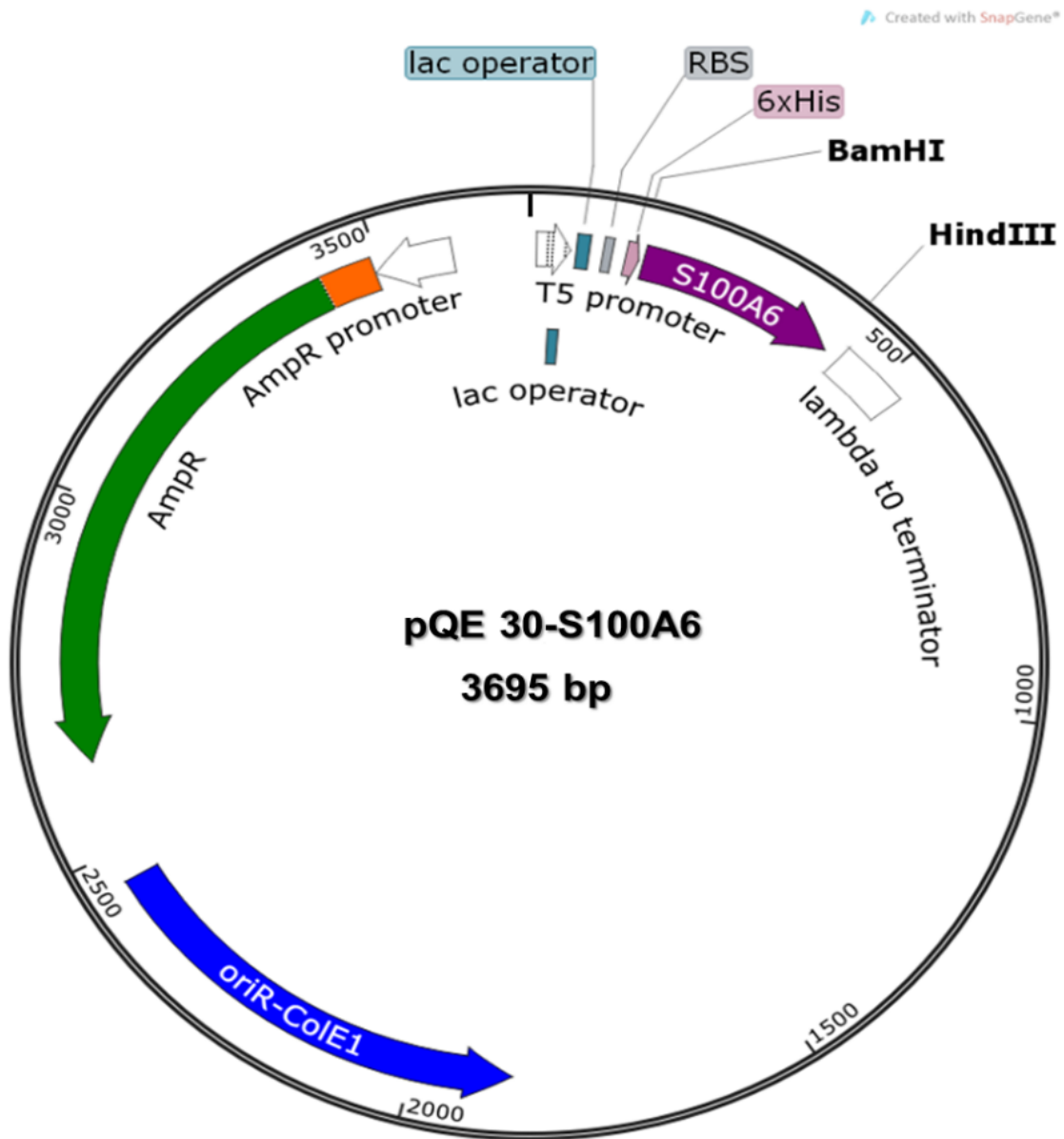


Figure 2-1: Plasmid map of S100A6 and M53 proteins

### 2.3.10 Equipments

**Table 2-6: General equipments used during this study**

<b>Equipment</b>	<b>Company</b>	<b>Catalogue number</b>
AGFA Curix 60 film developer	AGFA Healthcare, UK	
Amaxa® Nucleofector® electroporation device	Lonza, UK	
BDFACS Aria II	BD Biosciences	
BDFACS Canto II	BD Biosciences	
Centrifuge 5415R machine	Eppendorf, UK	
CL-XPosure film	Thermo Scientific, UK	34089
Cover Glass 22 x 22 mm	VWR International, UK	831-0124
Electroporation Cuvettes 2mm	GeneFlow, UK	E6-0060
Electroporation Cuvettes 4mm	GeneFlow, UK	E6-0060
ELx808iu Ultra Microplate Reader	Bio-Tek Instruments Inc, USA	
Filter paper	Amersham Bioscience, UK	SE1141
Flat-bed Electrophoresis tank 30 x 25 cm	Flowgen Instruments, Lichfield, UK	
G:BOX gel doc	Syngene	
GeneAmp PCR system 2400	Perkin Elmer, USA	
Heraeus HeraCell CO <sub>2</sub> (carbon dioxide) incubator		
Immobilon-P polyvinylidene difluoride (PVDF) membrane	Millipore	PVH 00010
Microscope slides, twin frosted 76 mm x 36 mm, 1.00 to 1.2 mm thick	Fischer Scientific, UK)	FB58628
NanoDrop ND-1000 Spectrophotometer	Thermo Scientific, UK	
Pipettes	Gilson	
Protein gel electrophoresis apparatus	BioRad, UK	
Sigma Compact Centrifuge 2-5	SciQuip, UK	
Sorvall® Legend RT Table top refrigerated centrifuge	Harlow Scientific	
StepOnePlus™ Real-Time PCR Systems	Applied Biosystems	
UV transilluminator	UVP BioDox-H System	

### 2.3.11 Buffers and solutions preparations

**Table 2-7: Description of chemicals that used for preparation of buffers.**

<b>Buffers</b>	<b>Chemicals</b>
<b>Blocking buffer</b>	5 gm dried milk powder dissolved in Tris Buffered Saline Tween (TBS-T)
<b>Blot overlay buffer</b>	10% v/v NP-40 (0.5% v/v) final, 2mM DTT, 3% w/v BSA/H <sub>2</sub> O (0.5% v/v) final, 0.1M NaCl, 50 mM Tris-HCl pH 7.5, 0.25% v/v Gelatin, 1mM CaCl <sub>2</sub> , 5mM EGTA, pure S100A4 protein (5mg/ml), pure S100A6 (5 mg/ml).
<b>Blot overlay washing buffer</b>	10% v/v NP-40 (0.5% v/v) final, 2mM DTT, 0.1M NaCl, 50 mM Tris HCl pH 7.5.
<b>1-X gel loading buffer</b>	50 mM Tris-HCl pH 6.8, 2 % v/v SDS, 10 % v/v glycerol.
<b>2-X gel loading buffer</b>	100 mM Tris-HCl, pH 6.8, 4% v/v SDS, 20 % v/v glycerol, 0.018 % v/v bromophenol blue, 2% v/v β-mercaptoethanol.
<b>Destaining buffer</b>	40 % v/v methanol, 50% v/v H <sub>2</sub> O, 10 % v/v acetic acid.
<b>Immunogold labelling-buffer A</b>	1% w/v BSA, 1% w/v normal goat serum, 0.1% v/v Tween-20, 1% w/v Sodium Azide in PBS pH 7.4.
<b>Immunoprecipitation lysis buffer A</b>	0.1% v/v NP-40 (stock 10%; to make a stock add 1ml NP-40 to 9 ml of water; warm up to 60 °C and mix), 0.15M NaCl, 0.5 mM EDTA, 50 mM Tris-HCl pH 8.0. The following inhibitors were then added: 1mM DTT, 50 mM NaF, 0.1mM PMSF-25mg/ml, 0.1 mM Na <sub>3</sub> VO <sub>4</sub> , 10 mM β-glycerophosphate, 2mg/ml aprotinin, 2mg /ml leupeptin.
<b>Immunoprecipitation washing buffer B</b>	0.1% v/v NP-40, 100 mM NaCl, 10 mM Tris-HCl pH 7.0, 0.5 mM EDTA
<b>Immunoprecipitation washing buffer C</b>	10 mM Tris pH 7.0, 100 mM NaCl
<b>Immunoprecipitation elusion buffer.</b>	50 mM Glycine pH 2.7
<b>Immunoprecipitation neutralisation buffer.</b>	1 mM DTT, 100 mM NaCl, 25 mM Tris-HCl pH 7.5
<b>4 % v/v Paraformaldehyde</b>	16 g paraformaldehyde and 4 PBS tablets were added to 400 ml water; warmed up to 60 °C and stored at -20 C°.
<b>Phosphate Buffer Saline (PBS)</b>	One tablet PBS was dissolved in 100 ml distilled water.
<b>Protein loading buffer</b>	0.4% v/v Bromophenol blue mixed with 50% v/v β-mercaptoethanol.

<b>Protein running buffer 10X</b>	30g Tris base, 144g 99% w/v Glycine and 10 g 20% w/v SDS, topped up to 1L with distilled water.
<b>Protein running buffer 1X</b>	100 ml 10-X running buffer, 200 ml methanol, topped up to 1 L with distilled water.
<b>Protein transfer buffer 10X</b>	30g Tris base and 144g 99% w/v Glycine, topped up to 1L with distilled water.
<b>Protein transfer buffer 1X</b>	100 ml 10-X transfer buffer topped up with 900ml distilled water.
<b>Protein purification-buffer A</b>	6 M GuHCl, 0.1 M NaH <sub>2</sub> PO <sub>4</sub> , 0.01 M Tris-HCl, pH 8.0.
<b>Protein purification- buffer B</b>	7 M urea, 0.1 M NaH <sub>2</sub> PO <sub>4</sub> , 0.01 M Tris-HCl, pH 8.0.
<b>Protein purification-buffer C</b>	8 M urea, 0.1 M NaH <sub>2</sub> PO <sub>4</sub> , 0.01 M Tris-HCl, pH 6.3.
<b>Protein purification-buffer D</b>	8 M urea, 0.1 M NaH <sub>2</sub> PO <sub>4</sub> 0.01 M Tris-HCl, pH 7.0
<b>Protein purification-buffer E</b>	8 M urea, 0.1 M NaH <sub>2</sub> PO <sub>4</sub> , 0.01 M Tris-HCl, pH 4.5
<b>Protein purification-buffer F</b>	20 Mm MES,50 mM NaCl , pH 6.1
<b>Protein purification lysis buffer</b>	50 mM NaH <sub>2</sub> PO <sub>4</sub> , 300 mM NaCl, 10 mM imidazole, pH 8.0
<b>Protein purification washing buffer.</b>	50 mM NaH <sub>2</sub> PO <sub>4</sub> , 300 mM NaCl, 20 mM imidazole, pH 8.0
<b>Protein purification-Elution buffer.</b>	50 mM NaH <sub>2</sub> PO <sub>4</sub> , 300 mM NaCl, 250 mM imidazole, pH 8.0.
<b>Protein purification-Dialysis Buffer</b>	20 mM Hepes, 500 mM NaCl, 2 mM DTT, pH 8.0.
<b>Protein purification-Dialysis Buffer</b>	10 mM Hepes, 20 mM NaCl, 2 mM DTT, pH 8.0.
<b>TBS-T</b>	20 mM Tris-HCl, pH 8.0, 150 mM NaCl, 0.1% v/v Tween-20
<b>Trypsin/EDTA TAE (50X)</b>	242g Tris base, 57.1 ml glacial acetic acid, 100 ml 0.5M EDTA pH 8.0, topped up to 1L with distal water and stored at room temperature. TAE buffer was diluted to a 1X working solution prior to use.

## 2.4 Mammalian cell Culture methods

### 2.4.1 Cell culture technique

Cell culture work was carried out in a Class II laminar flow cabinet. To induce EMT, cell lines were cultured in DMEM, 10% v/v FBS and 1% v/v penicillin/streptomycin and maintained in a 37 °C incubator with 5% CO<sub>2</sub> and 100% humidity. Cells were grown in the presence of 2 µg/ml (1.95 µM) Doxycycline (Dox), which was added to the tissue culture media, from a stock solution of 2 mg/ml in water. All cell lines were tested negative for different types of Mycoplasma.

### 2.4.2 Cell passaging and seeding

Cells were regularly seeded at approximately 60-80% confluence. The cells should not be passaged more than twenty times. Cells were washed with PBS (160 mM NaCl, 3 mM KCl, 8 mM Na<sub>2</sub>HPO<sub>4</sub>, 1mM KH<sub>2</sub>PO<sub>4</sub>, pH 7.3) and cells were detached by incubating in trypsin/EDTA (0.5 mg/ml Trypsin, 0.22 mg/ml EDTA in PBS, pH 7.5) for 5-10 minutes (mins). Cells were resuspended in complete worm DMEM medium. Cells were pelleted by centrifuging the sample at 1000 rpm for 5 mins and resuspended in DMEM medium. Cells were seeded in flasks at the required density. Volumes of PBS, TE and media that needed for T25, T75 and T175 cm<sup>2</sup> flasks are detailed in (Table 2.8).

**Table 2-8: Volumes of PBS, TE and DMEM essential for Cells Passaging**

<b>Flask (cm<sup>2</sup>)</b>	<b>PBS (ml)</b>	<b>Trypsin/EDTA (ml)</b>	<b>Complete DEMEM added to neutralise TE (ml)</b>	<b>Total volume of Media (ml)</b>
<b>T25</b>	5	1	5	5
<b>T75</b>	10	2	15	10
<b>T175</b>	15	4	30	25

### **2.4.3 Cell counting**

Harvested cells were re-suspended in complete DMEM medium or serum free medium at concentration of approximately  $0.5\text{-}2 \times 10^6$  cells/ml. After washing cells with PBS, they were detached by adding 1X Trypsin. 10  $\mu\text{l}$  of cell suspension was placed on one chamber of a haemocytometer (depth = 0.1 mm). Average number of calculated cells from 4 sets of 16 corner squares (1 mm<sup>2</sup>/square) was then multiplied by 10,000 to reach a final concentration of cells/ml.

### **2.4.4 Long-term storage of cells**

To store cell lines for long time and using later for lab work, vials of cell lines were stored in liquid nitrogen. Cells were detached by adding 1X Trypsin, pelleted and re-suspended in freezing media (80% v/v complete DMEM, 10% v/v FBS, 10% v/v DMSO) at a concentration of approximately  $2\text{-}5 \times 10^6$ /ml cells and ml aliquoted into individual cryotubes. Cells were frozen in a  $-80$  °C freezer and then placed in liquid nitrogen. For resuscitation, vials were thawed in a  $37$  °C water bath, centrifuged at 1000 rpm and seeded at the appropriate density of DMEM medium.

### **2.4.5 Established integration of plasmid DNA**

Cells passaged 72 hrs prior to transfection were grown to 60-80% confluence. They were then co-transfected with 5  $\mu\text{g}$  of the required plasmid as well as 0.5  $\mu\text{g}$  pIRES-puro2 plasmid. This plasmid has puromycin resistance gene. Cells were seeded in three 96-well plates. 72 hrs-post transfections, the medium was replaced with selective medium (complete DMEM and 0.5  $\mu\text{g}/\text{ml}$  puromycin) and replaced every three days. After approximately 3 weeks, a fluorescence microplate reader (BMG Labtech Ltd., Germany) was used to detect potential positive colonies by screening for GFP fluorescence (excitation: 480; emission: 520) and confirmed using an epifluorescence microscope. Prospective colonies were washed twice with PBS trypsinised, placed on 12-well plates and further amplified in 6 well plates until growing in T25 flasks. Lysates were then collected and analysed for the stable incorporation of the protein of interest.

## **2.5 Transfection with Ingenio® Electroporation solution**

Cells passaged for 72 hrs prior to transfection were grown to 70-90% confluence. Cells were then washed three times with PBS, trypsinised and resuspended with DMEM, centrifuged at 1000 rpm for 5 mins. Pellets were resuspended with 1 ml PBS and top up to 10 ml PBS. Cells were counted using a hemocytometer and the equivalent of  $2.5 \times 10^6$  cells centrifuged at 1000 rpm for 5 mins.  $2.5 \times 10^6$  cells were added to 500  $\mu$ l PBS and centrifuged at 1000 rpm for 5 mins. The pellet was resuspended in 60  $\mu$ l pre-warmed Ingenio® Electroporation solution and 2  $\mu$ l siRNA (of a 100  $\mu$ M stock) or 2  $\mu$ g plasmid DNA added to create a cell suspension. This was transferred to a 4 mm cuvette and transfected using a Nucleofector™ (Lonza, UK) device which was set at 250V and 250 $\mu$ F. The cuvette was then flushed with 1 ml media and cells seeded at the required density and maintained in growth media ready for the required experiment after 48 hrs.

## **2.6 Transient transfection and creation of stable cell lines**

Cells from two T175 flasks at confluence (60-80%) were trypsinised and counted using a haemocytometer.  $2 \times 10^7$  cells were transferred into individual Eppendorf tubes and centrifuged at 10,000 rpm for 5 mins. The supernatant was removed, and the cell pellets were gently resuspended in 60  $\mu$ l of Ingenio® Electroporation solution. 2 $\mu$ g of (pIRESpuro2 and pEGFP-MHC-S1943) DNA plasmids were applied to cells. Cells were then transferred into electroporation cuvettes and electroporation was done as described in section (2.4). Cells were seeded into 96 well plates (100  $\mu$ l of medium containing transfected cells suspension for each well) and maintained at 37 C°. The media were replaced carefully every three days. Massive dead cells were removed leaving colonies of stable cells. After 4 weeks, fluorescence microscopy was used to detect the fluorescence signals in the single colonies. The single colonies were then transferred into 24 well plates. In two or three days, when the confluence of growth reached (80-90) %, the wells were rinsed with PBS and trypsinised with 100  $\mu$ l of trypsin and cells were transferred into a 6-well plate. All clones that show a strong fluorescence signal were propagated and analysed.

## **2.7 Chemical treatment**

### **2.7.1.1 Doxycycline treatment**

A431/ZEB2 cells expressing GFP-myosin IIA wild and mutant clones of heavy and light chains were treated with Dox (2µg/ml) on the day of seeding and left for 72 hours (hrs) before harvesting.

### **2.7.1.2 Cycloheximide treatment**

To detect the half-life and thereby the stability of protein, cycloheximide (CHX) is employed; it is an inhibitor of protein biosynthesis and blocks protein elongation. A stock was made up in absolute ethanol at a concentration of 100 mg/ml of CHX. Cells were seeded at a density of  $75 \times 10^6$  cells added in 35-mm dishes. After 72 hrs incubation, the medium was removed and complete medium with different concentrations of cycloheximide (ranging from 50-300 µg/ml) for at least 8 hrs chase. Subsequently, the optimized concentration 100 µg /ml cycloheximide (dissolved in medium) was added into each dish and harvested at 2,4, 6 and 8 hrs for further protein work. As a negative control, medium with DMSO was added to cells; untreated cells were considered as 0 time. Cell lysates were collected for Western blot analysis. Cyclin D1 was used as control of CHX activity. We then repeated a CHX assay after transfecting cells with siControl and siS100A4 /A6 for 48 hrs. The collected lysates were resolved on the SDS-PAGE. Membranes were then probed with anti-S100A4, anti-S100A6, anti-MHC IIA, anti-RLC and Anti-cyclin D1. The results from three independent experiments were analysed using image J and prism.

## **2.8 Protein Analysis methods**

### **2.8.1 Preparation of protein lysates.**

After growing cells to 80% confluence in small flasks (T25), the medium was aspirated, and cells were then washed gently once with PBS. Approximately 300 µl of 1X gel loading buffer was added; the lysates were scraped and transferred into a 1.5 ml Eppendorf tube and boiled for 10 mins. The lysates were sonicated for 15 sec to disrupt chromosomal DNA and centrifuged at 1000 rpm for 1 minute to pellet DNA material. Lysates were then stored at -20°C for later use in determination of protein quantification.

### **2.8.2 Protein quantification**

Protein concentration was quantified using Pierce (BCA) protein assay kit according to the manufacturer's protocol (Thermo Scientific). Briefly, 25  $\mu\text{l}$  of 9 known bovine serum albumin (BSA) standards (ranging from 2  $\mu\text{g}/\mu\text{l}$  to 0  $\mu\text{g}/\mu\text{l}$ ) and 5  $\mu\text{l}$  unknown protein sample with 20  $\mu\text{l}$  1 X gel loading buffer were added to 204  $\mu\text{l}$  BCA reagent (50 parts BCA reagent A with 1 part reagent B) in 96 well plates and incubated at 37 °C for 20 mins. Samples were allowed to cool at RT for 10 mins and measured at 562 nm using a BioSpectrophotometer (Sanyo, Japan) blanked against water. The absorbance for the blank (0  $\mu\text{g}/\mu\text{l}$ ) was subtracted from each sample and a straight line fitted to the graph of absorbance versus concentration to determine the unknowns.  $\beta$ -mercaptoethanol and bromophenol blue were added to each lysate to make equilibration to 1  $\mu\text{g}/\mu\text{l}$  and get a final concentration of 1% w/v and 0.006% w/v, respectively. For quantification of immunoprecipitation lysates, a Bradford assay was used. 10  $\mu\text{l}$  of unknown sample and 10  $\mu\text{l}$  of 5 known BSA standards was added to 1 ml Bradford reagent, vortexed and incubated at RT for 10 mins. Samples were measured at 595 nm and protein concentration calculated as described above.

### **2.8.3 Sodium Dodecyl Sulphate-Polyacrylamide Gel Electrophoresis (SDS-PAGE)**

Sodium dodecyl sulphate-polyacrylamide gel electrophoresis (SDS-PAGE) was used to resolve polypeptides and detect the expression of target proteins. The percentage of resolving gels ranged from 6 to 15% depending on the size of the antigen modifying the relative ratio of acrylamide/bis-acrylamide to water accordingly (Table 2.9).

**Table 2-9: Volume (ml) of components required to prepare 10 ml of resolving gel with different concentration. This table was adapted from (Maly and Nitsch, 2007).**

<b>Gel (%)</b>	<b>Water</b>	<b>30% acrylamide mix</b>	<b>1.5 M Tris (pH 8.8)</b>	<b>10% Ammonium Persulfate (APS)</b>	<b>TEMED</b>
<b>6</b>	5.3	2	2.5	0.1	0.008
<b>8</b>	4.6	2.7	2.5	0.1	0.006
<b>10</b>	4.0	3.3	2.5	0.1	0.004
<b>12</b>	3.3	4	2.5	0.1	0.004
<b>15</b>	2.3	5	2.5	0.1	0.004

Polymerisation of the resolving gel was initiated by the addition of 0.1% (w/v) ammonium persulphate and 0.1% v/v TEMED. To cast the gel, the final volume of solution was poured into assembled glass plates and 1000 µl of water-saturated butanol was overlaid to prevent evaporation and create a homogenous surface, 10 or 15 well comb placed in the top. The solution was then left to solidify for (10-15) mins. After gel polymerization, the butanol was removed, and the gel was washed twice with water.

A 5% stacking gel (for 5 ml: 3.4 ml water, 0.8 ml acrylamide mix, 1.25 ml 1M Tris-HCl, pH 6.8), 0.01ml 10% w/v SDS, 0.01 ml APS and 0.01 ml N,N,N',N'-Tetramethylethylenediamine (TEMED) was made and added on top of the resolving gel before inserting a 10-well or 15-well comb and leaving to solidify. After polymerization, the gel was placed into a page-running tank, and the comb was removed before filling the tank with 1X running buffer. Meanwhile, a ladder was added to the protein lysates and boiled for 5 mins at 95 °C and loaded on the resolving gel. A known volume of sample (5-20µl) was loaded separately into each well and the gel was run at 120 V for approximately 90 mins (Figure2.2). The bromophenol blue dye front was monitored to check for efficient electrophoresis.

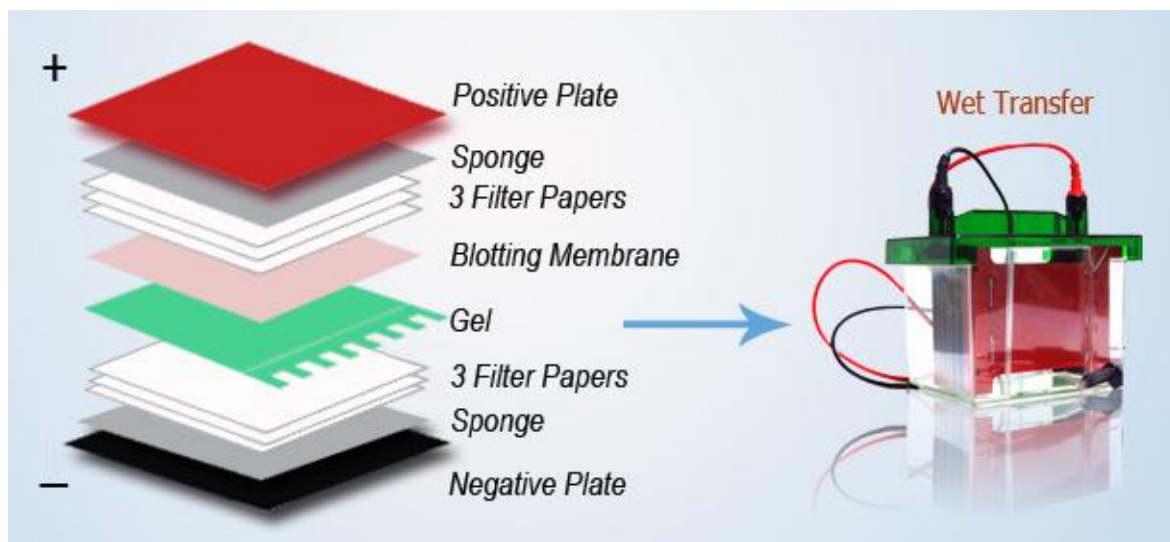


**Figure 2-2: Schematic illustration of Western blot apparatus.**

Illustration of the setup of the sandwich cassette in the transfer tank observed from the top for the Western blotting experiment (<http://www.western-blot.us/western-blot-protocol/wet-western-blot>).

### 2.8.3.1 Coomassie-blue staining

To visualise the resolved protein, the gel was washed with distilled water and stained with Coomassie stain (0.1% w/v Coomassie blue R-250, 40% v/v methanol and 10% v/v acetic acid) with agitation for about 16 hrs. The gel was then destained with destaining buffer (40% v/v methanol and 10% v/v acetic acid) and images were taken using a Canon Power Shot Digital Camera (Canon, UKL td).

### 2.8.3.2 Western Blotting

After completion of the running gel, the proteins were transferred onto a single polyvinylidene fluoride (PVDF) membrane. For this purpose, the gel was rinsed with water and placed onto the PVDF membrane by transfer apparatus. To make a sandwich, 4 pieces of 3 mm filter paper were soaked in 1X-transfer buffer and a piece of 0.2  $\mu\text{m}$  pore PVDF placed on top. The size of the pieces must match that of the gel. The PVDF membrane was put in the centre of the transfer apparatus after activating it in methanol followed by the gel. The membrane and gel were placed among 2 pieces of the filter paper above and 2 pieces below. The transfer cassette was properly orientated within the transfer tank, which was filled with transfer buffer. Protein transfer occurred at 25 volts for 16 hrs. The membrane was then

stained with 0.1% w/v Ponceau S for 5 mins to confirm successful protein transfer and then washed with water to remove the staining. After that, the membrane was rinsed with water three times and once with (TBS-T) to remove the stain. For blocking non-specific sites, the membrane was incubated in a blocking buffer (5% w/v milk TBS-T) for 30 mins at (RT) with shaking. Following the blocking step, Primary antibody at the appropriate concentration in 5 % TBS-T was applied to the membrane and incubated for 1 hour at RT or overnight at 4 °C with agitation (Table 2.2). Membrane was then washed 3 times in TBS-T for 5 mins, this ensured all unbound primary antibody is washed off the membrane. Subsequently, the appropriate horseradish peroxidase conjugated secondary antibody (Table 2.3) was then applied to the membrane and incubated for 30 mins. The membrane wash step was then repeated.

The peroxidase activity of the secondary antibody was then detected using the luminal-based Pierce® enhanced chemiluminescence (ECL) Western Blotting Substrate. Equal volumes of Detection Reagents 1 and 2 were combined and 1 ml incubated on the membrane for 1 min. The light signal produced is exploited by exposing the membrane to CL-X Posure film from Fisher Scientific (PN34089). Film using AGFA curix 60 films developer (AGFA Healthcare, UK) in the dark room for certain periods of time to detect the amount of light emitted or films were scanned with a Canon LIDE 60 scanner. The higher the protein concentration, the more intense light signal and the darker the film was produced. Protein expression levels can be quantified using ImageJ software.

### **2.8.3.3 Immunoprecipitation using Protein G agarose**

Cells were grown in 3 T175 flasks in the presence of Dox for 72 hrs and seeded at a density of  $1 \times 10^7$ . Medium was then removed, and cells were washed with 10 ml pre-chilled PBS. Cells were lifted by applying 4 ml 1X TE to each flask and incubated at 37 C° for 5-10 mins. TE was inactivated with 10 ml of medium containing 10% v/v serum and cells were transferred into 2 (50 ml) falcon tubes. Cell suspensions were spun for 5 mins at 1000 rpm. After aspiration of media, cells were rinsed with 10 ml pre-chilled PBS followed by centrifuging at 1000 rpm for 5 mins. Pellets were re-suspended in appropriate volume of pre-chilled immunoprecipitation (IP) lysis buffer A. Lysates were collected and clarified by centrifugation at 14,000 rpm for 10 mins at 4 C°. Supernatants were taken and added very

carefully to pre-chilled Eppendorf tubes to avoid any contact with the pellet. The sample was then incubated with an antibody (20 $\mu$ g/ml) for one hour at 4°C with shaking and 50  $\mu$ l of the sample was saved for further analysis (Input). 100 $\mu$ l of Protein G agarose beads (50% slurry diluted in IP buffer) was then applied and the sample was incubated overnight at 4°C under constant agitation.

Immune complexes were collected as a pellet by centrifuging of the lysate-antibody-agarose suspension at 10,000 g for 2 mins ensuring not to aspirate any of the pellet. 50 $\mu$ l of the supernatant was saved for further analysis as flow-through (FT) and the rest of solution was removed and discarded. Beads were washed three times with 750  $\mu$ l immunoprecipitation buffer B composed of 150 mM NaCl, 10 mM Tris-HCl, pH7.5, 0.5% v/v NP-40 and 0.5 mM EDTA supplemented with protease and phosphatase inhibitors. After washing the beads 3 times, we either added 50  $\mu$ l of 2 X-gel loading buffer, containing 0.018% v/v bromophenol blue and 2% v/v mercaptoethanol to the immunocomplex, which was boiled and separated on SDS-PAGE, or we eluted the protein from the beads. A protein was separated from the agarose-conjugated antibody by acidification with 50 mM Glycine pH 2.7 which was added and incubated on ice for 30 sec under constant mixing followed by centrifugation at 2,500 g for 2 mins at 4 C°. The supernatant was then transferred to a new tube. The elution step was repeated 4 times. For ATPase assay reaction, the eluted fractions were combined, but before that, each fraction was neutralized with 5  $\mu$ l ATPase buffer. 5  $\mu$ l of 1M Tris pH 8.0 was used for neutralisation of eluted fraction that used later for negative staining experiment. The eluted fractions were mixed and 25  $\mu$ l was saved for analysis. Eluted proteins were resolved on SDS-PAGE using equal volumes, followed by transferring the gels into membranes. The membranes were then probed against specific antibodies.

#### **2.8.3.4 Immunoprecipitation using GFP-Trap<sup>®</sup>-A beads**

The same previous protocol of immunoprecipitation was used as described in section (2.7.3.3), but instead of using anti-GFP antibody. We used GFP Trap<sup>®</sup>-A beads that contain GFP binding protein coupled with a monovalent matrix. 100  $\mu$ l beads slurry was pipetted into each pre-chilled Eppendorf tube. The samples were incubated overnight at 4°C with rotation. The lysates from antibody-beads suspensions were centrifuged at 2,500g for 2 mins, generating a pellet. 50 $\mu$ l from the supernatant was saved for analysis (FT) and the rest was

removed and discarded. Samples were then washed three times. 1st wash was with 750  $\mu$ l buffer A (150 mM NaCl, 0.5% v/v NP-40+inhibitors, 0.5mM EDTA,10 mM Tris pH 7.0); 2nd wash was with buffer B (100 mM NaCl and 0.1% v/v NP-40, 10 mM Tris pH 7.0), and 3rd wash was with buffer C (100 mM NaCl, 10 mM Tris pH 7.0). After addition washing buffer, the sample was centrifuged at 2,500 g for 2 mins. Bound proteins were separated from Trap®-A beads by acidification with 50 mM Glycine pH 2.7 (incubation time: 30 secs under constant mixing) followed by centrifugation at 2,500 g for 2 mins at 4 C°. The supernatant was transferred to a new tube. The elution step was repeated 4 times. 5 $\mu$ l of neutralisation buffer (100 mM NaCl, 1mM DTT, 25 mM Tris pH 7.5) was applied to each fraction. The eluted fractions were mixed and 25  $\mu$ l was saved for analysis.

#### **2.8.4 ATPase assay**

Samples with GFP-tagged myosin were eluted 5 times with 50  $\mu$ l of 50 mM glycine pH 2.7 and neutralized with 5  $\mu$ l 1X ATPase buffer. 60  $\mu$ l of the eluted GFP-tagged myosin solutions -Dox /+Dox were mixed with 10  $\mu$ l 1x ATPase buffer and 15  $\mu$ l of 200 mM actin. 10  $\mu$ l 1X ATPase buffer and 15  $\mu$ l of distilled water were added to another 60  $\mu$ l of the eluted -Dox /+Dox- GFP-tagged myosin. We repeated these steps by using glycine as a control instead of a sample (GFP-tagged myosin). The Mixture of actin and myosin IIA was incubated in a final volume of 95  $\mu$ l of ATPase buffer and kept on ice. The ATPase reaction was started by adding of 5  $\mu$ l of 100 mM ATP at timed intervals and the mixtures were incubated at 37 C° for 12 mins. The reaction was then stopped by adding 10% v/v of Trichloroacetic acid to give a final volume of 600  $\mu$ l. Precipitated protein was sedimented by centrifuging at 13,000 rpm for 5 mins. 500  $\mu$ l of the supernatant was taken and placed in a test tube. 1 ml of 1% ammonium molybdate in 0.5 M H<sub>2</sub>SO<sub>4</sub> was added into each tube and vortexed, then 0.5 ml of freshly prepared 10 g FeSO<sub>4</sub> dissolved in 25 ml 0.5 M H<sub>2</sub>SO<sub>4</sub> was added and vortexed. The solution was left for 5 mins to give time for the blue colour to develop. The concentration of inorganic phosphate was determined by measuring the absorbance at OD<sub>700</sub> nm using spectrophotometer.

10  $\mu$ l 10X ATPase buffer and 15  $\mu$ l distilled water were added to another 60  $\mu$ l of the eluted -Dox /+Dox-GFP-tagged myosin with 2mg/ml S100A4/A6 or without. We repeated these

steps by using glycine as a control instead of the sample (GFP-tagged myosin). The tubes were kept on ice. The same steps that mentioned above were repeated.

## **2.8.5 Immunocytochemistry**

### **2.8.5.1 Immunofluorescence**

To make fluorescent staining of protein antigens, secondary antibodies conjugated with fluorophores were used. These antigens were already bound to antigen-specific primary antibodies. Cells were cultured on ibidi dishes for 48 hrs. Cells were washed with PBS were fixed with paraformaldehyde (4% v/v PFA in PBS) for 15 mins, rinsed a further three times with PBS to remove excess PFA and permeabilized with 0.5% v/v triton X-100 (0.5% triton X-100 in PBS) for 5 mins, followed by PBS washing to remove excess detergent. Cells were incubated for 45 mins at RT with primary antibody diluted in 1X-staining buffer (complete DMEM) before additional washes. Cells were then incubated with 2 µg/ml fluorescent-conjugated secondary antibody for 45 mins at RT, washed three times and counter-stained using 0.5 µg/ml 4',6-diamidino-2-phenylindole (DAPI) to visualise nuclei. During optimisation, secondary antibody controls were conducted. Dilutions of antibodies were listed in Table (2.2) and (2.3). To mount coverslips, excess solution was drained off and a drop of mountant (Fluoromount-G) placed on the Ibidi dishes. 18 mm round coverslips were then placed cell-side down and pressure gently applied to spread the mountant and remove air bubbles. Cells were observed by using an Inverted Nikon TE2000S epifluorescence microscope (Nikon, Japan) equipped with a mercury Lamp. Plan Apo VC 60X oil 1.4 NA objective was used to image fixed samples. Nikon C1Si confocal laser scanning microscope with the laser light source (405 nm, 488 nm and 561 nm) was used and a CFI Plan Apochromat VC 60x/1.4 oil objective was also used to image fixed slices. Images were acquired using a EZ-C1 software (Nikon). No significant signal was detected above background for each secondary antibody within the different fluorescence channels.

### **2.8.5.2 Negative-staining electron microscopy**

3 µl of the sample\* (sample is described below) was empirically determined and applied on a hydrophilic (freshly glow discharged) gold-coated forever film grid using a Quorum Q150 TES coating unit. This was left for 3 mins to give time for the sample to adsorb. The grid was blotted with filter paper to remove excess solution. Immediately, the grid was rinsed

twice with (25 mM Tris buffer pH 7.5) and blotted. Following that, 2 drops of 1% uranyl acetate stain was then directly applied to the grid, blotted again to remove excess solution, and finally dried before imaging. Micrographs were recorded on a JEOL JEM-1400 transmission electron microscope at an accelerating voltage of 80Kv and working on the magnification of X100.000.

\*Samples; Myosin buffer (100 mM NaCl, 1 mM DTT, 25 mM Tris pH 7.5, 47.9 mM glycine, 47.9 mM Tris), (3.4 $\mu$ M myosin, 0.14 mM DTT, 71.4 mM NaCl, 34 mM glycine, 17.9 mM Tris, pH7.5) or (7.1 $\mu$ m S100A4, 0.14 mM DTT, 71.4 mM NaCl, 34 mM glycine, 35.7 $\mu$ M CaCl<sub>2</sub>, 17.9 mM Tris, pH7.5 ). (3.4  $\mu$ M myosin, 0.14 mM DTT, 71.4 mM NaCl, 34 mM glycine, 35.7 $\mu$ M CaCl<sub>2</sub>, 7.1 $\mu$ m S100A4, 17.9 mM Tris, pH7.5).

### **2.8.5.3 Electron microscopy immunogold labelling**

Cells for transmission electron microscopy (TEM) experiments were processed by the electron microscopy Suite, University of Leicester. Cells seeded on 9 mm glass coverslips were rinsed once with PBS and fixed overnight in 4% paraformaldehyde. Following that, they were rinsed twice with PBS and dehydrated in an ethanol series. Once dehydrated, LR white resin was infiltrated into cells and polymerised under a UV lamp at 4 °C for 24 hrs in a nitrogen-atmosphere (oxygen inhibits the polymerisation reaction). Thin sections of resin were then cut using an ultramicrotome and embedded on gold grids over a hexagonal mesh to hold the tissue sections in place. For the immunolabelling experiment, grids were first floated on drops of buffer A (1% w/v BSA, 1% v/v normal goat serum, 0.1 Tween-20, 1% w/v Sodium Azide in PBS, pH 7.4) for 30 mins to block non-specific sites and then they were transferred onto primary antibody (diluted in buffer A) for 2 hrs. Grids were washed 5 times in buffer A and then transferred to 0.5  $\mu$ g/ml goat anti-rabbit gold 30 nm or goat anti-mouse 15 nm gold secondary antibody for one hour before being given one wash in buffer A and 5 washes in ddH<sub>2</sub>O (Figure 2.3). The grids were left to dry for few mins. Control incubations with only secondary antibodies demonstrated a highly specific signal for each primary antibody with essentially no background labelling from secondary antibodies. Floating of grids ensured sections were only stained on one side; seepage that did occur on grids during labelling were discarded. Micrographs were recorded on a JEOL JEM-1400 transmission

electron microscope at an accelerating voltage of 80Kv. Multiple sections of cells were used and more than 300 images per sample were taken from 3 independent experiments.

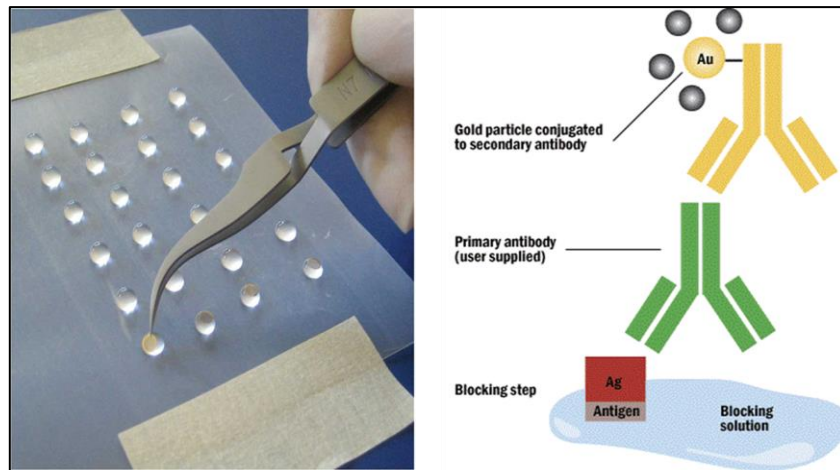


**Figure 2-3: Scheme of immunogold labelling**

Grids were floated on the drop of primary or secondary antibody and antigen was detected via a tagged antigen-specific antibody.

<http://www.nature.com/nprot/journal/v7/n9/full/nprot.2012.096.html>

To analyse the co-localisation of two antigens over a series of distances a modified version of Diggle's G function was used. We analysed the clustering of particles and the second reduced moment K function was evaluated for two types of particles 30 nm and 15 nm. The K function is the number of gold particles at distances shorter than a given distance from a typical particle divided by the average density of these particles. Depending on the size of the gold particles, X,Y co-ordinates for every particle were removed from each image using Image J and the nucleus allocated value of 1 or 2 and counter plugin. In this evaluation of cross K function, the blue points will be the gold particle of one type, while red points will be the gold particles of other type. The complete inter-point distance from each particle in set 1 to set 2 and vice versa of one image was then calculated using trigonometry. However, in order to extract repeated data, the distances were categorized in descending order and the minimum distance was chosen.

This was repeated for each image and all the nearest-neighbour distances clustered and distributed in a histogram from (0-1000) nm with 50 nm bins. The clustering induces an

increase in the density of particles in the neighbourhood of a typical particle. Consequently, the values of K function increase, i.e. The number of gold particles in set A at the distances shorter than a given particle in set B divided by the average density of the particles in set 1. In order to analyse the co-localisation patterns and produce the statistics, particles equal to the density of antigen 1 (gold particle 30 nm) and antigen 2 (gold particle 15 nm) for each image were randomly distributed within the area of one image (Figure 2.4).

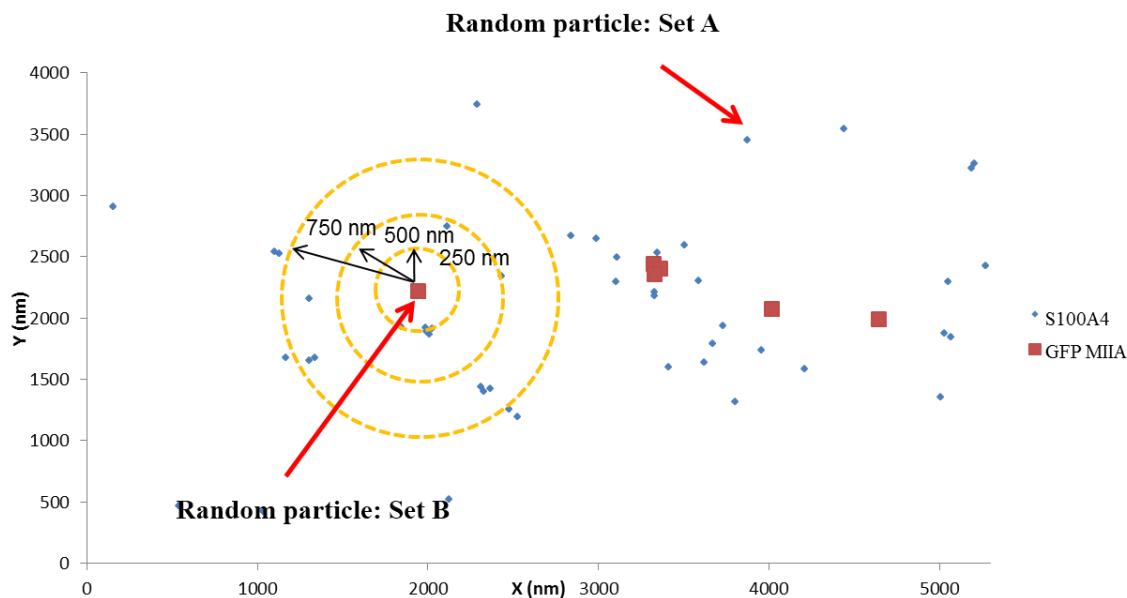


**Figure 2-4: Statistical evaluation of co-localisation of random particles**

K-function values were generated for distributions to assess the statistical significance of random particles data. *K* function which is the number of particles from set A within a certain distance of a particle of set B divided by the average density of set A. *K* function gives a measurement of co-localisation. Method based on (Philimonenko et al., 2000).

For each image, this process was simulated 100 times (Monte Carlo simulations), thus the 99% confidence intervals for complete spatial randomness could be calculated. All analysis was carried out using Microsoft Excel 2013 with a custom macro written in VB script (Irvine, 2012).

## **2.9 Technique of molecular biology**

### **2.9.1 DNA manipulation**

#### **2.9.1.1 Small scale isolation of plasmid DNA**

A plasmid DNA mini-prep isolation kit (Nucleobond, Macherey-Nagel, UK) was used for plasmid DNA purification. More than 20 µg of plasmid DNA can be isolated according to the manufacturer's instructions. Indeed, a single colony was isolated from a freshly-transformed agar plate and grown in 5 ml LB media (10 g/l peptone 140, 5 g/l yeast extract, 5 g/l sodium chloride) overnight. 2.5 ml from the overnight bacterial culture was centrifuged for 10 mins at 8,000 rpm. Supernatant was aspirated, and pellet was resuspended in 250 µl re-suspension solution by pipetting up and down. 250 µl of lysis buffer was added, incubated for 5 min at RT. 350 µl neutralisation buffer was then added and inverted up and down. The lysate was centrifuged for 10 mins at 13,000 rpm to pellet the flocculent. The supernatant was applied to a QIA-DNA-binding column and centrifuged at 13,000 rpm for 1 minute, flow-through was discarded and column washed twice with 70% v/v ethanol. To discard the ethanol, the column was centrifuged more at 13,000 rpm for one minute and flow through was discarded. Plasmid DNA was eluted in 50 µl elution buffer (5 mM Tris-HCl pH 6.8) and concentration determined spectrophotometrically with a NanoDrop (ThermoScientific, UK).

#### **2.9.1.2 Nucleic acid quantification**

Nucleic acid concentration and the total yield were determined using the NanoDrop ND-1000 Spectrophotometer (NanoDrop Technologies, USA). At the beginning, the pedestal and lid were cleaned with optical instrument cleaner. The programme was initialized with ultra-pure water and blanked with the buffer that used to dissolve the nucleic acid. Samples were applied onto the pedestal in 1µl volumes. Samples were measured in duplicate. Furthermore, the A260/A280 ratio was also measured and samples deemed pure if exceeding a value of 1.8.

#### **2.9.1.3 DNA gel electrophoresis**

To analyse plasmid DNA and DNA fragments, Tris-Acetate-EDTA (TAE) or Tris-Borate-EDTA (TBE) gel electrophoresis was used, depending on the size of analysed DNA. 100 ml 1X-TAE buffer (4.8 g/l Tris base, 1 mM EDTA, 1% v/v acetic acid) or 100 ml 1X-TBE buffer was mixed with 0.75-2.0 g agarose and boiled in a microwave until the mixture was

fully dissolved. After cooling of the solution with cold water, ethidium bromide was added to a final concentration of 1µg/ml. The solution was then poured into a pre-assembled horizontal gel electrophoresis tank with a 20-well comb and left to set for approximately 15-20 mins. Before filling the tank with TAE buffer or TBE buffer, the gel comb was removed. In the meantime, 5 X-loading buffer (50% v/v glycerol, 100 mM EDTA, 0.1% v/v bromophenol blue) was added to the suitable concentration of DNA making a total volume of 12 µl with TAE buffer or TBE buffer. Samples were then loaded into wells, together with a DNA marker and Electrophoresis carried out at 90 V for 30 mins. Gels were then visualised using a UV transilluminator (UVP BioDoc-H System, USA) and images captured using a Sony CCD Chip camera (Sony UK Ltd., UK).

#### **2.9.1.4 Site-directed mutagenesis**

Mutation of plasmid DNA was carried out according to the method described by the QuikChange® Site-Directed Mutagenesis kit (Stratagene, USA). Firstly, a Polymerase Chain Reaction (PCR) was performed to amplify template DNA using mutagenic oligonucleotide primers. Both primers contained the desired mutation and anneal to the same sequence on the opposite strands of plasmid. Primers were designed to be between 25 and 45 bases in length with a melting temperature ( $T_m$ ) of  $\geq 78$  °C, using the following equation to estimate the  $T_m$ .

$$T_m = 81.5 + 0.41(\%GC) 675/N - \% \text{ mismatch}$$

- N is the primer length in bases
- Values of % GC
- % mismatch is the number of base pairs required for mutation as a percentage of N.

For PCR, 100 ng template DNA, 1.5  $\mu$ l (10 $\mu$ M) of oligonucleotide forward and reverse primer, 25  $\mu$ l 2X KOD Hot Start Master Mix DNA polymerase (Novagen) was added to PCR tube and top up to a total volume of 50  $\mu$ l with DNase-free water and briefly centrifuged. The PCR reaction (GeneAmp) PCR system 2400 (Perkin Elmer, USA) was carried out as described in (Table 2.10).

**Table 2-10: PCR cycles for site-directed mutagenesis**

Step	Temperature (C°)	Time (s)	Cycles
<b>Initial denaturation</b>	<b>95</b>	<b>120</b>	<b>1</b>
<b>Denaturation</b>	<b>95</b>	<b>20</b>	<b>18</b>
<b>Annealing</b>	<b>60</b>	<b>10</b>	
<b>Extension</b>	<b>68</b>	<b>150</b>	
<b>Final Extension</b>	<b>68</b>	<b>300</b>	<b>1</b>

After amplification, 5  $\mu$ l of PCR product was analysed by DNA gel electrophoresis to check the presence of amplified DNA at the correct molecular weight. If it is correct, 1  $\mu$ l *Dpn I* (2 units/ $\mu$ l) was added directly to each amplification reaction and incubated at 37 °C for 1 hour to remove hemi-/methylated-DNA. Aliquot of frozen electro-competent. M15-*E.coli* cells were thawed for 15 mins on ice.

*DpnI*-treated DNA was transformed into electro-competent cells according to the manufacturer's protocol cells were thawed on ice for 15 mins and 20  $\mu$ l (per transformation) was transferred to pre-chilled Eppendorf tubes. 1  $\mu$ l of cloned DNA was added and gently mixed with a pipette and incubated on ice for 30 mins. Cells were then transferred to a 1mm cuvette and electroporated was performed using Amaxa nucleofector bacteria programm1. 200  $\mu$ l pre-warmed LB media was added and cells incubated with shaking at 250 rpm for 1 hour at 37 °C. 200  $\mu$ l of cell suspension was plated on a selective LB agar plate (10 g/l peptone 140, 5 g/l yeast extract, 5 g/l sodium chloride, 12 g/l agar plus 100  $\mu$ g/ml ampicillin) and incubated overnight at 37 °C. After that, two colonies were picked off and grown in 5

ml-selective media overnight at 37 °C. Sequence analysis revealed 100% homology to published sequences.

### 2.9.1.5 DNA cloning

Cell based DNA cloning involves separating a specific gene or DNA fragment from a larger chromosome using restriction enzymes. In order to clone a gene, DNA sequence needs a carrier that can take it into the cell. There are many kinds of vectors are isolated from larger plasmids that occur naturally in bacterial cells. cDNA (M53/S100A6) was amplified in a 50 µL PCR reaction. Indeed, primers were designed to have restriction sites that coincide with restriction ends on vector (pQE 30). The reaction consists of template DNA (0.12 µg/ µl), using 1 µl, and 1.5 µl (10µM) forward and reverse primers. 25 µl 2X KOD Hot Start Master Mix (Novagen) (0.04U/µl) and 21 µl of ultra-pure water were used in the PCR reaction. Samples were mixed thoroughly and incubated for 5mins at RT. The used PCR programme is described in (Table 2.11). Amplified fragment was purified using spin columns NucleoSpin Gel and PCR Clean-up (Macherey-Nagel). 5 µl of the PCR product was visualised on 1.5% TBE agarose gel and the remaining product was used for the digestion reaction.

**Table 2-11: PCR cycles for cloning**

Step	Temperature (C°)	Time (s)	Cycles
<b>Initial denaturation</b>	<b>95</b>	<b>120</b>	<b>1</b>
<b>Denaturation</b>	<b>95</b>	<b>20</b>	<b>25</b>
<b>Annealing</b>	<b>62</b>	<b>10</b>	
<b>Extension</b>	<b>70</b>	<b>150</b>	
<b>Final Extension</b>	<b>70</b>	<b>300</b>	<b>1</b>

DNA was cloned into a selected expression plasmid vector after double digestion using the appropriate restriction enzymes (Table2.12). The reaction was incubated at 37 °C for 2 hrs.

**Table 2-12: Digestion of the DNA and the plasmid vector with the restriction enzymes**

	DNA (M53/S100A6)	Plasmid vector (PQE30)
	20 $\mu$ l	2.5 $\mu$ l
<b>Bam HI-HF</b>	1 $\mu$ l	1 $\mu$ l
<b>Hind III-HF</b>	1 $\mu$ l	1 $\mu$ l
<b>Cut smart buffer 10X</b>	5 $\mu$ l	5 $\mu$ l
<b>B720 10X</b>		
<b>Ultra-pure water</b>	3 $\mu$ l	5.5 $\mu$ l

Next, 2.5  $\mu$ l *Dpn* 1 enzyme and 3  $\mu$ l 10X NEB Buffer was applied to the product to remove hemi and methylated DNA. To inactivate the reaction, the sample was heated at 80 °C for 15 mins. To prevent self-ligation of plasmid vector in ligation reaction, the terminal 5'-phosphate groups was removed by using alkaline phosphatase; the terminal 5'-phosphate residues from single-or double stranded DNA or RNA was removed. This dephosphorylation reaction is essential to inhibit the self-ligation of vector molecules. Thus, digested product from the plasmid vector was mixed with 1.5  $\mu$ l Antarctic phosphatase M0289 (NEB), 3  $\mu$ l 10X Antarctic phosphatase reaction buffer (1/10 of restriction digestion) and 10.5  $\mu$ l of ultra-pure water in a final reaction volume of 30  $\mu$ l. The sample was incubated at 37 C° for 1 hour. Following this, the reaction was inactivated by heating the sample at 70 C° for 5 mins.

The digested fragments were purified using spin columns NucleoSpin Gel and PCR Clean-up (Macherey-Nagel). The digested products from DNA fragment and plasmid was visualised on a 1% TBE agarose gel or 1% TAE agarose gels. The purified DNA fragment was cloned into the plasmid vector by ligation of the DNA fragment into the plasmid vector. 20  $\mu$ l ligation reaction consists from 0.5  $\mu$ l insert, 2  $\mu$ l pQE30 vector, 1 $\mu$ l T4 DNA ligase NEB M0202 and 2  $\mu$ l 10X T4 DNA ligase buffer. The sample was topped up to 20  $\mu$ l with ultra-pure water and incubated for 2 hrs at RT. DNA ligase catalyzes the end-to-end joining of the DNA by forming a phosphodiester bond between the 3'hydroxyl and the 5'phosphate

ends of nucleic acid molecules(Sambrook et al., 2001). 5 $\mu$ l of ligation mixture was chemically transformed into electro-competent M15-*E.coli* cells strain using Nucleofection.

M15-*E.coli* cells were thawed on ice for 15 mins and 20  $\mu$ l (per transformation) was transferred to pre-chilled Eppendorf tubes. 5  $\mu$ l of cloned DNA was added and gently mixed with a pipette and incubated on ice for 30 mins. Cells were then transferred to M15-*E.coli* cells as described previously in section (2.8.1.4). Sequence analysis after cloning revealed 100% homology to published sequences.

### **2.9.2 Small-scale protein expression trials**

Recombinant proteins were expressed and purified from M15-*E.coli* cells. The protocol was taken from Qiagen. For small-scale protein trials, bacterial colonies from efficient fresh growth of overnight transformed bacterial culture were picked up and grown overnight in 5 ml LB medium supplemented with 100 mg /ml ampicillin for 3 hrs at 37 °C. The bacterial culture was inoculated into 100 ml LB-ampicillin medium and incubated overnight at 37 °C. The fresh overnight culture was inoculated into 4 L LB-ampicillin medium and incubated at 37 °C until the absorbance had reached a value of  $\sim$ 0.6 at OD<sub>600</sub>. 1ml was taken and centrifuged at 4,000 rpm for 10 mins at 4 °C. 1 mM (Isopropyl-1-thio- $\beta$ -D galactopyranoside) IPTG was added and incubation continued at 37 °C with rotation for 4 hrs in which protein expression was induced. 1ml was taken and centrifuged at 4,000 rpm for 10 mins at 4 °C. The pellets from induced and non-induced protein were resuspended in 50  $\mu$ l BPS buffer and 250  $\mu$ l 2X-gel loading buffer was added. Proteins expression was analysed by SDS-PAGE.

### **2.9.3 Large scale protein expression and purification**

For large-scale grow-ups, a single colony was grown in 5 ml LB media for approximately 8 hrs and used to inoculate 200 ml media and grown for 37 °C with shaking. Eight flasks of 1 liter LB media were then inoculated with 20 ml overnight culture, induced with IPTG at  $\sim$ 0.6 at OD<sub>600</sub> and grown for 48 hrs at 30 °C. Bacteria were harvested by centrifugation at 4000 g for 20 mins and the pellet was frozen at -80 ° C overnight.

#### **2.9.3.1 Protein Purification under Native technique**

The protocol of native isolation was obtained from (Bornhorst and Falke, 2000). Cells were harvested by centrifugation at 4,000 rpm for 15 mins at 4°C, and cell pellets were

resuspended in a minimal volume of lysis buffer (50 mM, NaH<sub>2</sub>PO<sub>4</sub>, 300 mM NaCl, and 10 mM imidazole pH 8.0) supplemented with protease cocktail inhibitor tablet (Roche) without EDTA. All steps in this procedure are carried out at 4°C to minimize protein degradation. The cells were lysed by freezing/thawing and sonicated (6×30 pulses) with 30 sec intervals using sonicated using a MSE Soniprep 150 (MSE, Lower Sydenham, UK) 6 times for 30 sec. After sonication, the lysate was centrifuged at 4,000 rpm for 20 mins, and the cell-free extract was incubated with Ni-NTA resin equilibrated in lysis buffer overnight with rotation. On the next day, a column (Pharmacia, UK) previously packed with Ni<sup>2+</sup> NTA Nickel agarose was then equilibrated with lysis buffer and cell-free extract loaded on the column and attached to a peristaltic pump at a flow rate of 1 ml/minute. The column was washed with 150 ml lysis buffer and at least 500 ml washing buffer (50 mM NaH<sub>2</sub>PO<sub>4</sub>, 300 mM NaCl, and 20 mM imidazole pH 8.0) until the absorbance at 280 nm was minimal, indicating that all non-specific proteins had been washed off. A gradient maker with 100 ml elution buffer (250 mM imidazole in 50 mM NaH<sub>2</sub>PO<sub>4</sub> and 300 mM NaCl pH 8.0) was assembled, connected to the column. This column was used to elute protein and 2 ml fractions collected by a fraction collector (GE Healthcare,UK). Eluted fractions were analysed spectrophotometrically by measuring the absorbance at 280 nm and all fractions that containing eluted protein were assessed by SDS-PAGE. The protein at the correct molecular weight was concentrated using a centrifugal 3000 Dalton molecular weight cut-off filter unit (Millipore, USA) until a volume of approximately 1 ml had been reached. Protein-containing fractions were pooled and dialysed against (20 mM HEPES, 150 mM NaCl, and 1 mM DTT pH 8.0) buffer using column packed with Sephacryl S-75 High Resolution matrix (GE Healthcare, UK) and pre-equilibrated overnight at 4°C. After dialysis, protein fractions were centrifuged to get rid of any precipitation and the fractions were again checked for the presence of protein, frozen in aliquots and stored at -80 C°. The protein was assessed by using Coomassie stain after resolving on SDS-PAGE. In terms of M53 protein, fractions were pooled and dialysed against (20 mM MES, 50 mM NaCl pH 6.1) buffer. On the next day, fractions were again checked for the presence of protein, pooled and concentrated to yield 1 ml of purified protein.

### **2.9.3.2 Protein Purification under Denaturing Conditions**

Bacterial pellets prepared from 8L of IPTG-stimulated culture were thawed and resuspended in 40 ml of Buffer B (7 M urea, 0.1 M NaH<sub>2</sub>PO<sub>4</sub>, 0.01 M Tris-HCl pH 8.0). Cells were

sonicated on ice with 30 sec intervals using an MSE Soniprep 150 sonicator until the solution becomes translucent, indicating that lysis was complete. All next steps were carried out at 4°C to minimize protein degradation. The lysate was centrifuged at 4,000 rpm for 20 mins at 4°C, and then the cell-free extract was incubated with Ni-NTA resin equilibrated in buffer B with rotation overnight at 4°C. The Ni<sup>2+</sup>-NTA Nickel resin was then washed as described above with buffer C (8 M urea, 0.1 M NaH<sub>2</sub>PO<sub>4</sub>, 0.01 M Tris-HCl pH 7.0) until the absorbance at 280 nm was less than 0.1, indicating that all non-specific proteins had been washed off. The cells were either centrifuged for 5 mins at 1000 rpm, and 500 µl 1X Laemmle buffer was added to the lysate and boiled for 5 mins. Cells were then centrifuged for 5 mins at 10,000g or eluted using buffer E (8 M urea, 0.1 M NaH<sub>2</sub>PO<sub>4</sub>, 0.01 M Tris-HCl pH 4.5). Eluted fractions were analysed spectrophotometrically by measuring the absorbance at 280 nm. Protein-containing fractions were then assessed by SDS-PAGE. The protein at the correct molecular weight was concentrated using a centrifugal 3000 Dalton molecular weight cut-off filter unit (Millipore, USA) until a volume of approximately 1 ml had been reached. Protein-containing fractions were pooled and dialysed as described in section (2.8.3.1). After dialysis, the protein solution was centrifuged, and supernatant was frozen in aliquots and stored at -80 °C. The protein expression was assessed, by resolving the lysates on SDS-PAGE, following by Coomassie blue stain. To purify the proteins with a high concentration, we replaced buffer B with buffer A (6 M GuHCl, 0.1 M NaH<sub>2</sub>PO<sub>4</sub>, 0.01 M Tris-HCl pH 8.0). In fact, proteins could be purified under native or denaturing conditions (Figure 2.5).

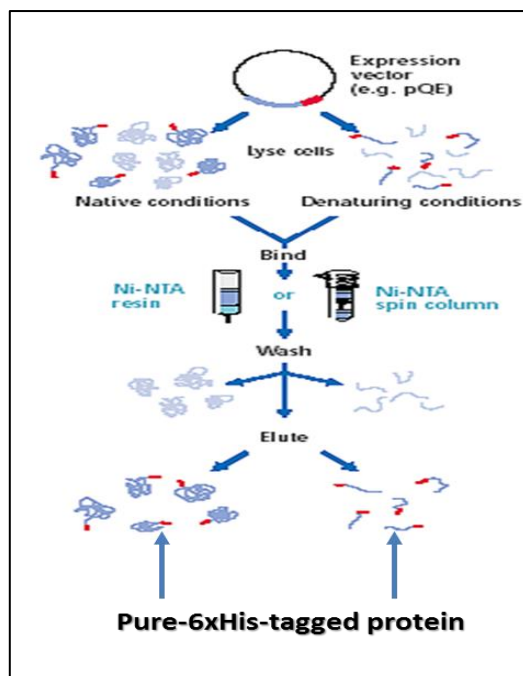


**Figure 2-5: Scheme of protein purification system with Ni-NTA .**

The purification of recombinant his-tagged proteins consists of cell lysis/extraction, binding, washing, and elution. His60 Nickel resin allows one-step protein purification under either native or denaturing conditions. Purified recombinant his-tagged proteins can be eluted with imidazole, or by a reduction in pH.

([http://www.ebiotrade.com/buyf/products/qiagen/qiaexpress\\_protein\\_purification\\_system.htm](http://www.ebiotrade.com/buyf/products/qiagen/qiaexpress_protein_purification_system.htm)).

## 2.10 Blot overlay

Blot overlay is an approach to study potential protein-protein interactions *in vitro*. The recombinant target proteins are resolved by gel electrophoresis and transferred onto appropriate membranes and then incubated in the presence of the protein of interest. A Blot overlay buffer with the following composition was prepared: 0.5% NP-40, 2mM DTT, 0.5% v/v BSA/H<sub>2</sub>O, 100 mM NaCl, 50 mM Tris-Cl pH7.5, 0.25% w/v Gelatin, 1mM CaCl<sub>2</sub> or 5mM EGTA, pure S100A4 protein (5µg/ml) or pure S100A6 protein (5µg/ml).

After transferring the proteins to membranes by Western blotting, they were washed with TBS-T, then immersed in the blot overlay buffer and left overnight at 4°C with shaking. On the next day, the membranes were washed with a washing buffer (0.5% v/v NP-40, 2 mM DTT, 0.1M NaCl, 50 mM Tris HCl pH 7.5) for 5 mins. The washing step was repeated four

times. The membranes were then incubated in a primary antibody anti-S100A4/A6 antibody diluted in milk TBS-T for 1 hour at RT or overnight at 4°C. After three washes with TBS-T, the membranes were incubated for 1 hour in a secondary antibody diluted in milk TBS-T and then washed three times with TBS-T before application of enhanced ECL reagent. On completion, the membranes were placed within a plastic film and then positioned in an autoradiography cassette. X-ray film was placed over the membrane for a variety of exposure times and developed as described in section (2.7.3.2).

## **2.11 Turbidity assay**

The turbidity of the protein was measured at an appropriate absorbance of 300 nm using a spectrophotometer. 10  $\mu$ M of protein (Hmyo 3B) was added to buffer containing 20 mM NaCl, 20 mM HEPES and 0.1 mM  $\text{Ca}^{2+}$ . The turbidity was measured at  $A_{300}$  nm after the incubation for 1200 sec using 10 mm-path length and 0.1 ml microcuvette (105,250-QS; Hellma, Southend-on-Sea, UK). The ionic strength of the solution was measured with frequent addition of 20 mM aliquots of NaCl and the absorbance was measured after each addition to follow the association and dissociation of the protein (myosin IIA). Data was fitted to a sigmoid curve using GraphPad Prism. The turbidity assay shows a midpoint value of approximately 150 mM NaCl. Following that, 10  $\mu$ M of the protein (Hmyo3B/M200) was prepared in buffer containing (150 mM NaCl, 20 mM HEPES and 0.1 mM  $\text{Ca}^{2+}$  pH 7.5). The (Hmyo3B/M200) filament aggregation was detected from increasing the turbidity of the solution. 20  $\mu$ M S100A6/A4 was added every 1200 sec. Data were collected and analysed using GraphPad Prism.

## **2.12 Analysis and statistics**

### **2.12.1 Sequence alignment**

Alignment using Clustal W (<http://www.ebi.ac.uk/Tools/msa/clustalw2/>); shading using BOXSHADE 3.3 (<http://www.mobyle.pasteur.fr/cgi-bin/portal.py/>).

### **2.12.2 Statistics**

A student's T-test was used to compare the mean of two groups. For comparison of more than two groups, a one-way ANOVA was used followed by a Dunnett's Multiple

Comparison test. All statistics was carried out using Graph Pad Prism Version 5. \*  $P < 0.05$ ;  
\*\*  $P < 0.01$ ; \*\*\*  $P < 0.001$ .

**Chapter 3 : S100A4 regulates the equilibrium between 10S and 6S forms of non-muscle myosin IIA**

### 3.2 Introduction

ZEB2 is considered as an important EMT transcription factor because it is one of the major repressors of E-cadherin (Yilmaz and Christofori, 2009). During EMT, significant cytoskeletal rearrangements occur where the role of actin and myosin are important. The actomyosin complex produces contractile forces that allow loss of cell to cell adhesions mediating cell migration (Dulyaninova et al., 2007). NM IIA is a motor protein which propels actin filaments by converting chemical energy into mechanical work (Juanes-García et al., 2016) ; (Kiss et al., 2016). This protein exists as monomers of folded 10S and unfolded extended 6S forms. The latter is capable of assembling into filaments (Kiboku et al., 2013). NM IIA filament assembly is largely controlled through the reversible phosphorylation of myosin regulatory light chain at Ser19 and Thr18 sites (Sakurada et al., 1998) ; (Heissler and Manstein, 2013b). However, the stability of the NM IIA filaments is controlled by phosphorylation of MHC IIA on S1943 by CK2 (Juanes-García et al., 2016) ; (Vicente-Manzanares, 2013, Kriajevska et al., 2000). In addition to NM IIA phosphorylation, it was established that S100A4 binds to the C-terminal end of NM IIA promoting filament disassembly (Ramagopal et al., 2013, Elliott et al., 2012, Badyal et al., 2011, Kriajevska et al., 1994).

Most studies investigating the molecular mechanism of the dynamic 10S-6S transition have been performed *in vitro*, using smooth muscle myosin purified from tissues and reconstituted with RLC mutant (Kiboku et al., 2013). The transition from a 6S to 10S state has been analysed by viscosity, fluorescence and sedimentation velocity measurements (Trybus et al., 1982). However, electron microscopic studies revealed that unphosphorylated myosin forms a folded conformation, referred to the 10S form based on its sedimentation coefficient (Jung et al., 2008). Another study by Milton et al., (2011) provided evidence for the existence of the 10S conformation of myosin *in vivo*. The mechanism of 10S to 6S transition was studied in smooth muscle myosin using an anisotropy decay study (Rosenfeld and Rener, 1994), where they demonstrated that the rotational association time for 10S myosin is approximately 4-fold longer than that for 6S form. This study also revealed a decrease in the nucleotide release rate by converting 6S myosin to the 10S form.

In the present study, human epidermoid carcinoma A431 cells, were used. Doxycycline (Dox) is a tetracycline derivative which controls gene expression via the Tet system. Dox interacts with the rtTA transcription factor, allowing it to bind DNA at the target gene promoter. This model relies on inducible expression of EMT regulators in epithelial tumour cells. Treating cells with Dox leads to rapid expression of ZEB2, thereby inducing EMT (Irvine, 2012); (Mejlvang et al., 2007).

In present chapter, transmission electron microscopy (TEM) in combination with double immunogold labeling technique was employed to analyse the co-localisation between S100A4 and GFP-tagged-NM IIA in cells. In addition, the effect of the phosphorylation of RLC and MHC on the S100A4-myosin IIA interaction in cells have been examined in cells. Thus, cells expressing double mutants of RLC either phosphodeficient or phosphomimetic Ser19 and Thr18 were generated by using phosphodeficient alanine substitutions (T18A\S19A) or phosphomimetic aspartic acid substitutions (T18D\S19D) (Beach et al., 2011b). We also generated a model of cells expressing phosphodeficient (S1943A) or phosphomimetic (S1943D/E) MHC IIA in which serine was replaced with either alanine or aspartic acid/glutamic acid, respectively.

### **3.3 Aims**

1. To analyse the S100A4- NM IIA interaction in cells using confocal and TEM microscopy.
2. To examine the effect of S100A4 on regulating the equilibrium between 10S and 6S conformations of myosin monomers.
3. To investigate the formation of S100A4-myosin IIA complexes *in vitro* using immunoprecipitation assay.
4. To assess the effect of RLC and MHC IIA phosphorylation on 10S-6S transition in cells.

## 3.4 Results

### 3.4.1 Investigation of S100A4-myosin IIA complexes during EMT

To investigate the interaction between S100A4 and myosin IIA *in vitro* and *in vivo*, A431/ZEB2-WT cells were maintained in the absence and presence of Dox for 72 hrs.

#### 3.4.1.1 ZEB2 induces epithelial to mesenchymal transition in A431-WT cells

A431-ZEB2 is a previously established model of EMT in which the squamous epidermoid carcinoma cell line A431 has been engineered to allow doxycycline (Dox) inducible expression of ZEB2. Expression of ZEB2 leads to an EMT phenotype, with morphological alteration, inhibition of epithelial genes and activation of mesenchymal markers (Korpál et al., 2008, Mejlvang et al., 2007).

A morphological change was observed after 72 hrs cultivation of cells in the presence of Dox (Figure 3.1). The highly compact, clustered and rounded cell line was converted by Dox into a scattered, fibroblast-like phenotype, with loss of cell-cell adhesion. The majority of cells had become individual with large lamellipodial protrusions. This phenotype is typical of mesenchymal cells.

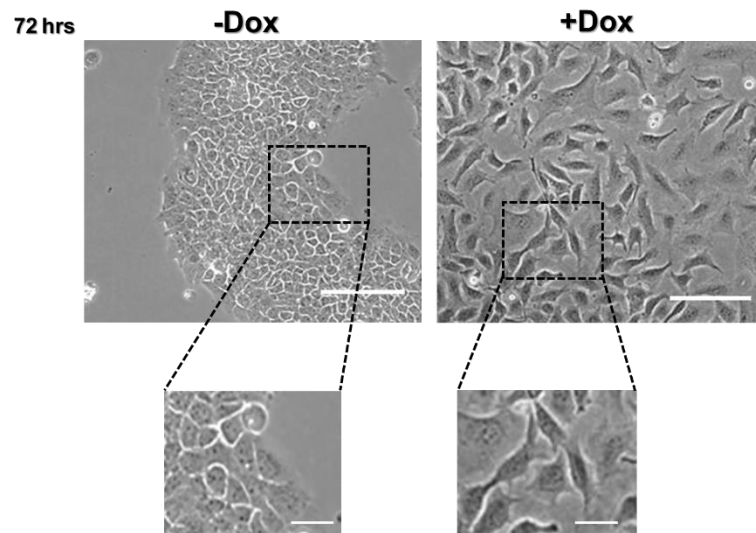


**Figure 3-1: EMT induction in A431/ ZEB2-WT cells**

A431/ZEB2-WT cells were cultured in the absence and presence of Dox for 72 hrs. Cells acquired a mesenchymal phenotype after Dox treatment. Phase-contrast images were taken using a 20x objective. Scale bar = 30µm. Images were magnified to show mesenchymal traits. Scale bar= 10 µm.

### 3.4.1.2 S100A4 expression is activated during ZEB2-induced EMT

Before examining the S100A4-myosin IIA complex in A431/ZEB2-WT cells, expression of S100A4 was analysed after Dox treatment, where EMT was induced by ZEB2 which is an E-cadherin repressor. A431/ZEB2-WT cells expressing GFP tagged myosin were grown in the absence and presence of Dox for 72 hrs. Subsequently, lysates were collected and immunoblotted using antibodies against ZEB2, GFP, MHC IIA, S100A4, E-cadherin, vimentin and  $\alpha$ -tubulin. The level of S100A4 expression was increased significantly after 72 hrs ZEB2 induction, concomitant with up-regulation of other mesenchymal markers, such as vimentin, and down-regulation of the epithelial marker E-cadherin (Figure 3.2), as expected from other *in vitro* studies (Mejlvang et al., 2007, Korpala et al., 2008). The expression of MHC IIA in A431/ZEB2-WT cells was observed as a double band in both treated and untreated cells with Dox. Moreover, expression of GFP was also detected in A431/ZEB2 cells. These results suggest that ZEB2 induces activation of S100A4 during EMT, whilst there was no alteration in MHC IIA expression.

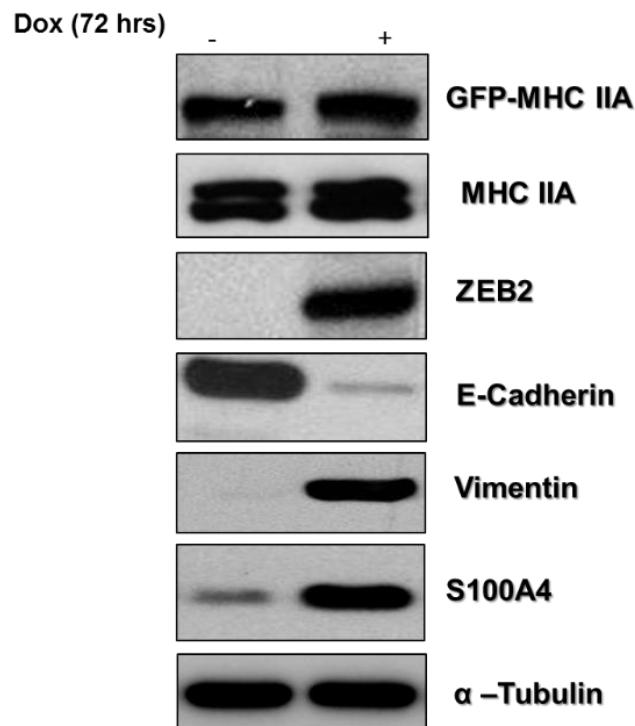


**Figure 3-2: Activation of S100A4 expression during EMT**

A431/ZEB2- WT cells were grown in the absence and presence of Dox for 72 hrs. Lysates were collected and resolved on SDS-PAGE. Membranes were probed with antibodies against GFP, MHC IIA, ZEB2, Vimentin, S100A4, and E-cadherin.  $\alpha$ -Tubulin was used as protein loading control.

### **3.4.1.3 Assessment of S100A4-GFP-myosin IIA interaction by co-immunoprecipitation**

To analyse an interaction of S100A4 with GFP-tagged myosin IIA in A431/ZEB2 cell model, a co-immunoprecipitation assay was carried out. Dox treatment A431/ZEB2-WT cells were lysed in lysis buffer consisting of immunoprecipitation (IP) buffer supplemented with protease and phosphatase inhibitors. S100A4 was immunoprecipitated using S100A4 antibody and then immunoblotted with antibodies against GFP and S100A4. Western blot analysis showed a strong band corresponding to S100A4 and a weak band corresponding to GFP (Figure 3.3-A), indicating that S100A4 is able to interact with GFP-myosin IIA in cell lysates. GFP was also immunoprecipitated from A431/ZEB2-WT cells and immunoblotted with anti-GFP and anti-S100A4 antibodies (Figure 3.3-B). A significant precipitation of GFP from cells was detected, but only a faint band corresponding to S100A4 was observed, indicating that only a part of myosin interacts with S100A4. As a control, HA-probe Y-11 antibody (Epitope mapping within an internal region of the influenza hemagglutinin (HA) protein) was used for immunoprecipitation and cell lysates were immunoblotted for S100A4. There was no significant precipitation of influenza HA protein from cells and there was no bands corresponding to S100A4. The clear bands of input reflect the total protein extracted from the cells after lysis and before immunoprecipitation, whereas non detectable bands in the flow-through indicates that the antibody successfully bound to the beads confirming the levels of efficiency and specificity of the immunoprecipitation assay. This was done to analyse the ability of S100A4 to form complex with myosin IIA in cell lysates.

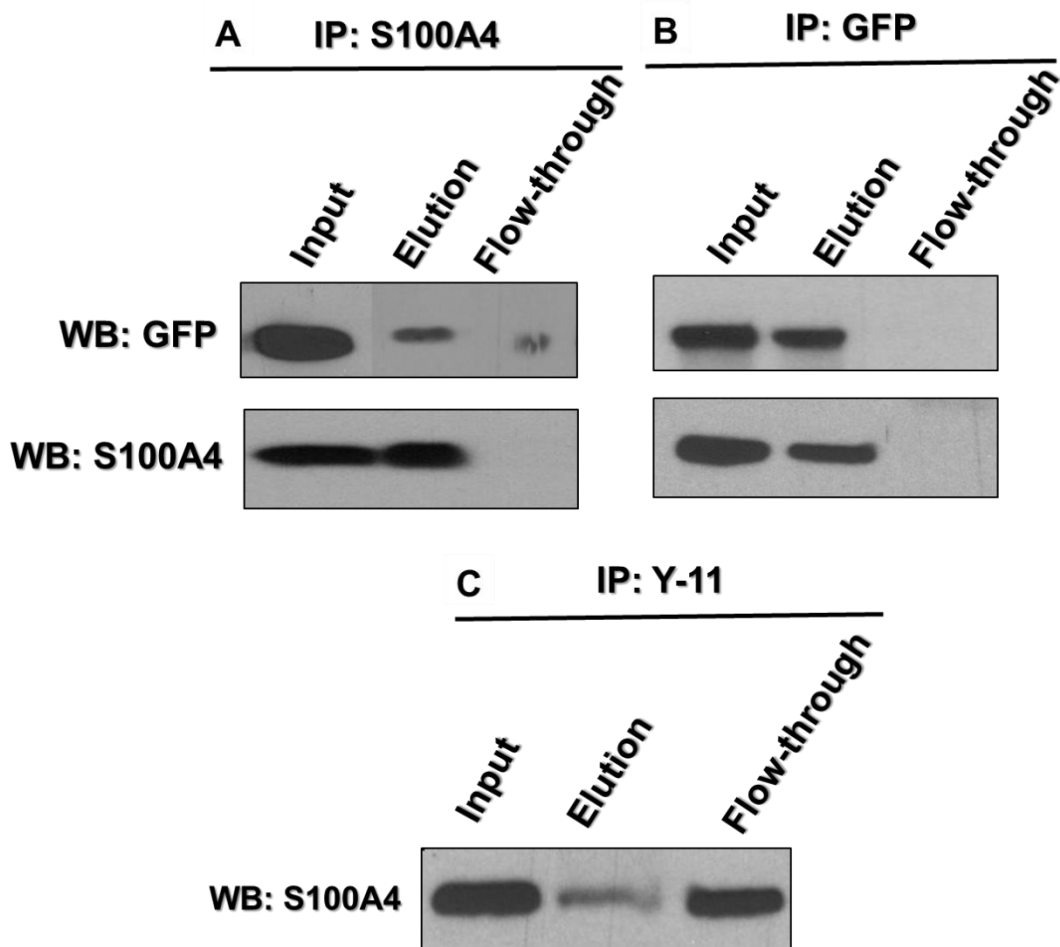


**Figure 3-3: Immunoprecipitation of S100A4 and GFP from A431/ZEB2-WT**

Doxt treated A431/ZEB2-WT cells were lysed in immunoprecipitation (IP) buffer. A-S100A4-protein complexes were immunoprecipitated with a monoclonal mouse anti-S100A4 antibody. B-GFP-protein complexes were also precipitated from these cells by polyclonal rabbit anti-GFP antibody. Lysates were resolved on SDS-PAGE and membranes were stained for S100A4 and GFP. C- Control, HA-probe Y-11 antibody was used for immunoprecipitation and cell lysates were resolved on SDS-PAGE and membranes were stained for S100A4. The total protein extracted from cells was shown in input, while flow-through indicates unbound fraction. Results representative of two separate experiments.

### 3.4.1.4 Characterisation of S100A4-GFP-myosin complexes in cells

#### 3.4.1.4.1 Localisation of S100A4 and myosin IIA in cells as assessed by confocal microscopy

In order to study the localisation of S100A4 and GFP-myosin IIA proteins in cells, immunofluorescence analysis was performed followed by confocal microscopy. Dox treated A431/ZEB2-WT cells were fixed with 4% v/v PFA and permeabilised followed by immunofluorescent staining with antibodies for S100A4 and GFP. GFP-myosin IIA was localised throughout the cytoplasm and partly at the edges of the cell, and S100A4 expression was exhibited in the cytoplasm and nucleus as was reported in other cell lines (Min et al., 2008, Kikuchi et al., 2006). A partial diffuse granular staining of both NM IIA and S100A4 with some enrichment around the cell edges was also observed (Figure 3.4).

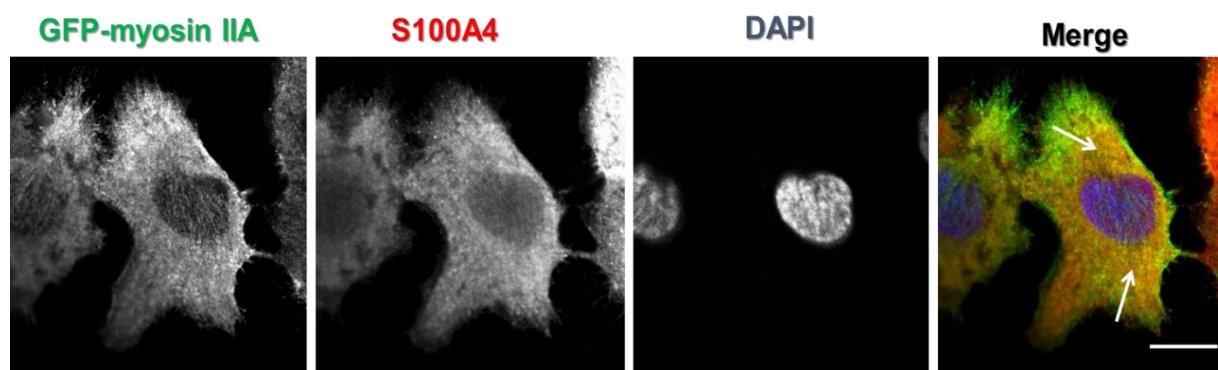


**Figure 3-4: Localisation of S100A4 and GFP-myosin IIA in A431/ ZEB2-WT cells**

Dox treated A431/ZEB2-WT cells were fixed with 4% v/v PFA, permeabilised and fluorescently immunolabelled with anti-GFP (Alexa Fluor 488), anti-S100A4 (Alexa Fluor 598) and DAPI (to visualise nuclei). Cells were analysed using confocal microscopy. White arrows show area of co-localisation. Scale bar = 8  $\mu$ m. Red = S100A4; Green = GFP; Blue = DAPI. Images were collected by Nikon confocal microscope with a C1Si 60x objective.

#### 3.4.1.4.2 S100A4 and GFP- $\alpha$ -Tubulin do not co-localise in A431/ZEB2-WT expressing GFP- $\alpha$ -Tubulin

For further experiments, another cytoskeleton protein  $\alpha$ -Tubulin that has been identified to interact weakly with S100A4 (Chen et al., 2001) was selected. Thus, a stable clone of A431/ZEB2 expressing GFP- $\alpha$ -Tubulin was used. This clone was previously generated in the lab and confirmed the expression of GFP and endogenous  $\alpha$ -tubulin (Irvine, 2012). Confocal analysis was used to assess the localisation of GFP- $\alpha$ -Tubulin and S100A4 in A431/ZEB2-G-Tubulin cells, and localisation of GFP-MHC IIA and S100A4 in A431/ZEB2-G-MHC IIA (Figure 3.5). It was found that GFP- $\alpha$ -Tubulin has a similar localisation to GFP-MHC IIA ; both proteins and S100A4 show partial diffuse granular staining throughout the cell. Therefore, this cell line was used as a negative control for electron microscopy experiments.

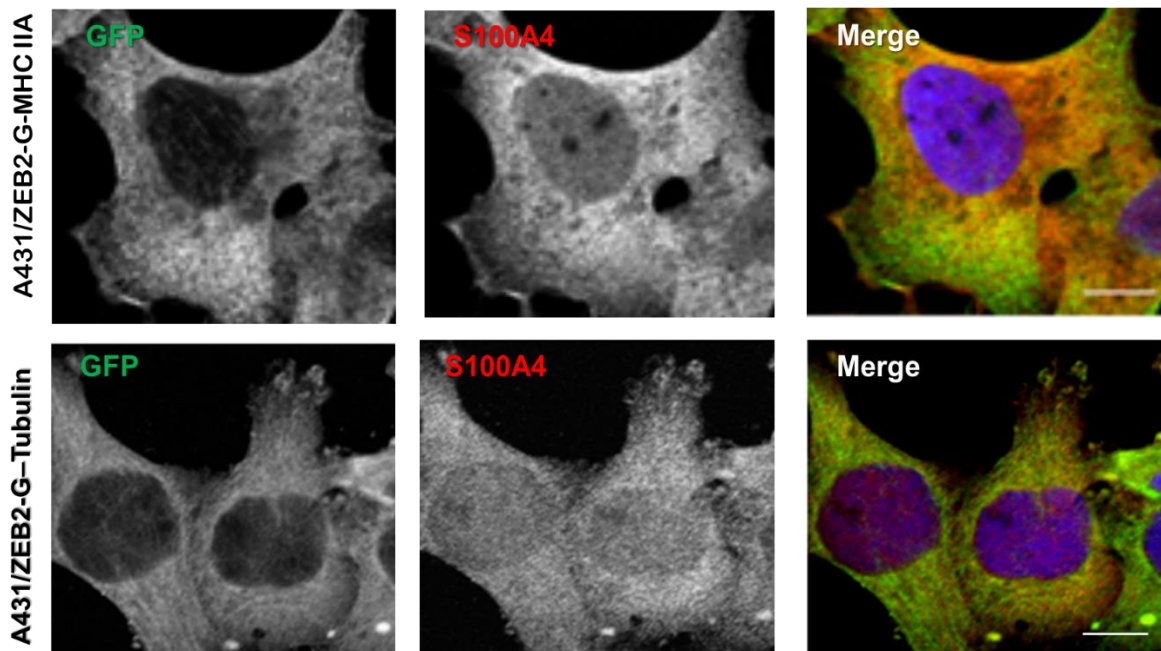


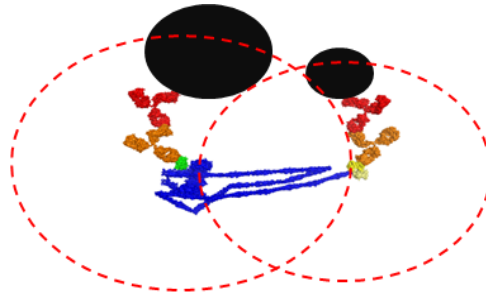
**Figure 3-5: Localisation of  $\alpha$ -Tubulin in A431/ZEB2 cells**

Dox treated A431/ZEB2-G-Tubulin, and A431/ZEB2-G-MHC IIA cells were fluorescently stained for GFP (green) and S100A4 (red). Scale bar =5 $\mu$ m.

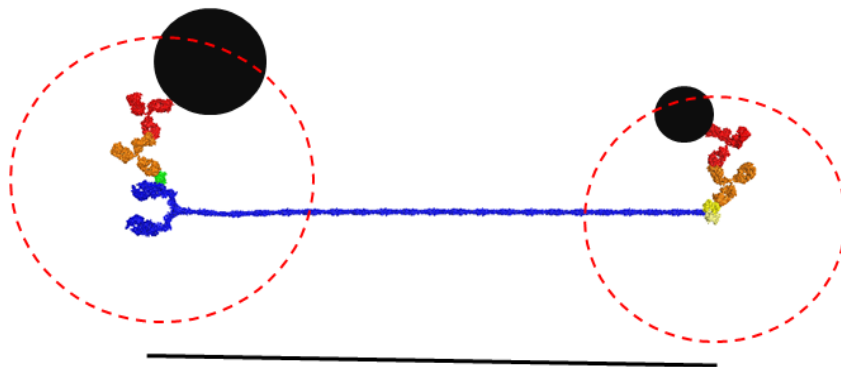
#### **3.4.1.4.3 Co-localisation of S100A4 and GFP-tagged myosin in cells by Transmission Electron Microscopy (TEM)-immunogold labelling**

Immunogold labelling is an approach to analyse the localisation of proteins of interest in cells and tissues (Orlov et al., 2015). Co-localisation experiments can be tested by different sizes of gold particles to visualise different proteins. Immunogold labelling of resin embedded sections of cells is used for detecting various antigens by immunolabeling with a primary antibody against the target molecule, followed by a secondary antibody (against the primary antibody) conjugated with gold particles. It is known that the length of myosin molecule from head to tail is about 150 nm corresponding to the 6S form (reviewed in (Liu et al., 2013a) whilst 50 nm reflects the 10S state in which the rod is folded back upon itself (Trybus et al., 1982) as shown in (Figure3.6). The work started by (Irvine, 2012) who developed the statistical analysis.

Although these distances estimate the lengths of a 10S and 6S myosin molecule, some variation might occur due to the extra addition of antibodies, shrinkage or swelling of tissue during the fixation, dehydration and embedding procedure, and size of gold particles. In fact, possible scenarios based on various locations of gold particles and antibodies were displayed (data not shown; personal communication, Prof. C.R. Bagshaw) and established that there should still be two distinctive peaks consistent with 10S and 6S myosin monomers between 25-75 nm and 125-175 nm, respectively and confirmed that the 6S state remains in an extended conformation.



**10S myosin: 50 nm**



**6S myosin: 150 nm**

**Figure 3-6: Schematic representing the possible distances of the two forms of myosin molecule 10S and 6S.**

Primary antibodies (orange) attached to either GFP/MHC IIA (green) or S100A4/GFP (yellow). Secondary antibodies (red) attached to the primary antibodies and a gold particle of 30 nm (GFP/MHC IIA) or 15 nm S100A4/GFP. Image courtesy of Dr Igor Barsukov.

#### **3.4.1.4.3.1 Quantitative TEM immunogold-labelling**

The intracellular co-localisation of S100A4 and NM IIA has been studied by confocal microscopy technique as described above. However, due to the limited resolution of standard light microscopy, this observation cannot be considered as a convincing evidence for detecting a direct protein-protein interaction. TEM has the same basic principles as the light microscope, however due to shorter wave length of electrons compared to photons, a higher optical resolution is achievable (Melo et al., 2014). Electron microscope uses a beam of electrons to illuminate specimens and electromagnetic lenses to magnify the images. TEM was chosen as it has previously been shown to visualise micro-localisation of some signaling proteins (Prior et al., 2003) TEM can reveal the finest details of internal structure in some cases as small as individual atoms with biological material that is limited by processing procedures carried out prior to visualization in TEM (Griffiths and Lucocq, 2014). Co-localisation experiments can be analysed by using different sizes of gold particles to visualise each antigen. Immunogold labelling of ultrathin sections of cells is used for detecting various antigens by immunolabeling with a primary antibody against the target molecule, followed by a secondary antibody (against the primary antibody) conjugated with gold nanoparticles (Philimonenko et al., 2000).

Previous work in the lab by has detected the co-localisation between S100A4 and monomeric forms of myosin IIA 10S and 6S in cells (Irvine, 2012). In this project, TEM was used to investigate the formation myosin II-S100A4 complexes in cells confirming the presence of the 10S state in cells.

#### **3.4.1.4.3.2 Optimisation of immunogold labelling protocol for TEM**

Dox treated A431/ZEB2-WT cell resin embedded sections were collected onto the gold grids and labelled individually for mouse anti-S100A4, rabbit anti-GFP, rabbit anti-myosin heavy chain IIA and mouse anti-GFP primary antibodies. 15 nm gold labelled Goat anti-mouse and 30 nm Goat anti-rabbit secondary antibodies were used, and samples were blocked before adding primary antibody. Subsequently, the antibody was applied to the resin embedded sections that binds with the antigen through a specific site called an epitope. Immunogold labeling depends exclusively on the antibody-antigen reaction. After exposure to primary antibody, gold conjugated secondary antibodies were applied in which they bind with specific primary antibodies in a microenvironment (Murtey, 2016).

Different dilutions were tested, and the optimum dilution was selected by choosing the concentration with the strongest labelling, but the lowest level of background before experiments with double labelling were performed. Images were taken using a TEM with digital imaging shown in (Figure 3.7) and (Figure 3.8) in which the labelling is mainly on the cell edges.

Accordingly, cell sections were immunogold labelled at specific concentrations for monoclonal S100A4 antibody (75 $\mu$ g/ml) and a polyclonal GFP (5 $\mu$ g/ml) antibodies or myosin heavy chain IIA (100  $\mu$ g/ml) and monoclonal mouse GFP (100  $\mu$ g/ml) antibodies.

Control sections were exposed to secondary antibody only to demonstrate specificity to the primary antibody. No such labelling was observed in these controls (Figure 3.9). In addition to this control, it is necessary to be sure that the secondary antibodies interact specifically with the appropriate primary antibodies. Furthermore, the secondary antibody should not cross-react with the opposing primary antibody. This was tested by labelling cells with primary antibody and then incubating with the opposing secondary antibody. For instance, primary mouse antibody was incubated with goat anti-rabbit secondary antibody. Using different gold particles visualise both epitopes on the same sections.

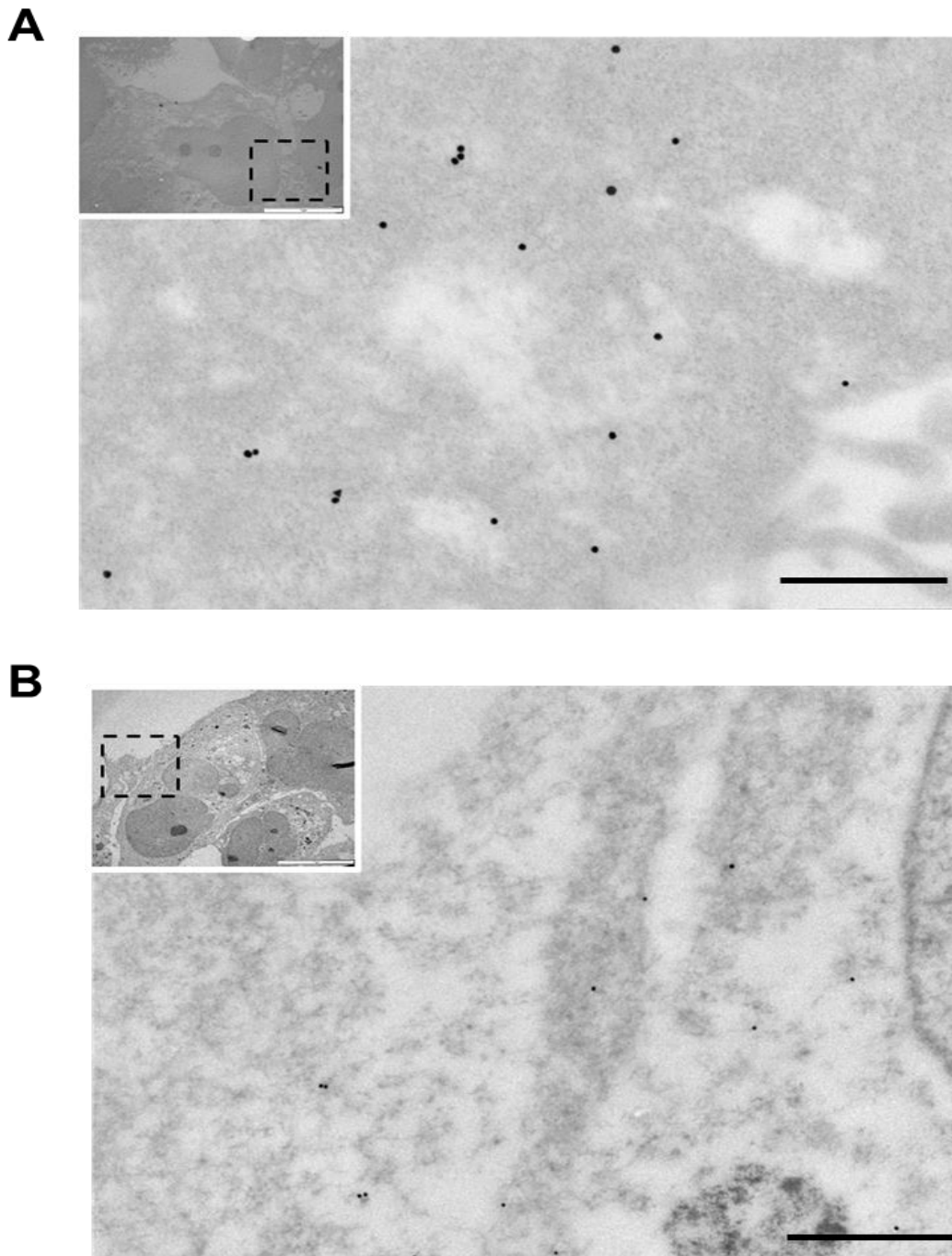


**Figure 3-7: Electron micrographs of single immunogold labeling of A431/ZEB2-WT cells for GFP or S100A4.**

Dox treated A431/ZEB2-WT cells were immunolabelled with A-Rabbit anti-GFP antibody and visualised with 30 nm gold goat anti-rabbit antibody. B- Mouse anti-S100A4 antibody visualised with 15 nm gold goat anti-mouse antibody. Scale bar = 500 nm; inset = 5 $\mu$ m.

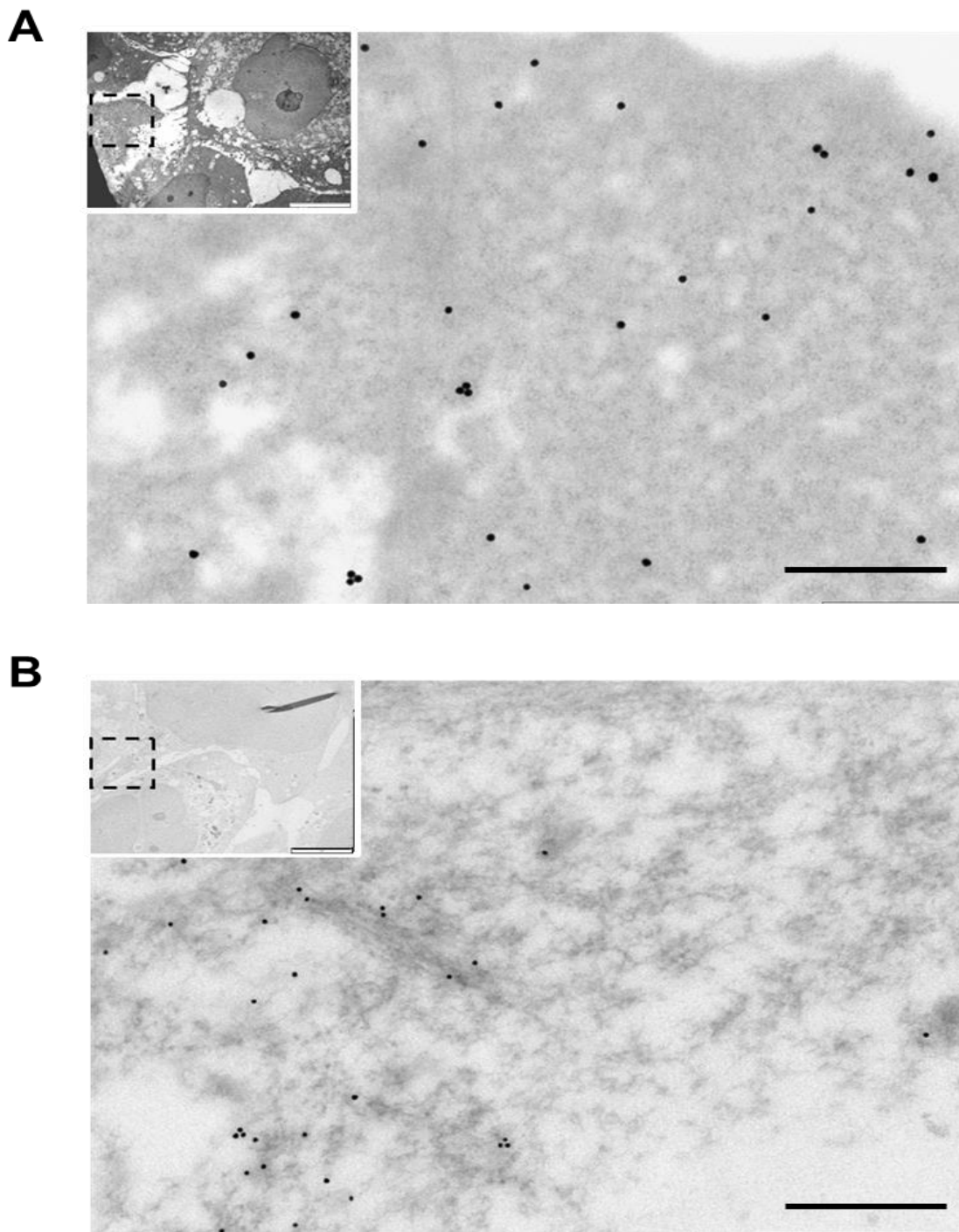


**Figure 3-8: Electron micrographs of single immunogold labeling of A431/ZEB2-WT cells for myosin heavy chain IIA or GFP.**

Dox treated A431/ZEB2-WT cells were labelled with A-Rabbit anti-myosin IIA antibody and visualised with 30 nm gold goat anti-rabbit antibody. B-Mouse anti-GFP antibody visualised with 15 nm gold goat anti-mouse antibody. Scale bar = 500 nm; inset =5 $\mu$ m.

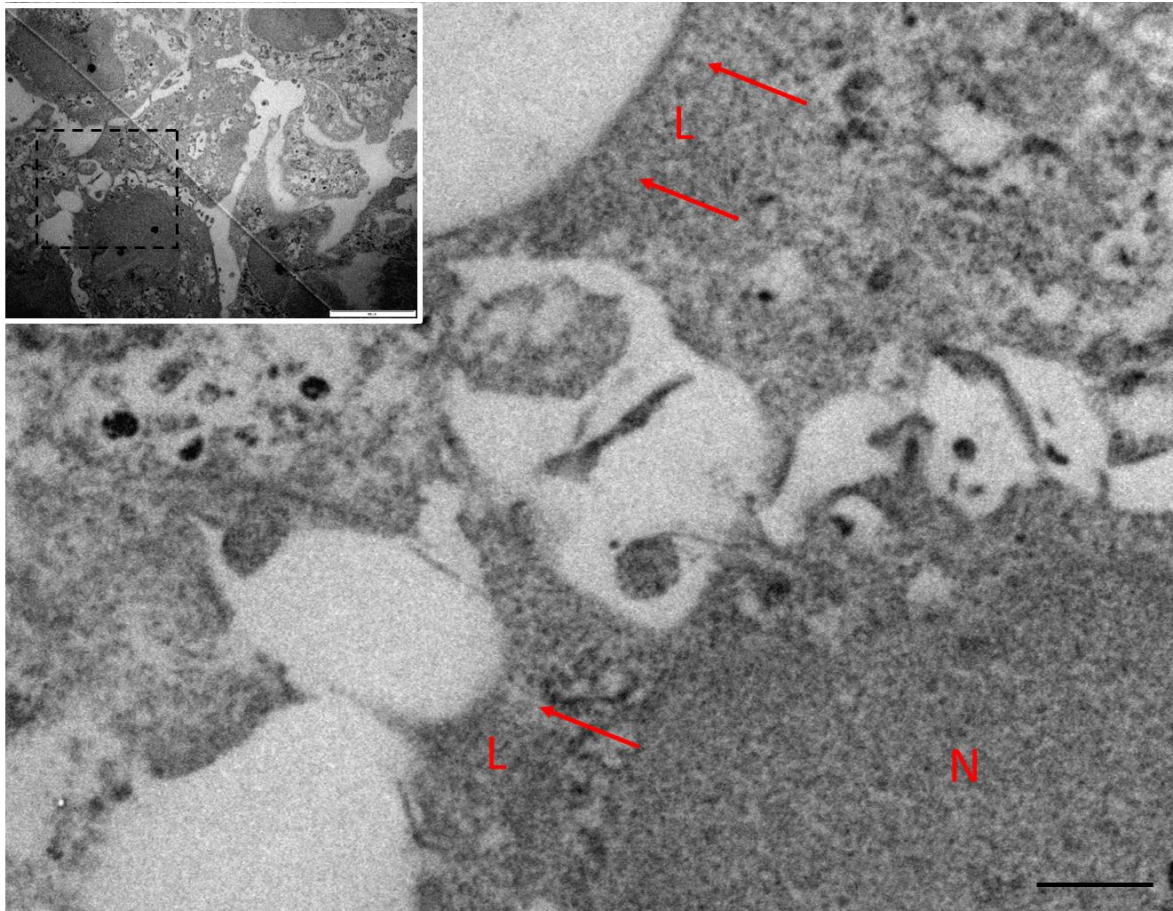


**Figure 3-9: Electron micrograph of immunogold labelling of A431/ ZEB2-WT cells for secondary antibody only.**

Dox treated A431/ ZEB2-WT cells were labelled against secondary antibody only. Red arrows indicate actin-myosin complex. Scale bar for upper panel= 10 $\mu$ m. Scale bar for lower panel= 2  $\mu$ m. N: Nucleus. L: Leading edge.

#### **3.4.1.4.3.3 S100A4 binds to both monomeric forms of myosin IIA in cells**

To investigate the interaction of S100A4 with GFP tagged myosin IIA in cells, immunogold labelling was carried out. Ultrathin resin sections of A431/ ZEB2-WT cells were double-immunogold labelled with anti-GFP and anti-S100A4 antibodies and visualised using 30 nm and 15 nm gold goat anti-rabbit and anti-mouse particles, respectively. Many images of cells were taken for statistical analysis based on the criteria that both particles were detected and the total number did not exceed 100 particles on the image. To analyse the interaction

between S100A4 and GFP-tagged myosin IIA, the XY-co-ordinates were identified for every particle and extracted from each image using a modified version of the nucleus counter plugin in Image J. According to the predicted lengths of 10S and 6S, which were approximately 50 nm and 150 nm, respectively (Figure 3.10), nearest neighbour statistical analysis was carried out. Statistical methods for spectral point pattern analysis were used to assess co-localisation between S100A4 and GFP-myosin IIA. These methods have been used in biological studies to analyse co-localisation of gold particles in electron microscopy (Prior et al., 2003, Rusakov et al., 1995). They can detect the actual distances that objects co-localise at. Thus, these methods are better than light microscopy co-localisation technique that was previously used.

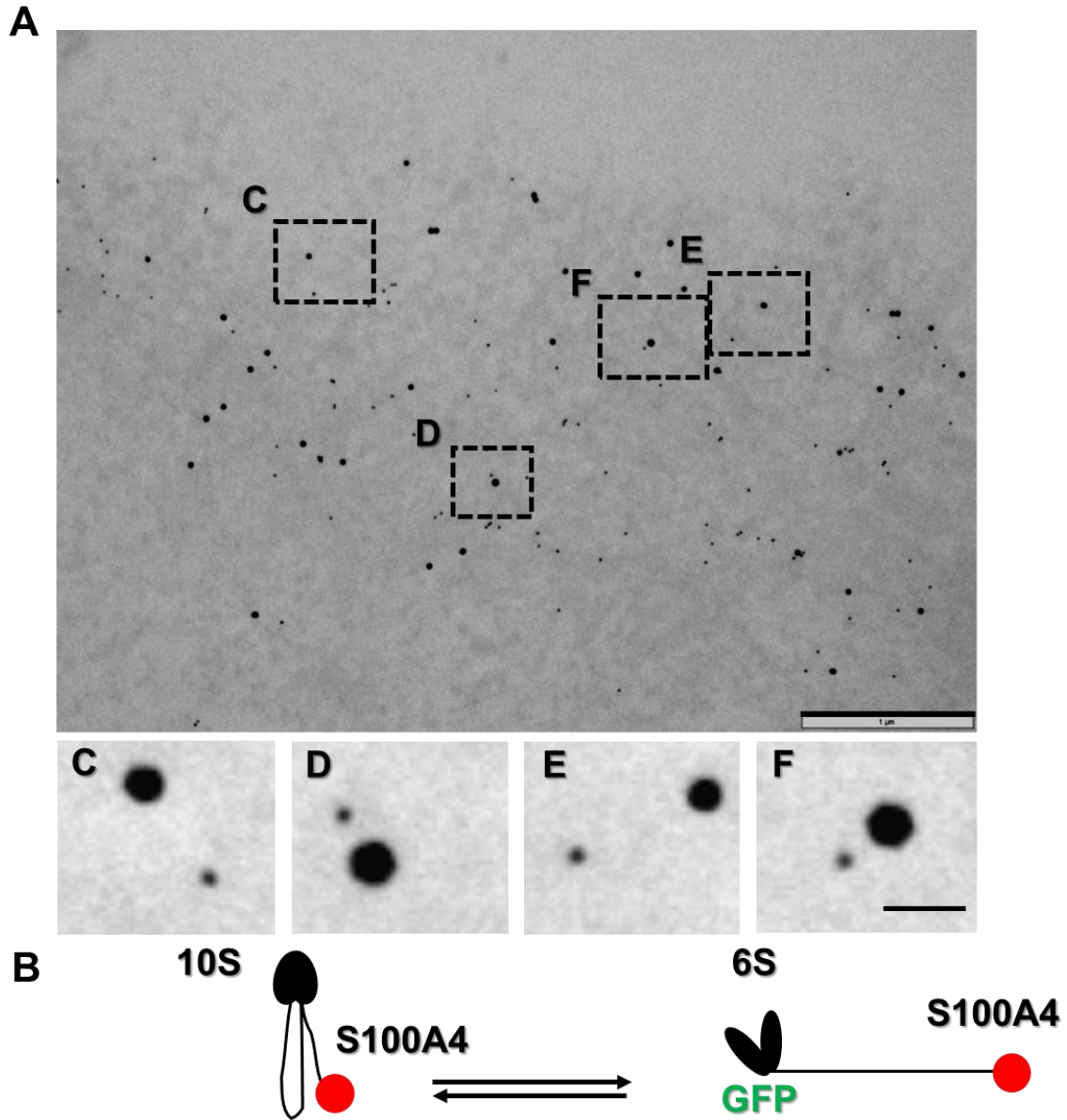


**Figure 3-10: Electron micrographs of double immunogold labelling of S100A4 and GFP in A431/ ZEB2-WT cells**

Dox treated A431/ ZEB2-WT cells were labelled for GFP and S100A4 and visualised using 30 nm and 15 nm gold-goat conjugated secondary antibodies, respectively. Scale bar = 1 μm. C, D, E, F are magnified views to show the intense co-localisation between S100A4 and GFP-myosin IIA at distances C-150 nm; D- 66 nm, E- 180 nm, F- 70 nm; Scale bar = 100 nm. B-S100A4 interacts with both 10S and 6S conformations of myosin IIA monomers.

The statistical approach was developed by Dr Straatman (Core Facility Imaging Manager) as part of a study of (Irvine, 2012). Particle distribution in multiple fields was analysed by image J followed by statistical analysis based on the distance between pairs of particles from two sets (i.e. antigen A and antigen B). The data were plotted as a histogram with co-localisation distance between particles on the X-axis and the % frequency at the particular distance on the Y-axis. Therefore, Diggle's G function that calculates the co-localisation of two types of particles over a range of distances was applied. Statistical analysis was based on comparison the experimental data to 99% confidence interval (CI) for Complete Spatial Randomness (CSR) generated from 100 Monte Carlo stimulations equal to the density of particles for each image. When experimental values exceed the 99% CI, there is statistically significant co-localisation P value of  $< 0.01$  at that specific distance (Philimonenko et al., 2000). The analysis was carried out using a custom Excel macro written in (Visual Basic for Applications) VBA (Microsoft, USA).

All experiments were done in triplicate, the co-localisation was detected at statistically significant peaks corresponding to 50 nm, 100 nm and 150 nm. The distances between particles consistent with the length of myosin monomers 10S and 6S, respectively (Figure 3.12-A). This suggests that S100A4-myosin complexes exist in cells. The previous study (Irvine, 2012) also found that S100A4 interacts with NM IIA at two distances between 25-75 nm and between 125-150 nm which likely reflect 10S and 6S myosin monomers, respectively.

As a negative control, sections of A431/ZEB2- $\alpha$ -Tubulin constructs were immunogold labeled for GFP and S100A4 antibodies (Figure 3.11). The statistical significance of the data was assessed using the same protocol. Co-localisation analysis from three separate experiments demonstrated no significant peaks (Figure 3.12-B).

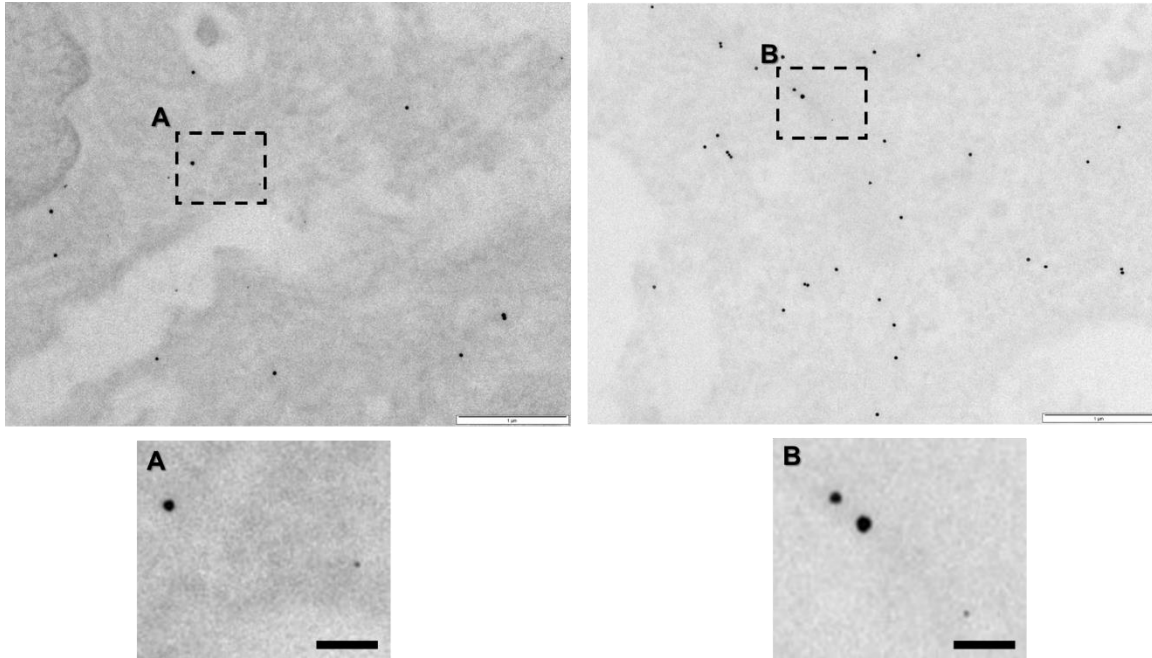


**Figure 3-11: Electron micrographs of immunogold labelling of A431/ZEB2 cells expressing GFP- $\alpha$ -Tubulin stained for S100A4 and GFP antibodies.**

Dox treated A431/ZEB2 cells expressing GFP- $\alpha$ -Tubulin were immunolabelled for S100A4 and GFP, using 30 nm and 15 nm gold-conjugated secondary antibodies, respectively. A, B- Images are zoomed in views show the distances between GFP- $\alpha$ -Tubulin and S100A4 particles; A-671 nm; B-382 nm. Scale bar =1 $\mu$ m. Scale bar for magnified images = 200 nm.

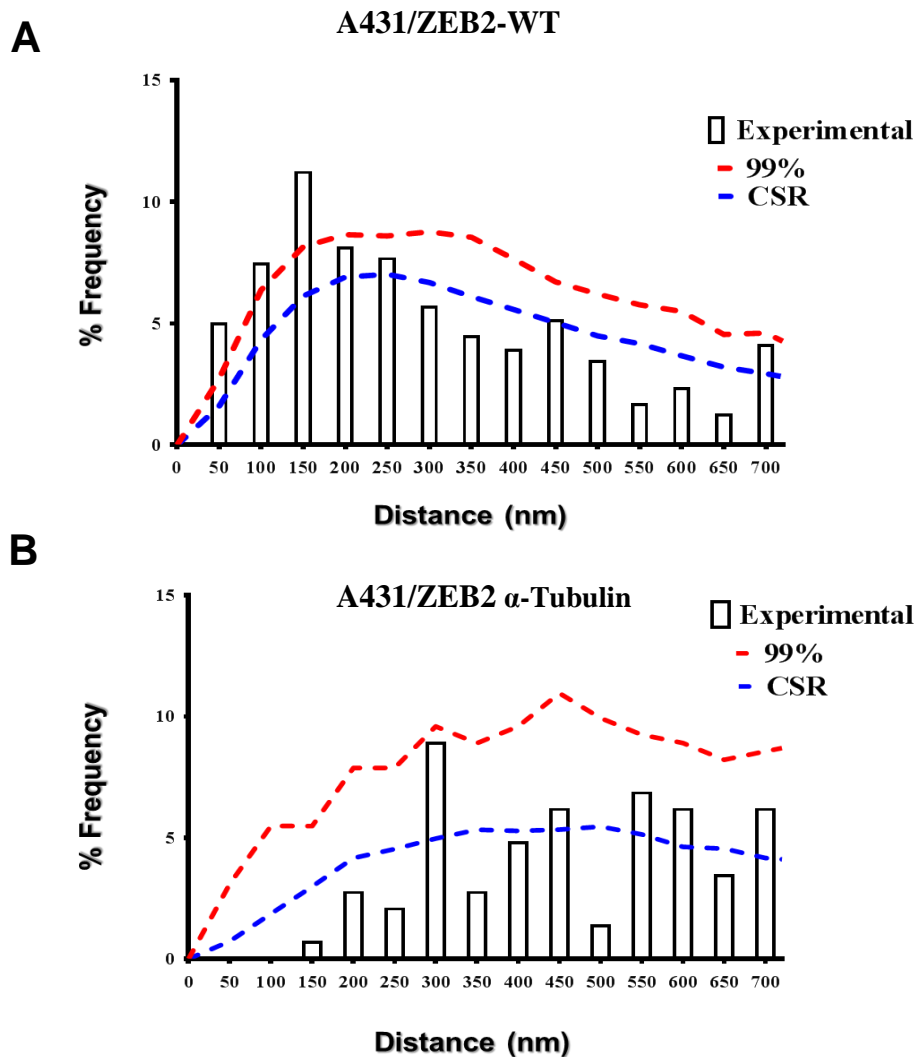


**Figure 3-12: Co-localisation of S100A4 and GFP-myosin IIA in A431/ ZEB2-WT and A431/ ZEB2 - $\alpha$ -Tubulin cells.**

Resin embedded sections of Dox treated A431/ ZEB2-WT and A431/ ZEB2- $\alpha$ -Tubulin cells were immunolabelled with anti-S100A4 and anti-GFP antibodies. Nearest-neighbour analysis was performed to determine the co-localisation of S100A4 and GFP in cells. Blue dashed line represents random distribution between small particles (15nm) and large particles (30 nm); Complete Spatial Randomness (CSR) calculated from 100 Monte Carlo simulations for each image. Nearest neighbour distances between 30 nm and 15 nm particles equal the experimental data from S100A4 and GFP co-localisation. Frequency indicates the nearest neighbour distance between S100A4 and GFP-myosin IIA at a particular distance, thus providing the co-localisation between them. Red dashed line reflects the 99% confidence interval calculated from the Monte Carlo simulations; at any point where the experimental data goes above 99% CI, co-localisation was considered as statistically significant at that specific distances. A- Significant co-localisation of S100A4 and GFP at three peaks corresponding to 50 nm, 100 nm and 150 nm reflecting 10S and 6S conformations. B-There was no statistically significant co-localisation between GFP- $\alpha$ -tubulin and S100A4. X-axis distances plotted in 50 nm. These results represent the analysis of 700 images of three independent experiments.

This data indicates that there was no interaction between GFP- $\alpha$ -Tubulin and S100A4. As a conclusion; data provide a strong evidence that S100A4 can interact with both folded 10S and unfolded 6S forms of NM IIA monomers *in vivo*.

#### **3.4.1.4.3.4 RNAi- mediated depletion of S100A4 in A431/ZEB2-WT cells**

To detect the functional role of S100A4 in regulating filament assembly of NM IIA *in vivo*, knock down of S100A4 was performed. Cells were transfected with either a non-targeting (siControl) or S100A4-targeting siRNA (siS100A4) and incubated in the presence of Dox for 48 hrs. Western blot analysis revealed decreased S100A4 protein levels in siS100A4 cells compared with siControl cells confirming the suppression of S100A4. The expression pattern of GFP and MHC IIA exhibited no changes upon knockdown of S100A4 (Figure 3.13-A). Subsequently, cells were fixed, embedded, ultramicrotomed and resin sections were collected on the grids. Resin embedded cells were then immunogold labelled for GFP and S100A4. Images were collected and analysed using nearest-neighbour analysis for S100A4 and GFP-myosin IIA. The result showed that S100A4 interacted with both monomeric states of myosin IIA by demonstrating distinctive peaks corresponding to 50 nm, 100 nm and 150 nm which are consistent with 10S and 6S myosin IIA conformations (Figure 3.13-B). In contrast, nearest neighbour co-localisation analysis from three independent experiments showed no significant peaks detected in siS100A4 cells. Therefore, it was used as a negative control (Figure 3.13-C).

### A431/ZEB2-WT

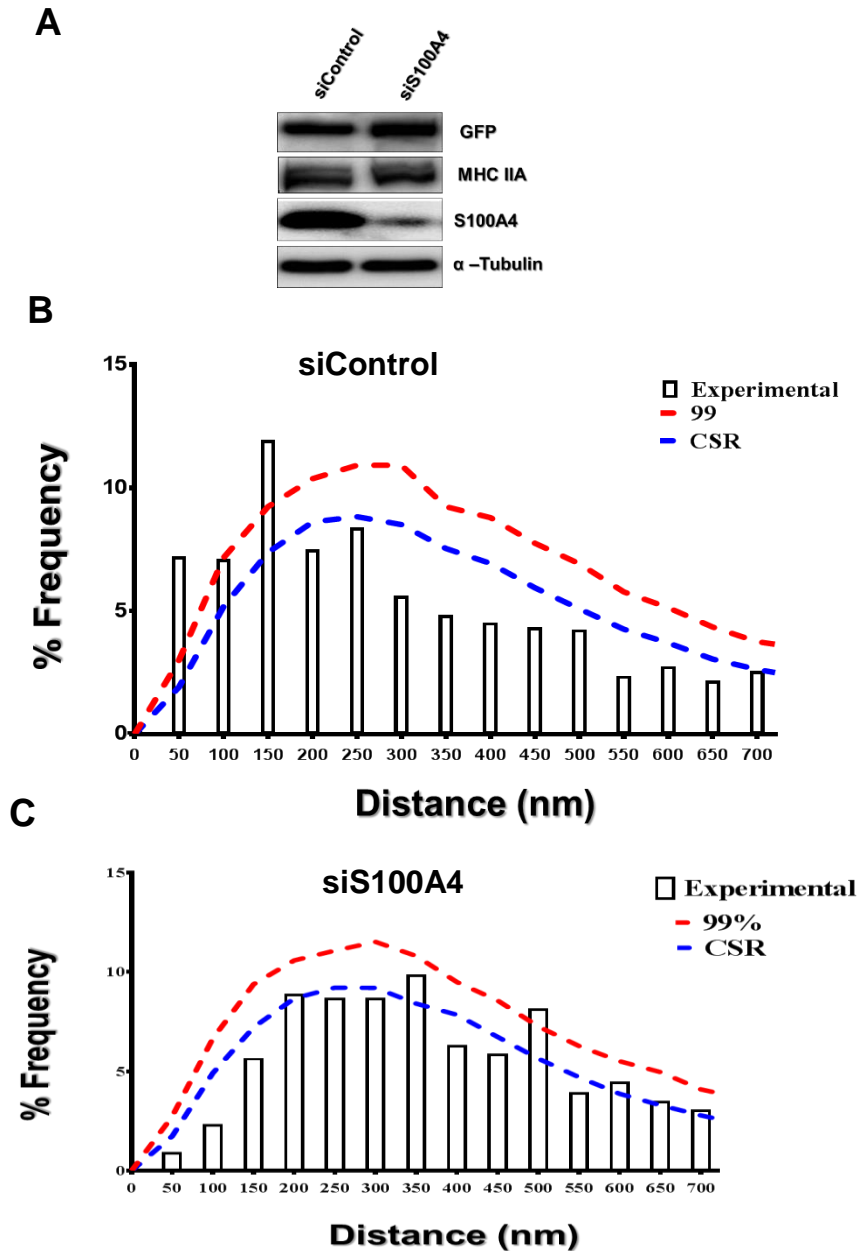


**Figure 3-13: Characterisation of S100A4 Knockdown in A431/ZEB2-WT cells**

Dox treated A431/ZEB2-WT cells were transfected with either a non-targeting (siControl) or targeting S100A4 siRNA (siS100A4). A-Cells were lysed, and proteins were analysed by Western blotting. Membranes were probed for GFP, MHC IIA and S100A4.  $\alpha$ -Tubulin was used as protein loading control. B and C- Resin embedded sections of cells were labelled against GFP and S100A4. Nearest-neighbour analysis was performed from three pooled experiments to detect the co-localisation between S100A4 and GFP-myosin IIA. B-The co-localisation was detected at three statistical significance peaks; 50 nm, 100 nm and 150 nm, respectively. C-As a result of S100A4 knockdown, no peaks were detected. Blue dashed line represents random distribution between small particles (15nm) and large particles (30 nm); Complete Spatial Randomness (CSR). 99% confidence interval (CI). These results represent the analysis of 800 images of three separate experiments.

#### **3.4.1.4.3.5 S100A4 promotes monomeric forms of myosin IIA**

Subsequently, the effect of S100A4 in maintaining the monomeric fractions of myosin IIA in cells was examined; using the technique of immunogold labelling in siControl and siS100A4 cells (Figure 3.14). In this experiment, we used antibodies for myosin N-terminus (anti-GFP) and C-terminus (anti-MHC IIA) antibodies that were prepared using C-terminus myosin heavy chain peptide analysis of particles distribution was performed reflecting myosin conformations based on distances between 2 sizes of particles that reflect positions of the N-and C-termini of myosin molecules. Three independent experiments detected two statistically significant peaks corresponding to 50 nm and 150 nm, consistent with there are being two monomeric forms of myosin IIA in cells; 10S and 6S, respectively (Figure 3.15-A), whereas in the absence of S100A4, the significant peaks were detected at 250 nm and 350 nm distances as shown in (Figure 3.15-B). This may indicate an increase in NM IIA filaments formation as the result of S100A4 depletion. Using this data and the previous data, it could be concluded that S100A4 plays an important role in preventing NM IIA filament formation rather than just promoting myosin monomers (Figure 3.15-C).

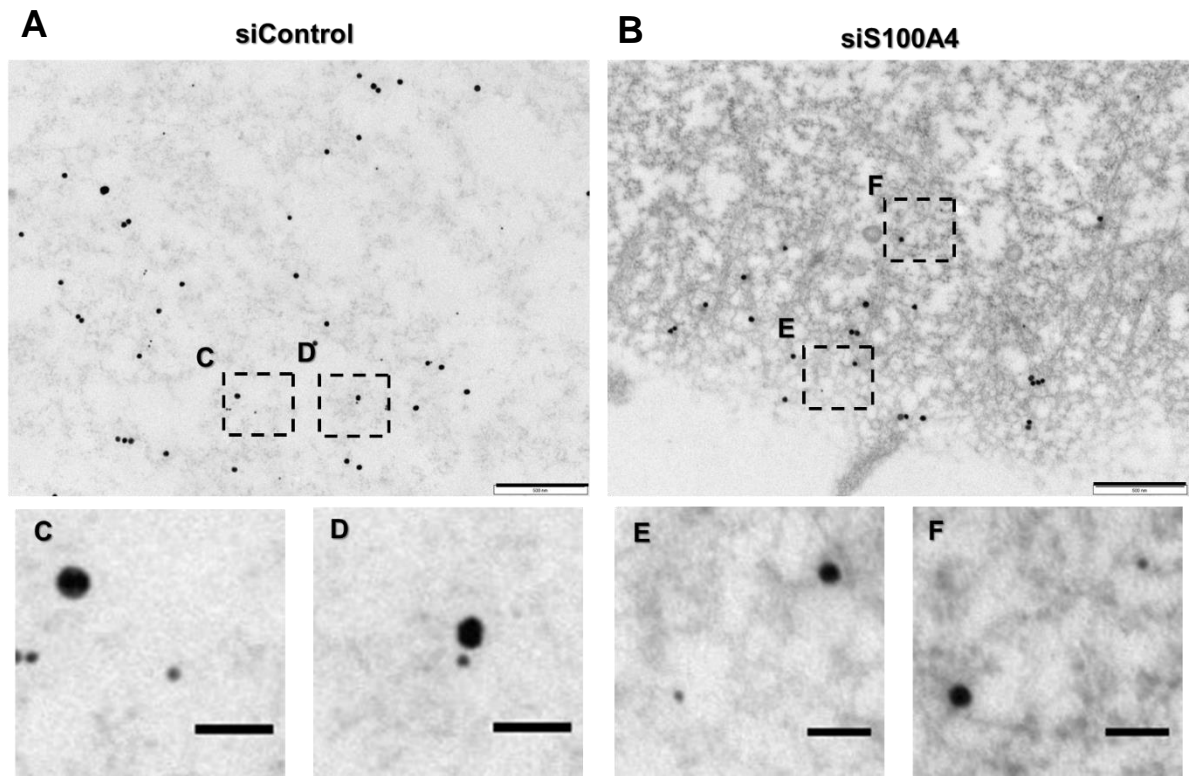


**Figure 3-14: Electron micrographs of immunogold labelling of siControl and siS100A4 cells for MHC IIA and GFP.**

Resin embedded sections of Dox treated siControl (A) and siS100A4 (B) cells were labelled for MHC IIA and GFP and visualised using 30 nm and 15 nm gold-conjugated secondary antibodies, respectively. A and B are overviews with images magnified in C, D, E and F to show the distances between GFP and MHC IIA particles; C-150 nm; D-30 nm, E- 335 nm, F- 350 nm. Scale bar =500 nm. Scale bar for magnified images = 80nm.

### A431/ZEB2-WT

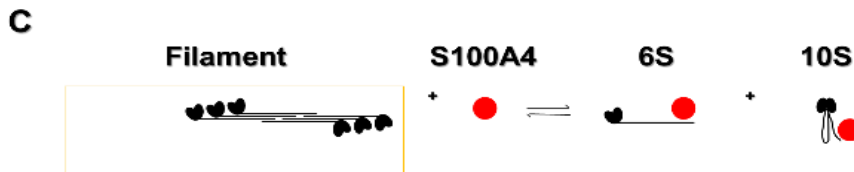
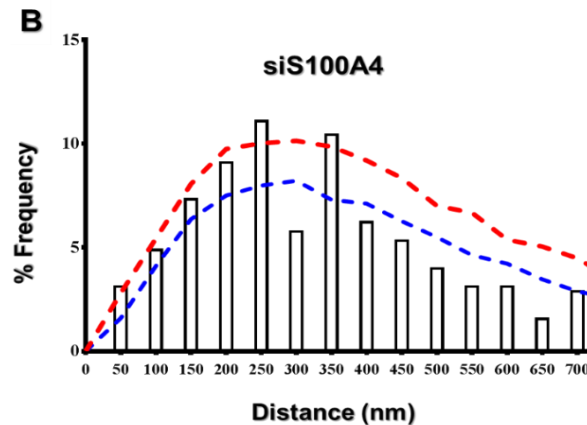
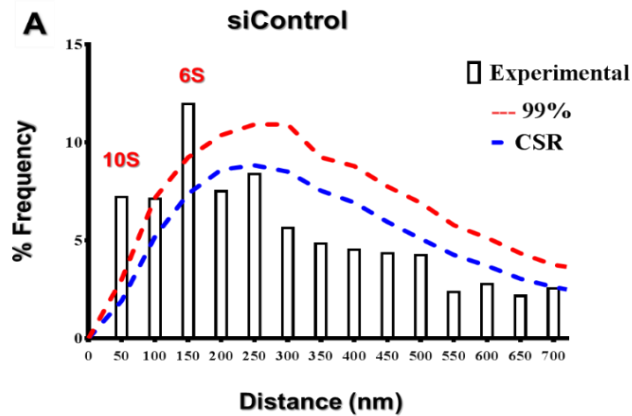


**Figure 3-15: Knockdown S100A4 leads to assembly of myosin IIA into filaments**

Resin embedded sections of siControl and siS100A4 cells were immunolabelled with anti-GFP and anti-MHC IIA antibodies and visualised using 15 nm and 30 nm gold-conjugated secondary antibodies, respectively. A-Nearest neighbour co-localisation analysis of three independent experiments detected the significant co-localisation between GFP and S100A4 at two significant peaks corresponding to 50 nm and 150 nm reflecting the presence of both 10S and 6S myosin IIA monomers in cells, respectively, whereas in B, the peaks were detected at 250 nm and 350 nm distances reflecting the presence of polymerization of myosin IIA into filaments. C-Binding of S100A4 to myosin IIA promotes the monomeric, unassembled state of myosin. Blue dashed line reflects random distribution between small particles (15nm) and large particles (30 nm) (CSR). 99%

confidence interval (CI). These results represent the analysis of 900 images of three independent experiments.

#### **3.4.1.4.4 Myosin Regulatory light chain (MRLC) phosphorylation is inhibited by the ROCK inhibitor Y27632.**

Previous studies documented a critical role of inhibition of RLC phosphorylation in switching myosin IIA from unfolded assembled 6S to the folded assembled 10S conformation (Breckenridge et al., 2009). Activity of myosin is regulated by phosphorylation of the RLC of NM IIA by MLCK and Rho kinase (Conti and Adelstein, 2008). Previous data obtained in our laboratory (Irvine, 2012), provides evidence that ROCK is the main kinase that phosphorylates MRLCs. Therefore, we inhibited the main kinase responsible for the phosphorylation of RLC in our cell model. Upon 72 hrs cultivation in the presence of Dox, A431/ZEBE2-WT cells were treated either with DMSO (vehicle) or 10 $\mu$ M Y27632 to inhibit ROCK which is controlling RLC phosphorylation at Ser19 and Thr18.

Clear cellular morphological changes were associated with Y27632 treatment. The phenotypical effects of ROCK inhibition were characterised by the formation of multiple long, spindle-like cellular protrusions (Figure 3.16-A). In addition, immunofluorescence staining illustrated a partial co-localisation between S100A4 and GFP-MHC IIA in treated cells with Y27632. There was a decrease in myosin IIA filaments assembly in treated cells (Figure 3.16-B).

Cell lysates from the same experiment were collected for blot analysis. Immunoblot data subsequently showed that ROCK inhibition led to a significant reduction in the RLC phosphorylation at Ser19/Thr18 (Di-p-RLC). In addition, it was found that there was no significant difference in the level of expression of RLC after treatment of cells with Y27632 (Figure 3.16-C).

**Dox (72 hrs)**

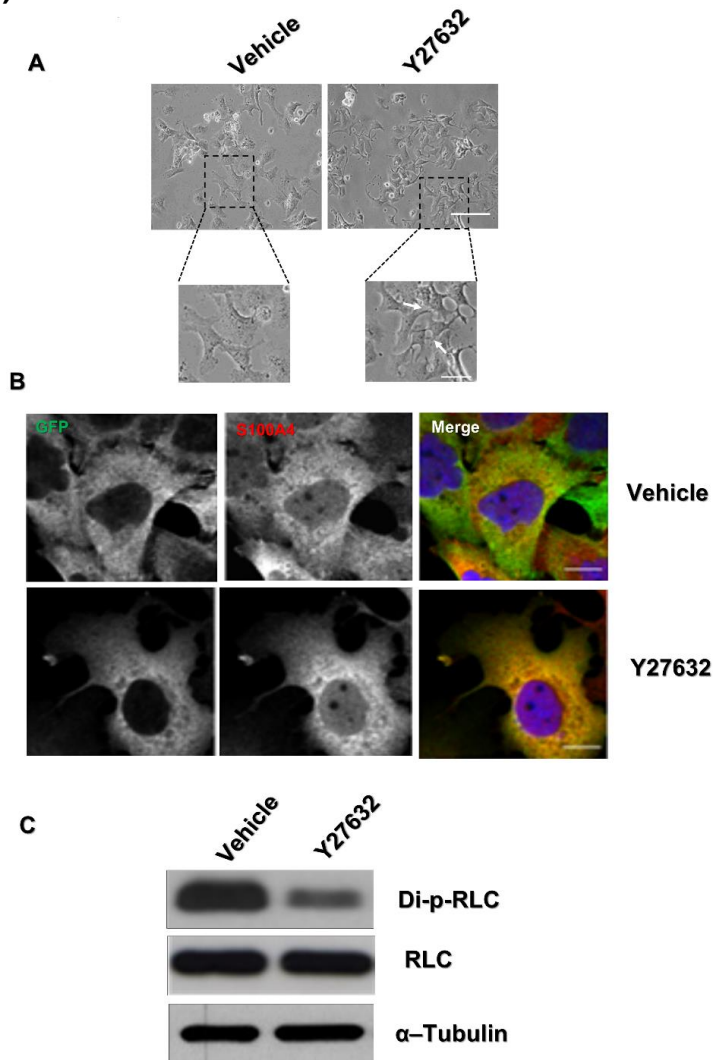


**Figure 3-16: Inhibition of the MRLC phosphorylation by the ROCK inhibitor Y27632**

Dox treated A431/ZEB2-WT cells were treated with DMSO (vehicle), or 10  $\mu$ M Y27632 for 2 hrs. A-Representative images of cells prior to lysis exhibit multiple spindle-like protrusions. Scale bar = 20  $\mu$ m. Magnified region of black boxes in (A). White arrows indicating formation of large lamellipodia, characteristic of mesenchymal cells. Scale bar = 10  $\mu$ m. B-Immunofluorescence staining of vehicle and Y27632 treated cells for GFP and S100A4. Merge images of GFP and S100A4 signals was shown as yellow colour illustrating a co-localisation between both proteins. C- Cell lysates were collected for Western blot analysis. Membranes were probed for (Di-p-RLC) and RLC.  $\alpha$ -Tubulin was used as a protein loading control.

#### **3.4.1.4.5 Inhibition of RLC phosphorylation obliterates the co-localisation between S100A4 and a GFP-myosin IIA at a distance reflects 10S conformation.**

As phosphorylation of RLC at S19/Thr18 favours the switch myosin IIA from 10S to 6S conformation, we predicted that inhibition RLC phosphorylation by Y27632 would reduce the population of 6S molecules (Liao et al., 2007). Therefore, Y27632 treated cells were stained for GFP and S100A4 using the immunogold labelling technique (Figure 3.17) and the same nearest neighbour analysis was performed. Data show a significant co-localisation of S100A4 and GFP at one distance corresponding to 50 nm consistent with the hypothesis that this distance reflects 10S form (Figure 3.18-A).

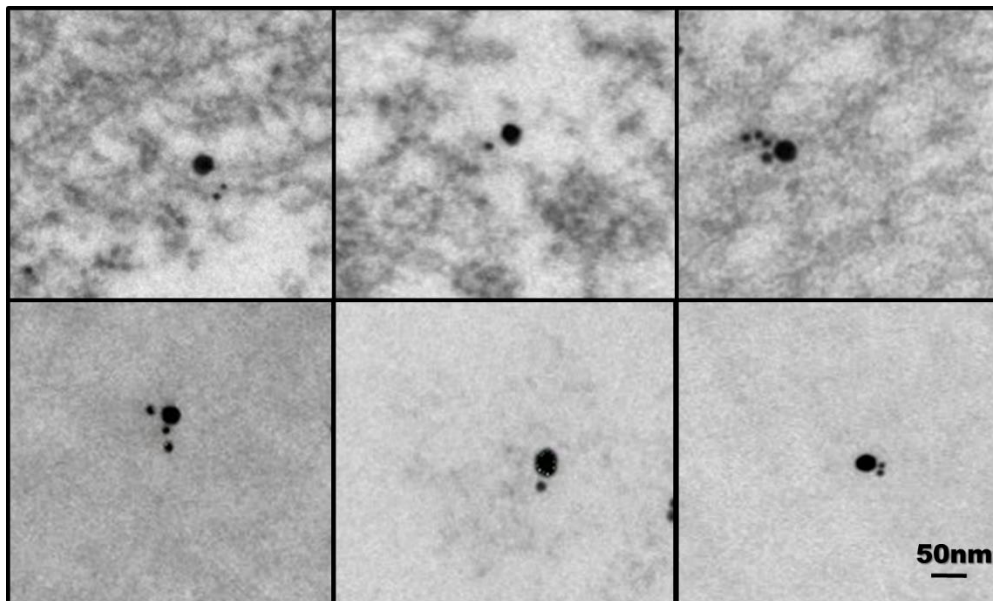


**Figure 3-17: GFP and S100A4 co-localised at distances consistent with 10S conformation as a result of inhibition of RLC phosphorylation.**

Representative images of A431/ZEB2-WT cells treated with 10 $\mu$ M Y27632 for 2 hrs and labelled with anti-GFP (30 nm gold) and anti-S100A4 (15 nm gold) antibodies. Scale bar= 50 nm. Signals were detected at distances less than 50 nm.

Further, we investigated the existence of myosin IIA in Y27632 treated cells. Resin embedded cell sections were immunolabelled for GFP and MHC IIA. Nearest neighbour

analysis of TEM images were then carried out to detect the localization of myosin IIA in cells. Data from three independent experiments demonstrated two statistically significant peaks in untreated cells at two distances 50 nm and 150 nm which are consistent with 10S and 6S conformations of myosin monomers. However, in cells treated with Y27632, only one significant peak corresponding to 50 nm was detected indicating the presence of myosin IIA in the 10S form (Figure 3.18-B). Taken together, these data suggest that 10S and 6S conformations of myosin IIA exist in cells. In addition, attenuation of RLC phosphorylation prevents the formation of 6S state and promotes 10S myosin monomer. In conclusion, phosphorylation of RLC is important for formation of myosin 10S state.

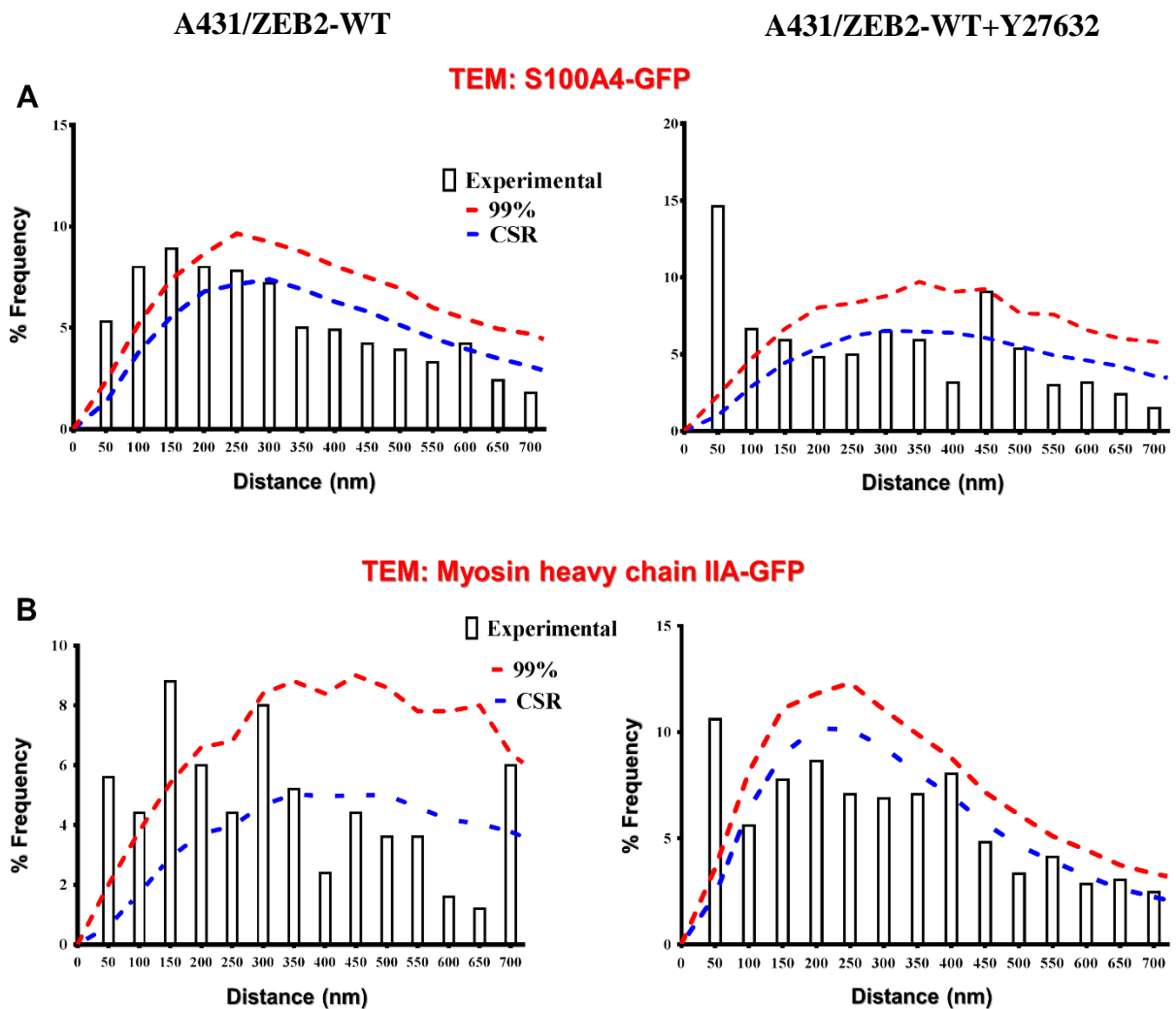


**Figure 3-18: Inhibition of RLC phosphorylation results in co-localisation between S100A4 and myosin IIA at one significant peak consistent with 10S myosin monomer**

Resin embedded sections of A431/ZEB2-WT cells under control condition or following treatment with 10 $\mu$ M Y27632 for 2 hrs were immunolabelled for S100A4 and GFP (A) and MHC IIA and GFP (B). Nearest-neighbour analysis of three independent experiments showed the significant co-localisation of the proteins. A- S100A4 co-localised with GFP-myosin IIA in the presence of Y27632 at one peak 50 nm represents 10S. B- Two significant peaks were detected in untreated cells at 50 nm and 150 nm consistent with 10S and 6S myosin IIA monomers, while only one significant peak was detected at 50 nm in Y27632 treated cells indicating that myosin IIA is present in a folded 10S and an extended 6S monomers in cells. Blue dashed line reflects random distribution between small particles (15nm) and large particles (30 nm) (CSR). 99% confidence interval (CI). These results represents the analysis of 2000 images of three separate experiments

#### 3.4.1.4.5.1 Attenuation of RLC phosphorylation by the ROCK inhibitor Y27632.

The depletion of RLC phosphorylation by treating cells with the ROCK inhibitor Y27632 and suppression of S100A4 protein were next analysed by Western blotting. A431/ZEB2-WT cells were transfected with either a non-targeting (siControl) or S100A4-targeting siRNA (siRNA) and grown in the presence of Dox for 48 hrs. Subsequently, cells were treated with 10  $\mu$ M Y27632 for 2 hrs. Lysates were then collected and run on SDS-PAGE. Membranes were blotted for GFP, MHC IIA, RLC and S100A4. It was observed that the level of RLC phosphorylation at Ser19 and Thr18 was reduced markedly in cells treated with Y27632. In addition, a considerable decrease in S100A4 expression in siS100A4 cells was demonstrated when compared with siControl (Figure 3.19). However, the level of myosin expression did not change in siControl and siS100A4 cells. In conclusion, this experiment proved that S100A4 is knocked down by RNAi and RLC is dephosphorylated in the presence of Y27632.

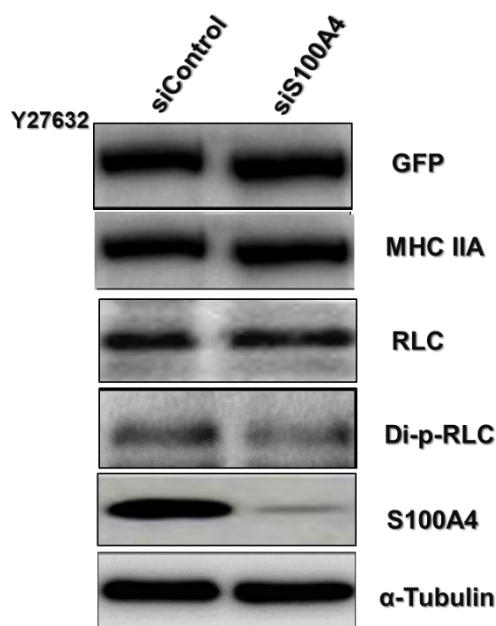


**Figure 3-19: ROCK inhibition blocked RLC phosphorylation on Thr18/Ser19.**

siControl and siS100A4 cells were treated with 10  $\mu$ M Y27632 for 2 hrs. Cell lysates were collected, and protein expressions was assessed by immunoblot analysis for S100A4, MHC IIA, GFP, RLC (Ser19/Thr18) and Di-p-RLC.  $\alpha$ - Tubulin was used as a protein loading control.

#### **3.4.1.4.5.2 S100A4 regulates 10S-6S transition**

Based upon the results of the previous experiment which confirmed that the binding of S100A4 to myosin IIA promotes the monomeric form of myosin IIA, further investigation was made to assess whether S100A4 can regulate a switch of myosin IIA from 6S to 10S. Thus, resin embedded sections of siControl or siS100A4 cells treated with 10 $\mu$ M Y27632 were immunogold labelled with the anti-MHC IIA and anti-GFP antibodies using the same immunogold labelling technique. The nearest neighbour co-localisation analysis of gold particles was performed. Although we detected statistically significant peak corresponding to 50 nm reflecting 10S in siControl+Y27632 cells (Figure 3.20-A), a shift of the peak from 50 nm to 150 nm was observed in siS100A4+Y27632 cells (Figure 3.20-B). The current data highlight the importance of S100A4 in maintaining myosin monomer in 10S form.

A431/ZEB2-WT+Y27632

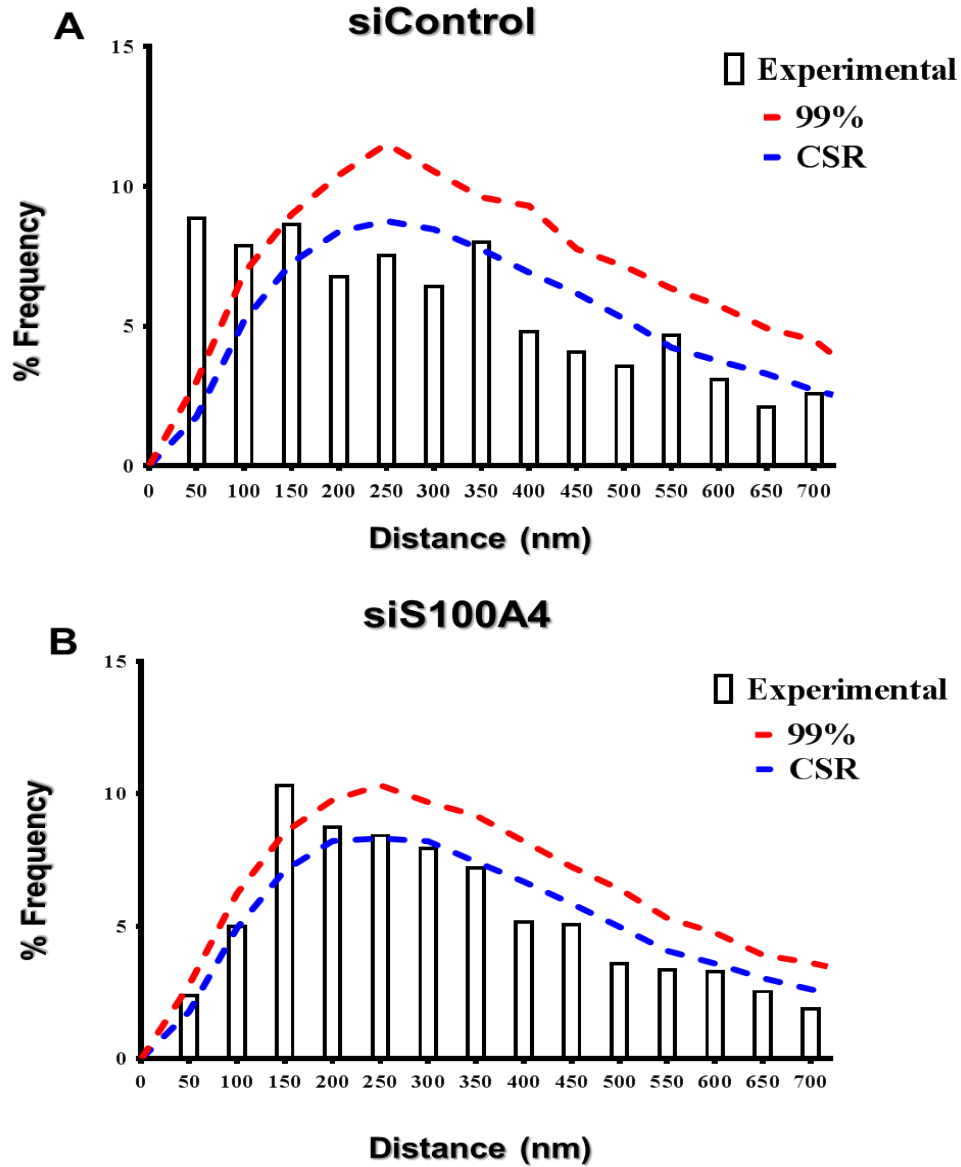


**Figure 3-20: Coupling S100A4 knockdown and ROCK inhibition alter myosin IIA confirmation.**

siControl and siS100A4 cells were treated with ROCK inhibitor 10 $\mu$ M Y27632. Sections of resin embedded cells were labelled for myosin IIA and GFP using 30 and 15 nm gold-conjugated secondary antibodies, respectively. Nearest-neighbour co-localisation analysis was conducted for siControl cells (A) and siS100A4 cells (B). A-The presence of a significant peak at 50 nm is consistent with the 10S myosin monomer. B-The presence of a significant peak at 150 nm is consistent with the extended 6S myosin monomer. Blue dashed line reflects random distribution between small particles (15nm) and large particles (30 nm) (CSR). 99% confidence interval (CI). These results represent the analysis of 860 images. Results are representative of experiments performed on three separate experiments.

### **3.4.2 Effect of RLC phosphorylation on S100A4-myosin IIA interaction.**

To further study the role and localization of myosin in cells, GFP-fused RLCs were used. However, the exact kinetic properties of myosin light chain when bound with GFP are poorly understood (Trybus, 1994). Importantly, it has not yet been demonstrated whether a RLC fused with GFP at its N-terminus can maintain the normal phosphorylation-dependent controlling of NM IIA, or serve as a substrate for myosin light chain kinase. The GFP molecule, which has a molecular weight approximately one and a half times that of RLC and thus it does not have an effect on myosin conformation or even prevent the normal enzymatic activity of myosin (Kengyel et al., 2010).

Although previous data showed that inhibiting phosphorylation of the RLC promotes the 10S conformation of myosin monomer as described in section (3.3.1.4.5), the functional significance of the RLC phosphorylation on S100A4-myosin IIA interaction remains uninvestigated. To address this problem, we produced phosphodeficient (T18A/S19A) and phosphomimetic (T18D/S19D) mutants of Ser19 and Thr18. RLC cell lines were expressed as GFP-fusion proteins (Beach et al., 2011b) and Dox treated cells were used for further analysis.

### **3.4.2.1 Assessing the activation of EMT-associated genes during ZEB2-induced EMT in RLC clones of A431 cells.**

Investigation was made into whether RLC phosphorylation and dephosphorylation has an effect on EMT. A431-ZEB2 cells expressing RLC-WT and mutants were cultured with and without Dox for 72 hrs, and cells were lysed for immunoblotting to verify the expression of ZEB2, E-cadherin, GFP, vimentin and S100A4 proteins. The western blot shows a substantial increase in the ZEB2, S100A4 and vimentin expression in cells treated with Dox which was detected in a highest level in T18D\S19D cells. In parallel, a notable decrease of E-cadherin expression during EMT was observed which was more obvious in T18D\S19D cells. Indeed, in T18A\S19A cells, S100A4 expression was lower than its expression in other cell lines (Figure 3.21). This might be due to clonal selection or it could result from the majority of S100A4 being present in protein aggregates in cell. This finding provides a conclusion that EMT was not dependent on myosin mutants.

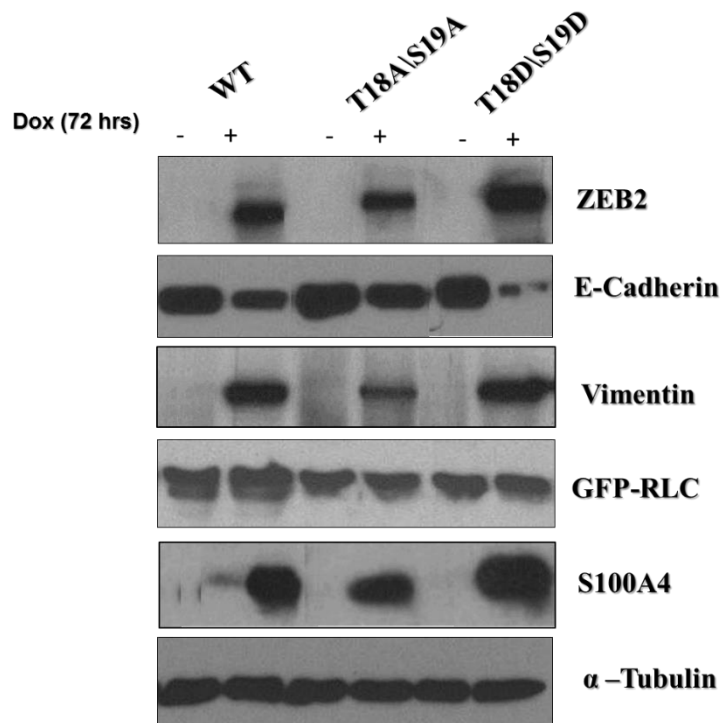


**Figure 3-21: Characterization of cells expressing GFP-tagged mutants of the RLC**

Cells expressing RLC-WT, phosphodeficient T18A/S19A and phosphomimetic T18D/S19D cells were maintained in the absence and presence of Dox for 72 hrs. Lysates were prepared and separated by SDS-PAGE. Membranes were blotted and stained against ZEB2, Vimentin, GFP, S100A4, and E-cadherin.  $\alpha$ -Tubulin was used as a loading control.

### 3.4.2.2 Assessment of the S100A4-myosin IIA interaction in cells expressing RLC-WT and mutants by co-immunoprecipitation

Based on the above results, we chose to test the interaction between S100A4 and GFP in cell lysates expressing RLC-WT, phosphodeficient T18A/S19A and phosphomimetic T18D/S19D. GFP and S100A4 were successfully immunoprecipitated from cell lysates using anti-GFP and anti-S100A4 antibodies, respectively. Subsequently, immunoprecipitated GFP fraction was probed with anti-S100A4 and anti-GFP antibodies. In addition, immunoprecipitated S100A4 was immunoblotted with anti-GFP and anti-S100A4 antibodies

(Figure 3.22). The data show clear bands that correspond to GFP and S100A4 being detected from immunoprecipitated GFP and S100A4, respectively. However, faint bands reflecting GFP were detected from immunoprecipitated S100A4 which immunoblotted with anti-GFP (Figure 3.22-A). In terms of S100A4, there is an obvious expression of S100A4 being immunoprecipitated from GFP in RLC-WT cells, but the highest level of S100A4 expression was estimated in T18A\S19A cells and the lowest signal was detected in T18D\S19D cells (Figure 3.22-B). Input and flow-through or unbound proteins were also immunoblotted for GFP and S100A4. From these results, we can conclude that S100A4 can interact with GFP-myosin IIA in cell lysates expressing phosphodeficient and phosphomimetic mutants of RLC, but some of S100A4 molecules can make a complex with GFP-myosin IIA. In addition, these findings support our immunoprecipitation results using A431/ZEB2-WT cells. As a control, HA-probe Y-11 antibody was used for immunoprecipitation and cell lysates were immunoblotted for S100A4 (Figure 3. 22-C). We did not detect a clear band which indicates there was no interaction between S100A4 and HA-Y-11 protein. In conclusion, S100A4 was successfully immunoprecipitated from cell lysates using anti-GFP and anti-S100A4 antibodies.

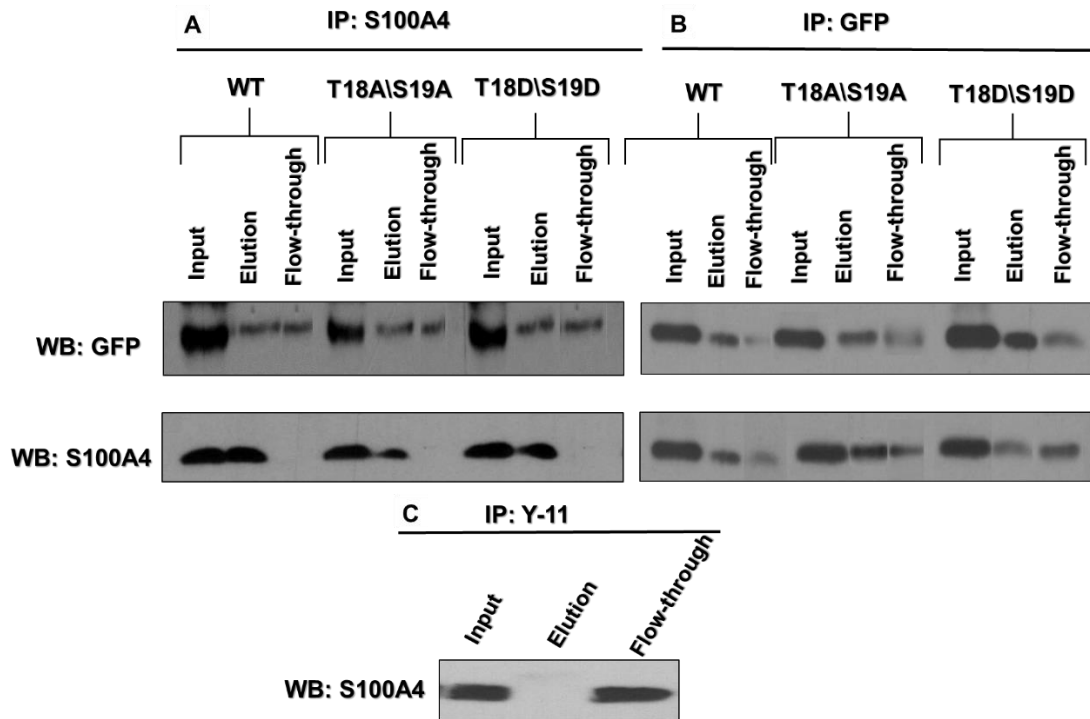


**Figure 3-22: Immunoprecipitation of S100A4 and GFP-myosin IIA from cells expressing RLC-WT and mutants.**

Dox treated RLC-WT, T18A/S19A and T18D/S19D cells were lysed in IP buffer. A- S100A4-protein complexes were immunoprecipitated with a monoclonal mouse S100A4 antibody, lysates were resolved by SDS-PAGE. Blotted membranes were stained against GFP and S100A4. B-GFP-protein complexes were immunoprecipitated with a polyclonal rabbit anti-GFP antibody and cell lysates were then analysed by Western blotting using specific antibodies for GFP as well as for S100A4. C- IP: Y-11 (control). The total protein extracted from cells was shown in input, elution indicates bound protein, while flow-through indicates unbound fraction. Results representative of two separate experiments.

### 3.4.2.3 Assessment of S100A4-myosin IIA localization in cells expressing phospho-RLC- mutants by confocal microscopy

To evaluate the effect of myosin light chain phosphorylation on S100A4 and myosin distribution in cells, immunofluorescence staining analysed by confocal microscopy was then performed. The distribution of S100A4 and GFP-myosin IIA proteins within cells expressing RLC-WT, phosphodeficient T18A/S19A and phosphomimetic T18D/S19D cells was

compared. Cells were fluorescently stained with monoclonal anti-S100A4 and polyclonal rabbit anti-GFP antibodies. S100A4 distribution did not change significantly between mutants and control, but less nuclear localisation was observed in T18D/S19D cells. Additionally, the result exhibited a strong effect of RLC phosphorylation on myosin II A assembly which was characterised specifically in T18D/S19D cells (Figure 3.23). In contrast, T18A/S18A cells seemed to have less myosin II filaments in the compared with T18D/S19D cells. Moreover, a strong co-localisation between S100A4 and GFP-myosin IIA was detected apparently in a phosphodeficient T18A/S19A cells.

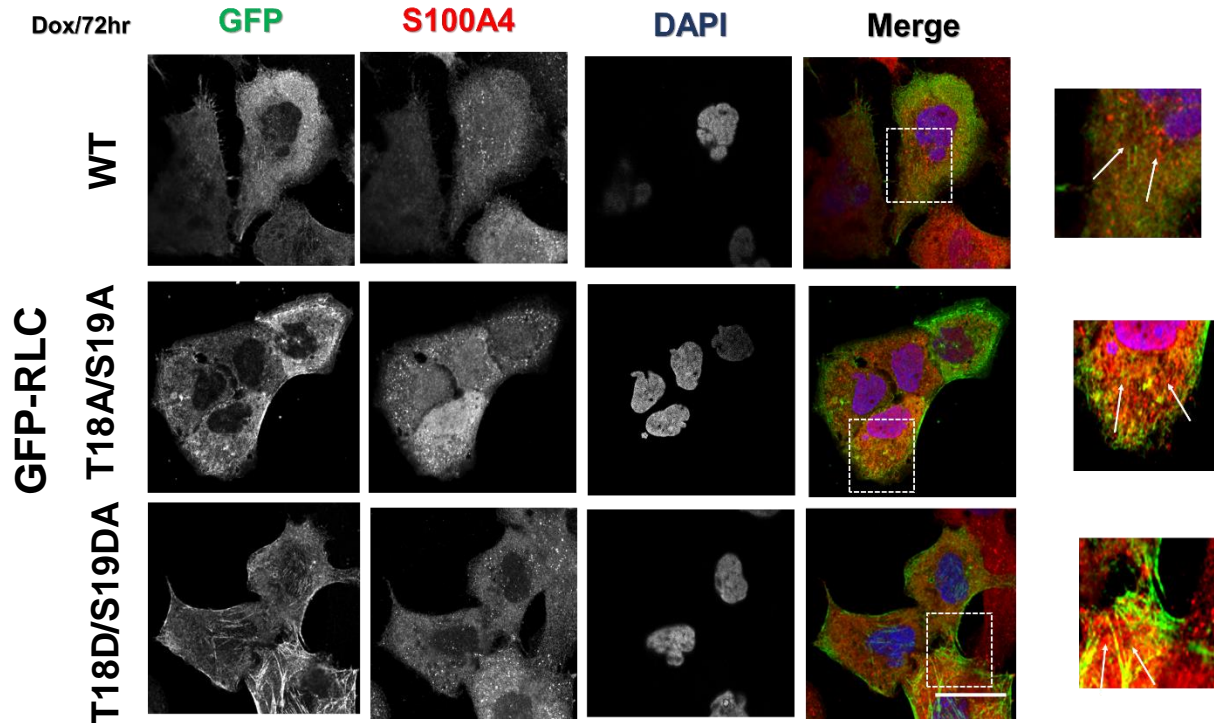


**Figure 3-23: Localisation of S100A4 and GFP-myosin IIA in cells expressing RLC-WT and mutants during EMT.**

Dox treated cells expressing GFP-RLC-WT, T18A/S19A, T18D/S19D cells were fixed with 4% PFA, permeabilised and fluorescently stained for GFP (left panels), S100A4 (middle left panels), followed by staining the nuclei with DAPI (middle right panels). Right panels show the combined images of the three panels (Merge). Scale bar = 8  $\mu$ m. White arrows show the regions of co-localisation between S100A4 and GFP-myosin IIA. White arrows indicating the area of co-localisation between S100A4 and GFP-myosin IIA.

#### **3.4.2.4 S100A4 colocalises with GFP-myosin IIA in cells expressing RLC-WT and mutants.**

To further analyse S100A4-GFP-myosin IIA interaction in cells expressing RLC-WT and mutants, double immunogold labelling technique was carried out. Resin embedded sections of Dox treated RLC-WT cells were labelled with anti-GFP and anti-S100A4 antibodies (Figure 3.24). Regarding cells expressing RLC-WT, the nearest-neighbour statistical analysis display a significant co-localisation between S100A4 and GFP-myosin IIA at distances corresponding to 50 nm and 150 nm (Figure 3.25-A) which are consistent with both 10S and 6S myosin monomers, indicating a co-localisation between S100A4 and GFP-myosin IIA in RLC-WT cells confirming our observation in A431/ZEB2-WT cells.

In order to further analyse the effect of the RLC phosphorylation on S100A4-myosin IIA interaction in cells, we tested the localisation of myosin IIA in cells expressing RLC-WT using the same technique. Cells were immunogold labelled for GFP and MHC IIA. Data showed statistically significant co-localisation between GFP and MHC IIA at peaks corresponding to 50 nm and 150 nm distances (Figure 3.25-B) and (Figure 3.25-C) reflecting 10S and 6S conformations. These results proved that RLC phosphorylation does not have an effect on S100A4-GFP-myosin IIA interaction *in vivo*.

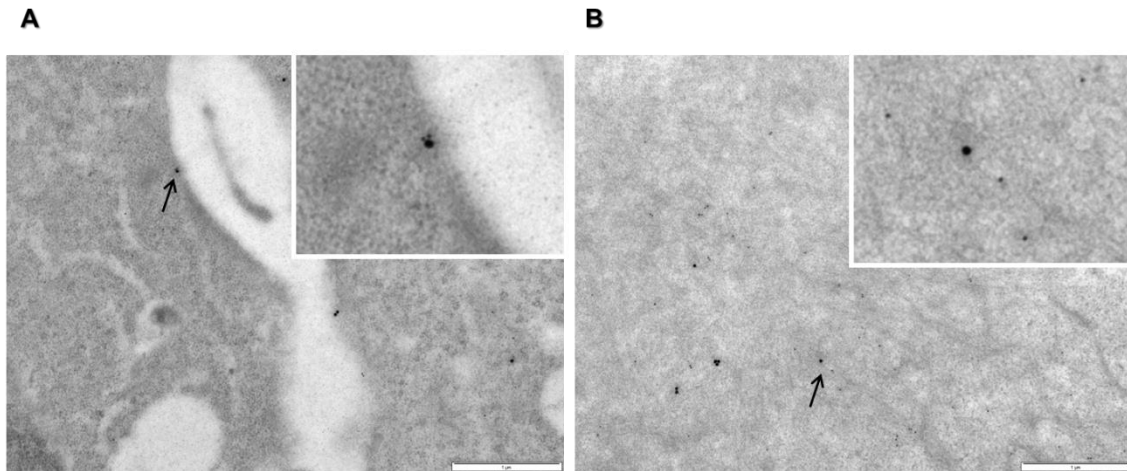


**Figure 3-24: Electron micrographs of double immunogold labelling of cells expressing RLC-WT for MHC IIA and GFP.**

Resin embedded sections of Dox treated of cells expressing RLC-WT were immunogold labelled for MHC IIA and GFP and visualised using 30 nm and 15 nm gold-conjugated secondary antibodies, respectively. The localisation of MHC IIA was detected at distances; A- 30 nm. B-145 nm. Scale bar =1 $\mu$ m.

## RLC-WT

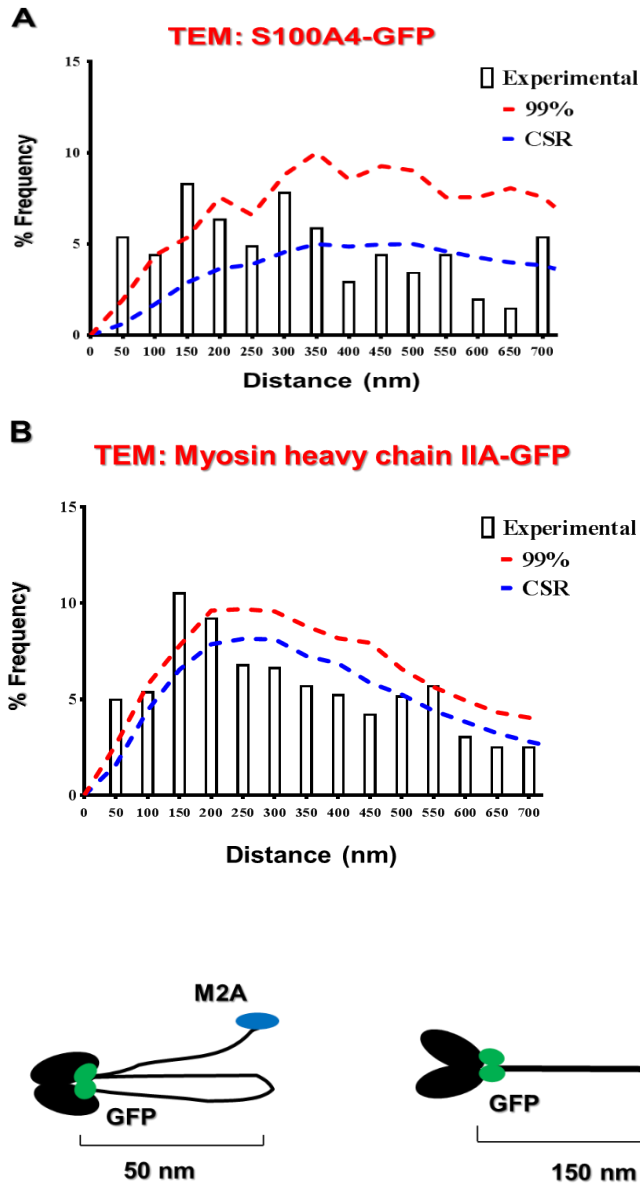


**Figure 3-25: S100A4 interacts with 10S and 6S myosin IIA monomers in RLC-WT cells**

Resin embedded sections of Dox treated cells expressing RLC-WT were immunolabelled for A-GFP and S100A4 and visualised using 30 and 15 nm gold-conjugated secondary antibodies, respectively. Nearest-neighbour co-localisation analysis of three independent experiments demonstrates statistical significant co-localisation of S100A4 with both 10S and 6S conformation of myosin IIA. B-MHC IIA and GFP antibodies and visualised using 30 and 15 nm gold-conjugated secondary antibodies, respectively. C-Myosin IIA exists as monomers of 10S and 6S forms. Blue dashed line reflects random distribution between small particles (15nm) and large particles (30 nm) (CSR). 99% confidence interval (CI). These results represent the analysis of 670 images of three independent experiments.

Moreover, we examined S100A4 and GFP-myosin IIA co-localisation in T18A/S19A and T18D/S19D cells. With respect to T18A/S19A, the nearest-neighbour statistical analysis show a single statistically significant peak at a distance corresponding to 50 nm, which reflects the 10S state of myosin IIA. In the same line with previous work in our laboratory (Irvine, 2012) who showed that inhibition of RLC phosphorylation switches myosin IIA monomer from 6S to 10S conformation which interacts significantly with S100A4. Of note, multiple peaks were detected in phosphomimetic T18D/S19D cells at the distances corresponding to 50 nm, 150, 200, 250, 300 nm and 350 nm (Figure 3.26-A). This finding indicates that the majority of myosin IIA presents in 6S conformation and filaments and S100A4 interacts with both. However, one peak corresponding to 50 nm is still present suggesting that some cells are still expressed RLC-WT. Phosphorylation of RLC at Ser19 and Thr18 promotes conformational changes of myosin IIA from 10S to 6S enables myosin to assemble into filaments (Barros et al., 2003). These multiple peaks indicating a presence of multiple myosin structures initiated by a presence of the phosphomimetic (DD) amino acids.

Myosin structures were analysed in cells expressing the RLC T18A/S19A and T18D/S19D mutants (Font-Burgada et al., 2016). T18D/S19D cells were immunolabelled with anti-GFP and anti-MHC IIA antibodies. Data show multiple peaks in T18D/S19D cells in comparison to one specific peak at 50 nm in T18A/S19A cells (Figure 3.26-B).

In conclusion, these findings confirmed the hypothesis that dephosphorylated RLC triggers the folded 10S conformation of myosin IIA in cells. Furthermore, the results show that S100A4 interacts significantly with only the 10S conformation of myosin in cells expressing the RLC-T18A/S19A mutant. We also observed for the first time that S100A4 can interact with myosin IIA filaments as seen in T18D/S19D cells.

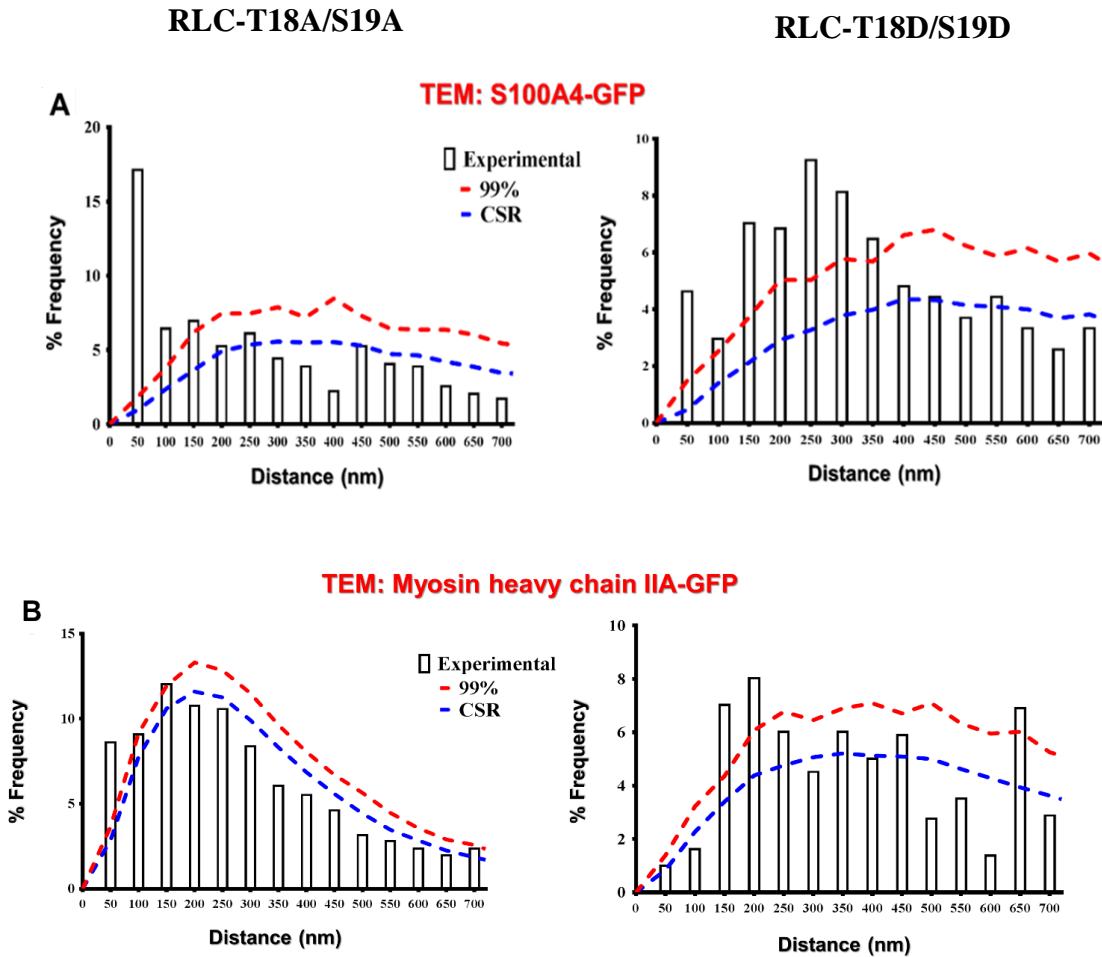


**Figure 3-26: S100A4 interacts only with 10S myosin monomer in T18A/S19A cells**

Resin embedded sections of Dox treated A431/ ZEB2 cells expressing phosphodeficient and phosphomimetic GFP-RLC-T18A/S19A or T18D/S19D were immunolabelled with A-anti-GFP and anti-S100A4 antibodies and visualised using 30 and 15 nm gold-conjugated secondary antibodies, respectively. B- anti-MHC IIA and anti-GFP antibodies and visualised using 30 and 15 nm gold-conjugated secondary antibodies, respectively. Nearest-neighbour co-localisation analysis of three independent experiments was carried out. Blue dashed line reflects random distribution between small particles (15nm) and large particles (30 nm) (CSR). 99% confidence interval (CI). These cells represent the analysis of 1750 images of three independent experiments.

#### **3.4.2.5 S100A4 promotes 10S conformation of myosin IIA in RLC-T18A\S19A cells**

Previous results confirmed that S100A4 maintains the balance between 10S and 6S states in cells. As such, the functional consequence of S100A4 knockdown on regulation myosin IIA dynamics in T18A\S19A cells was examined. Thus, cells were transfected with either non-targeting (siControl) or targeting S100A4 siRNA (siS100A4) and grown in the presence of Dox for 48 hrs. Consequently, the level of S100A4 expression was remarkably reduced in siS100A4 transfected T18A\S19A cells. In addition, it was observed that there was no difference in the level of RLC expression upon knockdown of S100A4 (Figure 3.27).

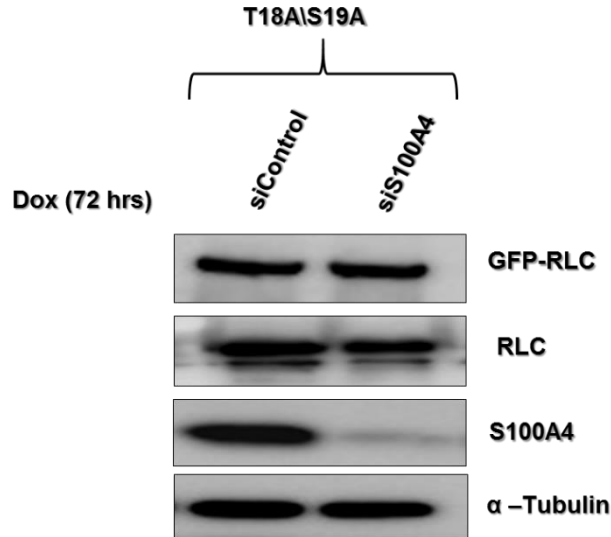


**Figure 3-27: RNAi-mediated knockdown of S100A4 in RLC-T18A/S19A cells.**

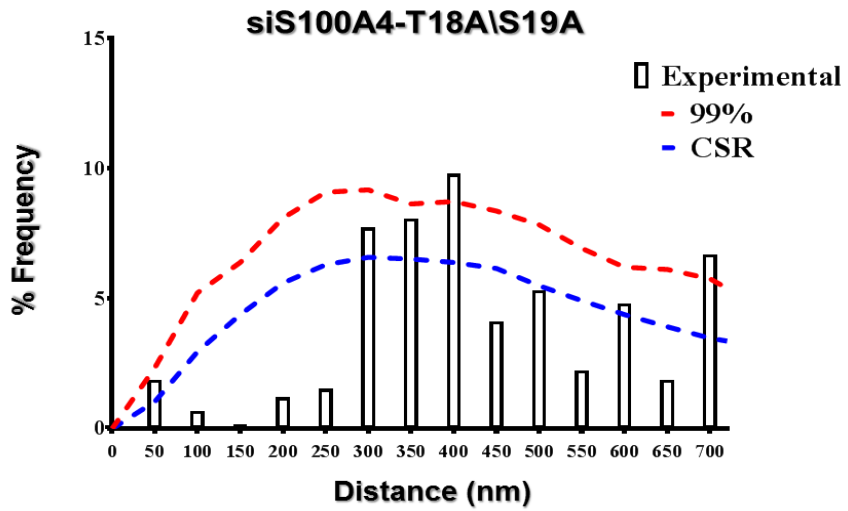
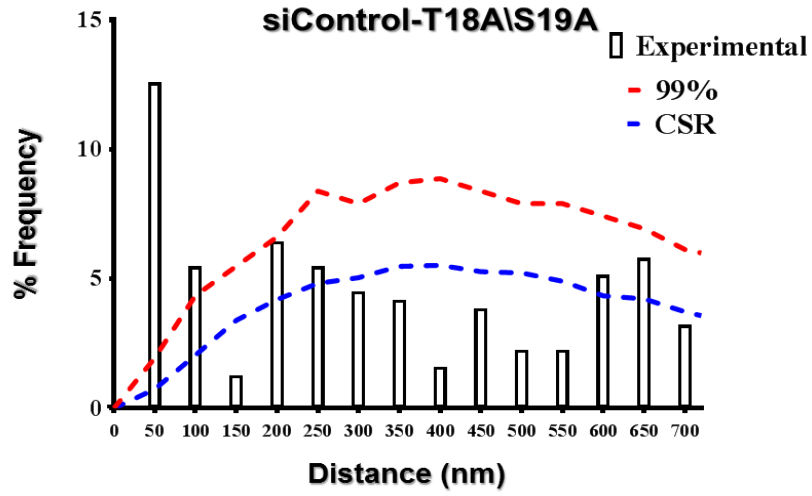
RLC-T18A/S19A cells were transfected either with siControl or siS100A4 and cultured in the presence of Dox for 48 hrs. Lysates were collected and proteins were analysed by Western blotting. Membranes were probed against GFP, RLC and S100A4.  $\alpha$ -Tubulin was used as a loading control.

Subsequently, we further tested the functional role of S100A4 in controlling 10S-6S transition in cells. Ultrathin resin sections of transfected cells were immunolabelled with anti-S100A4 and anti-GFP antibodies. Data from nearest neighbour statistical analysis detect the co-localisation between S100A4 and myosin IIA at one significant peak corresponding to 50 nm which reflects the bending form of myosin 10S. This result is in agreement with the previous data in section 3.3.1.4.4. This peak is consistent with there being only the 10S monomeric form of myosin in cells expressing the RLC-T18A/S19A mutant (Figure 3.28-A). As a result of S100A4 suppression, no specific peaks were detected in siS100A4 transfected T18A/S19A cells. However, it is necessary to further prove the role of S100A4 in maintaining myosin IIA in 10S form. Thus, to test this observation, double immunogold labelling for MHC IIA and GFP was carried out. Resin embedded cell sections were labelled for MHC IIA and GFP. As illustrated in (Figure 3.28-B), myosin IIA molecules were present as 10S conformation in siControl which was detected as one specific peak 50 nm. In contrast, in siS100A4 cells, the conformation of myosin IIA molecules were significantly estimated at distances corresponding to 150, 200 and the least 250 nm. In spite of RLC

dephosphorylation, myosin IIA exists as extended 6S monomeric form and possibly some intermediate structures of myosin IIA filaments could be detected. Considering these results, the folded form of 10S form was estimated in phosphodeficient siControl transfected T18A/S19A cells, while 6S myosin monomer and some filaments was shown in siS100A4 transfected T18A/S19A cells. To conclude, S100A4 can contribute to regulate an equilibrium between 10S and 6S states of myosin monomers and controls assembly/disassembly of myosin IIA into filaments in cells.

# TEM: S100A4-GFP

## A



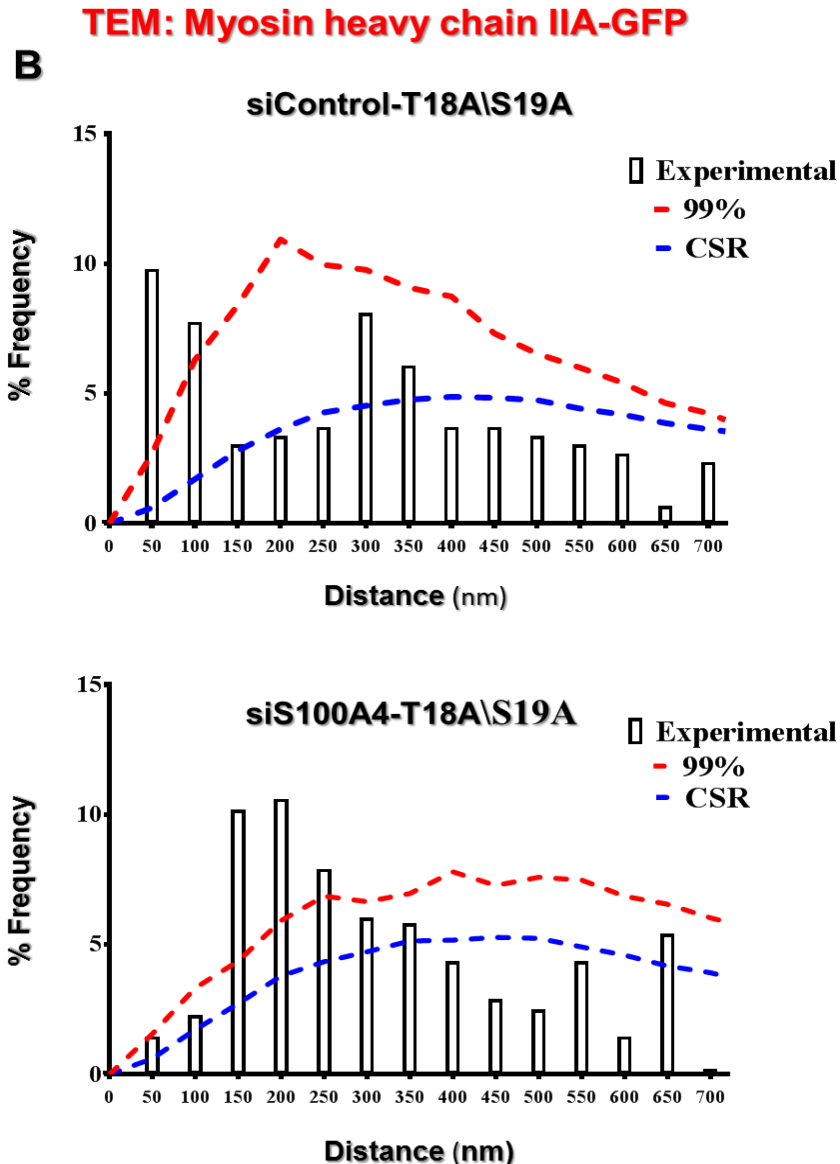


**Figure 3-28: Knockdown of S100A4 promotes assembly of myosin IIA into filaments in RLC- T18A\S19A mutants**

Resin embedded sections of siControl-T18A\S19A and siS100A4-T18A\S19A cells were immunolabelled with anti-S100A4 and anti-GFP antibodies, visualised using 15 nm and 30 nm gold-conjugated secondary antibodies, respectively (A) and Anti-MHC IIA and anti-GFP antibodies, visualised using 30 and 15 nm gold-conjugated secondary antibodies, respectively (B). A-. The co-localisation analysis detected only one statistically significant peak of 50 nm which reflects 10S myosin monomer. B-. The co-localisation analysis data estimated the significant peak at a distance of 50 nm in siControl cells which illustrates the existence of myosin IIA monomer into 10S form, while the peaks shift to 150, 200 and 250 nm in siS100A4 cells indicating the existence of myosin IIA into assembled 6S form and intermediate structures might be formed during formation of filamentous myosin. Results represents the analysis of 690 images from three independent experiments.

### **3.4.3 Effect of MHC phosphorylation on S100A4-myosin IIA interaction**

We previously described the effect of regulatory light chain phosphorylation on S100A4-GFP-myosin IIA interaction in cells. This was followed by analysis of the impact of the myosin heavy chain phosphorylation on S100A4-GFP-myosin IIA. Therefore, mutants of myosin heavy chain IIA constructs as GFP fusions were created including a model of phosphodeficient and phosphomimetic MHC IIA (Dulyaninova et al., 2007). pEGP plasmid contains GFP-tagged WT and mutants of MHC was used. A431/ZEB2 cells were transfected with the plasmid and cultivated in the presence of puromycin. Ser1943 was substituted with alanine, aspartic or glutamic acid in both the full-length GFP-MHC IIA and myosin IIA rods. Subsequently, myosin specific mutants of heavy chains were used to probe the effect of myosin heavy chain phosphorylation on the S100A4 binding.

Kriajevska and colleagues (Kriajevska et al., 2000) reported that phosphomutant Ser1943D does not influence on the S100A4-myosin IIA interaction. Later, data from (Dulyaninova et al., 2007) showed a 7- fold reduction in the binding affinity of S100A4 to myosin IIA as result of phosphorylation of MHC at Ser1943. Conversely, it was shown that Ser1943 phosphorylation did not affect the interaction of myosin IIA with S100A4 using phosphomimetic mutants of myosin IIA replacing Ser1943 with either Asp or Glu. In spite of overlapping with S100A4 binding site, it was shown that phosphorylation of MHC at S1916 does not affect the interaction with S100A4. In subsequent experiments described in this chapter, A431/ZEB2 cells expressing GFP-MHC phosphodeficient S1943A and phosphomimetic S1943D/E cells were cultured in the presence of Dox for 72 hrs that triggered expression of ZEB2.

#### **3.4.3.1 The effect of myosin heavy chain mutation on EMT**

Next, we analysed the effect of myosin heavy chain phosphorylation on ZEB2-induced EMT and activation of S100A4 expression. Western blot analysis showed that S100A4 was actively expressed in the MHC-phosphodeficient S1943A and phosphomimetic S1943D/E cells. It was shown that the MHC IIA mutation did not have an effect on EMT. A similar level of expression of S100A4 and vimentin was detected in S1943D and S1943E and cells. However, it was expressed more highly in S1943A cells. The expression of myosin IIA heavy

chain and GFP did not affect EMT as we detected an equivalent level of expression of this proteins in all mutants. In addition, we detected a dramatic increase in the expression level of ZEB2 in S1943E cells compared with S1943A and S1943D mutants. The expression of E-cadherin was decreased in cells expressing GFP-MHC phosphodeficient and phosphomimetic mutants during EMT. However, it was higher in S1943A cells compared to other mutants (Figure 3.29).

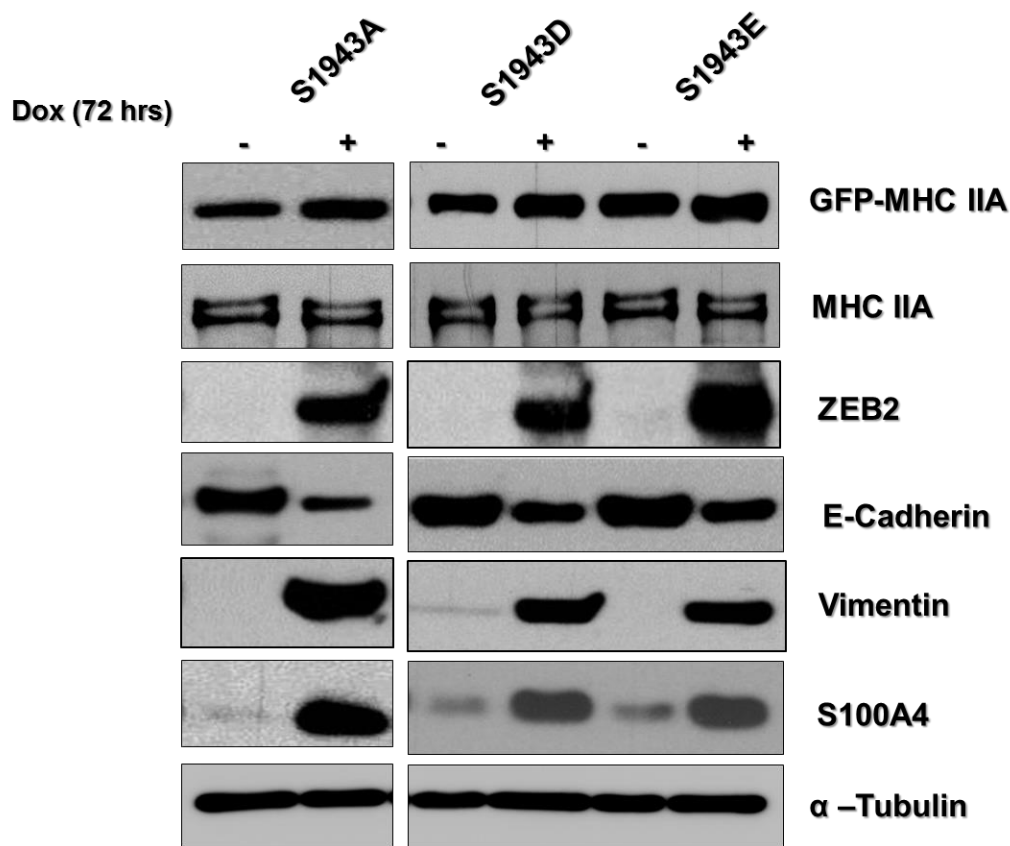


**Figure 3-29: Western blot analysis of lysates of A431/ZEB2 cells expressing MHC phosphodeficient and phosphomimetic cells.**

MHC-S1943A, S1943D and S1943E cells were maintained in the absence and the presence of Dox for 72 hrs. Cell lysates were resolved on SDS-PAGE. Membranes were stained for GFP, vimentin, S100A4 and E-cadherin.  $\alpha$ -Tubulin was used as a loading control.

### **3.4.3.2 Assessment of myosin heavy chain phosphorylation on S100A4-myosin interaction in cells**

To study the interaction of S100A4 with GFP-myosin IIA in cells expressing phosphodeficient and phosphomimetic mutants, co-immunoprecipitation assay was carried out. To test this, S100A4 and GFP-myosin IIA complexes were immunoprecipitated from cell lysates using either monoclonal anti-S100A4 or polyclonal anti-GFP antibodies. Briefly, cells were lysed, and beads were washed by IP buffer three times. Protein complexes were evaluated by immunoprobings with S100A4 and GFP antibodies. As shown in (Figure 3.30), a clear expression of GFP and S100A4 were readily detected from immunoprecipitated S100A4 in S1943A and S1943D/E cells indicating the formation of S100A4-myosin IIA complexes (3.30-A). The immunoprecipitated GFP-myosin IIA was also blotted with anti-GFP and anti-S00A4 antibodies. Strong bands that corresponded to GFP were detected in phosphodeficient and phosphomimetic mutants, while S100A4 expression was decrease in S1943D/E cells, noticeably weaker in S1943A mutant (3.30-B). This result provides a conclusion that phosphorylation of MHC does not have an effect on the interaction between S100A4-myosin IIA *in vitro*. As a negative control, cell lysates were incubated with HA-Y-11 antibody and blotted for S100A4 and GFP (NA).

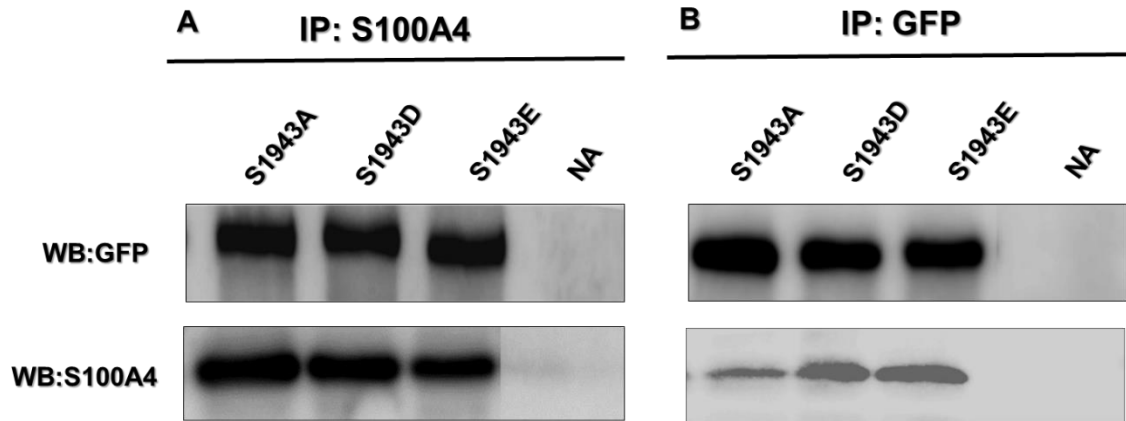


**Figure 3-30: S100A4-myosin IIA complexes were detected in A431/ZEB2 cells expressing phosphodeficient and phosphomimetic MHC IIA mutants.**

Lysates from A431/ZEB2 cells expressing phosphodeficient and phosphomimetic MHC IIA mutants treated with Dox were used for IP. Cells were lysed in IP buffer. A-S100A4-protein complexes were immunoprecipitated with a monoclonal mouse anti-S100A4 antibody, eluted from beads and resolved on SDS-PAGE. Membranes were blotted against GFP and S100A4. B-GFP-protein complexes were immunoprecipitated with a polyclonal rabbit anti-GFP antibody. Western blot analysis was then performed using specific antibodies for GFP as well as for S100A4. NA (control; IP-Y-11).

### **3.4.3.3 Assessment of S100A4-myosin IIA localization in cells expressing phospho-MHC IIA- mutants by confocal microscopy.**

To further examine the effect of MHC IIA phosphorylation on the co-localisation of S100A4 and GFP-myosin IIA in cells, immunofluorescence staining was performed. Thus, cells expressing MHC IIA-phosphodeficient S1943A and phosphomimetic S1943D/E mutants were stained for GFP-myosin IIA and S100A4. In general, cells expressing MHC-phosphomimetic S1943D/E mutants exhibited more mesenchymal traits with visible lamellipodial protrusions compared with cells expressing phosphodeficient S1943A. Cells expressing S1943A mutant displayed a diffuse distribution of both proteins throughout the cytoplasm and the area of co-localisation was detected along the stress fibres network and around the nucleus. However, a considerable reduction of filaments was observed in S1943D/E cells. (Dulyaninova et al., 2007) study suggested that cells expressing MCH IIA S1943D and S1943E exhibited a decrease in the formation of myosin filaments compared with the wild type, whereas cells expressing the S1943A mutant displayed an enhanced network of filaments. In addition, it was shown that S100A4 distribution did not change markedly in cells expressing different myosin mutants. Furthermore, a strong co-localisation between S100A4 and GFP-myosin IIA was detected in cells expressing S1943D and S1943E mutants (Figure 3.31). This observation indicates that MHC phosphorylation facilitates S100A4-myosin interaction.

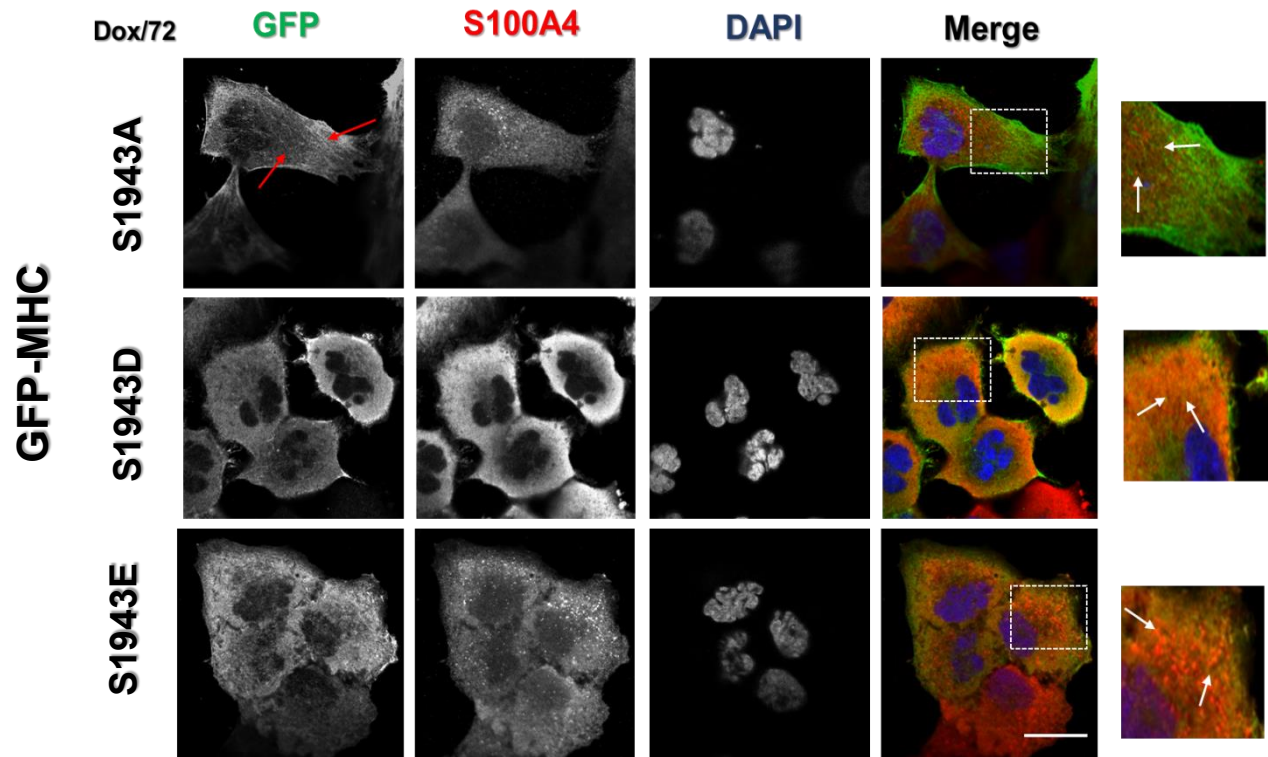


**Figure 3-31: Localisation of S100A4 and GFP-myosin IIA in cells expressing MHC IIA mutants.**

Dox treated S1943A and S1943D/1943E cells were fixed with 4% PFA, permeabilized and fluorescently stained with anti-GFP antibody (left panels), anti-S100A4 antibody (middle left panels), followed by staining nuclei with DAPI (middle right panels). Right panels show the combined images of the three panels (Merge). White arrows in selected zoomed images presented on the right of the merge panels show the area of co-localisation between S100A4 and GFP-myosin IIA, while red arrows show the distribution of the myosin IIA filaments in 1943A cells. Scale bar = 8  $\mu$ m

#### **3.4.3.4 S100A4 co-localises with GFP-myosin IIA in cells expressing MHC IIA mutants**

To investigate the interaction between S100A4 and myosin IIA in phosphodeficient MHC-S1943A cells, immunogold labelling technique was performed. Cells were immunolabelled for S100A4 and GFP. The nearest-neighbour statistical analysis revealed a significant co-localisation between the proteins which was detected as a strong peak corresponding to 150

nm (Figure 3.32-A). However, multiple small peaks at distances 50, 100 and 200 nm were shown. These distances most likely reflect the intermediate structures that possibly formed during polymerisation of myosin IIA into filaments. Subsequently, sections of cells expressing MHC-S1943A mutant were labelled for myosin IIA and GFP to analyse the composition of myosin IIA molecules. Three distinctive peaks were observed at distances corresponding to 100 and 150 nm (Figure 3.32-B). These peaks are consistent with 6S myosin IIA monomers. However, unexpected peak corresponding to 50 nm was present indicating that some proportion of myosin IIA was in 10S conformation. This could be due to the partial phosphorylation of myosin IIA in cells expressing S1943A mutant.

## MHC-S1943A

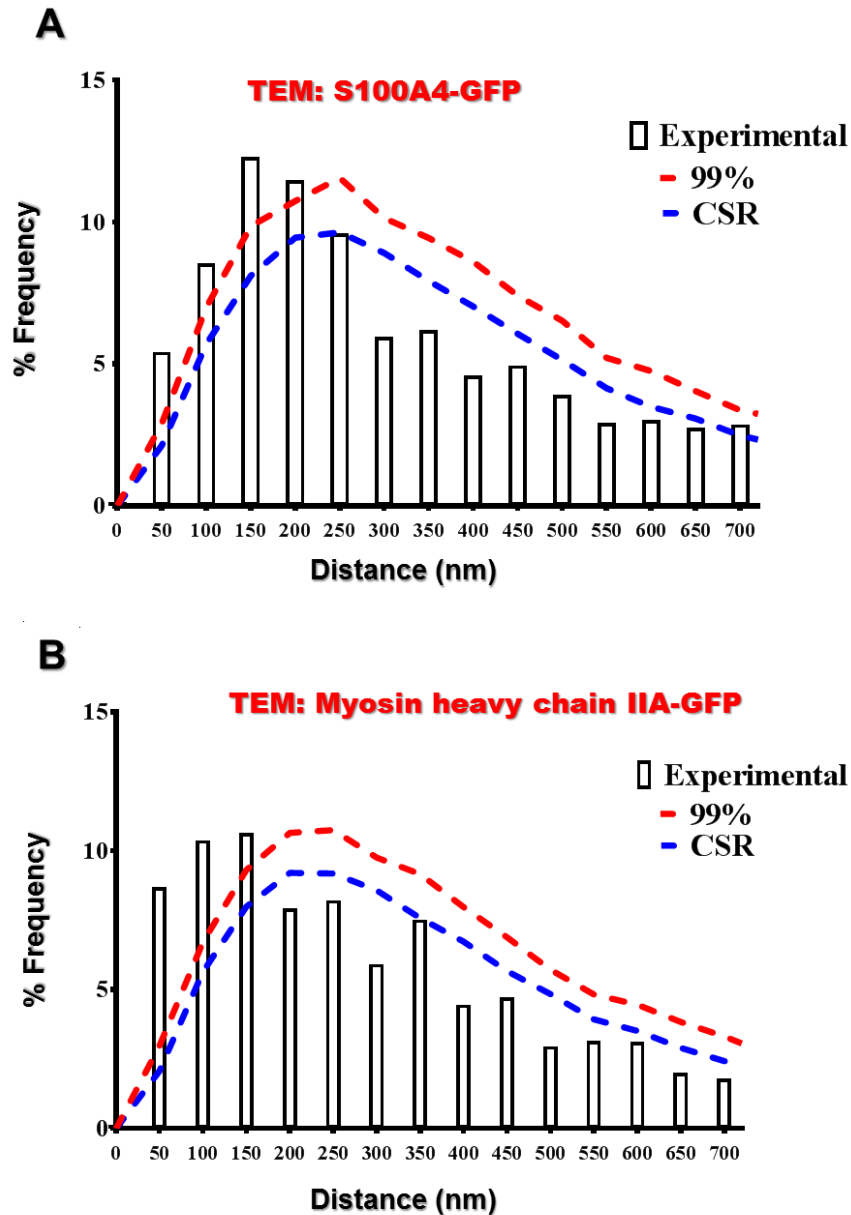


**Figure 3-32: Dephosphorylation of MHC IIA promotes formation of 6S assembly-competent conformation.**

Resin embedded sections of Dox treated MHC-S1943A cells were immunolabelled for A- GFP and S100A4 and visualised using 30 and 15 nm gold-conjugated secondary antibodies, respectively. The images were collected and nearest-neighbour statistical analysis was used. The data detect multiple peaks at distances corresponding to 50, 100, 150, and 200 nm. B- Sections of resin embedded cells were labelled with antibodies against MHC IIA and GFP and visualised using 30 and 15 nm gold-conjugated secondary antibodies, respectively. Three distinctive peaks corresponding to 50, 100 and 150 nm were estimated. Blue dashed line reflects random distribution of small particles (15nm) and large particles (30 nm) (CSR). 99% confidence interval (CI).

#### **3.4.3.5 S100A4 promotes 10S conformation of myosin IIA in MHC-S1943D cells**

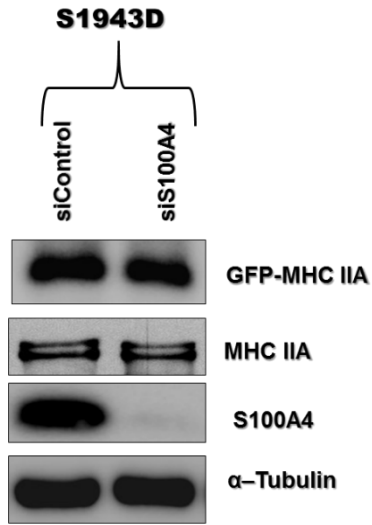
To further examine the functional role of S100A4 in regulation the 6S–10S transition and underlying mechanism controlling myosin IIA assembly, knockdown of S100A4 in cells expressing phosphomimetic myosin heavy chain was performed. Cells were transfected with non-targeting S100A4 and targeting S100A4 siRNA and they were grown in the presence of Dox for 48 hrs.

Western blot analysis showed an efficient knockdown of S100A4 in siS1004 transfected S1943D cells compared with siControl transfected S1943D cells which was characterised as a significant down-regulation of S100A4 expression in siS1004 transfected S1943D cells (Figure 3.33-A). Subsequently, cell sections were immunogold labelled for S100A4 and GFP. Analysis of S100A4-myosin complexes seemed to be specific only at one peak, corresponding to 50 nm in siControl transfected S1943D cells, which consistent with 10S conformation of myosin monomer (Figure 3.33-B). Majority of studies have suggested that phosphorylation of myosin heavy chain induces the 10S conformation of myosin IIA monomer and prevents filaments formation (Dulyaninova et al., 2005, Billington et al., 2013a, Li and Bresnick, 2006). To validate this finding, the same protocol was used to label cells against myosin IIA and GFP (Figure 3.33-C). It was shown that in the absence of S100A4 two peaks were detected corresponding to 150 and 250 nm which indicates the existence of myosin IIA in 6S conformation as preexisting state for myosin IIA polymerization. We used the same approach in analysing cells expressing S1943E and we have reached the same result (Figure 7.7 in appendix).

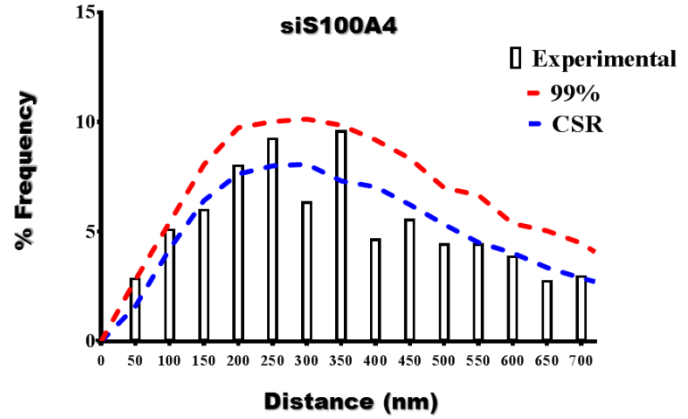
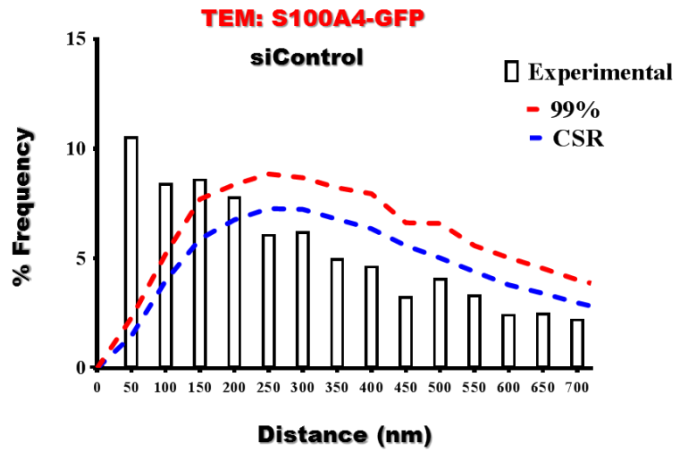
Taken together, these findings suggest a role for S100A4 in regulating 10S-6S equilibrium in cells. S100A4 can form a complex with myosin IIA in cells expressing MHC IIA mutants.

# MHC-S1943D

**A**



**B**



## MHC-S1943D

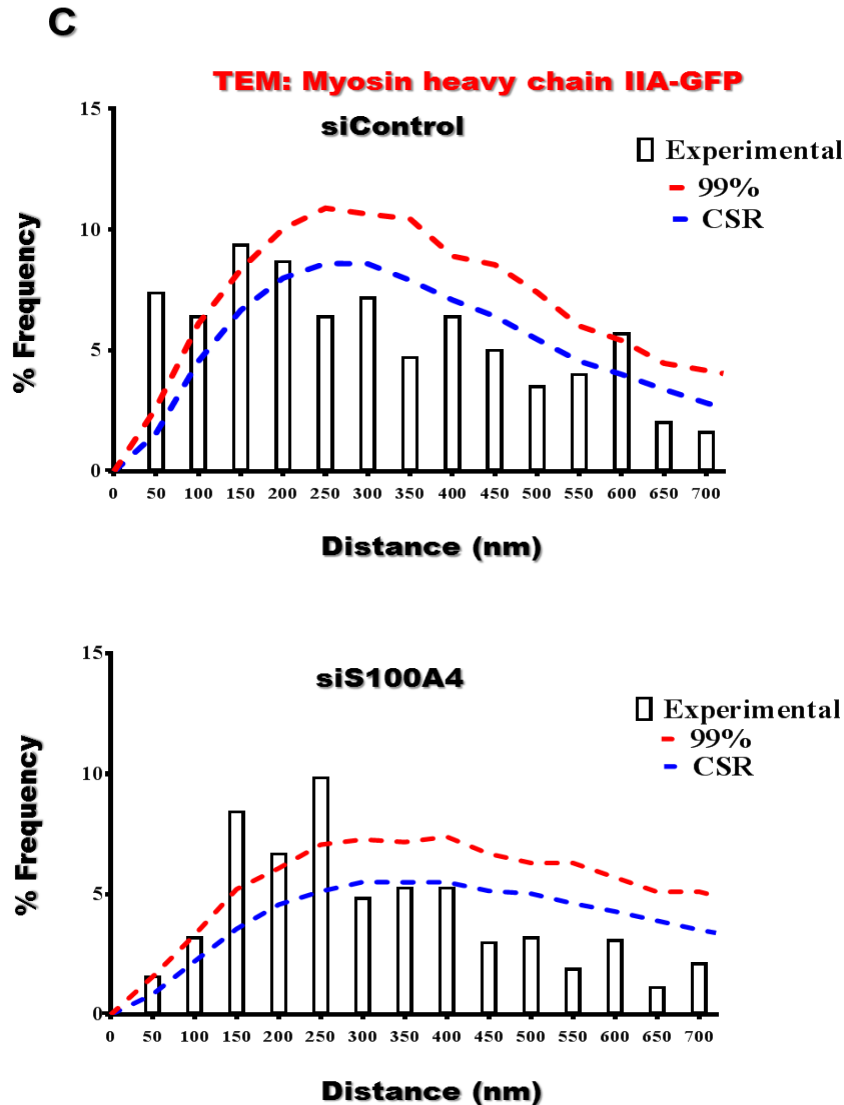


**Figure 3-33: Knockdown of S100A4 in MHC-S1943D cells leads to a dramatic shift of myosin IIA monomer from 10S toward 6S form.**

A- Western blot analysis analysis of proteins expression in siControl transfected S1943D and siS100A4 transfected S1943D cells. Cells were resolved on SDS PAGE and membranes were blotted for S100A4, GFP, MHC IIA.  $\alpha$ - Tubulin was used as a loading control. B- Sections of resin embedded siControl/siS100A4 cells were immunogold labelled for GFP and S100A4, and visualised using 30 and 15 nm gold-conjugated secondary antibodies, respectively. The nearest neighbour co-localisation analysis of two independent experiments shows only one statistically significance peak between 25-75 nm. C- Sections of resin embedded siControl/siS100A4 cells were immunolabelled for MHC IIA and GFP and visualised using 30 and 15 nm gold-conjugated secondary antibodies, respectively. One statistical significant peak was detected at 50 nm in siControl cells, while two peaks of statistical significance at 150 and 250 nm were detected in siS100A4 cells. Blue dashed line reflects random distribution of small particles (15nm) and large particles (30 nm) (CSR). 99% confidence interval (CI).

### 3.5 Discussion

S100A4 expression modulates the migratory properties of a wide range of cell types by its interaction with several target proteins such as the heavy chain of NM IIA (Kriajevska et al., 1994). The results in this chapter investigated the molecular mechanism underlying S100A4 function in EMT and provide in cells data highlighting its role in regulating of myosin activity. The aim of this chapter was to characterise NM IIA-S100A4 interaction in cells and to identify the effect of this interaction on the cytoskeletal dynamics. In this study, we chose to analyse this interaction in human epidermoid carcinoma A431 cells with a Tet-On inducible expression of ZEB2, a master regulator of EMT (Mejlvang et al., 2007).

Since the assembly of non-myosin IIA into filaments is regulated mainly by phosphorylation of the regulatory light chain at Ser19 and Thr18 as well as by phosphorylation of heavy chain at Ser 1916 and Ser 1943 (Juanes-García et al., 2016), it was of interest to analyse how this phosphorylation affect the S100A4-myosin IIA interaction in cells. For this purpose, we generated cell lines constitutively expressing phosphomimetic and phosphodeficient mutants of GFP-tagged RLC and MHC constructs. As phospho-site mutations at Ser19 and Thr18A, aspartic acid substitutions (RLC-D) are used to mimic phosphorylation, whereas a constitutive phosphodeficient mutant is mimicked by alanine substitutions (RLC-A). Likewise, Ser 1943 was substituted with either aspartic acid (Ser 1943D) /glutamic acid (Ser 1943E) or alanine (Ser 1943A).

Western blotting confirmed expression of S100A4 and indicated that the expression of GFP-NM IIA was approximately equal to the endogenous NM IIA. In addition, immunofluorescence analysis of S100A4 and GFP-myosin IIA expression in A431/ZEB2 cells show an obvious distribution of both proteins throughout the cytoplasm associated with nuclear localisation of S100A4. Furthermore, images exhibited little distribution of stress fibers in cells expressing Thr18A distribution and S1943D/E mutants. In contrast, a cytoplasmic distribution of myosin IIA was displayed in T18D/S19D and S1943A cells expressing which was correlated with increased stress stress fibers network (Figure 3.23) and (Figure 3.31). This observation is consistent with (Beach and Egelhoff, 2009) study who reported that GFP-tagged RLC constructs with alanine substitutions at the activating Thr18/Ser19 sites were still able to co-localise with other proteins. In agreement with Dulyaninova

and colleagues studies (Dulyaninova and Bresnick, 2013, Dulyaninova et al., 2007) reported that MDA-MB-231 cells expressing GFP-MHC-S1943E and S1943D mutants displayed a decrease filament assembly into stress fibers, whereas cells expressing GFP-reflects prominent stress fibers networks and strong cortical localization.

### **3.5.1 Evaluation of S100A4-myosin IIA complexes in A431/ZEB2 cells**

Biochemical studies established that S100A4 interacts with the C-terminal end of the MHC IIA coiled coil region and causes disassembly of myosin-IIA filaments; however, the mechanism by which S100A4 mediates myosin IIA depolymerization is still not well known (Kriajevska et al., 1994, Badyal et al., 2011, Ramagopal et al., 2013). It was reported that myosin peptides containing 15 residues bind to S100A4 with micromolar affinity that is compatible with a site involving a single EF-hand cleft (Malashkevich et al., 2008). Kinetic studies on myosin tail fragment suggests that S100A4 binds to the filament with moderate affinity in the presence of  $Ca^{2+}$  and actively dissociates the filaments to yield a S100A4-NM IIA “monomer” complex with nanomolar affinity (Badyal et al., 2011). Additionally, NMR analysis has shown that S100A4 dimer binds to a single myosin heavy chain in asymmetrical configuration. Conformational changes occur in S100A4 upon calcium-binding resulting in exposure of a hydrophobic cleft. This cleft serves as a site for myosin IIA binding (Elliott et al., 2012). Additionally, (Ramagopal et al., 2013) studied the X-ray crystal structure of the S100A4-myosin IIA complex suggesting a mechanism in which a single myosin IIA 1908-1923 peptide binding across the S100A4 dimer interface. Consequently, S100A4 induces partial unwinding of the myosin-IIA coiled-coil, and thereby promotes myosin-IIA filament disassembly. Data from recent study have shown that mutation of the two calcium-binding EF-hands in one S100A4 monomer caused a 30-60 fold decrease in the binding affinity for non-muscle myosin associated with reduced ability of S100A4 to regulate the monomer-polymer equilibrium of NM IIA (Chen, 2016).

There are many studies have confirmed the interaction between myosin IIA and S100A4 *in vitro*, *but in vivo* evidence supporting the formation of S100A4-myosin IIA complexes is more limited. The association between S100A4 and non-muscle myosin heavy chain was analysed in HeLa cells. The fluorescence resonance energy transfer-derived changes was determined in the fluorescence lifetime of enhanced cyan fluorescent protein (CFP) fused to

S100A4 in the presence of a recombinant fragment of the C-terminal region of NMHC IIA (Zhang et al., 2005), whereby S100A4-myosin IIA complexes were detected in MTC cell line which enhanced the invasive behaviour of cancer cells (Li and Bresnick, 2006). Furthermore, (Kim and Helfman, 2003) observed partial co-localisation between intact myosin IIA and S100A4 at the periphery of MDA-MB-231 cells by the light microscopy. The overexpression of S100A4 in macrophages mediates macrophages recruitment and promotes myosin filament disassembly leading to cellular formation of pseudopodial protrusions during chemotaxis (Dulyaninova and Bresnick, 2013).

In this chapter, a number of approaches were taken to examine the S100A4–GFP-myosin IIA complexes in A431/ZEB2 cells, focused on understanding the molecular mechanism underlying the role of S100A4 in regulating myosin dynamics. Co-immunoprecipitation analysis detected the S100A4-GFP-myosin IIA complexes in cells expressing phosphodeficient and phosphomimetic RLC and MHC IIA. Although GFP containing complexes were successfully immunoprecipitated from A431/ZEB2 cell lysates, a weak band reflecting traces of S100A4 in complex was detected by Western blotting indicating that not all myosin molecules can interact with S100A4 dimers. However, Western blot analysis showed GFP-tagged myosin was successfully precipitated from T18A/S19A and S1943D/E cells forming a complex with S100A4 which was characterised as strong band corresponding to S100A4 expression. Immunoprecipitated S100A4 was more efficient to detect myosin. IP approach for detection of S100A4-myosin complex in cell lysates and conditioned medium has been used by diverse groups. Consistent with (Chaabane et al., 2015), this group showed that S100A4 released from cells by immunoprecipitation to form complexes with other proteins. In addition, this observation is in agreement with other study (Li and Bresnick, 2006) showing that the myosin-IIA S100A4 binding site antibodies were successfully assessed by immunoprecipitation analysis using HeLa cell lysates. Similar to that (Bowers et al., 2012) suggested that immunoprecipitated S100A4 was effectively detected NM IIA from wild type A549 cells.

In the present work we also studied the S100A4-myosin IIA interaction *in vivo* by immunoelectron microscopy technique. We frequently observed the co-localisation between S100A4 and GFP-myosin IIA with gold particles separated by at distances of less than 200

nm, consistent with 10S and 6S myosin monomers. Nearest neighbour statistical analysis of TEM immunogold labelling detected the co-localisation of S100A4 with folded and extended monomers in cells as demonstrated in previous study from our laboratory (Irvine, 2012). However, analysis of the immunogold particle separation has several complications. Colloidal gold particles only stain the surface of tissue embedded in LR white resin (Stangel et al., 1987) which gives rise to a low efficiency of labelling compared with immunofluorescence labelling of non-embedded samples. As such, the observed co-localisation of gold particles about 2 to 4% has to be compared with that arise from chance encounter. Another problem in our interpretation is that close co-localisation between the epitops could arise from myosin in the filamentous state, S100A4 bound to the tail of one myosin molecule lying close to the GFP-labelled head of another myosin. While this might occur, we do not consider it to be the dominant state, because little co-localisation is seen between myosin filaments in stress fibers and S100A4 at the level of the light microscope.

A combination of Diggle's nearest neighbour function and Monte Carlo simulation showed that myosin molecules are localised at two statistically significant distances corresponding to 50 nm and 150 nm which are consistent with 10S and 6S monomers, respectively (Figure 3.12). These data not only detected the co-localisation of S100A4 and GFP-myosin IIA, but also displays the existence of myosin IIA in 10S and 6S conformations in cells, in agreement with (Irvine, 2012) finding. In addition, increased co-localisation with a compact 10S conformer is seen following treatment of cells with Y27632, an agent known to decrease the extent of myosin filament formation by abolishing myosin light chain phosphorylation resulting in switching myosin IIA from the unfolded 6S or filaments to folded 10S conformation (Figure 3.18).

Our results considered that S100A4 is not the only factor regulate monomer-polymer equilibrium, but it is likely that S100A4 binding shifts the balance toward the 10S monomer. In agreement with (Ford et al., 1997) suggested that the formation of the 10S state was a factor might contribute to promote solubilisation of intact myosin IIA filament by S100A4. Consequently, the majority of myosin IIA binding to S100A4 is expected to be in monomeric conformation. Previous work revealed that BM4 which is a monoclonal antibody interacts with C-terminal end of myosin in a position similar to the S100A4 binding site and blocks

myosin filaments assembly *in vitro*. Indeed, this antibody was isolated from chicken intestinal epithelial brush border cells. Furthermore, BM4 significantly decreased the actin-activated MgATPase activity of phosphorylated myosin associated with conversion of myosin filaments to a folded 10S monomer (Citi and Kenderick-Jones, 1987). This study also showed myosin-BM4 complexes by the rotary shadowing-immunoelectron microscopy technique. Interestingly, similar to BM4, S100A4 interaction with NM II in the presence of Ca<sup>2+</sup> causes the destabilisation myosin filaments and inhibits the actin-activated MgATPase activity of myosin *in vitro* (Ford et al., 1997).

Most of the published studies investigating the molecular mechanism of the 10S-6S transition have been carried *in vitro*. For instance, the 10S is the favorable form of myosin compared with 6S myosin as detected by the Kinetic and sedimentation studies (Rosenfeld and Rener, 1994, Trybus et al., 1982) In addition, (Milton et al., 2011) provided a direct evidence for existence of 10S myosin *in vivo*. The previous structural study of myosin (Horowitz et al., 1994) suggested that folded monomeric state of myosin has been detected in smooth muscle cells. The detailed structure of 10S myosin was studied by the negative staining electron microscopy technique (Burgess et al., 2007).

### **3.5.2 Effect of phosphorylation of MHC and MLC on S100A4-myosin IIA interaction in A431/ZEB2 cells.**

Phosphorylation of both RLC by ROCK and MLCK and MHC by PKC and CK2 provide a mechanism for modulating the assembly of myosin IIA filaments (Dulyaninova and Bresnick, 2013). Nearest neighbour statistical analysis of immunogold labelling of cells expressing phosphodeficient and phosphomimetic mutants indicated a significant detection of S100A4-GFP-myosin IIA interaction in these cell lines. Specific interaction between S100A4 and 10S myosin IIA was detected in T18A/S19A cells (Figure 3.28-A). Consistent with this, S100A4 binds only to folded monomer in phosphomimetic S1943D cells (3.33). An unexpected 50 nm peak was detected in T18D/S19D cells indicating that part of myosin is still unphosphorylated. Unpredicted peaks between 100 and 350 nm were estimated (Figure 3.26-A) indicating that S100A4 interacts with 6S and filamentous forms with a possible formation of intermediate structure during assembly of myosin IIA into filaments. The fact

that mutation of Thr18 and Ser19 to D prevented the formation of a banded myosin and promoted extended 6S state favouring filament formation (Walsh, 2011).

These results further reinforce the importance of S100A4 and RLC phosphorylation in regulating myosin IIA assembly and suggest the alternative mechanism for regulation 10S to 6S equilibrium by the interaction with S100A4 protein. Previously, published data reported that dephosphorylated RLC maintains myosin IIA in the “off state”, while phosphomimetic mutation of RLC (T18D/S19D) shifts the conformational equilibrium toward the open 6S state (Espinoza-Fonseca et al., 2014). In fact, RLC phosphorylation modulates enzymatic and the motor activity of vertebrate non-muscle and smooth muscle myosins (Komatsu et al., 2000). Additionally, cells expressing phosphomimetic mutants of RLC exhibit stable filament formation *in vitro* and *in vivo* in the absence of ATP and 10S conformation in the presence of ATP (Vasquez et al., 2016). Another *in vitro* study observed that phosphorylation of RLC does not play a crucial role on the assembly of myosin filaments (Liu et al., 2017). The data from other research suggested that RLC Ser1/Ser2/Thr9 phosphorylation does not significantly control myosin II assembly during cytokinesis and cell migration in HeLa cells, while RLC Thr18/Ser19 phosphorylation is critical for myosin II assembly (Beach et al., 2011).

Our results showed that myosin heavy chain phosphorylation does not have an effect on S100A4 binding site. The two important phospho sites of MHC are located at Ser1916 and Ser1943 that are phosphorylated by PKC and CK2, respectively (Breckenridge et al., 2009, Dulyaninova and Bresnick, 2013, Betapudi et al., 2011, Kriajevska et al., 2000). Phosphorylation of myosin heavy chain significantly inhibits filaments formation (Dulyaninova et al., 2005). Subsequent study (Dulyaninova et al., 2007) reported that MHC IIA phosphorylation may trigger filament disassembly, thereby providing a mechanism for recycling of myosin monomers and turnover of myosin filaments. Phosphorylation of NMHC IIA at Ser 1943 controls its interaction with S100A4 which may regulate NM IIA dynamics and stability (Juanes-García et al., 2016). Consequently, phosphorylation of NMHC IIA is another mechanism for controlling myosin IIA assembly. Interestingly, the phosphorylation at Ser 1943 occurs at the site of myosin rod domain that interacts with S100A4. In agreement with (Kriajevska et al., 2000) who suggested that phosphorylation of MHC IIA at Ser1943

by CK2 did not affect S100A4 binding. However, this finding was later disputed by (Dulyaninova et al., 2005) who reported that CK2 phosphorylation of MHC IIA (residues 1339-1961) decrease S100A4 binding affinity by 7 fold and inhibits its effect in promoting filament assembly. Later, Dulyaninova and colleagues found that phosphomimetic mutants of Ser 1943 did not modify the interaction with myosin regulatory molecules such as S100A4 (Dulyaninova et al., 2007). Recent research has established that phosphorylation of NMHC IIA at Ser 1943 controls the contraction of airway smooth muscle by regulating the assembly of adhesion Junction signalling complexes which is required for actin polymerisation (Zhang and Gunst, 2016).

### **3.4 Conclusion**

Phosphorylation of light and heavy chains regulates myosin polymerisation. However, this phosphorylation does not have an effect on S100A4-myosin IIA interaction in cells. Our results show that the expression of S100A4 is a second important determinant of myosin dynamics in cells. S100A4 is required for the presence of the monomeric fraction. In the absence of ROCK activity, S100A4 controls 6S/10S equilibrium and modulates myosin IIA filament formation in cells. Interestingly, S100A4 can interact with myosin IIA filaments and form transient unstable complex which further disrupt into myosin monomers where the 10S form is the most stable. Figure (3.34) illustrates the S100A4 binding site on MHC IIA and the role of S100A4 in regulating myosin IIA dynamics in cells and shows also the role of the RLC and MHC IIA phosphorylation in controlling myosin IIA filament assembly.

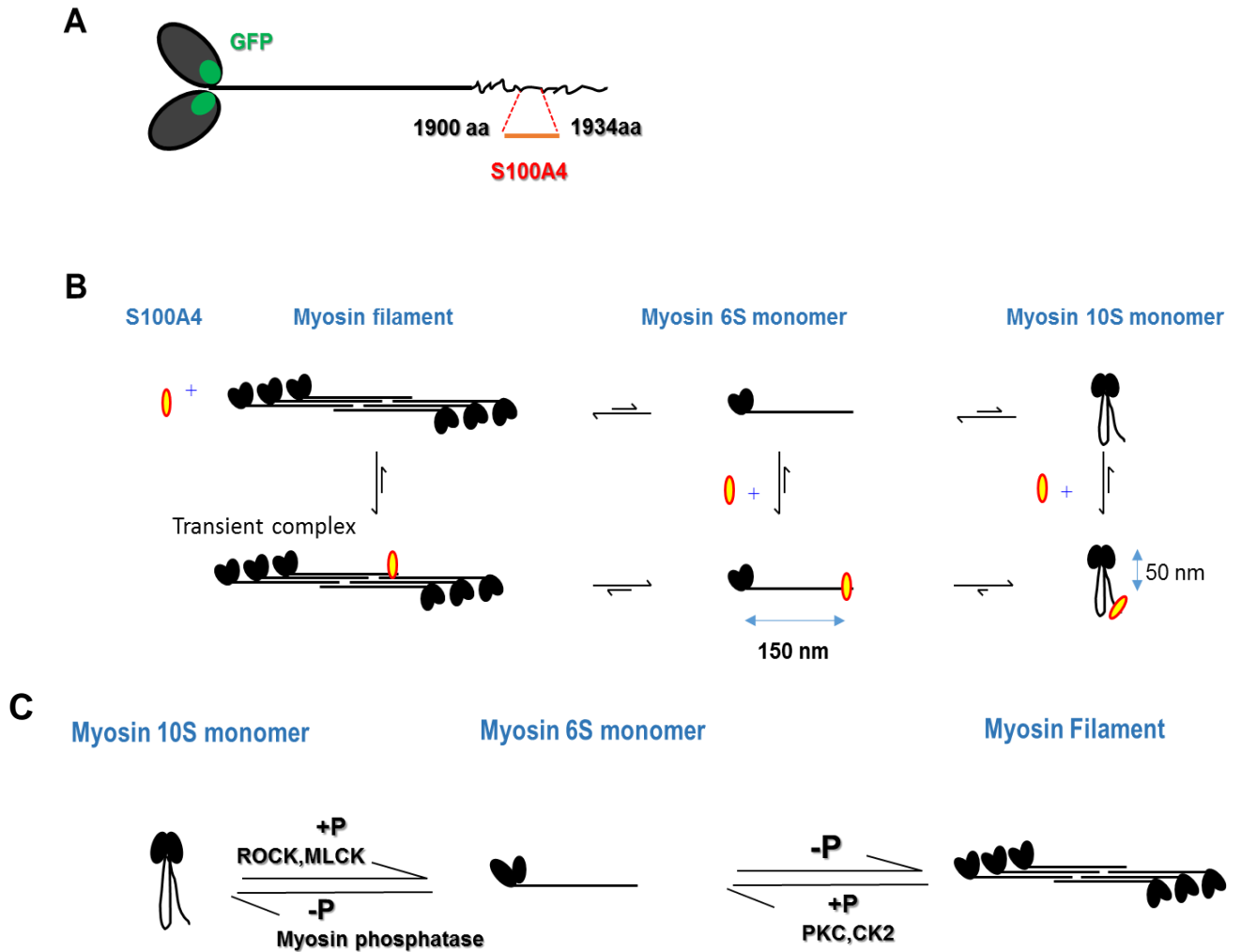


**Figure 3-34: A regulatory mechanism of S100A4 and myosin phosphorylation in controlling myosin IIA dynamics.**

A- Schematic representative of GFP-tagged myosin IIA. S100A4 binds to myosin heavy chain between (1900-1934) aa. B- S100A4 binds myosin filaments promoting transient unstable complex which further dissociates into 6S and 10S myosin monomers, where the 10S conformation is the most stable conformation. C- Phosphorylation of the RLC of myosin IIA at either Ser 19 or Thr 18 causes unfolding of the myosin molecules into extended 6S conformation. Phosphorylated 6S state mediates the formation of bipolar filament. MHC IIA phosphorylation promotes myosin IIA monomers, which is regulated by PKC and CK2.

**Chapter 4 Study of S100A4-myosin IIA complexes by negative staining**

## 4.2 Introduction

The formation of S100A4-GFP-myosin complexes in cells was described in the previous chapter. This chapter focuses mainly on myosin IIA features, by using negative staining electron microscopy. GFP-tagged myosin IIA was extracted from Dox treated A431/ZEB2-WT cells by immunoprecipitation and stored at -80 C°. Electron micrographs of myosin IIA in low salt buffer displayed aggregation of myosin filaments which has previously been demonstrated. (Billington et al., 2013b) suggested that aggregation of myosin into filaments was visualised in low salt concentration buffer. Myosin II structure was also previously visualised by rotary shadowing staining method, in which electron micrographs detecting bundles of large filamentous aggregates of myosin IIA prepared from samples lysed in low salt strength solutions (Badyal et al., 2011) was observed.

Rho-associated protein kinases are serine/threonine kinases that created actin-myosin cytoskeletal changes through phosphorylation of myosin light chain at Ser19 and Thr18 (Liao et al., 2007). Inhibitors of kinases, such as Y27632 suppress the phosphorylation of MLC (Vasquez et al., 2016, Kaneko-Kawano et al., 2012). In this chapter, myosin IIA molecules were observed as filaments in low salt buffer, when myosin IIA was extracted from cells treated with Y27632. Likewise, clusters of 10S aggregates were detected on electron images of S100A4-myosin IIA complexes or addition of S100A4 to the myosin solution.

The aim of this chapter was to analyse the S100A4-myosin IIA complexes *in vitro* by negative staining technique, and determine whether S100A4 has a role in supporting formation of the folded form of myosin IIA.

## 4.3 Results

### 4.3.1 Analysis of the myosin immunoprecipitated from A431/ZEB2-WT cells by negative-staining electron microscopy

In this chapter, we have extended earlier work on intact muscle myosin molecules, and we tested the feature of NM IIA molecules *in vitro* by negative staining technique and TEM. Initially, GFP-tagged myosin IIA molecules were immunoprecipitated from Dox treated A431/ZEB2-WT cells. Cells were lysed with IP buffer A and immunoprecipitation was carried out using anti-GFP antibody (20µg/ml) in combination with Protein G agarose (100 µg/ml). The amount of isolated myosin was analysed by Western blotting using anti-GFP antibody. As it shown in (Figure 4.1-A), myosin IIA was efficiently precipitated, input shows the amount of the used protein, and no protein was detected in a flow-through fraction.

In general, high salt concentration initiates myosin filament disassembly but impairs the negative staining. We selected a standard composition of the myosin buffer with salt concentration of 100 mM as it showed myosin disassembly with minimum stain artefact (100 mM NaCl, 1mM DTT, 47.6 mM glycine, 25 mM Tris, pH 7.5).

Negative staining was then carried out using carbon film gold mesh grids as described in (Materials and Method). Gold grids were used, because gold is an inert metal that will not react with the buffers.

As a control, we negatively stained a sample of the myosin buffer applied on the gold grids (Figure 4.1-B). Based on the image analysis, electron micrographs generally illustrate a large aggregates of myosin filaments. Images showed large aggregates of myosin molecules isolated with anti-GFP antibody. These aggregates consist of two types of aggregates linked via antibodies and via myosin aggregates on its own. The majority of filaments have a compact appearance, in which the heads are tightly packed against the filament backbone; myosin filaments exhibit comma shaped heads attached to a long thin tails (Figure 4.1-C).

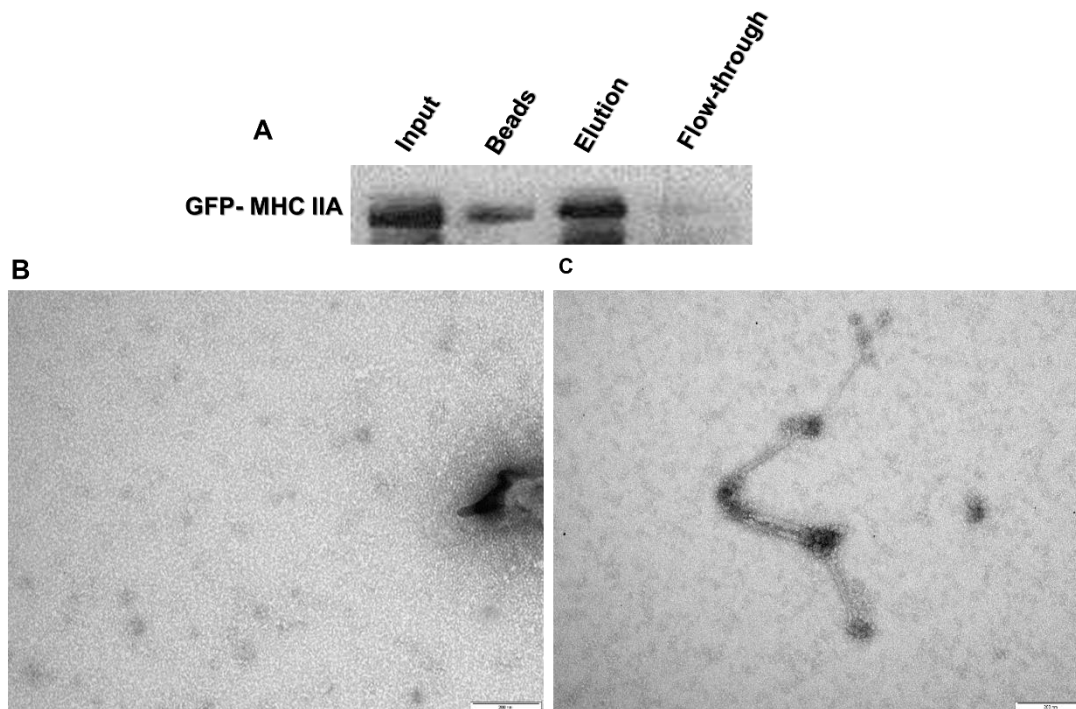


**Figure 4-1: Myosin IIA forms filament bundles in 100 mM salt buffer.**

A- Western blot analysis of GFP-myosin IIA eluted from A431/ZEB2-WT cells by anti-GFP antibody following incubation with protein G agarose beads. B- Negatively staining of myosin buffer which was used as a negative control. C- Negatively staining of immunoprecipitated myosin IIA samples that applied on the gold grids. Scale bar = 200 nm.

#### **4.3.2 Analysis of S100A4-GFP-myosin IIA complexes by negative staining electron microscopy.**

Before analysis of S100A4-myosin IIA complexes by negative staining, we isolated myosin molecules by using the same technique with GFP-Trap®-A beads instead of a mixture of anti-GFP/protein G agarose beads. The amount of isolated myosin was analysed by Western blotting using anti-GFP antibody. The total protein extracted from cells was shown in an input, whereas flow-through indicates unbound protein (4.2-A). This approach was selected in order to avoid a presence of the antibodies that initiated additional aggregation of myosin. Myosin buffer was used as a negative control (4.2-B). Recombinant S100A4 protein was purified under native condition to be used for the negative staining experiment. Electron micrographs showed the presence of small particles of S100A4 (Figure 4.2-C).

Large aggregates of myosin particles were observed as bundles of filaments in a 100 mM salt buffer (100 mM NaCl, 1mM DTT, 47.6 mM glycine, 25 mM Tris, pH 7.5) with compact heads. These aggregates were detected as a field of myosin bipolar filaments demonstrating extensive arrays arranged in head-to-head pattern (Figure 4.2-D). One study showed that myosin IIA molecules form bundles of 250-300 nm of polymerised filaments, known as a backbone at 100 mM salt buffer (Billington et al., 2013a). Myosin IIA sample was then mixed with S100A4 in the presence of 0.1mM CaCl<sub>2</sub> in which samples were diluted in myosin buffer to achieve the final concentration of 7.0 μM S100A4 and 3.5 μM myosin IIA. After incubation for 2 hrs at RT, negative staining was performed.

Myosin light chain phosphorylation is a signal to myosin assembly into filaments (Heissler and Manstein, 2013b). In order to prevent this aggregation of myosin, cells were treated with ROCK inhibitor (10 μM Y27632) before isolation of myosin IIA by immunoprecipitation. Cell lysates were used for Western bolt analysis. It was shown a low level of phosphorylated RLC (Di-p-RLC) expression in treated cells in comparison with untreated ones, whereas a similar expression level of S100A4 was observed in both cell cultures (Figure 4.3).

Samples were then applied on the gold grids and negatively stained. Small aggregates or possible single molecules of folded 10S myosin monomers were observed (Figure 4.2-E).

In the next experiment, myosin IIA was extracted from cells treated with 10 μM Y27632. The ROCK inhibitor (Y27632) blocks MLC phosphorylation as confirmed by Western blot analysis (4.3). Myosin sample eluted from treated cells was diluted to achieve final concentration of 3.5 μM and negative staining was carried out. The sample was then mixed with 7.0 μM S100A4 and followed by negative staining. We did not observe any clear difference following addition of S100A4 to Y27632 treated cells as both samples (with and without S100A4) displayed the smaller clusters of possible folded form of myosin (Figure 4.2-F). Therefore, it will be proposed that S100A4 might initiate aggregation of folded form 10S of myosin.

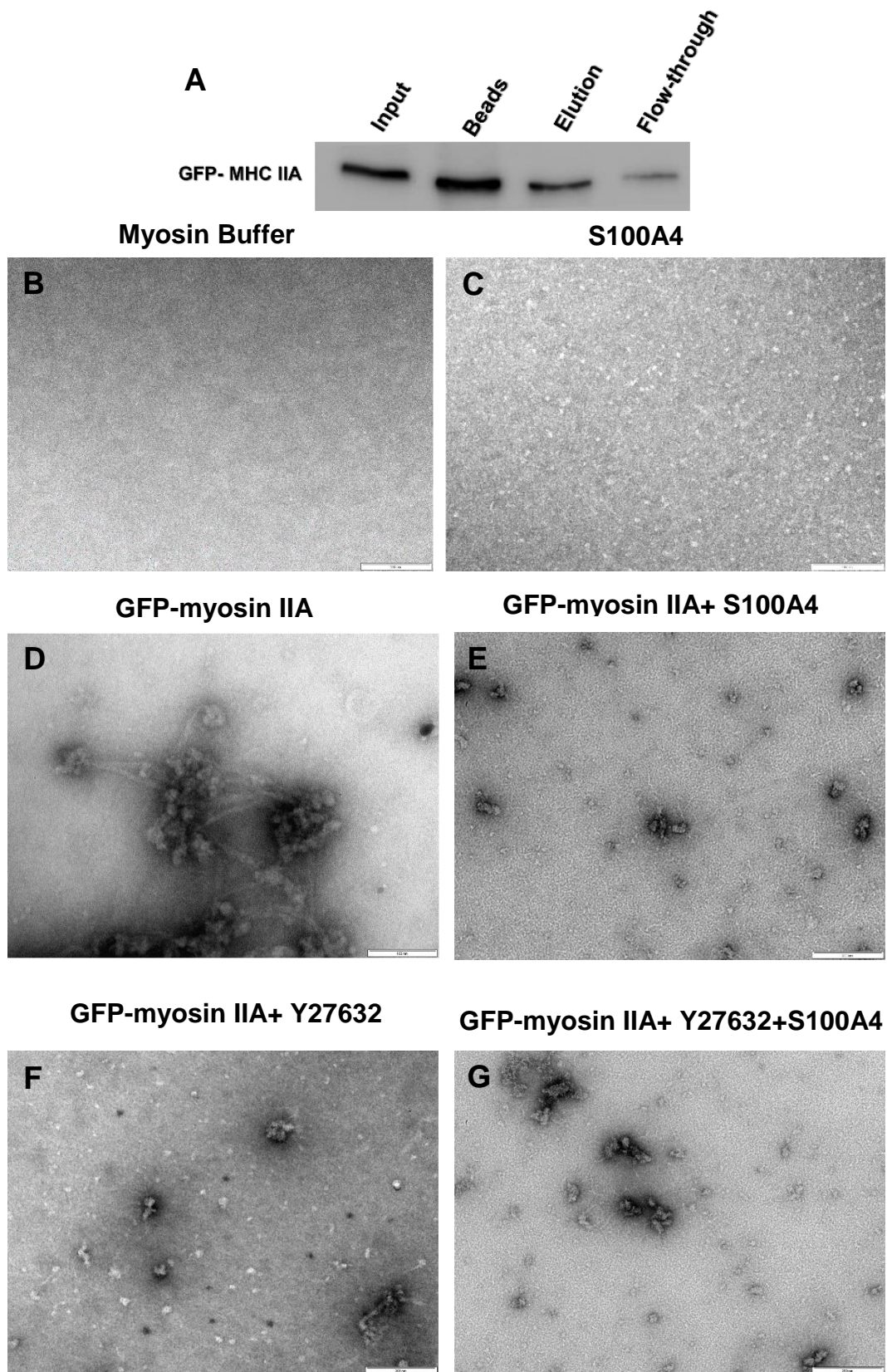


**Figure 4-2: S100A4 supports 10S form of myosin IIA as an alternative role of RLC phosphorylation.**

A-Western blot analysis of GFP-myosin IIA that was immunoprecipitated from A431/ZEB2-WT cells. Beads reflect immunocomplex and elution reveals the amount of protein that separated from the complex. Input reflects the amount of protein that used, whereas flow-through indicates unbound fractions. B- myosin buffer. C-Electron micrograph of S100A4 protein. D- GFP-myosin IIA in 100 mM salt buffer; myosin molecules were visualised as large aggregates of filaments. E- Electron micrograph of negatively stained mixture of GFP-myosin IIA and S100A4. F-GFP-myosin IIA was extracted from A431/ZEB2-WT cells and treated with ROCK inhibitor (10  $\mu$ M Y27632) for 2 hrs; small clusters of possible folded 10S myosin aggregates were observed. G- Electron micrograph of negatively stained of GFP-myosin IIA isolated from treated cells with 10  $\mu$ M Y27632 and mixed with S100A4. Scale bar = 200 nm. This experiment is a representative of three independent experiments.

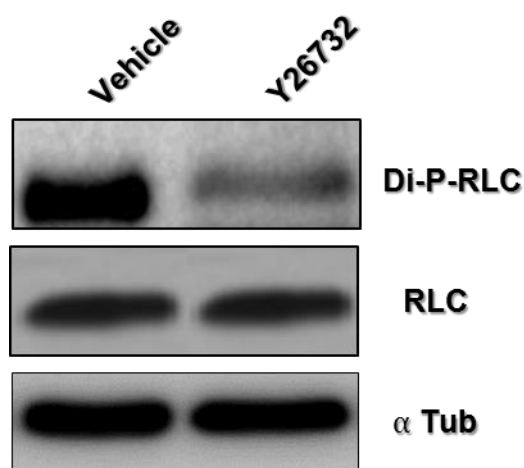


**Figure 4-3: ROCK inhibitor (Y27632) blocks MLC phosphorylation.**

Dox treated A431/ZEB2-WT cells were cultured for 2 hrs in the presence of 10  $\mu$ M DMSO (Vehicle) or 10  $\mu$ M Y27632 before lysis. Cell lysates were analysed to confirm the effect of treatment. The proteins were resolved on SDS-PAGE. Membranes were probed for Di-p-RLC and RLC.  $\alpha$ - Tubulin was used as a protein loading control.

#### 4.4 Discussion

Binding of S100A4 to myosin IIA stabilises its monomeric state and destabilises formation of myosin filaments contributing to cancer cells spreading and invasion (Li and Bresnick, 2006). However, detection of S100A4-myosin IIA complexes is still under investigation. The aim of this chapter was to analyse of S100A4-myosin IIA complexes *in vitro* using negative staining electron microscopy approach.

According to the negative staining electron microscopy results, we observed the properties of NM II filaments formation in 100 mM salt. Myosin filament were detected in low-salt buffer, in which it was distinguished the features of myosin IIA aggregates as it was described previously by (Billington et al., 2013b, Lister et al., 2004, Burgess et al., 2004) studies. The folded state of myosin IIA was possibly observed in the myosin IIA samples isolated from cells treated with Y27632 inhibitor that blocks phosphorylation of the myosin light chains by Rho-associated protein kinase. From co-immunoprecipitation and immunogold labelling experiments, we hypothesized that S100A4-myosin IIA complexes can be detected *in vitro* and in cells. However, we could not observe complexes of S100A4 and myosin IIA by negative staining, but it was detected aggregates of myosin in 10S conformation in the presence of S100A4. It could be proposed that in addition to the main function of S100A4 in promoting disassembly of the myosin filaments, there is another role of S100A4 in supporting the formation of 10S aggregates as shown by negative staining electron microscopy results. This result supports our previous findings in chapter 3 when we knocked down S100A4 by siRNA and observed formation of myosin filaments. However, further work using electron cryomicroscopy will be required to determine S100A4-myosin complexes in more detail.

In conclusion, in addition to the crucial role of the RLC phosphorylation in driving the myosin IIA's conformations, S100A4 also regulates the 10S/6S equilibrium by supporting the formation of the 10S conformation of myosin IIA.

## **Chapter 5 : S100A6 is a new regulator of myosin dynamics**

## 5.2 Introduction

Since it has been demonstrated that S100A4 binds to the C-terminal end of the myosin heavy chain and induces disassembly of myosin IIA filaments, it was identified that other S100 proteins can interact with myosin IIA. With respect to the structure-function relationship between S100 proteins, it was established in *in vivo* study that S100P is partially co-localised with NMII filaments. This interaction leads to dissociation of myosin filament which causes significant reduction in cellular adhesion, and thereby enhance cell migration (Du et al., 2012). It was hypothesised that S100A6 protein which has a similar structure to S100A4 can interact with NM IIA *in vivo* and *in vitro*. According to the preliminary data obtained by the master student (Elvira Diamantopoulou, MSc thesis, University of Leicester), fragment 3 of myosin heavy chain (Hmyo3) was a potential target for S100A6. The interaction between them was detected by blot overlay. Thus, it was set out to identify whether S100A6 has a potential effect on myosin IIA dynamics. Like S100A4, S100A6 expression is upregulated during EMT. Several studies had pointed to a role of S100A6 in cancer metastasis (Marenholz et al., 2006, Duan et al., 2014, Wang et al., 2010a, Melle et al., 2008).

In this chapter, we focused on analysing the binding site of S100A6 on the NMHC IIA molecule which was mapped by blot overlay technique. Subsequently, we narrowed the site of the interaction through preparation overlapping truncated fragments from Hmyo3B and proved the site of the interaction is present in the M53 fragment. The S100A6 binding site on myosin IIA is present in a M53 protein fragment of 53 aa consisting of 1296-1349 residues. This fragment is located in the coiled-coil region of myosin IIA. The nearest statistical co-localisation analysis confirmed our finding, as it was shown that S100A6 interacts with the coiled coil region of NM IIA.

NM IIA is an actin-based motor protein and myosin ATPase activity is involved in stress fibers formation (Watanabe et al., 2007). The driving force for migration in non-muscle cells arises mainly from the actomyosin filaments which tend to play a crucial role during cancer metastasis via force generation resulting from ATP hydrolysis (Billington et al., 2013). One study showed that actin-activated ATPase activity of myosin IIA was decreased during metastasis of cancer cells, such as skin squamous cell carcinoma (Schramek et al., 2014)

Schramek et al., 2014). S100A4 inhibits actin-activated ATPase activity of myosin IIA led to a decrease in the assembly of actomyosin IIA into filaments (Li et al., 2010). The ATPase activity of the actomyosin IIA complex was measured in the presence of S100A4 and S100A6.

We validated the hypothesis that S100A6 is similar to S100A4 as it promotes filament disassembly and thereby, the monomeric state of myosin IIA was triggered. Using a turbidity assay, we were able to show the effect of ionic strength on the aggregation of myosin IIA into filament and we measured the solubility of myosin IIA in the presence of S100A4 or S100A6 as well.

MHC IIA stability occurs by interacting of the third segment of MHC IIA with RLC. Myosin regulatory light chains are required to maintain the stability of MHC IIA and cellular integrity (Park et al., 2011). We investigated the effect of S100A4/A6 on MHC IIA IIA stability. Thus, we used a blocker of the protein synthesis and measured the half-life of the myosin heavy chain.

### **5.3 Aims**

- 1- To measure the ATPase activity of GFP-tagged myosin IIA isolated from A431/ZEB2 cells grown in absence and presence of Dox.
- 2- To assess the effect of S100A4 and S100A6 on the ATPase activity of actomyosin IIA complex.
- 3- To characterise S100A6 binding site with NM IIA *in vitro* by blot overlay assay.
- 4- To investigate the level of co-localisation between S100A6 and myosin IIA *in vivo* using confocal and electron microscopy.
- 5- To examine the effect of S100A4/ S100A6 on myosin stability.

## **5.4 Results**

### **5.4.1 Assessment of ATPase activity of myosin IIA extracted during EMT.**

To measure the ATPase activity of the myosin IIA isolated from A431/ZEB2-WT cells during EMT, ATPase assay was carried out. The effect of S100A4 and S100A6 on the ATPase activity of actomyosin complex were also investigated.

#### **5.4.1.1 Extraction of myosin IIA for the ATPase assay**

Myosin IIA was isolated from A431/ZEB2-WT cells. Firstly, A431/ZEB2-WT cells were grown in absence and presence of Dox for 72 hrs and myosin IIA was immunoprecipitated from cells using rabbit anti-GFP antibody and protein G agarose. Eluted myosin IIA was analysed by Western blotting using rabbit anti-GFP antibody. The optimal concentration of rabbit anti-GFP (15µg/ml) was empirically selected.

#### **5.4.1.2 ATPase activity of actomyosin IIA complex is down-regulated during EMT**

A432/ZEB2-WT cells were grown in absence and presence of Dox for 72 hrs. GFP-tagged myosin IIA was isolated and eluted from beads using rabbit anti-GFP antibody and protein G agarose. Efficiency of the isolation was confirmed by Western blot analysis (Figure 5.1-A). The strong bands of input reflects the total protein extracted from the cells after lysis and before immunoprecipitation, while not detectable bands in flow-through indicates the efficiency of the immunoprecipitation. Freshly isolated myosin was then used for ATPase assay experiment. Inorganic phosphate was measured by adding ammonium molybdate and iron sulphate. Consequently, green molybdophosphoric acid was formed and absorbance was measured at OD A<sub>700</sub> nm. Notably, data from three separated experiments exhibited a significant down-regulation of myosin ATPase activity during EMT \*\* P= 0.0081 (Figure 5.1-B).

Phosphorylation of RLC increases the affinity of myosin heavy chain for F-actin, thereby enhancing ATPase activity and thus induces cell contractility (Beach and Egelhoff, 2009)

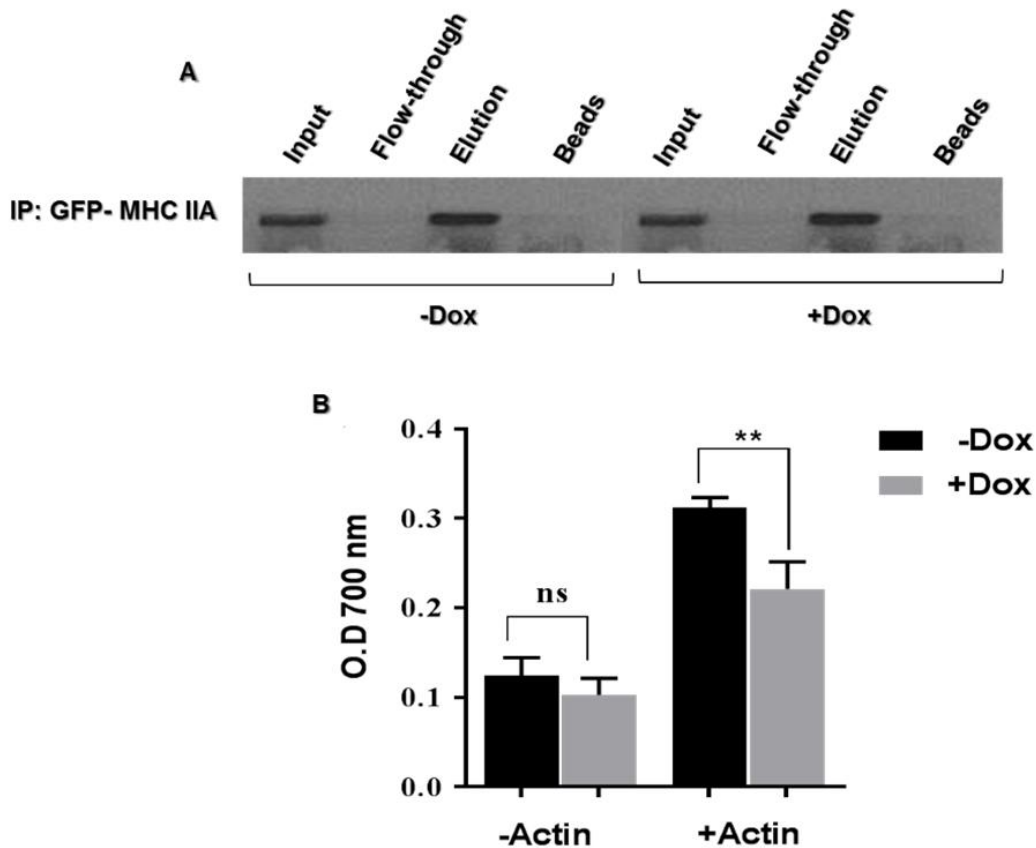


**Figure 5-1: Measurement of ATPase activity of the isolated GFP-tagged myosin IIA from A431/ZEB2-WT cells grown in the absence and presence of Dox.**

GFP-tagged myosin IIA was isolated from A431/ZEB2-WT cells grown in absence and presence of Dox for 72 hrs. A- Eluted GFP-MHC IIA was analysed on 8% SDS-PAGE and blotted using rabbit anti-GFP antibody. Myosin was successfully isolated from cells (input) and efficiently interacted with protein G beads (flow-through). B- ATPase activity of myosin IIA grown in absence and presence of Dox was measured. Results represent the mean of three independent experiments performed in triplicate. There was a statistical significant decrease of ATPase activity of actomyosin complex during EMT. Unpaired t-test was used to assess the statistical significance. \*\* P= 0.0081. Error bars are SEM.

### 5.4.1.3 S100A4 /A6 modulates Actin-activated ATPase of myosin IIA

Subsequently, the effect of S100A4/S100A6 on the actin-activated ATPase activity of myosin IIA was examined. As such, ATPase activity was measured in the presence of S100A4 protein or S100A6 protein. Interestingly, data from three separate experiments showed that S100A4 and S100A6 display a significant inhibition of the actin-activated ATPase activity of myosin IIA. The ATPase activity was reduced by approximately 4-fold in the presence of S100A4 and 3-fold in the presence of S100A6 (Figure 5.2); \*\*\*\* P < 0.0001 and \*\*\* P= 0.0001 for S100A4 and S100A6, respectively.

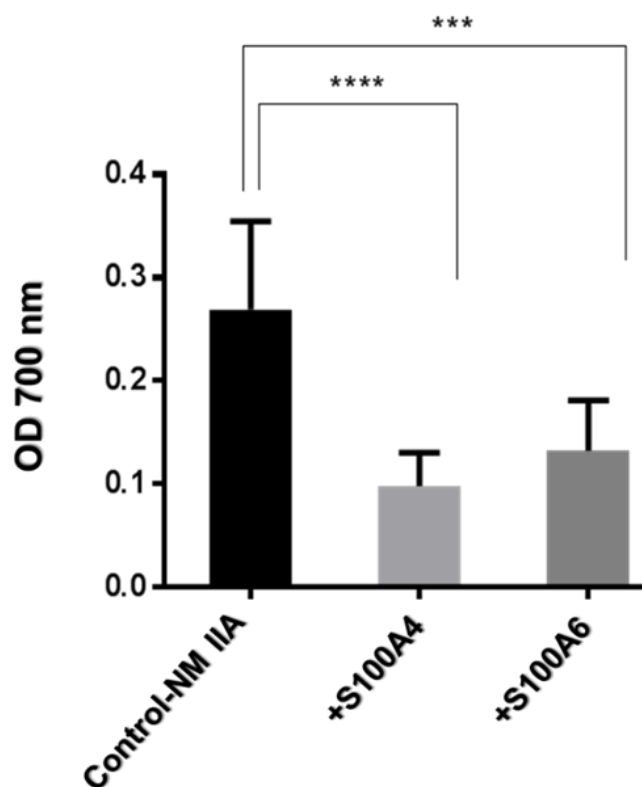


**Figure 5-2: S100A4/A6 inhibits the actin-activated ATPase activity of GFP-tagged myosin IIA during EMT.**

Actin-activated ATPase activity of the isolated myosin IIA from A431/ZEB2-WT cells maintained in the presence of Dox for 72 hrs was measured in the presence of S100A4/S100A6. Data from three independent experiments showed that the ATPase activity of myosin IIA was significantly reduced in the presence of S100A4/S100A6. Errors bars represent SEM. \*\*\*\*P < 0.0001 for S100A4 and \*\*\*P= 0.0001 for S100A6. Statistical analysis was done using a One-way ANOVA followed by Dunnett's multiple Comparison Test.

#### **5.4.2 Study of NMHC IIA half-life by cycloheximide chase assay**

Once S100A4/S100A6 reduced the ATPase activity of myosin IIA, further investigation was carried out to analyse the influence of S100A4/S100A6 interaction on MHC IIA stability. Initially, we tried to determine the half-life of NM IIA by treating A431/ZEB2-WT cells with an inhibitor of protein synthesis cycloheximide (CHX). CHX is a well-known inhibitor of protein synthesis and therefore, it is used to measure the protein-half-life (Zhou, 2004, Patel et al., 2002).

To ascertain the half-life of myosin IIA, A431/ZEB2-WT cells were treated with CHX after optimization its concentration. The selected concentration of CHX (100 $\mu$ g/ml) were used to treat cells at four different time points between 0 and 8 hrs chase. Lysates were then prepared and analysed by Western blotting (Figure 5.3). The expression of MHC IIA protein was down-regulated after 4 hrs CHX treatment. However, the significant effect of CHX on MHC IIA half-life was detected after 6 hrs treatment; as a faint band corresponding to MHC IIA presence. Cyclin D1 is synthesized rapidly and accumulated during G1 phase and degraded in the S phase (Eeckhoute et al., 2006). In A431 cells, a direct repression of cyclin D1 expression is mediated by ZEB2 leading to arrest the cell cycle during EMT (Mejlvang et al., 2007). Due to the short half-life of cyclin D1, it was used as a control. Western blot analysis showed S100A4 and S100A6 long-lived proteins with a half-life more than 8 hrs.

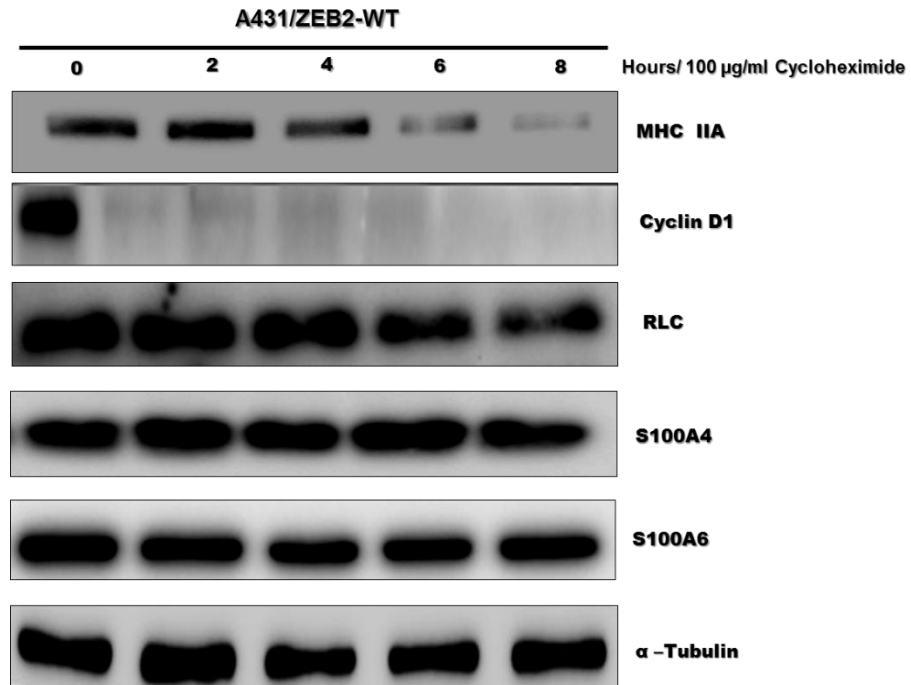


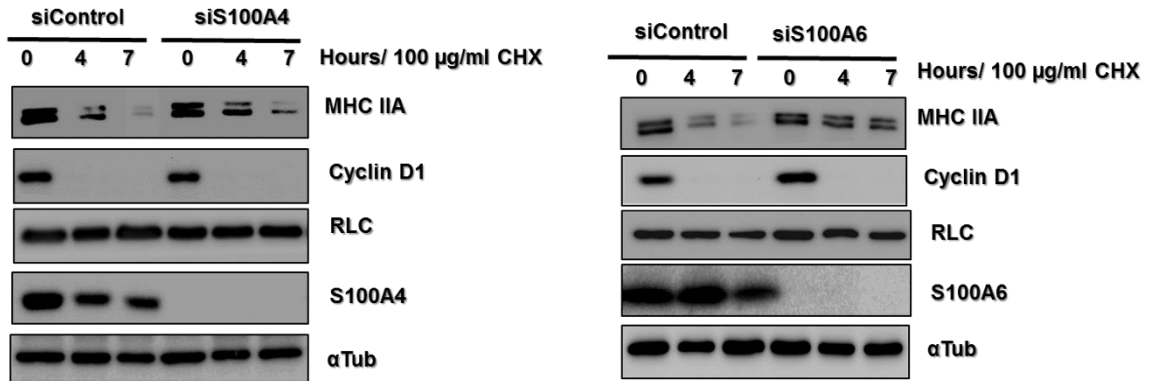
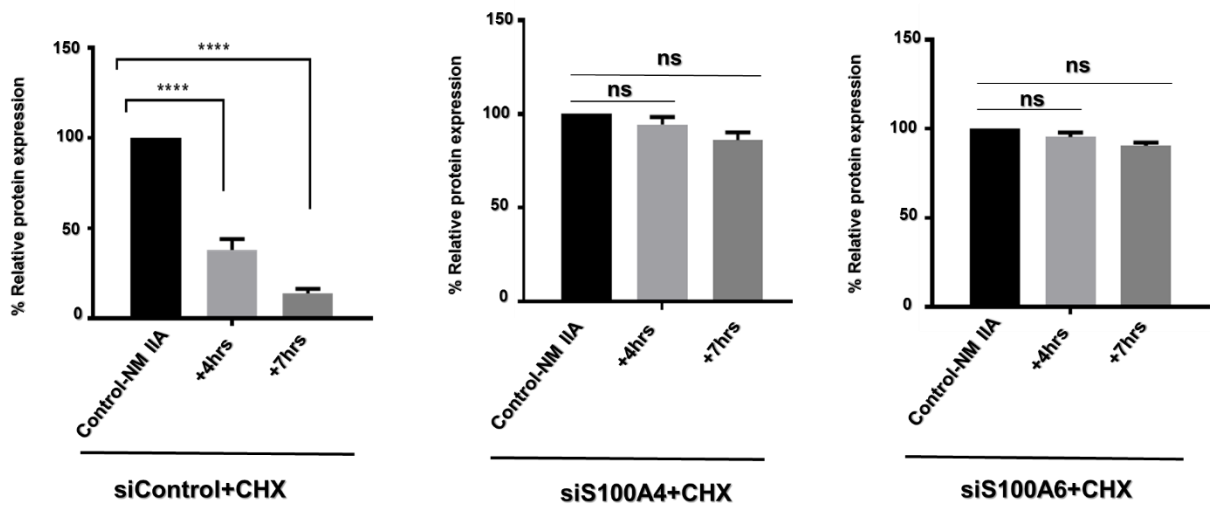
**Figure 5-3: Measurement of proteins half-life in A431/ZEB2-WT cells.**

Dox-treated A431/ ZEB2-WT cells were incubated in the presence of 100 µg/ml CHX for different time points between (0-8) hrs. Lysates were collected for Western blot analysis to determine the half-life of MHC IIA, RLC, S100A4 and S100A6. Cyclin D1 was used as control.  $\alpha$ -tubulin was used as a protein loading control. This experiment was repeated three times.

In order to characterise the effect of S100A4/S100A6 on myosin IIA half-life, A431/ZEB2-WT cells were transfected with either siControl or siS100A4 or siS100A6 and seeded on 6 cm petri dish for 48 hrs in the presence of Dox. Cells were then incubated with 100µg/ml of CHX in a time-course of 0, 4 and 7 hrs and cell lysates were analysed by Western blotting, in which the expression of S100A4, S100A6 and RLC was measured (Figure 5.4-A). The NMHC IIA bands intensity were measured using image J and normalized to  $\alpha$ -tubulin.

Data from three independent experiments demonstrated a significant decrease in the myosin heavy chain expression in siControl cells at time points 4 and 7 hrs, \*\*\*\*P < 0.0001. However, it was found that there was no significant changes in MHC IIA expression in siS100A4 and siS100A6 cells in comparison with siControl cells (Figure 5.4-B).

In conclusion, the obvious decrease in MHC IIA half-life was detected as a result of CHX treatment. However, S100A4 and S100A6 have an effect in increasing the myosin IIA half-life.

**A****B**

**Figure 5-4: The effect of S100A4/S100A6 on the MHC IIA half-life**

Dox treated A431/ ZEB2-WT cells were transfected with either siControl or siS100A4/S100A6. Cells were treated with 100 μg/ml CHX for 4 and 7 hrs and lysates were collected for Western blot analysis. A-A significant reduction of S100A4 and S100A6 expression in siS100A4 and siS100A6 transfected cells was detected, respectively. A remarkable decrease in the MHC IIA expression was estimated after CHX treatment. Cyclin D1 was used as control of the CHX assay. B-Data from three separate experiments show a significant decrease of MHC IIA expression upon CHX treatment, and data was presented as mean ± SEM. P values were determined by a One-way ANOVA followed by a Dunnett's Multiple comparison test; \*\*\*\*= P < 0.0001 for (4-7) hrs CHX treatment, whereas no significant impact of S100A4/S100A6 on MHC IIA stability. This experiment is a representative of three separate experiments.

### **5.4.3 S100A6 co-localises with myosin IIA**

ATPase assay showed that S100A6 has an effect on actin-activated ATPase activity of myosin IIA. Therefore, further investigations were made to analyse whether S100A6 has a direct interaction with myosin IIA.

#### **5.4.3.1 Characterisation of S100A6-myosin IIA complexes *in vitro* by co-immunoprecipitation assay**

A co-immunoprecipitation data described in chapter 3 confirmed that S100A4 interacts with myosin IIA and form complexes in A431/ZEB2 cells. In this section, we analysed whether S100A6-myosin IIA complexes can be detected in cell lysates by immunoprecipitation assay. Specifically, A431/ZEB2-WT cell lysates were incubated with anti-S100A6 or anti-GFP antibody for 1 hour and precipitated with protein G agarose beads. Subsequently, the lysates were separated by SDS-PAGE and immunoblotted for GFP and S100A6 to detect S100A6-GFP complexes. Anti-GFP antibody was used to detect GFP expression following the precipitation by anti-GFP or anti-S100A6. Simultaneously, anti-S100A6 antibody was used to detect S100A6 expression following the precipitation by anti-GFP or anti-S100A6 antibody. In terms of immunoprecipitated S100A6, Western blot analysis revealed the expression of both GFP and S100A6 as clear bands. Regarding the immunoprecipitation of GFP, a high level of GFP expression was detected by Western blotting, while a weak band reflects S100A6 was observed (Figure 5.5). Consequently, we conclude that S100A6 can form a complex with NM IIA in cell lysates.

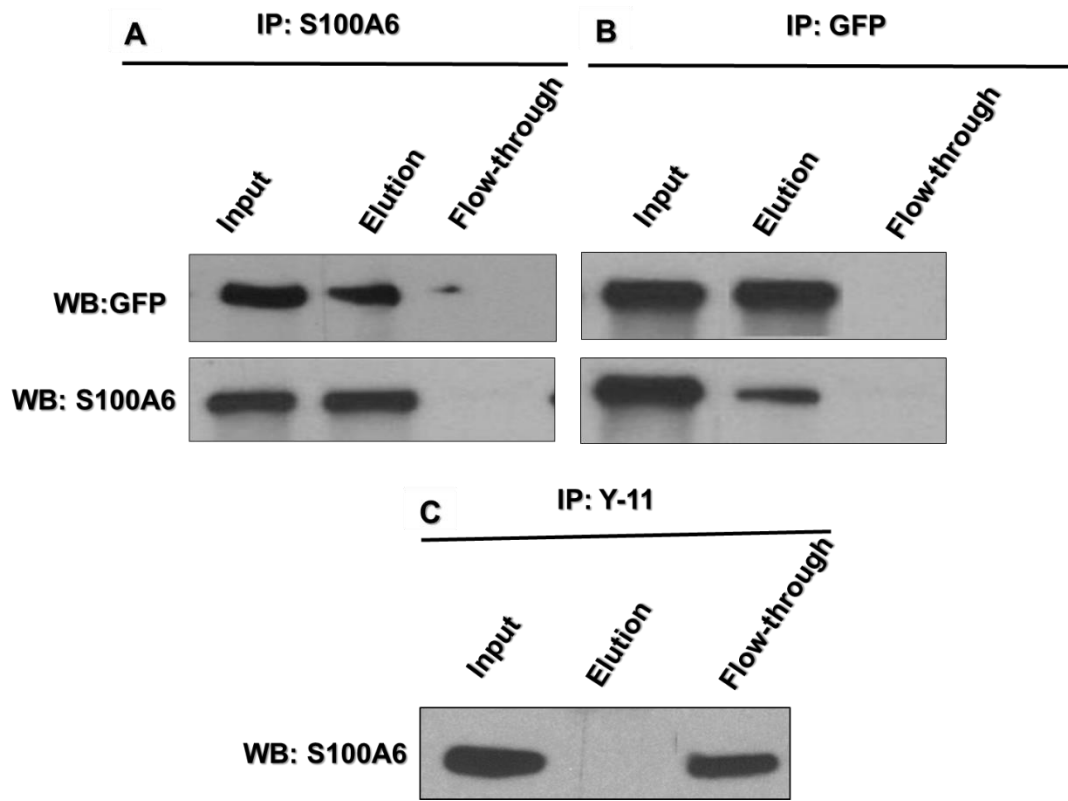


**Figure 5-5: Co-immunoprecipitation of GFP and S100A6 from A431/ZEB2-WT cells**

Dox treated A431/ ZEB2-WT cells expressing GFP-MHC IIA were lysed in IP buffer. A-S100A6-protein complexes were immunoprecipitated by a monoclonal mouse anti-S100A6 antibody in combination with protein G agarose beads, lysates were resolved on SDS-PAGE and immunoblotted with anti-GFP and anti-S100A6 antibodies. B-GFP-protein complexes were immunoprecipitated by a polyclonal rabbit anti-GFP antibody in combination with protein G agarose beads, lysates were separated on SDS-PAGE and then analysed by Western blotting using specific antibodies for GFP as well as for S100A6. C- Control (IP: Y-11). The total protein extracted from cells was shown in an input, whereas flow-through indicates unbound protein.

#### **5.4.3.2 Localisation of S100A6 in A431/ZEB2 cells expressing RLC and MHC WT and mutants.**

In the next experiment, we analysed the expression of S100A6 in A431/ZEB2 cells expressing WT or mutants of the RLC and MHC. As such, all cell lines were maintained in the absence and presence of Dox for 72 hrs, harvested and the whole protein cell lysates were analysed by Western blotting. It was observed that a significant up-regulation of S100A6 expression occurred during EMT in all cell lines which appeared to be expressed highly in cells expressing phosphodeficient and phosphomimetic mutants of RLC and MHC (Figure 5.6-A) and (Figure 5.7-A). Subsequently, the localisation of S100A6 in cells were assessed by confocal studies. Thus, cells were fixed and fluorescently stained for GFP and S100A6. Like S100A4, S100A6 was distributed throughout the nucleus and cytoplasm. Intriguingly, partial co-localisation of S100A6 and myosin IIA was detected with the distribution of both proteins throughout the cytoplasm and increasing the intensity along the filaments network towards the periphery of the cells (Figure 5.6-B) and (Figure 5.7-B).

In conclusion, S100A6 was detected in nucleus and cytoplasm with variable expression between cells and partial co-localisation with myosin IIA. S100A6 was expressed in A431/Z2B2 cells expressing MHC and RLC-WT and mutants.

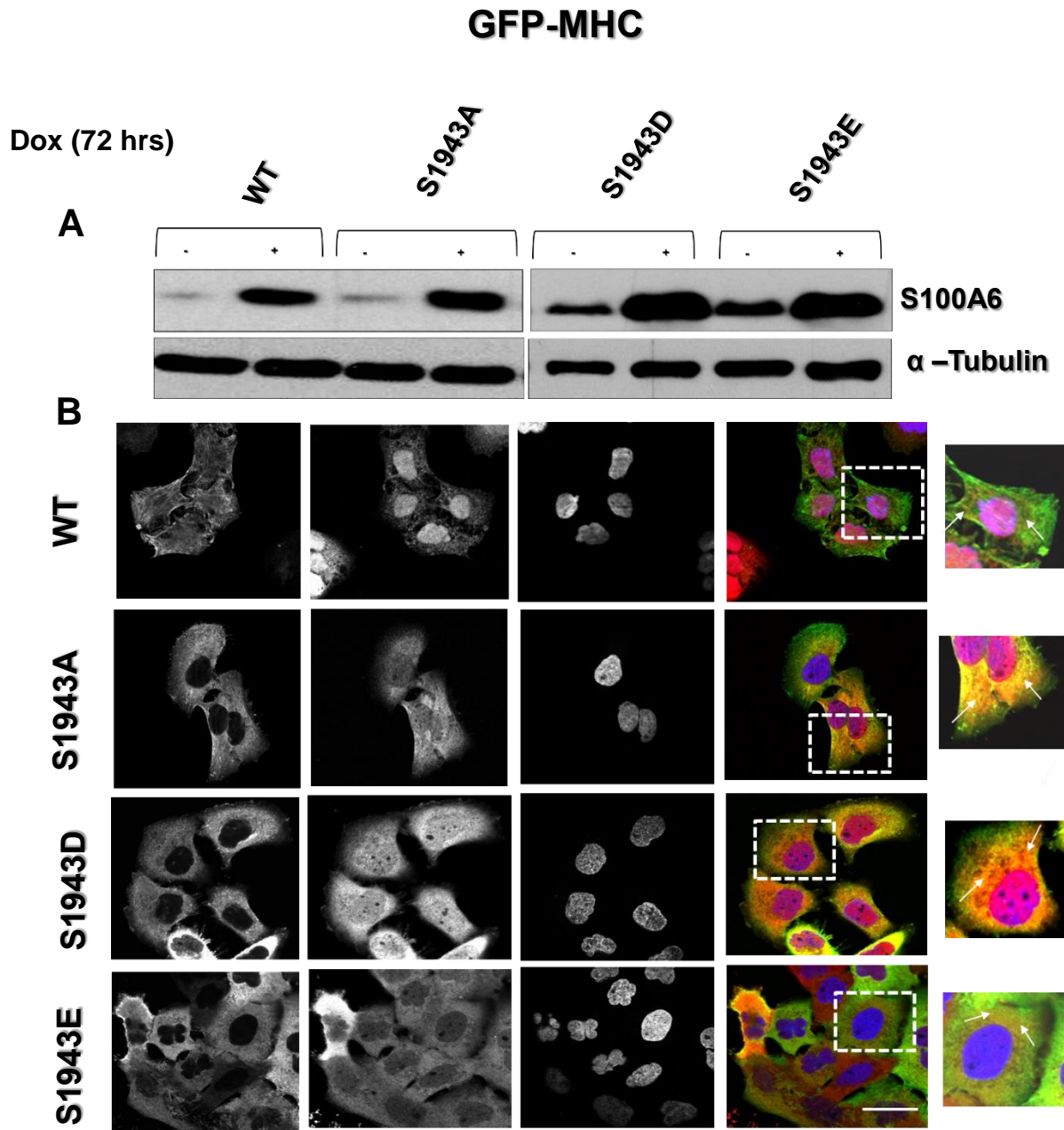


**Figure 5-6: Immunofluorescence staining of A431/ZEB2 cells expressing WT and mutants of the MHC IIA.**

Dox treated A431/ZEB2 cells expressing WT, phosphodeficient S1943A, and phosphomimetic S1943D/E mutants of the MHC IIA were grown in the absence and presence of Dox for 72 hrs. Cells were lysed, resolved on SDS-PAGE and blotted for S100A6.  $\alpha$ -Tubulin was used as a protein loading control. B-Cells were fixed with 4% PFA and fluorescently stained against GFP (green) and S100A6 (red). Images were collected by Nikon confocal microscopy. White arrows indicate area of S100A6-MHC co-localisation. Scale bar = 10  $\mu$ m.

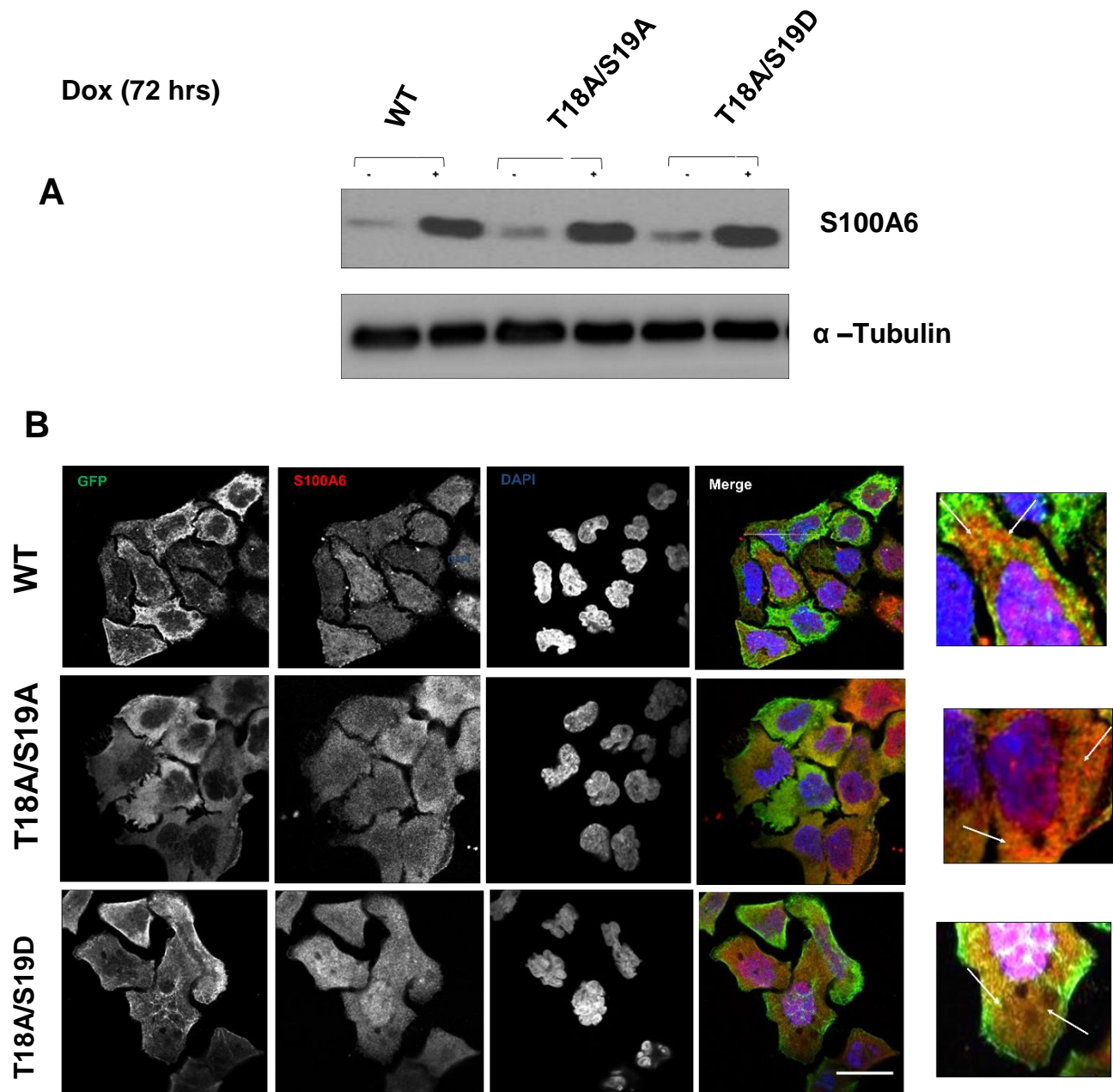


**Figure 5-7: Immunofluorescence staining of A431/ZEB2 cells expressing GFP-tagged myosin light chains mutants.**

Dox treated A431/ZEB2 cells expressing RLC-WT, phosphodeficient T18A/S18A and phosphomimetic T18D/S18D mutants were grown in the absence and presence of Dox for 72 hrs. Cells were lysed, and proteins were analysed by Western blotting using anti-S100A6 antibody.  $\alpha$ -Tubulin was used as a protein loading control. Cells were fixed with 4% PFA and fluorescently stained against GFP (green) and S100A6 (red). Images were collected by Nikon confocal microscopy. White arrows indicate area of S100A6-RLC co-localisation. Scale bar = 10  $\mu$ m.

#### 5.4.3.3 Assessment of S100A6-GFP-myosin IIA complexes in A431/ZEB2-WT cells by TEM immunogold labelling.

Since S100A6-myosin IIA complexes have been identified in cell lysates, we next investigated the existence of these complexes in cells. Thus, immunogold labelling approach was used to analyse the S100A6-GFP-myosin IIA interaction in A431/ZEB2-WT cells. As such, the nearest neighbour statistical co-localisation analysis of gold particles was performed as described previously in chapter 3. Before double labelling experiment was carried out, optimal concentration of anti-S100A6 antibody (50 $\mu$ g/ml) was detected by an individual staining of resin embedded sections of cells with different dilutions of monoclonal mouse anti-S100A6 antibody (Figure 5.8).

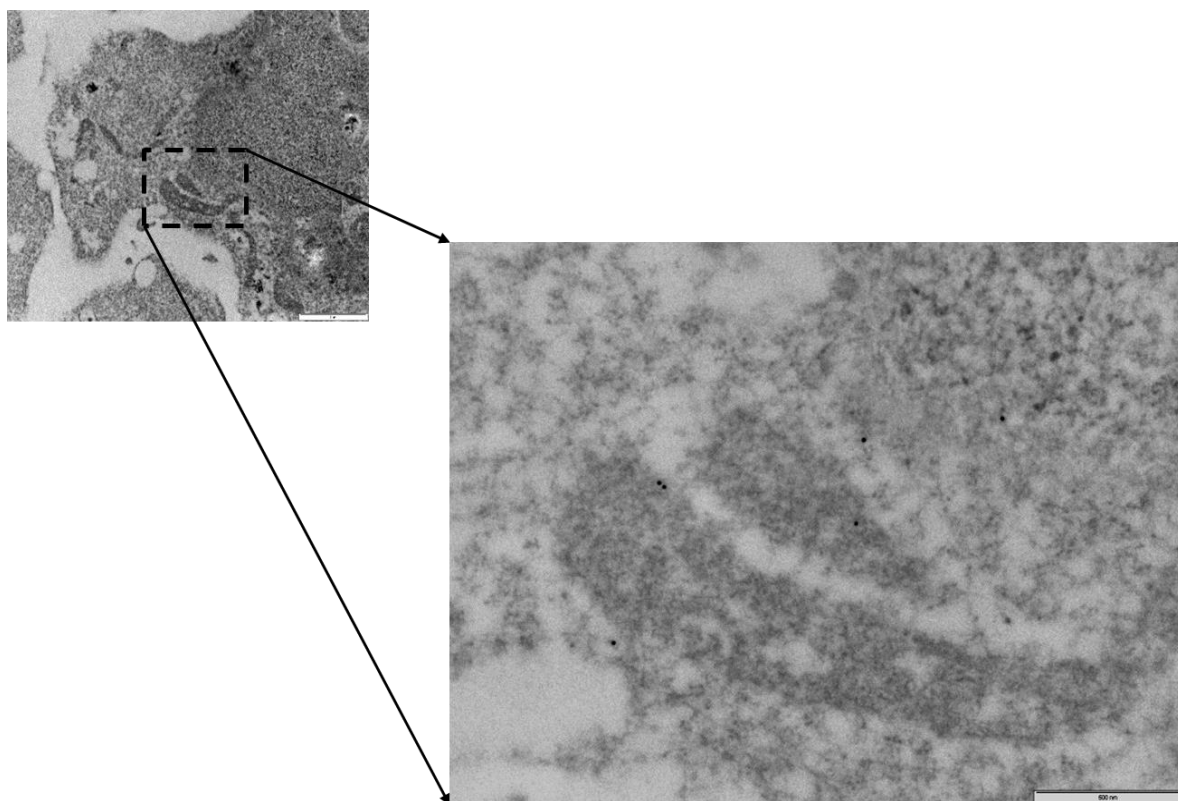


**Figure 5-8: Electron micrograph of A431/ZEB2-WT cells immunogold labelled for S100A6**

Dox treated A431/ZEB2-WT cells were labelled with optimized concentration of S100A6 (50 $\mu$ g/ml) and visualised with 15 nm gold particles. Scale bar for top panel= 2 $\mu$ m. Scale bar for lower panel = 500 nm.

In the next experiment, A431/ZEB2-WT cells were treated with 10  $\mu$ M Y27632 for 2 hrs. Western blot analysis shows a high level of S100A6 expression during EMT in both untreated and treated A431/ZEB2-WT cells with Y27632 (Figure 5.9).

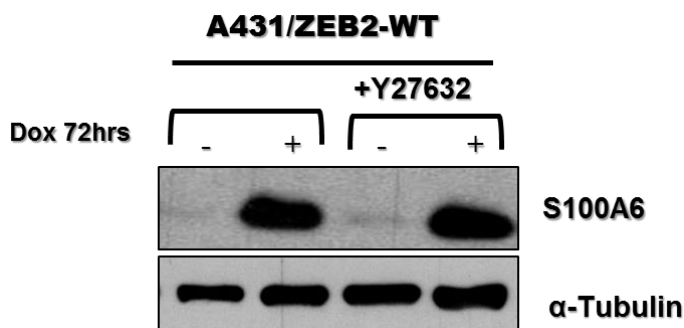


**Figure 5-9: S100A6 expression is increased in A431/ZEB2-WT untreated and treated cells with Y27632 during EMT.**

Dox treated A431/ZEB2-WT cells were treated for 2 hrs with 10 $\mu$ M Y27632. Untreated and treated cell lysates were immunoblotted for S100A6.  $\alpha$ -Tubulin was used as a protein loading control.

Resin embedded sections of A431/ZEB2-WT untreated and treated cells with Y27632 were immunolabelled for S100A6 and GFP and imaged (Figure 5.10). Data from nearest neighbour statistical co-localisation analysis detected the significant co-localisation between S100A6 and myosin IIA at one peak corresponding to 100 nm in untreated cells which reflects the coiled coil region of myosin IIA (Figure 5.11-A), whereas in Y27632 treated cells one significant peak was detected at 50 nm which is consistent with folded form of myosin 10S (Figure 5.11-B).

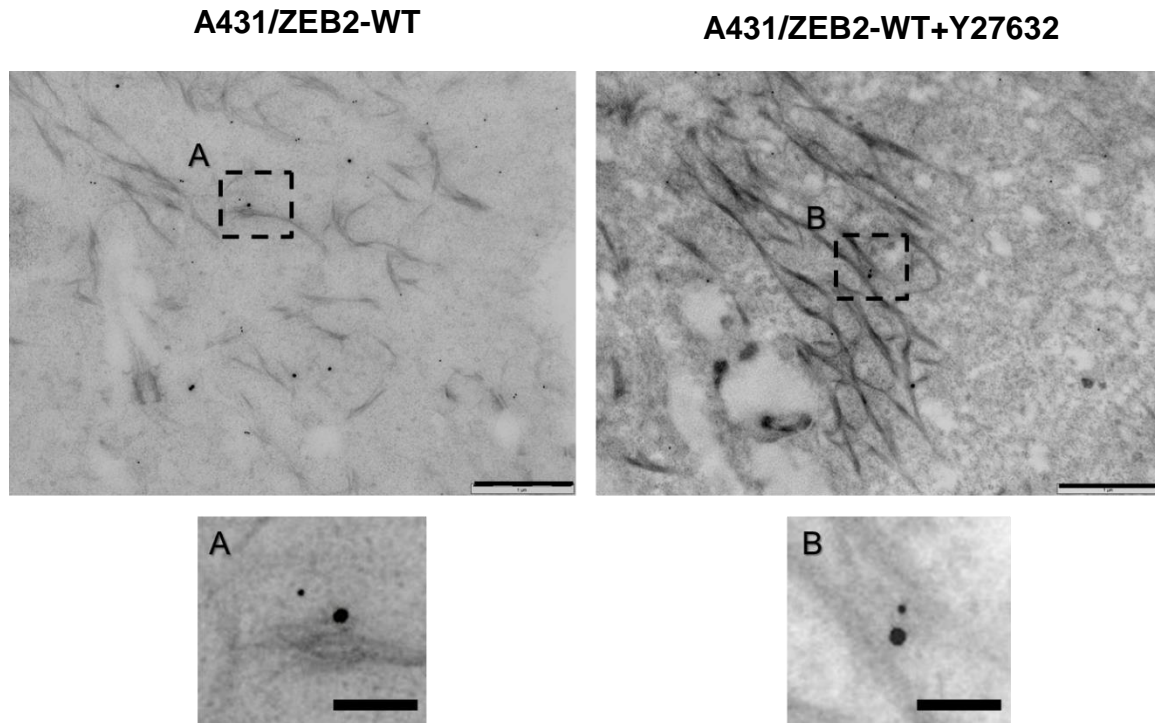


**Figure 5-10:** Electron micrographs of immunogold labelled A431/ZEB2-WT and A431/ZEB2-WT +Y27632 cells for S100A6 and GFP.

Resin embedded sections of Dox treated A431/ZEB2-WT and A431/ZEB2-WT+ Y27632 cells were immunolabelled with anti-S100A6 and anti-GFP antibodies and visualised using 15 nm and 30 nm gold-conjugated secondary antibodies, respectively. (A) and (B) overview magnified images. Distances between S100A6 and GFP-myosin IIA particles in magnified electron micrographs are A= 100 nm, B= 55 nm. Scale bar = 1 $\mu$ m. Scale bar of magnified images = 200 nm.

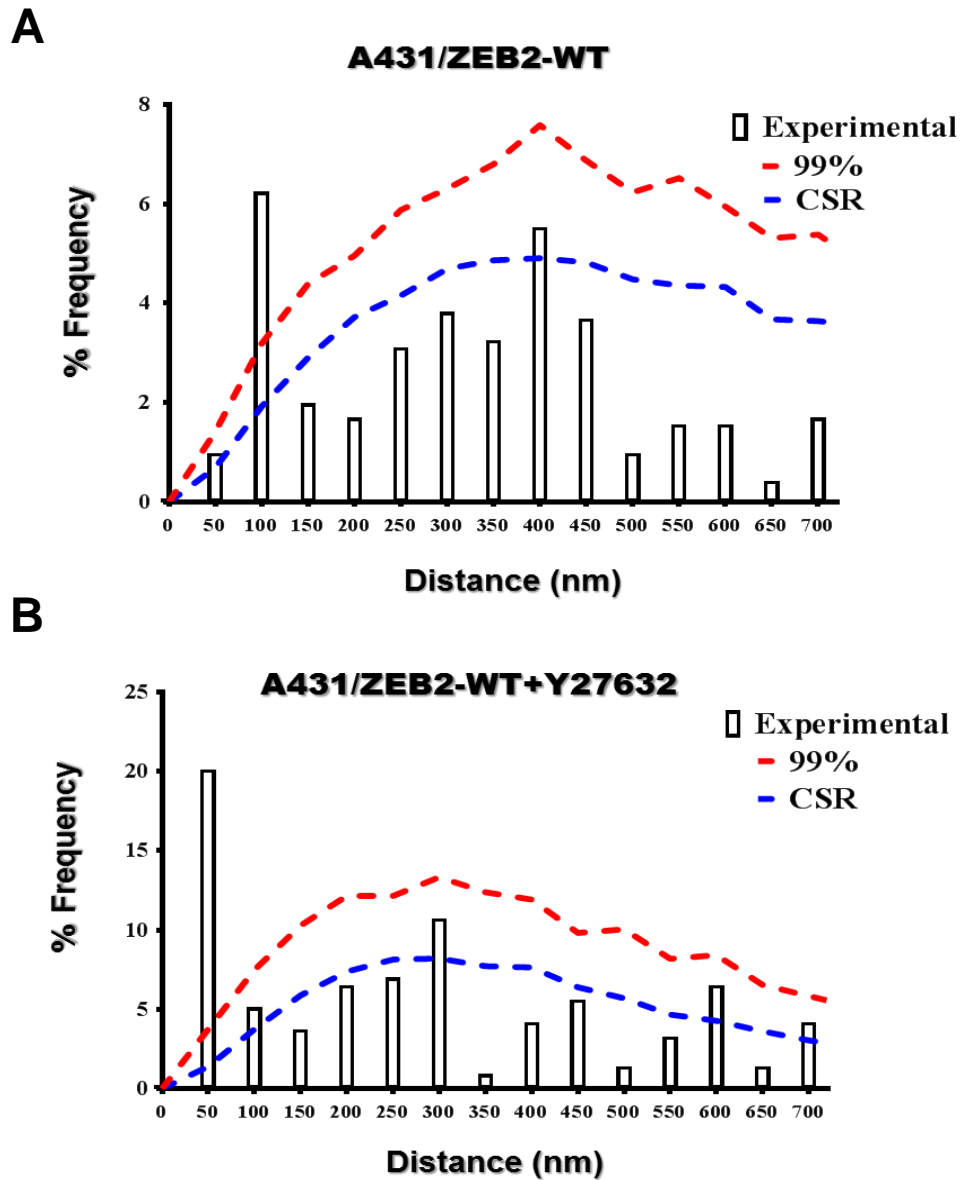


**Figure 5-11: Co-localisation of S100A6 with-myosin IIA in control cells and after treatment with Y27632.**

Resin embedded sections of Dox treated A431/ZEB2-WT cells A431/ZEB2-WT+ Y27632 cells were immunolabelled for S100A6 and GFP. A- Nearest neighbour statistical analysis indicates only one specific peak corresponding to 100 nm in untreated cells. B- Nearest neighbour statistical analysis indicates one significant peak corresponding to 50 nm in Y27632 treated cells.

#### 5.4.4 Mapping of the S100A6 binding site.

Based on nearest neighbour analysis in section 5.3.3.3, we predicted a new binding site of S100A6 with NMHC IIA. Therefore, blot-overlay assay was performed to search for the S100A6 binding site on NMHC IIA molecule. Recombinant overlapped fragments of human NMHC IIA protein shown in (Figure 5.12) were used for the blot-overlay.

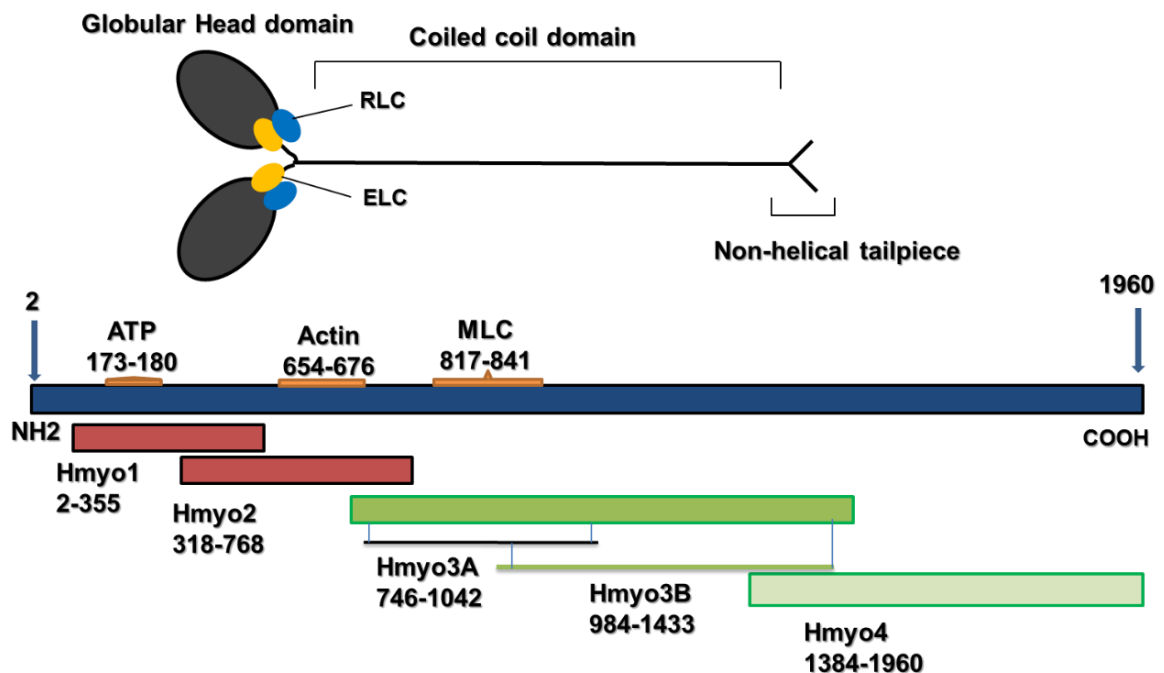


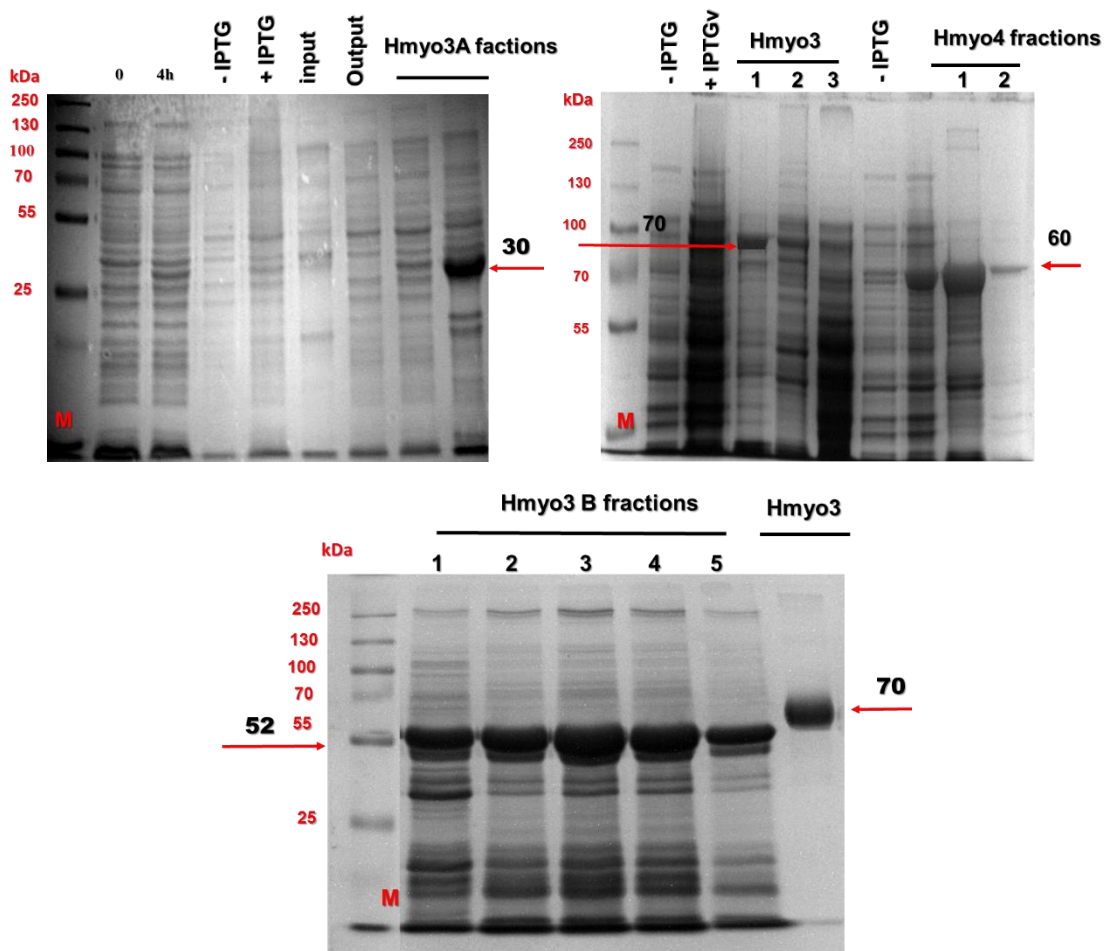
**Figure 5-12: A schematic map of the recombinant NMHC IIA protein fragments**

A scheme of the NM IIA monomer (top) and recombinant human MHC IIA protein fragments (bottom). The amino acid residues are numbered (Kriajevska, 1998).

#### 5.4.5 Expression and purification of the myosin recombinant proteins

Polyhistidine-tagged recombinant myosin fragments were cloned in pQE30 vector and expressed in M15 bacterial cells. Polyhistidine is an affinity tag that provides expression vectors for protein expression and purification reagents. Histidine forms coordination bonds

with immobilized transition metal ions, such as,  $\text{Cu}^{2+}$ ,  $\text{Ni}^{2+}$ ,  $\text{Zn}^{2+}$ , and  $\text{Fe}^{2+}$ , which can be used to purify polyhistidine fusion proteins (Kimple et al., 2013). pQE30 expression system is an efficient approach for expression of the recombinant proteins (Krause et al., 2010). Small scale protein expression was conducted. Lysates of bacterial clones expressing recombinant myosin fragments were prepared and used for blot-overlay analysis. Since S100 proteins are transducers of calcium signaling and change their conformation in the presence of calcium, blot-overlay assay was performed in the presence of calcium and EGTA as a control. For lysates preparation, overnight bacterial cultures were diluted 10 times and then grown in the absence and presence of 1mM IPTG for 4 hrs. This approach was used to prepare the lysates of NMHC IIA (Hmyo1, Hmyo2 and Hmyo3) after IPTG-induction. However, when the recombinant proteins were less stable, a purification was used. The selection of protocol depends on the stability and solubility of the protein (Ward and Swiatek, 2009). If the recombinant protein was in inclusion bodies, purification under denaturing condition was performed. Bacterial pellets were resuspended in lysis buffer containing GuHCl and soluble protein was applied to Ni-NTA resin overnight. The resin was washed to remove non-specific binding proteins. Proteins were then eluted from Ni-NTA resin using a buffer containing urea pH 4.5. The eluted fractions of the recombinant NMHC IIA protein fragments (Hmyo) were resolved on SDS-PAGE and then stained with Coomassie blue as shown in (Figure 5.13). The detected bands corresponded to the expression of the recombinant proteins. The sequence of Hmyo 3B was shown in (Figure7.1).



### Coomassie blue staining

**Figure 5-13: Coomassie blue staining of the purified NMHC IIA fragments under denaturing condition**

Recombinant proteins of Hmyo 3, Hmyo 3A, Hmyo 3B and Hmyo 4 fragment were purified under denaturing condition and resolved on SDS-PAGE followed by Coomassie blue staining. The bands were characterized at approximately 70, 60, 52, and 30 kDa (red arrows) corresponding to the expressed recombinant Hmyo3, Hmyo4, Hmyo 3B and Hmyo3A proteins, respectively. The expressed Hmyo3 (70kDa) was used as a control.

#### **5.4.6 Analysis of non-muscle myosin heavy chain IIA interaction with S100A6 by blot overlay**

To examine expression of NMHC IIA fragments, bacterial lysates of recombinant NMHC IIA fragments (Hmyo1, Hmyo 2) and semi-purified proteins (Hmyo3, Hmyo 4 and Hmyo3A) and purified protein Hmyo3 B were resolved on two SDS-PAGE. The first gel was stained with Coomassie blue to confirm the expression of the proteins (Figure 5.14-A), another gel was used for transferring of proteins onto the membranes for blot overlay analysis using S100A4 or S100A6 protein in the presence of 1mM Ca<sup>2+</sup> or 5mM EGTA (Figure 5.14-B). This technique is particularly useful to study protein-protein interaction *in vitro*. Regarding to blot overlay result, it was observed that both S100A4 and S100A6 interacted with Hmyo4 fragment. The interactions were abolished in the presence of EGTA. This means that both proteins interacted with the C-terminal end of the NMHC IIA. In addition, the new binding of S100A6 was detected in Hmyo 3B fragment which is derived from the coiled coil region of NMHC IIA.

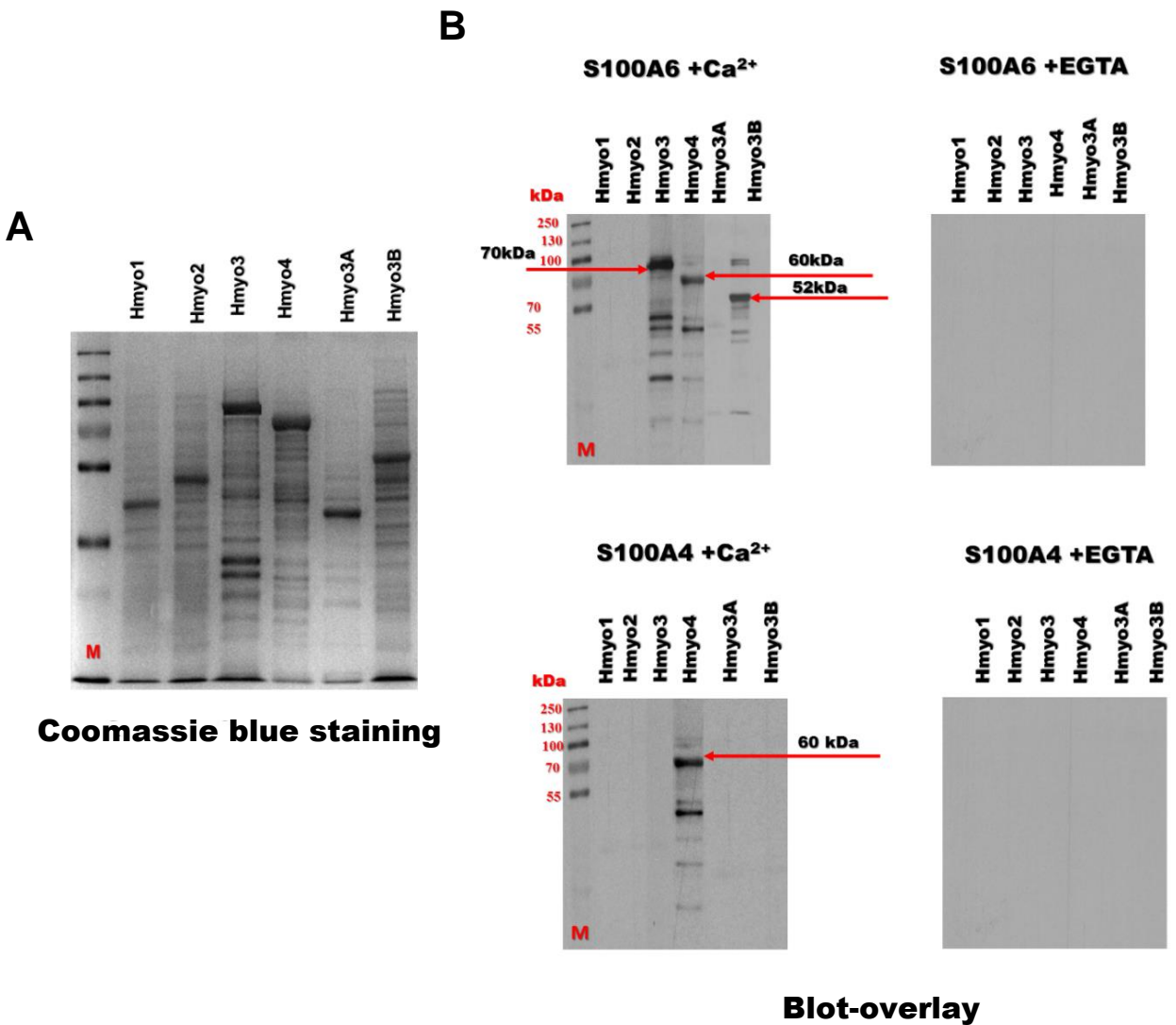


**Figure 5-14: Detection of a new site of interaction of S100A6 with myosin heavy chain IIA by blot overlay.**

Recombinant myosin heavy chain IIA protein fragments were prepared. Bacterial lysates expressing recombinant NMHC IIA fragments were prepared from M15 cells and resolved on a two 12% SDS-PAGE. A-The first gel was stained with Coomassie blue. B-The second gel was used for transferring of proteins onto membranes that were incubated overnight with 5 $\mu$ g/ml of S100A4/A6 in buffer containing either 1mM CaCl<sub>2</sub> or 5 mM EGTA following staining with anti-S100A4 or anti-S100A6 antibodies.

#### **5.4.6.1 Mapping of the S100A6 binding site on the Hmyo 3B fragment**

Blot overlay showed that S100A6 as S100A4 interacts with both Hmyo 4 and Hmyo 3B. So, this new site of the S100A6 interaction is located inside the myosin rod domain.

##### **5.4.6.1.1 Incorporation of stop codons into Hmyo 3B fragment by site-directed mutagenesis**

To ascertain the localisation of S100A6 binding region on Hmyo3B fragment, fragments of Hmyo 3B with different lengths were generated and then they were used to analyse the interaction with S100A6. Polymerase chain reaction (PCR)-based site-directed mutagenesis was carried out according to QuikChange® site-Directed Mutagenesis (Stratagene, USA) protocol. Forward primers were first designed to have desired mutation in the middle of each primer inducing a TAG stop codon to terminate protein synthesis. DNA template was amplified with mutagenic oligonucleotide primers as described in (Materials and Methods) by a Polymerase Chain Reaction (PCR). To increase the efficiency of the reaction, PCR products were digested by *Dpn* I to remove hemi-/methylated-DNA and then transformed into competent *E.coli* M15 strain by nucleofection. Two single colonies were picked up and grown on the selective media overnight for plasmid DNA isolation. To ensure that the stop codons have been incorporated in the right locations and no other mutations had been arisen from the PCR amplification, sequencing was performed.

Expression of the recombinant Hmyo 3B stop1, stop2, stop3, stop4, and stop5 fragments were induced by IPTG; sequences were shown in (Figure 7.1). Bacterial lysates of 3B-stop1 and stop2 fragments were then run on two SDS-PAGE. One gel was stained with Coomassie blue to confirm the expression of the proteins (Figure 5.15-A) and another one was subjected to the blot overlay assay. It was found that there is no interaction between S100A6 and the truncated myosin fragments stop1, stop2 and stop3. However, S100A6 interacted with Hmyo3B-stop4 and stop5 fragments; 30 kDa and 38 kDa, respectively (984-1385) aa (Figure 5.15-B).

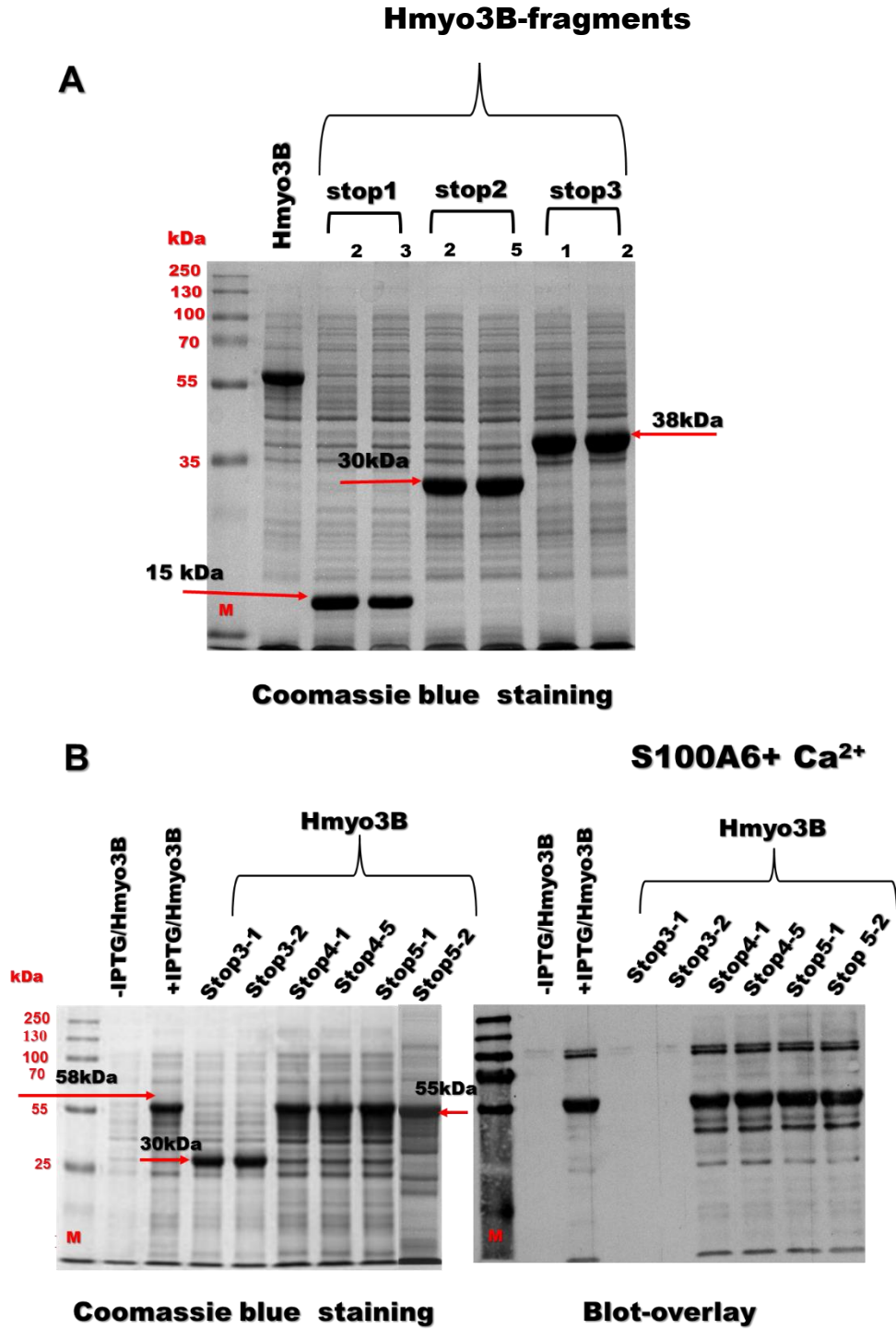


**Figure 5-15: Mapping of S100A6 binding sites on the MHC IIA.**

The recombinant Hmyo3B fragments were resolved on two SDS-PAGE. The gel was either stained with Coomassie blue or blotted (A) and (B). B-Blot overlay assay was performed in the presence of 1 mM CaCl<sub>2</sub>. S100A6 interacts only with Hmyo3B-stop4 and Hmyo3B-stop5 (984-1385) aa.

To confirm that the S100A6 binding site is included into the sequence of the identified region, a small recombinant protein (M53) containing a sequence which is a part of Hmyo 3B (S1296-1349E) residues was cloned in pQE30 and expressed as recombinant bacterial protein (Figure 5.16) which was then used for blot overlay analysis.

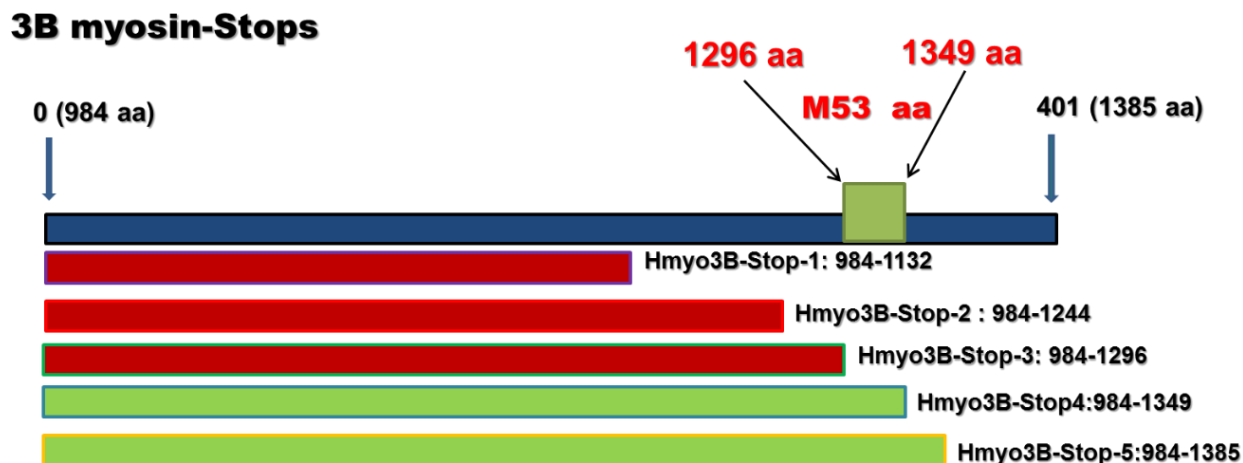


**Figure 5-16: Schematic represents mapping of new S100A6 binding site on rod domain of NMHC IIA.**

Mapping of the new S100A6 binding site on the myosin IIA coiled coil region was made by site-directed mutagenesis. 5 stop codons were incorporated into Hmyo 3B fragment via PCR using Hmyo3B plasmid as a template. S100A6 did not interact with Hmyo 3B-stop 1, stop 2 and stop 3 illustrating by red colour, but it interacted with Hmyo 3B-stop 4 and stop 5 showing by green colour. Green colour reflects M53 fragment consisting of the 53 amino acids (S1296-1349E) that was cloned and expressed.

cDNA of M53 (159 bp) was cloned into a selected expression vector pQE30 (3461 bp) after double digestion using Bam HI-HF and Hind III-HF restriction enzymes. The ligation of the insert (cDNA M53) and the plasmid pQE30 was done overnight using T4 DNA ligase enzyme to form pQE30+M53 (3584bp). Transformation into M15- *E.coli* competent bacteria cells was then achieved through the use of electroporation method (Figure 5.17-A). Cell suspension of bacteria was plated on a selective LB agar plate and incubated overnight at 37°C. The same experiment was used to clone cDNA of S100A6 (270 bp) into pQE30 vector (Figure 5.17-B). (Figure 7.2 and 7.3) shows the sequences of M53 fragment and S100A6 protein, respectively. Figure (7.4) shows the sequence of pQE30 vector.

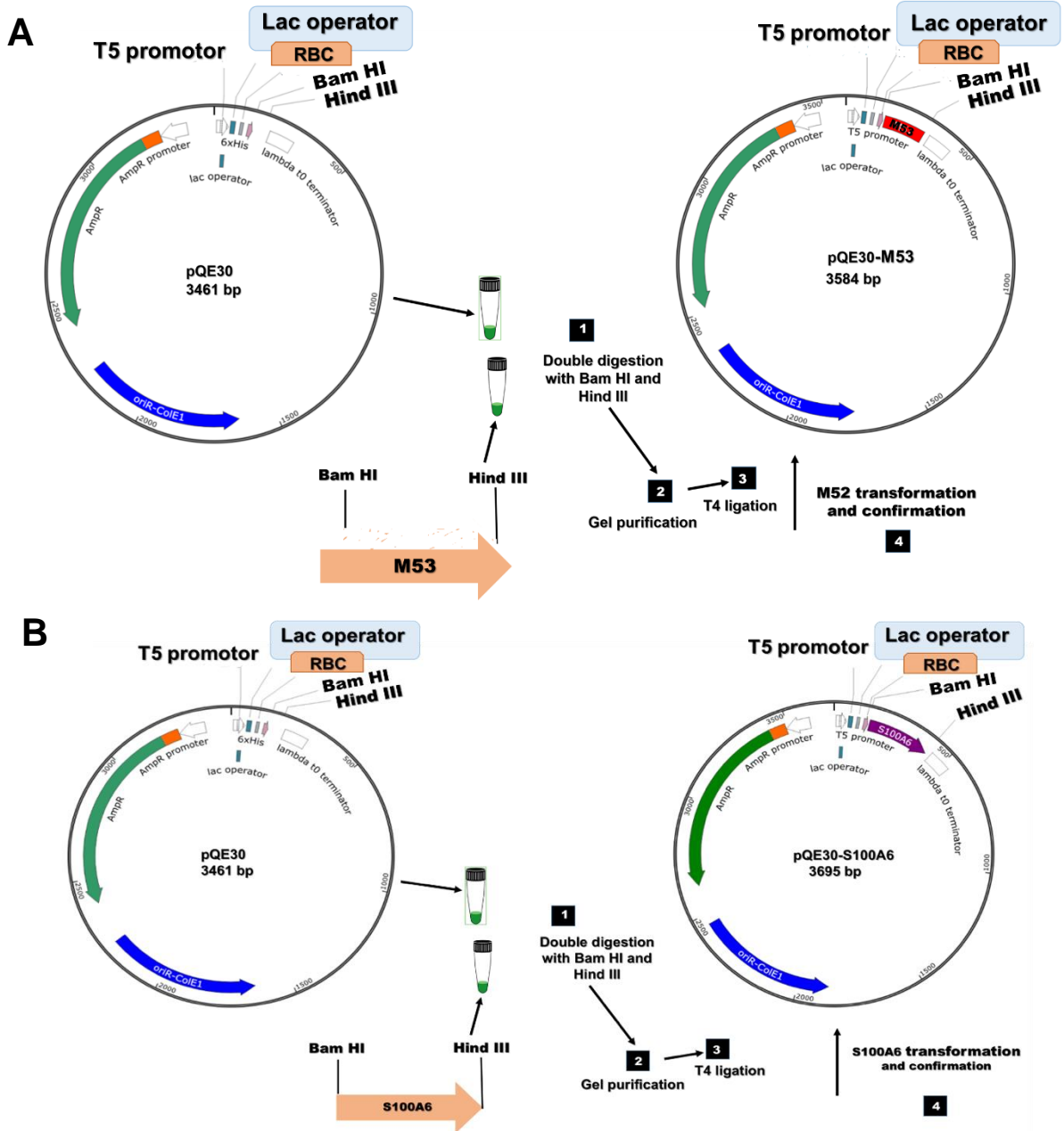


**Figure 5-17: Schematics of cloning of M53 and S100A6 DNA into pQE30 plasmid.**

A- cDNA of M53 (159 bp) was cloned into pQE30 vector after double digestion using Bam HI-HF and Hind III-HF restriction enzymes. B- cDNA of S100A6 (270 bp) was cloned into pQE30 vector after double digestion using the same enzymes. Ligation of the insert (cDNA M53 or S100A6) and PQE30 was done overnight and transformation was achieved through the use of electroporation of

M15-*E.coli* competent bacteria. Plasmid map produced using Snap Gene Viewer 283 and APE version 2.0.45.

The amino acids sequence of M53 protein (S1296-1349E) is shown in (Figure 5.18).

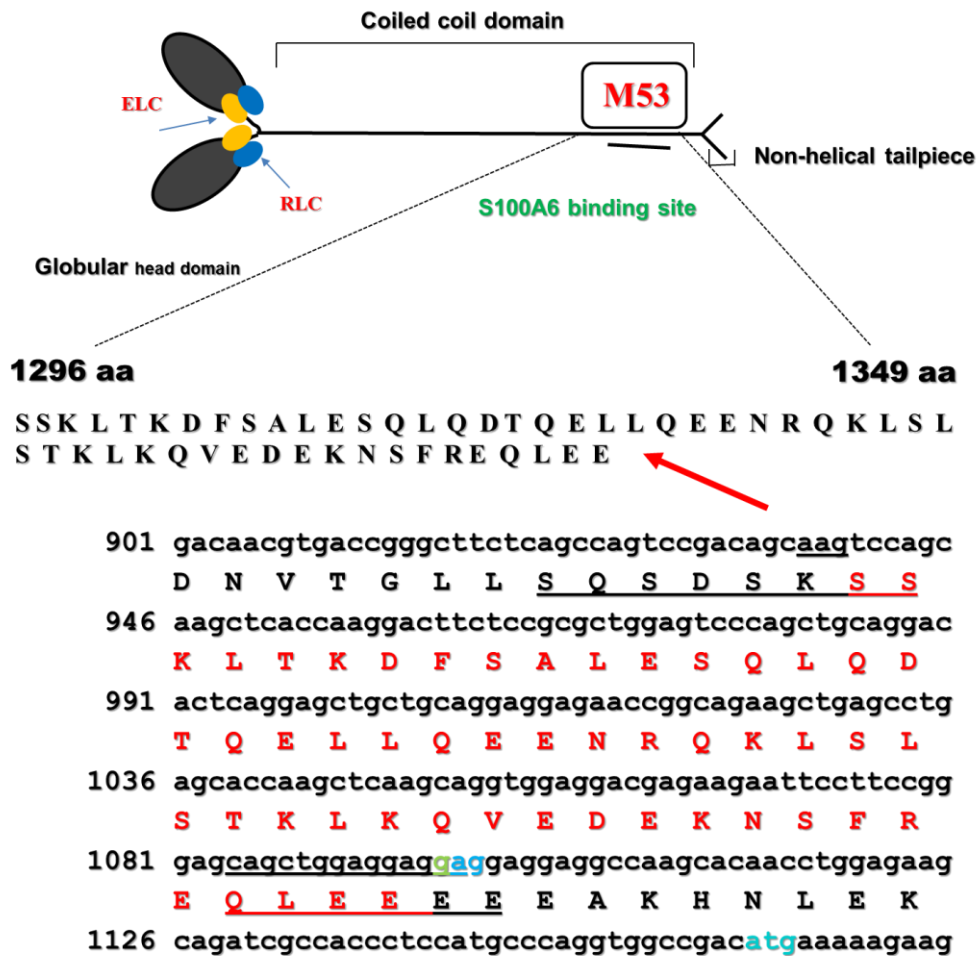


**Figure 5-18: M53 fragment is a part of rod coiled coil domain of NMHC IIA.**

M53 fragment is composed of 53 amino acids (S1296-E1349). This fragment is located in the middle of coiled coil region of NMHC IIA. Residues that represent the S100A6 binding site. The nucleotide and amino acid composition of the M53 fragment is shown.

#### 5.4.6.1.2 Large scale expression and purification of the M53 protein.

To examine the expression of M53 fragment, small-scale expression experiment was first conducted. After 4 hrs IPTG induction, lysates were collected and run on SDS-PAGE followed by staining the gel with Coomassie blue to check the expression of recombinant M53 protein (data not shown). Following this, large-scale isolation and transition was done to produce enough amount of proteins for NMR analysis and next biochemical experiments. 10 liters of bacterial broth were prepared for protein purification. Bacterial pellets were prepared after 4 hrs IPTG induction of recombinant M53 protein. Protein purification was undertaken under native condition and M53 protein fractions was eluted from Ni-NTA agarose column by imidazole. Purified M53 protein was analysed by SDS-PAGE and stained with Coomassie blue. M53 protein was observed as a single band corresponding to the correct molecular weight of M53 protein of 8 kDa. The same method was used to purify S100A6 protein under native condition to use this protein for further analysis (Figure 5.19).

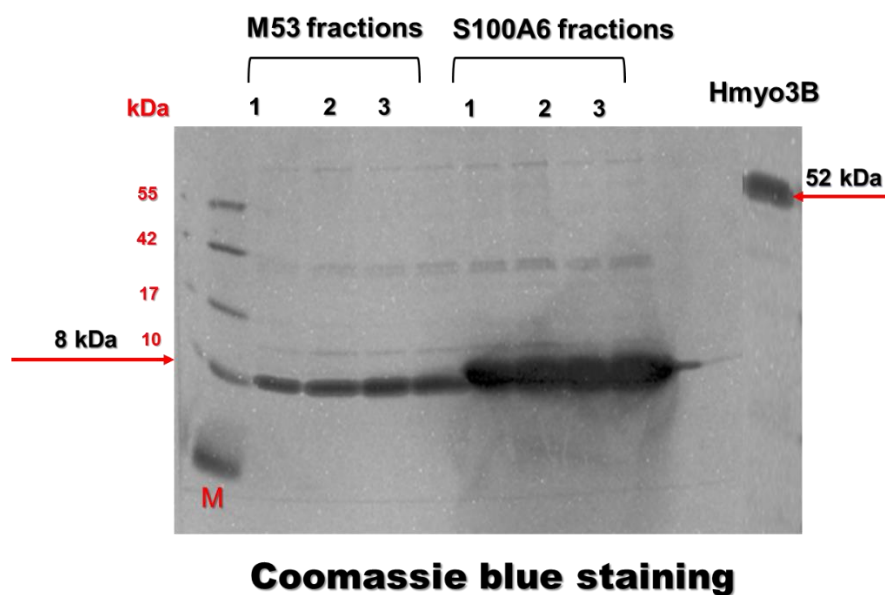


**Figure 5-19: Isolation of M53 and S100A6 proteins purified under native condition.**

To test the presence of M53 and S100A6 proteins, eluted fractions of M53 and S100A6 proteins under native conditions were resolved on 18% SDS-PAGE. The gel was then stained with Coomassie blue.

#### **5.4.6.1.3 Analysis of the S100A6 and M53 interaction by blot-overlay**

Based on the previous finding, blot overlay was carried out to confirm the possible direct interaction of S100A6 with M53 (8 kDa) fragment (S1296-E1349) which derived from the coiled coil region of NMHC IIA. Previous study by (Badyal et al., 2011) showed that S100A4 interacted with M200 fragment (Q1761–E1960) which is located within the C-terminal 200 aa of NMHC IIA. Blot overlay assay was carried out to verify the site of S100A6 interaction on the myosin heavy chain IIA.

Myosin heavy chain fragments were resolved on three 18% SDS-PAGE. One gel was stained with Coomassie blue to detect the expression of M53 protein (Figure 5.20-A). Another two gels were transferred to the membranes for incubation with S100A4 or S100A6 in the presence of  $\text{Ca}^{2+}$ . Blot overlay analysis shows a direct interaction of S100A6 with both M53 and Hmyo4-B fragments in the presence of calcium which were characterized as bands corresponding to 8 and 35 kDa, respectively (Figure 5.20-B). In contrast, S100A4 interacted in blot overlay assay with Hmyo4-B fragment (35 kDa) only in the presence of calcium (Figure 5.20-B). In conclusion, the results above have identified (S1296-E1349) of myosin heavy chain IIA as a core sequence for S100A6 binding.

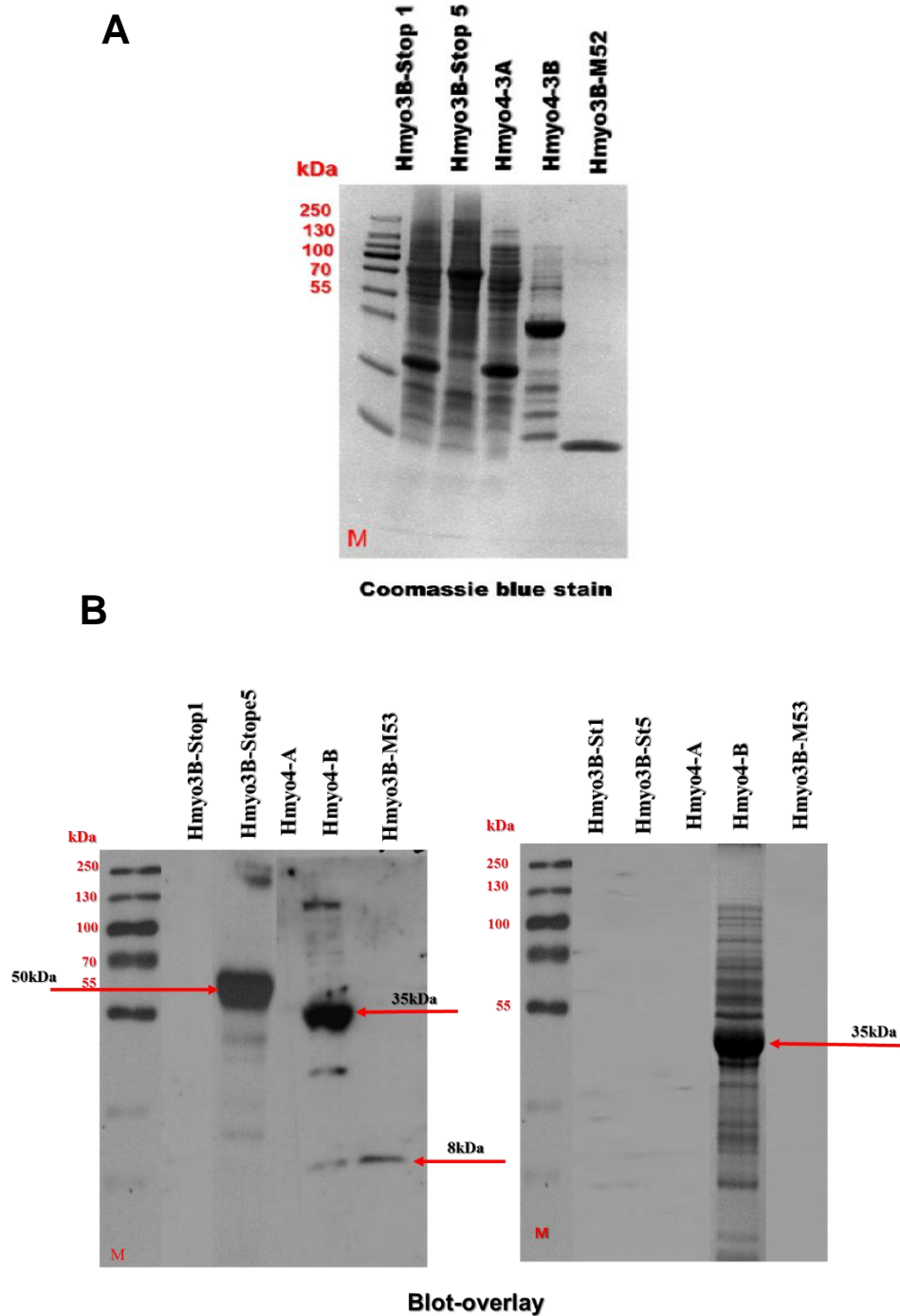


**Figure 5-20: Localisation of S100A6 and S100A4 binding sites on NMHC IIA by blot overlay analysis**

Crude and purified fragments of recombinant NM IIA fragments were run on 18% SDS-PAGE and either stained with Coomassie blue (A) or used for blot overlay assay (B); the proteins were transferred onto membranes and they were incubated overnight with 5 $\mu$ g/ml of S100A4 or S100A6 protein in buffer containing 0.1mM CaCl<sub>2</sub> followed by staining membranes with anti-S100A4 or anti-S100A6 antibodies.

#### **5.4.7 S100A4 and S100A6 are new regulators of myosin dynamics**

Since S100A6-myosin IIA interaction was confirmed, further *in vitro* investigations were performed to analyse the effect of S100A6 on myosin dynamics.

##### **5.4.7.1 The effect of ionic strength on myosin IIA aggregation**

As S100A6 interacted directly with Hmyo 3B, therefore this fragment was used to study the solubility of myosin IIA in the presence of S100A6 or S100A4 by turbidity assay. Before that, the turbidity assay was carried out to measure the solubility of Hymo3B fragment in high and low salt buffer.

10  $\mu\text{M}$  of Hmyo 3B was prepared in buffer containing 20 mM NaCl, 20 mM HEPES and 0.1 mM  $\text{Ca}^{2+}$ . The turbidity was measured at ODA<sub>300</sub> nm at an indicated time point 1200s. The ionic strength of the solution was steadily increased by adding 20 mM aliquots of NaCl and the turbidity was measured after each addition. Continuous measurement of the protein solubility was carried out until no turbidity was detected, because saturation had been reached. Plotting the absorbance versus NaCl concentration formed a sigmoid curve and provided midpoint value of 150 mM NaCl (Figure 5.21).

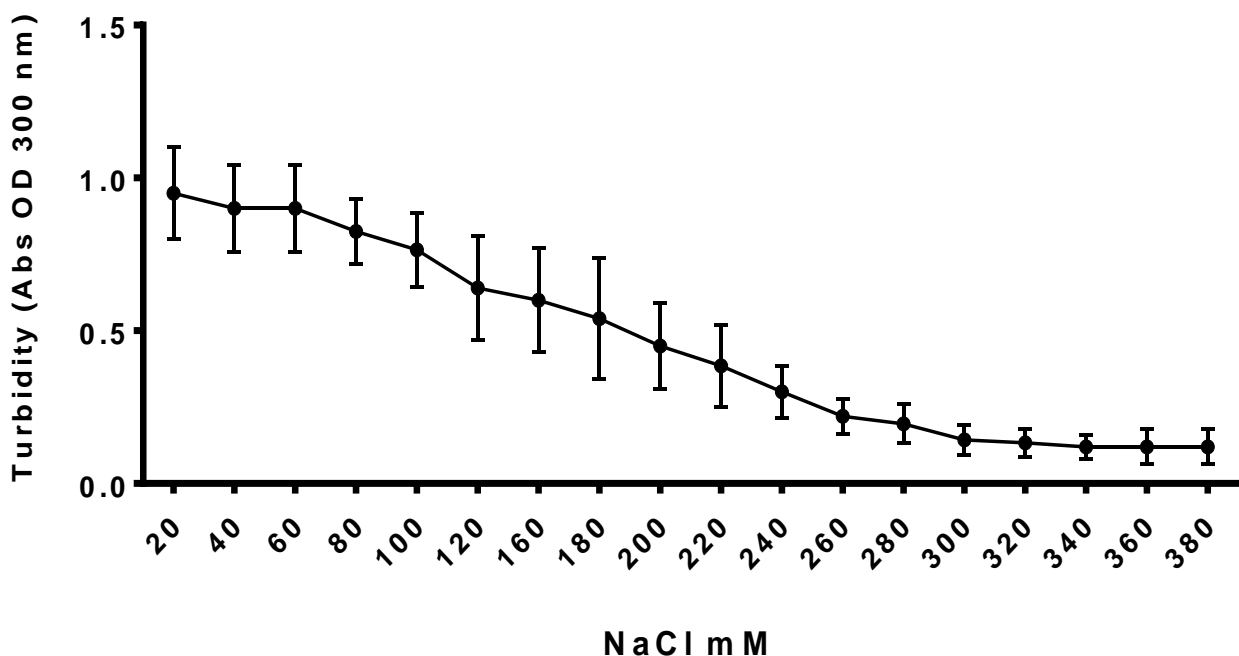


**Figure 5-21: Alteration of the Hmyo3B turbidity is controlled by NaCl concentration.**

10  $\mu$ M Hmyo3B was prepared in the buffer containing 20 mM NaCl, 20 mM Hepes, 0.1 mM  $\text{Ca}^{2+}$  at pH 7.5 and the absorbance was measured at  $A_{300}$  nm. 20 mM NaCl were added every 1200s and the absorbance was measured until a background level had been achieved (approximately 400 mM NaCl). The turbidity values were plotted against concentrations of NaCl and fitted to a sigmoid curve to yield midpoint for fragment Hmyo3B of 150 mM NaCl. The values were averaged from two independent experiments and the error bars represent standard deviation.

#### 5.4.7.2 Solubility of myosin fragments by S100A4/A6

Based on the previous finding, the turbidity assay was performed to assess the effect of S100A4/A6 on the Hmyo 3B and M200 fragments disassembly. Blot overlay experiment showed that S100A6 was able to interact with Hmyo 3B fragment. Consequently, it would be expected that S100A6 would solubilise Hmyo 3B filament which could be measured in turbidity assay. 10  $\mu$ M of Hmyo 3B was prepared in the buffer containing 150 mM NaCl and then 20  $\mu$ M S100A6/A4 was applied. The turbidity was measured at  $\text{ODA}_{300}$  nm in an indicated time point of 1200s until there was no change in turbidity. Data show that the turbidity significantly reduced in the presence of S100A6. Moreover, Hmyo 3B filament aggregate was fully solubilised by addition 80  $\mu$ M S100A6; \*\*\*\*P < 0.0001. Addition of 5 mM EGTA reversed the process, allowing Hmyo3B filaments to form (Figure 5.22-A).

With respect to S100A4, data show that there was no significant effect of S100A4 on the solubility of Hmyo 3B fragment in the presence of  $\text{Ca}^{2+}$  (Figure 5.22-B).

Since S100A4 binds to M200 fragment which is a part from C-terminal end of myosin IIA and actively promotes filament disassembly (Badyal et al., 2011), it is important to consider the effect of S100A6 on the M200 filament aggregation using the same technique. As shown in (Figure 5.22), S100A6/A4 specifically decreased the turbidity of M200 fragment in the presence of  $\text{Ca}^{2+}$ . Indeed, there was no changing of the absorbance after addition 60 $\mu\text{M}$  S100A6 to M200 fragment (Figure 5.23-A). However, S100A4 has a more significant effect on the solubility of M200 fragment than S100A6. M200 filament was fully dissociated in the presence of 40  $\mu\text{M}$  S100A4 (Figure 5. 23-B).

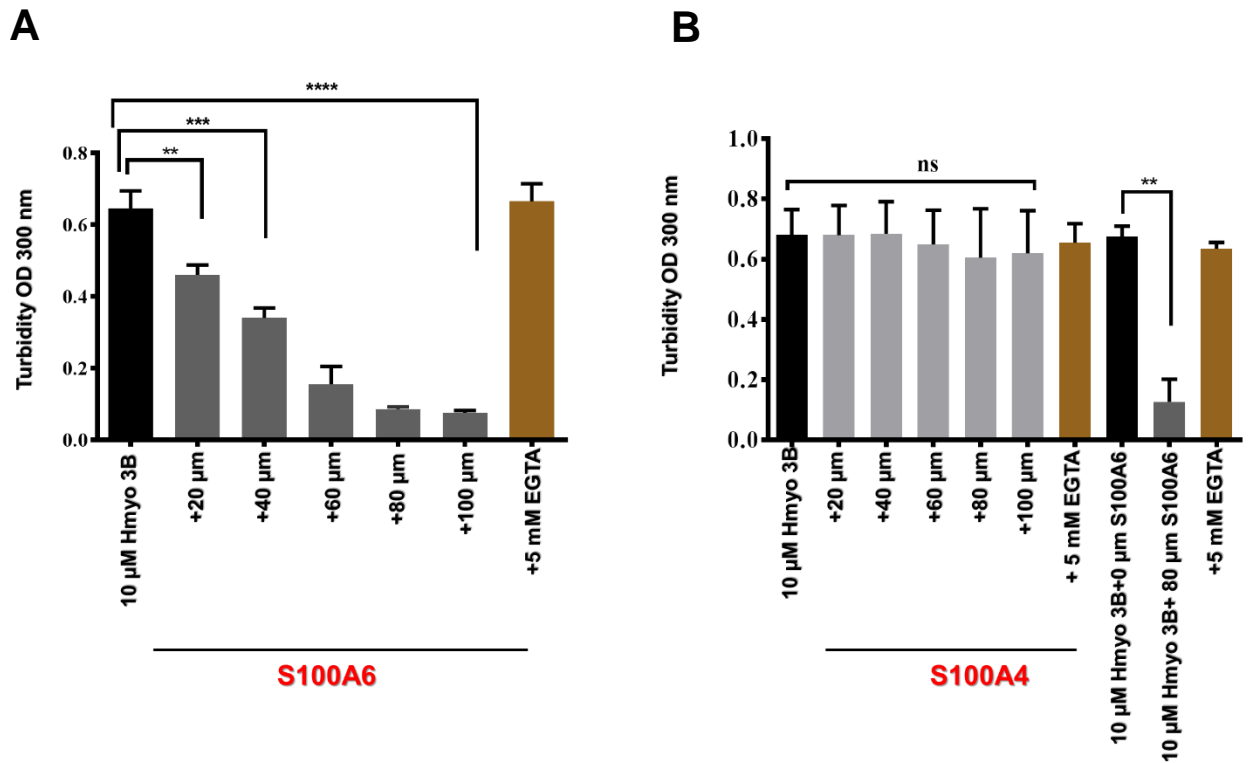


**Figure 5-22: Dissociation of Hmyo 3B filaments by S100A6.**

10μM of Hmyo 3B was prepared in the buffer containing 20 mM HEPES, 0.1 mM Ca<sup>2+</sup> at pH 7.5 to give a final concentration of NaCl of 150 mM and the turbidity measured at the absorbance of A<sub>300</sub>. A- 20 μM S100A6 was added at a time point of 1200s until there was no change in turbidity. 5mM EGTA was added to chelate Ca<sup>2+</sup> B- 20 μM S100A4 was added in a time point of 1200s, but no significant effect was detected. Results are represented of three separate experiments. Data was presented as mean ± SEM. P values were determined by a Two- way ANOVA followed by a Dunnett's Multiple comparison test; \*\*P= 0.0057, \*\*\*P = 0.0003, \*\*\*\*P < 0.0001.

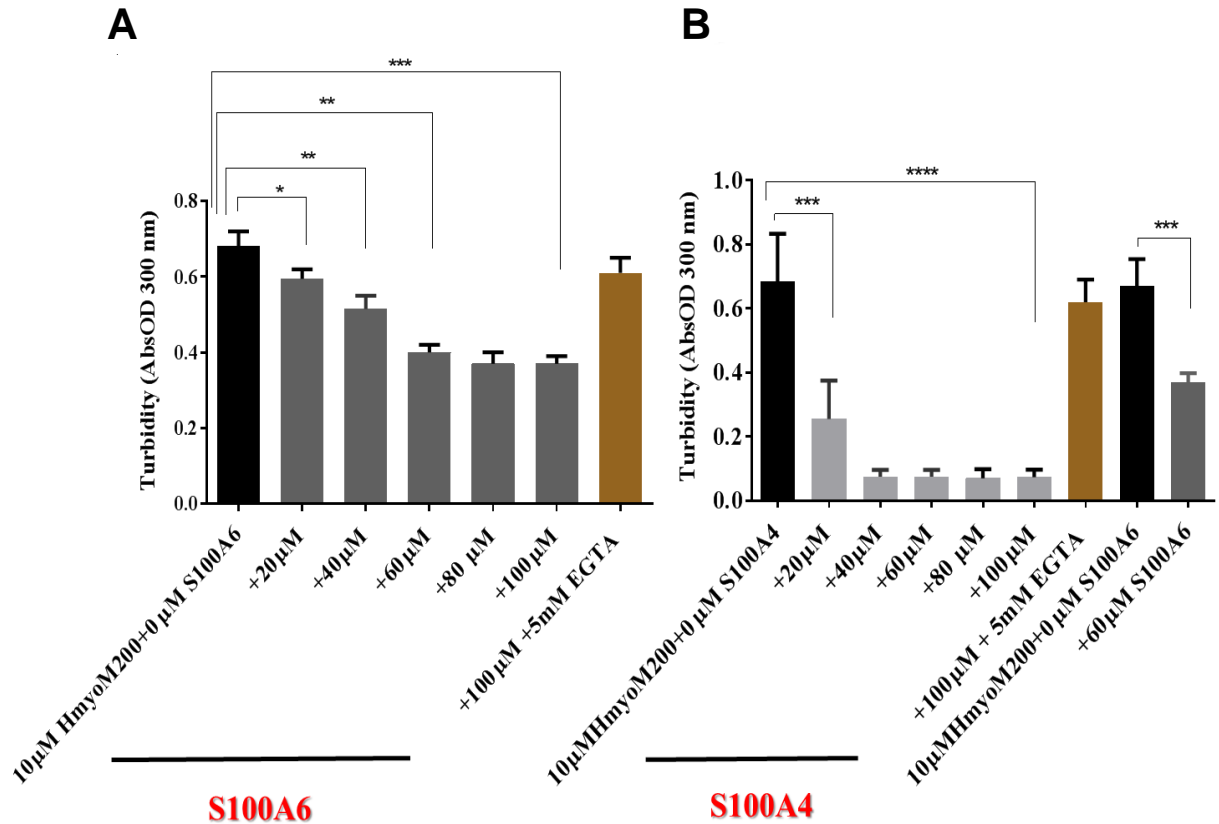


**Figure 5-23: Dissociation of M20 filaments by S100A4/S100A6.**

10 μM of M200 was prepared in the buffer containing 20 mM HEPES, 0.1 mM Ca<sup>2+</sup> at pH 7.5 to give a final concentration of NaCl of 150 mM. The turbidity of the solution was measured at the absorbance of A<sub>300</sub>. A- 20 μM S100A6 was added in an indicated time point of 1200s until until there was no change in turbidity. Data was presented as mean ± SEM. P values were determined by a Two-way ANOVA followed by a Dunnett's Multiple comparison test; \*P = 0.0290, \*\*P = 0.0017, \*\*\*p=0.0009. 5mM EGTA was added to chelate Ca<sup>2+</sup> B- 20 μM S100A4 until saturation point has been reached. \*\*\*P=0.0001, \*\*\*\*P < 0.0001. Results are represented of three separate experiments.

## 5.5 Discussion

As S100 proteins are involved in cytoskeletal dynamics, S100A6-NM IIA interaction was investigated in Dox treated A431-ZEB2 cells. After confirming the hypothesis, the aim was to identify the S100A6 binding site on NMHC IIA. For this purpose, overlapped MHC IIA fragments were prepared for analysis.

### 5.5.1 Co-localisation of S100A6 and NM IIA in cells

Following findings in this chapter, it was observed that a member of S100 proteins, S100A6 interacts with myosin IIA in a  $\text{Ca}^{2+}$  dependent manner. Our results show that like S100A4, S100A6 was localised within the nucleus and cytosol of A431/ZEB2 cells as observed by confocal studies (Figure 5.6-B) and (Figure 5.7-B). Some variability in S100A6 expression was estimated in cells. In agreement with (Mandinova et al., 1998, Sudo and Hidaka, 1998) who reported that S100A6 is mainly localised in the cellular cytoplasm and it forms a network structure around the nucleus as well. In addition, the results established that S100A6 was upregulated in A431/ZEB2 cells treated with Dox (Figure 5.6-A) and (Figure 5.7-A). *In vitro* study (Chen et al., 2015) reported that overexpression of S100A6 induces EMT and triggers cell motility and invasion. Co-immunoprecipitation analysis detects the interaction between S100A6 and GFP-myosin IIA in A431/ZEB2-WT cell lysates. However, a weak signal was shown when immunoprecipitated GFP complexes was immunoblotted for S100A6 antibody (Figure 5.5). Very limited studies have investigated the interaction between S100A6 and other target proteins (Hoyaux et al., 2000). One study showed that CacyBP/SIP interacted with S100A6 protein *in vitro* in a  $\text{Ca}^{2+}$  dependent manner which was evaluated by co-immunoprecipitation assay. Importantly, nearest-neighbor co-localisation analysis from immunogold labelling experiment suggested that a new binding site of S100A6 with NM IIA exists on the coiled coil region of NMHC IIA. Previous studies showed that S100A6, *in vitro*, interacts with several target proteins such as tropomyosin, annexins II and XI (Filipek et al., 2008, Luo et al., 2008, Breen and Tang, 2003, Hoyaux et al., 2000, Sudo and Hidaka, 1998).

### **5.5.2 S100A4 and S100A6 inhibit the actin - activated ATPase activity of NMC IIA**

The globular head domain of myosin IIA contains actin- and ATP-binding sites which are responsible for generating force. ATP binding initially decreases the affinity of myosin IIA for actin. Later, hydrolysis of ATP rapidly leads to a metastable ternary complex between myosin, ADP, and inorganic phosphate (Pi) (Rayment and Allingham, 2007). It is evident from our data that ATPase activity of actomyosin IIA complex was down-regulated in the presence of S100A4 and S100A6 (Figure 5.2). This result confirms the role of S100A4/A6 in controlling the myosin IIA dynamics in cells, as myosin is an actin-based motor protein and ATPase activity of actomyosin complex is characteristics of stress fibers formation (Watanabe et al., 2007). Other studies (Billington et al., 2013a, Beach and Egelhoff, 2009) reported that binding of myosin IIA to F-actin leads to hydrolysis of ATPase which generates force responsible for cell division. However, one study showed that ATPase activity of myosin IIA was diminished during metastasis of cancer cells, such as skin squamous cell carcinoma (Schramek et al., 2014). Myosin IIA and actin tend to play a crucial role during cancer cell migration via force generation resulting from ATP hydrolysis. Several studies have reported this issue, for example (Li et al., 2010) suggested that S100A4 inhibits ATPase activity of actomyosin IIA complex leading to a decrease in the assembly of actin-myosin IIA into filaments. Another study by (Donato, 2001) revealed that binding of S100A4 protein to NMHC IIA in a  $Ca^{2+}$  dependent manner results in the inhibition of actin-activated ATPase activity of myosin IIA promoting disassembly of myosin filaments. Several lines of evidence suggest that S100A4 binds to NM IIA in a  $Ca^{2+}$ -dependent manner and inhibits the actin-activated myosin MgATPase (Ford et al., 1997). Thus, S100A4 promotes the disassembly of myosin filaments and inhibits their reassembly (Ford et al., 1997; Li et al., 2003). Despite of the direct effect of S100A4/A6 on the actin-activated ATPase of myosin IIA, cycloheximide chase assay permitted us to conclude that S100A4/A6 do not have impact on myosin IIA half-life as RLCs that are critical for cell structure and maintaining stability of myosin heavy chain (Park et al., 2011).

### **5.5.3 S100A6 interacts with M53 fragment**

A binding site of S100A6 was mapped on NMHC IIA by blot overlay experiment. Blot overlay assay is a biological technique that provides a reliable method to test protein-protein interaction *in vitro* (Hall, 2004). Recombinant NMHC IIA fragments were used for blot

overlay. Some fragments were semi-purified due to their instability. During the protein purification experiments, certain parameters were taken into consideration, such as selection of technique, changing buffers, and pH of washing and elution buffers. High concentrations of salt and certain denaturants, such as 7 M urea or 6 M GuHCl, had an effect on our result. For this reason, purification of proteins from samples in different starting buffers is preferable. The denaturing technique is preferable, because the proteins can be isolated from inclusion bodies as strong denaturants (Terpe, 2003).

In this work, S100A4 binding site on NM IIA was confirmed to be on the tail region, whereas no interaction was demonstrated with the myosin rod domain. This finding is in agreement with (Kriajevska, 1998) study who suggested that S100A4-binding site is located within a 29-amino acid region, at the C-terminal end of the myosin heavy chain between (1909–1937) aa. Furthermore, another study reported that there was a negative impact on the binding parameters of the interaction of S100A4 with NMHC IIA when the two C-terminal residues were removed (Ismail et al., 2008). For the first time, it was shown that S100A6 interacts with the myosin IIA rod domain between (S1296-E1349) aa. Further analysis should be done to clarify the affinity and functional role of this interaction. In agreement with the preliminary data that was obtained by the master student (Elvira Diamantopoulou, MSc thesis, University of Leicester) who reported that the rod domain of myosin was a potential target for S100A6, which was characterized by blot overlay assay. This study shows also that S100A4 and S100A6 can interact with NM IIA tail. Other studies have also found a similar issue, for instance Fernandez-Fernandez and colleagues revealed that S100A4 and S100A6 bind to P53 TET domain which affects the transcriptional activity of p53 (Fernandez-Fernandez et al., 2008).

#### **5.5.4 S100A4/A6 dissociates NM IIA in turbidity assay.**

Turbidity of myosin IIA as measured in a standard spectrophotometer provides a useful way to follow the association and dissociation of myosin. The results show that the ionic strength of non-muscle myosin IIA was in the transition between dissociated (soluble) and associated (filamentous) myosin status. It was shown that approximately 300 mM NaCl completely solubilized the aggregates of coiled coil fragment. Ideally, a titration with increasing NaCl

should be consistent, meaning that when NaCl is in excess amount there is no change, and that indicates the equilibrium has been reached. Furthermore, turbidity assay was used to assess the effect of S100A4/A6 on myosin filament aggregation. It was shown that S100A4 binds to the tail fragment of MHC IIA and actively promotes disassembly rather than just binding to the myosin monomer and displacing the equilibrium. Similar measurements were made to investigate the dissociation of coiled coil and tail fragment in the presence of S100A6. However, regardless of the detailed mechanism, S100A6 solubilised coiled coil fragment aggregates simply by sequestering the free monomers. This study displays that S100A6 can solubilise coiled coil fragment of myosin IIA, while partial dissociation of myosin IIA tail fragment was detected in the presence of S100A6. In addition, it was shown that S100A4 can also solubilise myosin tail fragment. Similarly, (Badyal et al., 2011) reported that 2 molecules of S100A4 monomer was required to solubilise 1 molecules of myosin tail aggregate. Nevertheless, there was no effect of S100A4 on the aggregate properties of coiled coil fragment.

## **5.6 Conclusion**

S100A6 binding site was mapped on NMHC IIA which was represented on rod domain. Further analysis should be performed for an accurate mapping of binding site and investigate the affinity of the interaction. S100A4/A6 reduced the ATPase activity of NM IIA and actively promoted filament disassembly. However, S100A4/A6 did not influence myosin IIA stability.

## **Chapter 6 : General Discussion**

## 6.2 Discussion

The S100 proteins form a family of EF-hand calcium binding proteins. Specific proteins of the S100 family, S100A4 and S100A6 are implicated in different biological processes which are important in tumourgenesis and cancer progression. They exert their activity in promoting metastasis through interaction with their target proteins (Bresnick et al., 2015, Chen et al., 2014a) that have a regulatory impact on cell migration and invasion (Gross et al., 2014). The interaction of S100A4 with myosin IIA provides a linkage between the actomyosin cytoskeleton and modulation of cell migration (Li and Bresnick, 2006). The direct interaction of S100A4 with NF- $\kappa$ B, is also reputed to be involved in cancer cell proliferation and differentiation. S100A4, acting as either an intracellular or extracellular protein, can trigger cell migration using numerous pathways, such as the activation of MMPs through integrin receptors or through the RAGE signalling pathway, but the exact mechanism is still not well known (Wang et al., 2013). S100A6 also plays a key role in controlling cell migration during cancer metastasis, as it regulates the cytoskeletal dynamics via its interaction with intracellular target proteins, such as tropomyosin, annexin 11 and annexin 2 (Nedjadi et al., 2009).

This study has focused on analysis of the molecular mechanism of S100A4 on the regulation of myosin IIA dynamic. We tried also to address the question of the role of S100A6 in controlling the myosin IIA activity.

Activation of S100A4 and S100A6 expression has been shown during EMT. S100A4/A6-GFP-myosin IIA complexes were detected in cell lysates by co-immunoprecipitation analysis. Moreover, immunogold labelling of ultrathin sections of A431/ZEB2 cells were used for detecting the co-localisation of S100A4/A6 - myosin IIA in cells. The co-localisation experiments can be used to visualise different proteins as shown by (Philimonenko et al., 2000, Prior et al., 2003). According to the nearest neighbour statistical analysis of TEM immunogold labelling, data show that S100A4 interacts significantly with the 10S (50 nm) and 6S (150 nm) forms of myosin IIA monomers in cells. To analyse the effect of myosin light and heavy chains phosphorylation on S100A4 - myosin IIA interaction, the ROCK inhibitor Y27632 and myosin mutants have been used. As a consequence of inhibition of

myosin light chain phosphorylation by treating cells with Y27632, one significant peak corresponding to 50 nm was observed. This consistent with the hypothesis that this distance reflects 10S myosin monomer. It was proposed that a switching in myosin IIA conformation from the unfolded 6S or filaments to the folded 10S conformation. Furthermore, shift of the peak from the folded 10S to the extended 6S form is observed in the treated siS100A4 cells with Y27632. Taken together, these findings lead us to hypothesise that S100A4 plays a role in the regulation 6S/10S equilibrium and it is important in maintaining the 10S conformation of myosin IIA in cells, as shown in chapter 3. Analysis of the myosin conformation in cells expressing phosphodeficient and phosphomimetic mutants helped us to understand the effect of the phosphorylation of myosin light and heavy chains on the S100A4-myosin IIA interaction. Light and heavy chain phosphorylation regulates myosin IIA filament assembly. Strong co-localisation between S100A4 and GFP-myosin IIA was detected apparently in cells expressing phosphodeficient RLC-T18A\S19A or phosphomimetic S1943/E,D cells. In cells expressing phosphomimetic T18D\S19D mutants, co-localisation of S100A4 and myosin IIA was detected significantly at multiple distances corresponding to 6S myosin monomer and filaments and S100A4 interacts with both (Figure 3.26-A). However, one peak corresponding to 10S form was also demonstrated. This finding more likely indicates incomplete phosphorylation of RLC. Additionally, the results also provide further confirmation that the phosphorylation of myosin heavy and light chains has no effect on the S100A4-myosin IIA interaction in cells. In contrast to this finding, Li and his colleagues reported that phosphorylation of MHC IIA on Ser 1943 by CK2 prevents S100A4 binding and protects myosin disassembly (Li et al., 2003b). It was reported previously that phosphorylation of myosin IIA on Ser 1943 decreases filament formation and regulates the binding of S100A4 (Dulyaninova et al., 2005). In our work, it was demonstrated that phosphodeficient light chain and phosphomimetic heavy chain mutants reflect the assembly properties of non-phosphorylated and phosphorylated myosin IIA, respectively (Dulyaninova et al., 2007). Previous research has established by using FRAP analysis that a phosphomimetic S1943D displays an increase in filament turnover and reduced assembly compared with wild-type MHC IIA (Raab et al., 2012).

S100A4 increases the myosin turnover through two processes. Indeed, S100A4 provides a mechanism in maintaining a monomeric pool of activated myosin IIA by interaction with myosin IIA filaments and thereby, transient unstable complex can be initiated which further rapidly disassembles into myosin monomers, whereas 10S myosin monomer is the most stable conformation. In addition, myosin heavy chain phosphorylation provides another mechanism for recycling of myosin IIA monomers and the turnover of myosin IIA filaments. S100A6 can also play a role on regulating filament assembly/disassembly in cells.

The mechanism controlling myosin IIA activity is summarised in figure (6.1).

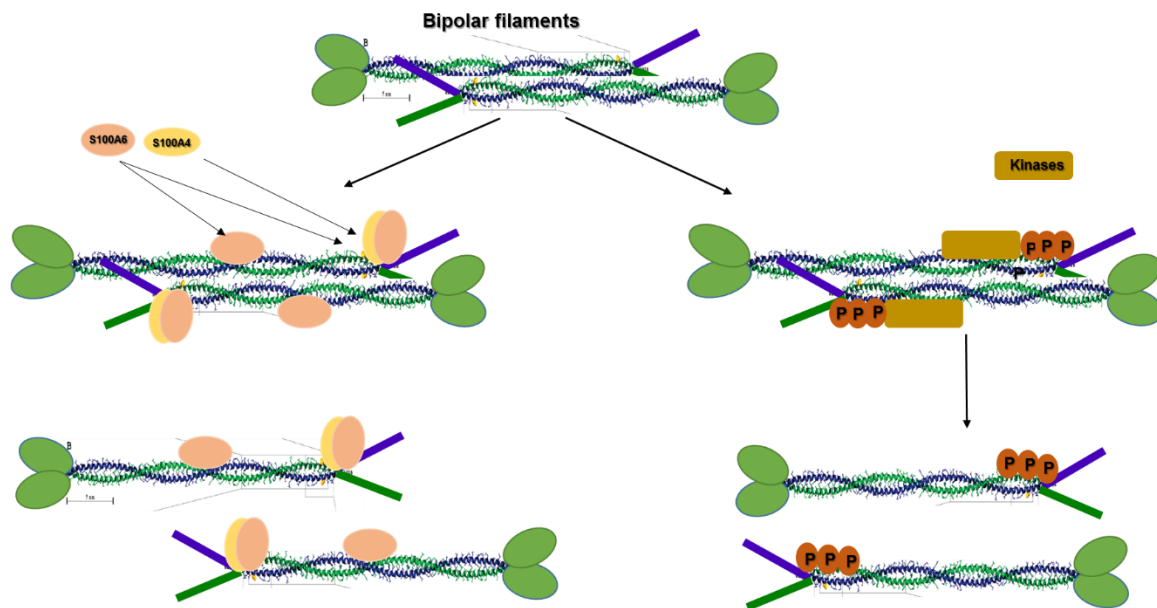


**Figure 6-1:** Schematic representative assembly/disassembly of non-muscle myosin II in the presence of calcium.

Proteins such as S100A4/A6 can interact with the region essential for the filament assembly and promote myosin depolymerisation. Phosphorylation of the MHC IIA contributes to destabilisation the electrostatic interaction between myosin IIA monomers, and thereby filament disassembly. Figure was adopted from (Clark et al., 2007).

Besides that, this study has provided a unique direct evidence for the role of S100A4 in promoting the 10S conformation of myosin in cells (chapter 3). Based on different studies, the molecular mechanism of 10S to 6S transition has been carried out only *in vitro* (Ikebe et al., 1994, Milton et al., 2011). It is likely that S100A4 binding shifts the balance towards the 10S monomer. A previous study proposed that the formation of the 10S state was a factor might contribute to promote solubilisation of intact myosin IIA filament by S100A4 (Ford et al., 1997). The folded myosin was first identified as a rapidly sedimenting peak 10S in the analytical ultracentrifuge of smooth muscle myosin preparations (Suzuki et al., 1978). However, another recent study has reported that human airway smooth muscle cells contain a significant pool of functional myosin in the 10S conformation that can assemble into filaments upon changing cellular conditions (Milton et al., 2011).

In chapter 4, data of negative stain electron microscopy showed that individual monomeric myosin molecules were detected in the presence of S100A4 and small clusters of possible folded myosin monomers were observed. A possible explanation for this might be that S100A4 might initiate aggregation of 10S state of myosin. A structural model of the folded 10S monomer of turkey gizzard smooth muscle myosin was analysed by negative stain electron microscopy (Burgess et al., 2007).

In terms of S100A6, the most interesting finding to emerge from the nearest neighbour statistical analysis is that a novel binding site of S100A6 with myosin IIA was detected as a one significant peak corresponding to 100 nm. This means that the binding site may be located on coiled coil rod domain. Therefore, S100A6 could play a role in filament assembly/disassembly of myosin IIA. Another important finding which supports this idea is the solubility of myosin IIA in the presence of S100A4/A6 in turbidity assay (chapter 5). Furthermore, a decrease in ATPase activity of actomyosin complex in cells undergoing EMT was observed in the presence of S100A4/A6. This result may be explained by the fact that that binding of S100A4/A6 to myosin IIA promotes filament disassembly, thereby decreasing the actin-activated ATPase activity.

Our data from the blot overlay assay identify a new S100A6 binding site on NMHC IIA. This is an interesting novel result shows that S100A6 binds directly to myosin heavy chain at two

different sites, but the effect on the solubility was observed only when S100A6 interacts with the rod domain. The precise binding site was mapped within a position of a 53 amino acids; S1296-E1349 present in M53 fragment.

NMR spectra with the  $^1\text{H}$ ,  $^{15}\text{N}$  heteronuclear single-quantum coherence spectrum was used to confirm S100A6-M53 interaction. It can be observed the free and the bound states of M53 protein (Figure 6.2).

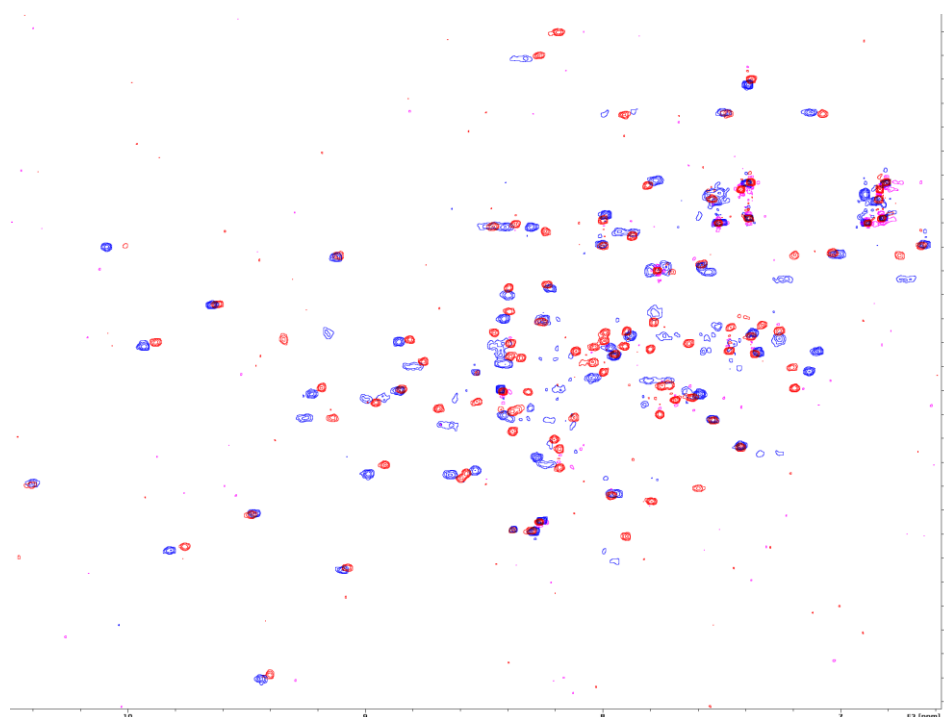


**Figure 6-2: Interaction of S100A6 with M53 peptide by NMR titration.**

NMR shows the  $^{15}\text{N}$ -HSQC overlays of S100A6 in the free form (blue) and in the presence of M53 (red). It is possible to characterise the interaction of S100A6 with M53.  $^1\text{H}$ ,  $^{15}\text{N}$ -HSQC spectrum of  $^{15}\text{N}$ -labeled (Igor L. Barsukov).

### 6.3 Conclusions and future work

1-S100A4 and S100A6 were activated during EMT

2- S100A4/A6 can form a complex with myosin IIA which was analysed by co-immunoprecipitation.

3- S100A4/A6 co-localise with myosin IIA in cells

4-Based on the presented results, S100A4 is a second important determinant of myosin dynamics in cells in addition to phosphorylation of light and heavy chains.

6-Our data shed a light on the importance of S100A4 in regulating 6S/10S equilibrium and modulates myosin IIA filament formation in cells.

7- Phosphorylation of myosin light and heavy chains do not have an effect on S100A4-myosin IIA interaction.

8- We also show for the first time that the S100A6 interacts with the coiled coil region of myosin. This finding suggests a possible regulatory role of S100A6 on myosin activity.

More research is required to determine the mode of M53-S100A6 interaction, and further work needs to be done to establish whether heavy and light chain phosphorylations have an effect on the S100A6-myosin IIA interaction in cells. The limiting time frame of the current work did not allow further analysis to characterise S100A4-myosin complexes using electron cryomicroscopy.

## Attending Conferences

### **Analysis of S100-myosin protein complexes by immunogold labelling and Transmission Electron Microscopy**

Ban H. Alwash<sup>1</sup>, Andrew Irvine<sup>1-2</sup>, Natalie Allcock<sup>3</sup>, Mohammed El-Mezgueldi<sup>2</sup>, Clive Bagshaw<sup>2</sup> and Marina Kriajevska<sup>1</sup>

<sup>1</sup> Department of Cancer Studies and Molecular Medicine, University of Leicester

<sup>2</sup> Department of Biochemistry, University of Leicester

<sup>3</sup> Advanced Imaging Facility, University of Leicester

Epithelial mesenchymal transition (EMT) is an embryonic program, which is activated in cancer. EMT stimulates dynamics of actomyosin facilitating cell locomotion and enabling metastatic dissemination of cancer cells. Non-muscle myosin II is a chemo-mechanical protein that exists as monomers of heavy and light chains. In response to the phosphorylation of light chains, monomeric myosin assembles in filaments. Multiple kinases, which are activated in EMT, regulate myosin assembly/disassembly. Conformation of myosin monomers was intensively studied *in vitro* by different biochemical and biophysical approaches but never directly investigated in cells. Inactive 50 nm monomers exist in 10S conformation, which transforms into 6S extended conformation upon phosphorylation. In addition, calcium-binding protein S100A4 regulates formation of the myosin IIA filaments via interaction with the C-terminus of the myosin heavy chain (MHCIIA).

The aim of this project was to study interactions between MHCIIA and S100 proteins in squamous carcinoma cells during EMT. Using TEM, we calculated distances between N-terminal GFP-tagged MHCIIA and S100A4/A6 by immunogold labelling. We collected multiple images and performed statistical analysis of the data. As the sizes of myosin molecules in 6S and 10S conformations are known, we were able to show that S100A4/A6 proteins interact with both myosin conformations *in vivo*.

## **S100 proteins in Epithelial to Mesenchymal Transition: their implications in cell motility and cytoskeletal dynamics**

Andrew F. Irvine<sup>1,2\*</sup>, Ban H.K. Alwash<sup>1\*</sup>, Qais Al Ismaeel<sup>1</sup>, Mohammed El-Mezgueldi<sup>2</sup>,  
,Natalie S. Allcock<sup>3</sup>, Seong Oak Park<sup>4</sup>, Sandip K. Badyal<sup>1,2</sup>, Jaswir Basran<sup>2</sup>, Igor L.  
Barsukov<sup>5</sup>, Jonathan McDearmid<sup>6</sup>, Kees Straatman<sup>4</sup>, Hyun Suk Jung<sup>4</sup>, Clive R.  
Bagshaw<sup>2,7</sup> and Marina Kriajevska<sup>1</sup>, \*\*.

<sup>1</sup> Cancer Research Centre in Leicester, UK

<sup>2</sup>Department of Biochemistry, University of Leicester, UK

<sup>3</sup>Electron Microscopy Facilities, University of Leicester, UK

<sup>4</sup>Division of Electron Microscopic Research, Korea Basic Science Institute, Korea

<sup>5</sup>Institute of Integrative Biology, Biosciences Building, University of Liverpool,

<sup>6</sup>Department of Neuroscience, Psychology and Behaviour, University of Leicester,

<sup>7</sup> Current address: Department of Chemistry & Biochemistry, University of California at Santa Cruz, USA

\*These authors equally contributed to the work.

\*\* Corresponding author: Marina Kriajevska Cancer Research Centre in Leicester, University of Leicester, Robert Kilpatrick Clinical Sciences Building

Epithelial mesenchymal transition (EMT) is implicated in tumour progression and is characterised by alterations in cell morphology and formation of highly motile cells.

During EMT, cytoskeleton undergoes global reorganisation; dynamic actin-myosin stress fibres are formed and modify cellular polarity. Non-muscle myosin II is a chemo-mechanical protein that converts cellular chemical energy into mechanical work. This protein exists as monomers of heavy and light chains. Assembly/disassembly of myosin filaments is primarily controlled by myosin light chain phosphorylation, which is activated during EMT. However, emerging evidence suggests that small calcium-binding proteins of the S100 family also play an active role in the dynamics of actin-myosin filaments, leading to increase the dissemination capability of tumour cells. Traditionally, studies on metastatic potential of human tumour cells are performed in mice, but, recently, transparent zebrafish became popular as a model system in cancer research.

The aim of this study was to analyse the interaction between NM IIA and S100A4 or S100A6 proteins and their implications in cell motility in human epidermoid carcinoma A431 cells with a Tet-On inducible expression of *Zeb2*, a master regulator of EMT.

It has been found that both S100A4 and S100A6 were strongly activated during ZEB2-induced EMT. ATPase activity of NM IIA was down regulated during the EMT. Both S100A4 and S100A6 have an inhibitory effect on the NM IIA ATPase activity. Using the transmission electron microscopy in combination with immune gold labelling, the interaction between S100A4 and S100A6 with NM IIA was identified. Moreover, silencing of S100A4/A6 affected dissemination A431 cells in Zebrafish embryos highlighting their role in EMT and tumour progression.

## **S100A4 binds to the extended and compact forms of non-muscle myosin in A431 cells undergoing Epithelial Mesenchymal Transition and modulates tumour cell dissemination in Zebrafish embryos.**

Ban H.K. Alwash<sup>1</sup>, Qais I.I. Al Ismael<sup>1</sup>, Andrew F. Irvine<sup>1,2</sup>, Natalie S. Allcock<sup>3</sup>, Jonathan McDearmid<sup>4</sup>, Mohammed El-Mezgueldi<sup>2</sup>, Clive R. Bagshaw<sup>2,5</sup>, and Marina Kriajevska<sup>1</sup>

<sup>1</sup> Cancer Research Centre in Leicester, UK

<sup>2</sup> Department of Biochemistry, University of Leicester, UK

<sup>3</sup> Electron Microscopy Facilities, University of Leicester, UK

<sup>4</sup> Department of Biology, University of Leicester, UK

<sup>5</sup> Current address: Department of Chemistry & Biochemistry, University of California at Santa Cruz, USA.

### **ABSTRACT**

#### **Background.**

S100A4 protein is a mesenchymal marker that is expressed in several forms of human cancer and implicated in regulation of cell motility and Epithelial Mesenchymal Transition (EMT) when cells lose epithelial polarity, scatter and gain mesenchymal phenotype. *In vitro*, S100A4 interacts with several molecular targets including non-muscle myosin IIA, a major actin-associated motor protein, which is involved in cell motility and cytokinesis.

#### **Observations.**

We studied expression and function of S100A4 in A431 cells, in which EMT was induced by a transcription factor ZEB2. We show that induction of S100A4 expression in this cell system promoted increased cell motility and dissemination in Zebrafish embryos.

During EMT, cytoskeleton undergoes global reorganisation when the dynamic actin-myosin stress fibres are formed. Nonmuscle myosin II is a chemo-mechanical protein that converts chemical energy into mechanical work. We detected a decrease in ATPase activity of non-muscle myosin IIA in cells undergoing EMT, a phenomenon that was largely S100A4-dependent.

Using transmission electron microscopy, we demonstrated that S100A4 and nonmuscle myosin IIA directly interact *in vivo*. Importantly, our approach allowed us to discriminate between different conformations of nonmuscle myosin within cells. The presence of two major monomeric myosin forms in a solution, compact 10S and extended 6S has been known for many years. However, the *in vivo* relevance of these conformations remains debated. Here we show that cytosol contains 10S and 6S forms of non-muscle myosin IIA, and both these forms interact with S100A4.

In conclusion, our work highlights the role of S100A4 in EMT. Our data show that S100A4 is up-regulated by ZEB2 and is implicated in the dynamic regulation myosin filaments by switching the balance towards monomeric myosin.

## **Calcium-binding protein S100A4 controls cytoskeletal dynamics and is required for the maintenance of a pool of 10S myosin IIA monomers.**

Ban H.K. Alwash<sup>1</sup>, Qais I.I. Al Ismae<sup>2</sup><sup>1</sup>, Andrew F. Irvine<sup>1,2</sup>, Natalie S. Allcock<sup>3</sup>, Jonathan McDearmid<sup>4</sup>, Mohammed El-Mezgueldi<sup>2</sup>, Clive R<sup>2,5</sup>. Bagshaw, and <sup>1</sup>Marina Kriajevska.

<sup>1</sup> Cancer Research Centre in Leicester, UK

<sup>2</sup> Department of Biochemistry, University of Leicester, UK

<sup>3</sup> Electron Microscopy Facilities, University of Leicester, UK

<sup>4</sup> Department of Biology, University of Leicester, UK

<sup>5</sup> Current address: Department of Chemistry & Biochemistry, University of California at Santa Cruz, USA.

### **ABSTRACT**

**Background:** S100A4 is a member of the S100 protein family that interacts *in vitro* with several molecular targets including heavy chain of non-muscle myosin IIA (NMIIA). S100A4 is expressed in various forms of human cancer and is broadly used as a marker of epithelial-mesenchymal transition (EMT). However, the function of S100A4 in EMT remains poorly understood.

**Results:** Here we study S100A4 protein function in the course of EMT. Induction of S100A4 enhanced cell dissociation and promoted motility of mesenchymal cells xenografted in zebrafish embryos. FRAP and TIRF microscopy analyses demonstrated that S100A4 stimulated rapid myosin turnover explaining its requirement for cell dissociation and cell motility at later stages of EMT. We employed a novel transition electron microscopy approach to study the representation of myosin isoforms and their interactions with S100A4 in cells undergoing an EMT. Our data confirmed that both 6S and 10S myosin isoforms do exist *in vivo*. To discriminate between these isoforms in S100A4/complexes, we applied ROCK inhibitors and polymerisation-deficient heavy and light chain myosin mutants. In these experiments we detected folded, assembly-incompetent 10S isoforms that were bound to S100A4, and these interactions were independent of light or heavy chain NMIIA phosphorylation.

**Conclusions:** We show that S100A4 protein interacts predominantly with the monomeric 10S isoform of NMIIA, contributing to the enhanced myosin dynamics. We propose that by controlling the balance between folded and unfolded myosin monomers, S100A4 promotes dissociation and migration of epithelial and mesenchymal cells respectively. In this study we uncover previously unknown function of S100A4 in EMT.

## **S100A4 binds to the extended and compact forms of non-muscle myosin IIA in A431 cells undergoing Epithelial-Mesenchymal Transition”**

Ban H.K. Alwash<sup>1</sup>, Qais I.I. Al Ismael<sup>1</sup>, Andrew F. Irvine<sup>1, 2</sup>, Natalie S. Allcock<sup>3</sup>, Jonathan McDearmid<sup>4</sup>, Mohammed El-Mezgueldi<sup>2</sup>, Clive R. Bagshaw<sup>2, 5</sup>, and Marina Kriajevska.<sup>1</sup>

<sup>1</sup> Cancer Research Centre in Leicester, UK

<sup>2</sup> Department of Biochemistry, University of Leicester, UK

<sup>3</sup> Electron Microscopy Facilities, University of Leicester, UK

<sup>4</sup> Department of Biology, University of Leicester, UK

<sup>5</sup> Current address: Department of Chemistry & Biochemistry, University of California at Santa Cruz, USA.

\*These authors equally contributed to the work.

### **ABSTRACT**

Epithelial-mesenchymal transition (EMT) is implicated in tumour progression and is characterised by alterations in cell morphology and formation of highly motile cells. EMT stimulates dynamics of actomyosin facilitating cell locomotion and enabling metastatic dissemination of cancer cells. Non-muscle myosin IIA is a chemo-mechanical protein that converts cellular chemical energy into mechanical work. This protein exists as monomers of heavy and light chains. Assembly/disassembly of myosin filaments is primarily controlled by myosin light chain phosphorylation, which is activated during EMT. However, emerging evidence suggests that small calcium-binding protein S100A4 also plays an active role in the dynamics of actin-myosin filaments, leading to increase the dissemination capability of tumour cells. The confirmation of myosin monomers was intensively studied *in vitro* by different biochemical and biophysical approaches but never directly investigated in cells. Inactive 50 nm monomer exists in 10S confirmation, which transforms into 6S extended conformation upon phosphorylation. In addition, calcium-binding protein S100A4 regulates the formation of the myosin IIA filaments via interaction with the C-terminus of the non-muscle myosin heavy chain (NMHCIIA). The aim of this project was to study interactions between NMHC IIA and S100A4 in squamous carcinoma cells during EMT. Using the transmission electron microscopy in combination with immune gold labelling, the interaction between S100A4 and NM IIA was identified. The distances between N-terminal GFP-tagged NMHC IIA and S100A4 was calculated by immunogold labelling. We collected multiple images and performed statistical analysis of the data. As the sizes of myosin molecules in 6S and 10S conformations are known, we were able to show that S100A4 proteins interact with both myosin conformations in cells.

## **Chapter 7 Appendix**

## Hymo3B-stop codons

5' gaggaccagaactgcaagctggccaaggaagaaactgctg3'  
E D Q N C K L A K E K K L L  
46 gaagacagaatagctgagttcaccaccaacctcacagaagaggag  
E D R I A E F T T N L T E E E  
91 gagaaatctaagagcctcgccaagctcaagaacaagcatgaggca  
E K S K S L A K L K N K H E A  
136 atgatactgacttgggaagagcgctccgcagggaggagaagcag  
M I T D L E E R L R R E E K Q  
181 cgacaggagctggagaagacccgccggaagctggagggagactcc  
R Q E L E K T R R K L E G D S  
226 acagacctcagcgaccagatcgccgagctccaggcccagatcgcg  
T D L S D Q I A E L Q A Q I A  
271 gagctcaagatgacagctggccaagaaagaggaggagctccaggcc  
E L K M Q L A K K E E E L Q A  
316 gccctggccagagtgggaagaggaagctgccagaagaacatggcc  
A L A R V E E E A A Q K N M A  
361 ctcaagaagatccgggagctggaatctcagatctctgaactccag  
L K K I R E L E S Q I S E L Q  
406 gaagacctggagtctgagcgtgcttccaggaataaagctgagaag  
E D L E S E R A S R N K A E K  
451 cagaaacgggaccttggggaagagctagaggctctgaaaacagag  
Q K R D L G E E L E A L K T E  
496 ttggaggacacgctggattccacagctgccagcaggagctcagg  
L E D T L D S T A A Q Q E L R  
541 tcaaaacgtgagcaggaggtgaacatcctgaagaagaccctggag  
S K R E Q E V N I L K K T L E  
586 gaggaggccaagaccacgaggcccagatccaggagatgaggcag  
E E A K T H E A Q I Q E M R Q  
631 aagcactcacaggccgtggaggagctggcggagcagctggagcag  
K H S Q A V E E L A E Q L E Q  
676 acgaagcgggtgaaagcaaacctcgagaaggcaaagcagactctg  
T K R V K A N L E K A K Q T L  
721 gagaacgagcggggggagctggccaacgaggtgaaggtgctgctg  
E N E R G E L A N E V K V L L  
766 cagggcaaaggggactcggagcacaagcgcaagaaagtggagggc  
Q G K G D S E H K R K K V E A  
811 cagctgcaggagctgcaggtcaagttcaacgaggagagcgcgctg  
Q L Q E L Q V K F N E G E R V  
856 cgcacagagctggccgacaaggtcaccaagctgcaggtggagctg  
R T E L A D K V T K L Q V E L  
901 gacaacgtgaccgggcttctcagccagctccgacagcaagtcagc  
D N V T G L L S Q S D S K S S  
946 aagctcaccaaggacttctccgctggagctccagctgcaggac  
K L T K D F S A L E S Q L Q D  
991 actcaggagctgctgcaggaggagaaccggcagaagctgagcctg  
T Q E L L Q E E N R Q K L S L  
1036 agcaccaagctcaagcaggtggaggacgagaagaattccttccgg  
S T K L K Q V E D E K N S F R  
1081 gagcagctggaggaggaggaggccaagcacaacctggagaag  
E Q L E E E E E A K H N L E K  
1126 cagatcgccaccctccatgccaggtggccgacatgaaaaagaag  
Q I A T L H A Q V A D M K K K  
1171 atggaggacagtggtggggtgctggaaactgctgaggaggtgaag  
M E D S V G C L E T A E E V K

1216 aggaagctccagaaggacctggagggcctgagccagcggcacgag  
R K L Q K D L E G L S Q R H E  
1261 gagaaggtggccgcctacgacaagctggagaagaccaagacgcgg  
E K V A A Y D K L E K T K T R  
1306 ctgcagcaggagctggacgacctgctggtggacctggaccaccag 1350  
L Q Q E L D D L L V D L D H Q

1. 3B-stop1F & 3B-stop1R

1F: GCTTCCAGGAATAAAGCTTAGAAGCAGAAACGG

1R: CCGTTTCTGCTTCTAAGCTTTATTCCTGGAAGC

Tm 63.2; 33 bp

2. 3B-stop2F & 3B-stop2R

2F: AAAGGGGACTAGGAGCACAAGCGCAAG

2R: CTTGCGCTTGTGCTCCTAGTCCCCTTT

Tm 62.8; 27 bp

3. 3B-stop3F & 3B-stop3R

3F: CAGTCCGACAGCTAGTCCAGCAAGCTC

3R: GAGCTTGCTGGACTAGCTGTCGGAAGT

Tm 64.3; 27 bp

3B-Stops

4. 3B-stop4F & 3B-stop4R

4F: CAGCTGGAGGAGTAGGAGGAGCCAAG

4R:CTTGGCCTCCTCCTACTCCTCCAGCTG

Tm 63 ; 27 bp

5. 3B-stop5F & 3B-stop5R

5F: CTGGAAACTGCTTAGGAGGTGAAGAGGAAG

5R:CTTCCTCTTCACCTCCTAAGCAGTTTCCAG

Tm 63 ; 30 bp

**Figure 7-1: The nucleotides and amino acids sequences of the Hmyo3B fragment designed with stop codons.**

overlapped truncated subfragments of Hmyo3B were designed by incorporation stop codons into Hmyo3B fragment. Blue colour letters indicate the positions of the sites for incorporation of the stop codons.

**M53**

S S K L T K D F S A L E S Q L Q D T Q E L L Q E E N  
R Q K L S L S T K L K Q V E D E K N S F R E Q L E  
E

901 gacaacgtgaccgggcttctcagccagtccgacagcaagtccagc  
D N V T G L L S Q S D S K S S  
946 aagctcaccaaggacttctccgcgctggagtcccagctgcaggac  
K L T K D F S A L E S Q L Q D  
991 actcaggagctgctgcaggaggagaaccggcagaagctgagcctg  
T Q E L L Q E E N R Q K L S L  
1036 agcaccaagctcaagcaggtggaggacgagaagaattccttccgg  
S T K L K Q V E D E K N S F R  
1081 gagcagctggaggaggaggaggaggccaagcacaacctggagaag  
E Q L E E E E E A K H N L E K  
1126 cagatcgccaccctccatgcccaggtggccgacatgaaaaagaag

**Forward M53**

**GTGT GGATCC** TCC AGC AAG CTC ACC AAG GAC TTC

Length 24/Tm 64.4/GC% 54.2 %

**Reverse M53:**

**GTGT AAGCTT** CTA CTC CTC CAG CTG CTC CCG

Length 21/Tm 65.69/ GC 65.7%

**M53-F**

CTGCAGGANACTCAGGAGCTGCTGCAGGAGGAGAACCGGCAGAAGCTGAGCCTGAGCACCAAGCTC  
AAGCAGGTGGAGGACGAGAAGAATTCCTTCCGGGAGCA**GCTGGAGGAGTAG**AAGCTTAATTAGCTG  
AGCTTGGACTCCTGTTGATAGATCCAGTAATGACCTCAGAACTCCATCTGGATTTGTTTCAGAACGC  
TCGGTTGCCCGCGGGCGTFTTTTATTGGTGAGAATCCAAGCTAGCTTGGCGAGATTTTCAGGAGCT  
AAGGAAGCTAAAATGGAGAAAAAATCACTGGATATAACCACCGTTGATATATCCCAATGGCATCGT  
AAAGAACATTTTGAGGCATTTTCAGTCAGTTGCTCAATGTACCTATAACCAGACCGTTTCAGCTGGAT  
ATTACGGCCTTTTTAAAGACCGTAAAGAAAAATAAGCACAAGTTTTATCCGGCCTTTTATTCACATT  
CTTGCCCGCCTGATGAATGCTCATCCGGAATTTTCGTATGGCAATGAAAGACGGTGAGCTGGTGATA

TGGGATAGTGTTACCCCTTGTTACACCGTTTTCCATGAGCAAACCTGAAACGTTTTTCATCGCTCTGG  
AGTGAATACCACGACGATTTCCGGCAGTTTCTACACATATATTCGCAAGATGTGGCGTGTTACGGT  
GAAAACCTGGCCTATTTCCCTAAAGGGTTTATTGAGAATATGTTTTTCGTCTCAGCCAATCCCTGG  
GGTGAGTTTACCAGTTTTGATTTAAACGTGGCCAATATGGACAACCTTCTCGCCCCCGTTTTCAC  
CATGGGCAAATATTATACGCAAGGCGACAAGGTGCTGATGCCGCTGGCGATTC  
NNNTCATCATGNCGNTTGNGATGGCTTCCATGTCGGCAGAATGCTTNATGAATTACNACAGTACTG  
CGATGANNNNNNNGGNNGGNNTAATTTTTTTNNNNNANTNNTGGNGCCNNAANNCTGGGGNAAT  
GACTCTCTAGCNNGNATNANTAAAACGAANNNNCANTCN

## M53-R

NGNNNNNNTTCNCGNCCTCCN

CCTGCTTGAGCTTGGTGCTCAGGCTCAGCTTCTGCCGTTCTCCTCCTGCAGCAGCTCCTGAGTGTCTGCA  
GCTGGGACTCCAGCGCGGAGAAGTCCTTGGTGAGCTTGGTGGAGGATCCGTGATGGTGTGATGGCA  
TCCTCTCAGTAGTTAATTTCTCCTTTAATGAATTCTGTGTGAAATTGTTATCCGCTCACAAATGAATCTATTAT  
AATTGTTATCCGCTCACAAAGCAAATAAATTTTTTATGATTTCTCGAGGTGAAGACGAAAGGGCCTCGTGAT  
ACGCCTATTTTATAGGTTAATGTCATGATAAATGGTTTCTTAGACGTCAGGTGGCACTTTTCGGGGAAA  
TGTGCGCGGAACCCCTATTTGTTATTTTTCTAAATACATTCAAATATGTATCCGCTCATGAGACAATAACCC  
TGATAAATGCTTCAATAATATTGAAAAGGAAGAGTATGAGTATTCAACATTTCCGTGTCGCCCTTATTCCCT  
TTTTGCGGCATTTGCTTCTGTTTTGCTCACCCAGAAACGCTGGTGAAAGTAAAAGATGCTGAAGATC  
AGTTGGGTGCACGAGTGGGTTACATCGAACTGGATCTCAACAGCGGTAAGATCCTTGAGAGTTTTCGCCCC  
GAAGAAGTTTTCCAATGATGAGCACTTTAAAGTTCTGCTATGTGGCGCGGTATTATCCCGTATTGACGCC  
GGGCAAGAGCAACTCGGTCGCCGCATACACTATTCTCA

NAATGACTNGGNTNGAGTACTCNCAGTCACAGAAAANCATCTTANGGATGGCATGACAGTAAGANAATT  
ATGCAGNGCTGCCATAACCATGAGTGANN

ANNACTGCGCCNANTNACTTCTGACNACGATCGNANGACCGANNANCTANNNGNTTTTTNNACAACN  
TNGGGNNNCATGTNNCTCANNNTGNTCGTNGNNNCNANCTNANGANNNTACNNANCNACNANGNN  
ANNNNNNATGCNNNNANNANGNNANNANNNNNNNNANCNNNNNNNNNAANNNTNNCNNNNANN  
NNNNNNNNNNNANNNACNNNNNGNAGGNGNNNANNNNNNNNGNNNNNTNNGNNNNNGNNNNNN  
NNNNNNNNNNNNGNNNNNNNNNNNNNNNGNNNNNNNNNNNNNNNNNNNNNNNNNNNN

NNNNNNNNNNNCNNNNNNNNNNNNNN.

## Reverse complement

TGAGAAAGTGTATGCGGCGACCGAGTTGCTTGGCCGGCGTCAATACGGGATAATACCGCGCCACATAG  
CAGAACTTTAAAAGTGCTCATCTTGGAAAACGTTCTTGGGGCGAAAACCTCAAGGATCTTACCGCTGTT  
GAGATCCAGTTCGATGTAACCCACTCGTGACCCAACTGATCTTACGATCTTTACTTTACCAGCGTTTCT  
GGGTGAGCAAAAACAGGAAGGCAAAATGCCGCAAAAAGGGAATAAGGGCGACACGGAAATGTTGAATA  
CTCATACTCTTCTTTTCAATATTATTGAAGCATTTATCAGGGTTATTGTCTCATGAGCGGATACATATTTGA  
ATGTATTTAGAAAAATAACAAATAGGGGTTCCGCGCACATTTCCCCGAAAAGTGCCACCTGACGTCTAAG

AAACCATTATTATCATGACATTAACCTATAAAAAATAGGCGTATCACGAGGCCCTTTCGTCTTCACCTCGAGAA  
 ATCATAAAAAATTTATTTGCTTTGTGAGCGGATAACAATTATAATAGATTCAATTGTGAGCGGATAACAATT  
 TCACACAGAATTCATTAAGAGGAGAAATTAACCTATGAGAGGATCGCATCACCATCACCATCACGGATCCTC  
 CAGCAAGCTCACCAAGGACTTCTCCGCGCTGGAGTCCCAGCTGCAGGACACTCAGGAGCTGCTGCAGGAG  
 GAGAACCGGCAGAAGCTGAGCCTGAGCACCAGCTCAAGCAGG.

```
TCCAGCAAGCTCACCAAGGACTTCTCCGCGCTGGAGTCCCAGCTGCAGGACACTCAGGAG 60
|||||
Sbjct 646 TCCAGCAAGCTCACCAAGGACTTCTCCGCGCTGGAGTCCCAGCTGCAGGACACTCAGGAG
705 61 CTGCTGCAGGAGGAGAACCGGCAGAAGCTGAGCCTGAGCACCAGCTCAAGCAGG 115
|||||
Sbjct 706 CTGCTGCAGGAGGAGAACCGGCAGAAGCTGAGCCTGAGCACCAGCTCAAGCAGG 760
```

**Figure 7-2: Sequence of M53 fragment of NM IIA**

Forward and reverse primers were used for M53 DNA plasmid synthesis by PCR amplification using Hmyo3B as a templet.

**S100A6**

```
315 atggcatgccccctggatcaggccattggcctcctcgtggccatc
M A C P L D Q A I G L L V A I
360 ttccacaagtactccggcagggagggtgacaagcacaccctgagc
F H K Y S G R E G D K H T L S
405 aagaaggagctgaaggagctgatccagaaggagctcaccattggc
K K E L K E L I Q K E L T I G
450 tcgaagctgcaggatgctgaaattgcaaggctgatggaagacttg
S K L Q D A E I A R L M E D L
495 gaccggaacaaggaccaggaggtgaacttccaggagtatgtcacc
D R N K D Q E V N F Q E Y V T
540 ttctgggggcttggctttgatctacaatgaagccctcaagggc
F L G A L A L I Y N E A L K G
585 tga
```

**$T_m = 4^{\circ}\text{C} \times (\text{number of G's and C's in the primer}) + 2^{\circ}\text{C} \times (\text{number of A's and T's in the primer})$**

$T_m = 69.3 + (0.41 \times \text{GC \%}) - (650/\text{length}).$

Overhang + BamHI :

GTGT GGATCC

Overhang + HindIII :

GTGT AAGCTT

## S100A6 Reverse

CCTATAGNTNTAGGNGTNNNNNTCTNNNTNTTNAANNNAANANNAAGACAATCTTTCTTTCATANGTTT  
NCGNNNCNATGTANTGAGGCCCCCCAAAAAAGNTTNCNNAATNNTATCTCATNATATCNCGTCCNNG  
GNGNGGGGGGGCCCCCNCAAAAAANNNNAACCNCCNNGTATGANNTGNNGATCCNTNTCNCNCGNAN  
GCCACNGNNNNANNTGAGATGTCNNNACNGCNCNCTTATNTCANTGTGNTTTNAGTNGNGNNNNCANC  
NGCNGGCACNNGNCATAANNNTGTTNNTTTNAATNNNNGGGCAGTNGTNCNTTCGCTGNCNGNNNAN  
NTTTTNNNNCCNNTNTGCGTACGGNAGGTNNNNNTGGTNANAGNNTCCNAACNATNNGTNGGNCCGT  
GCNNGCGACNNNCNNGCNTGATATTNNANTNTNGTNTNGCTACGCGGTGGCNNNNTNNGTNCNGTNN  
TNCNNGTANANGTNATTCNNATANNANNNCNCTCNGCTGTTNNACTGANGTTNNTCGNCCTNTNTNN  
NCGNGNNNNATATGNGACNAGCGTNGAGNGGNCGNCNNNNTANNNGTGANTANNTNGTNANTANCTC  
NNGCCNGCTCNGNNGGNCGNTTGANNNGNANTNTNNTANNTGTGANCANTGNNCGNTCNGTANNA  
GTTANGGNAGTGCAGGCCTNNTGNNNTNTNCCNTNGNNNNNTNNCGNTNTTACNCNTACNTCTTTNT  
NGAGNNNACGN TTCNGCANAATNCTCNANNNGTNNTTCTNTCTNNTTTCTNTNTTCGCCNNNAGN  
NGGGTTATTGTNNNNNTNNNNNANGGNTAGCNTNNTTNNNGNGNNCCANNNGNNNNNGAANTGC  
TANTATNTANNNTNNNATNCACNTNNNTTANGNTTCGTGATNGTCANANNGCNTTGANNNGNNCNA  
CTCGTTCTNNTTNGATTAGTANNATNATNTNGNNGGTAGACNTNTGNCNGGNTNNGCNNTANGTNA  
NTNNNTATATNNNTNAGNGANNGGCTNNNNNTTNTCNTNTNNTNANCNCCATGTNNGTGNCCNGTN  
NATNTNACAANANGATNTNAGTATCAANNNTNCNTTGNATNCAATNNNATCNGATTGATTTNNNNCN  
TGCGTNANACTTCTNCCGATGTANANANTCNANGTNGTNGCNNNNTCNTANTCGNCTNTTNCANTNGN  
CNTCNCGANNANCGANTNGNCNTGTNTGGCGNTNTGNTNNNNNGCNNNTNGNNGANANNNGNNCG  
TTTTGNCNGNNGNCGCTNCTTATTAGGNTNNTNTGCGTCNNNANCCTATGNTCGNNGCANTATNNGCN  
CTNNGCGGNTNGNNNCTATNTNCATNNNNNATTCTNGTATTTNTTTNNNTNTGGNNNNNANTNTNNTC  
ACNNNNNTANGACANNNTNNGGTAGACNNANTNNNNANATNNNTTANATNACTCTANNAGAGANT  
AGTGNNTCTGNATTANANNCCAGGNCCTTTNANANAAAGACAGCNCNCAGNNCNGTNTNTNGCAC  
NGNATNTAGTTNCCGCATATNGNNTCNTGTNTGTNCNNNTCNCNGTNTCATGCNNTCTNCATTNNGAN  
TACACGANTAATNGNGNGANNNGTNGANATNTGGAGTTGTNNAGNGCATGTGCNTGANNTTTTAGNTC  
NNGCTTCNATTGTTNGNACNTNTGGTCTNGCANNTGNGCGCNATTNGTTNTGNTNNGANNNNNGGCTN  
NNTCTCCTNNGANTNGNGNNNTATANNAGNTATGNATGATNNTCNATATAGGACCGNGCNGNATANC  
GTGTANCGANGNACGGTATCGACTNGNNGTGGNTTAGGAGCANCGGNCAGNCTGNGNTNNAANANN  
N.

## **S100A6- Reverse complement**

GCGAAAACCTCAAGGATCTTACCGCTGTTGAGATCCAGTTCGATGTAACCCACTCGTGACCCAACTGATC  
TTCAGCATCTTTTACTTTACCAGCGTTTCTGGGTGAGCAAAAACAGGAAGGCAAAATGCGCAAAAAGG  
GAATAAGGGCGACACGGAAATGTTGAATACTCATACTCTTCTTTTCAATATTATTGAAGCATTTATCAGG  
GTTATTGTCTCATGAGCGGATACATATTTGAATGTATTTAGAAAATAAACAATAGGGGTTCCGCGCACAT  
TTCCCCGAAAAGTGCCACCTGACGTCTAAGAAACCATTATTATCATGACATTAACCTATAAAAATAGGCGTA  
TCACGAGGCCCTTTCGTCTTCACTCGAGAAAATCATAAAAAATTTATTTGCTTTGTGAGCGGATAACAATTAT  
AATAGATTCAATTGTGAGCGGATAACAATTTACACAGAATTCATTAAGAGGAGAAATTA ACTATGAGAG  
GATCGCATCACCATCACCATCACGGATCCATGGCATGCCCCCTGGATCAGGCCATTGGCCTCCTCGTGGCCA  
TCTTCCACAAGTACTCCGGCAGGGAGGGTGACAAGCACACCCTGAGCAAGAAGGAGCTGAAGGAGCTGAT

CCAGAAGGAGCTCACCATTGGCTCGAAGCTGCAGGATGCTGAAATTGCAAGGCTGATGGAAGACTTGGAC  
CGGAACAAGGACCAGGAGGTGAACTTCCAGGAGTATGTC.

Query 313 CCATGGCATGCCCCCTGGATCAGGCCATTGGCCTCCTCGTGGCCATCTTCCACAAGTACT  
372  
Sbjct 531 CCATGGCATGCCCCCTGGATCAGGCCATTGGCCTCCTCGTGGCCATCTTCCACAAGTACT  
590  
Query 373 CCGGCAGGGAGGGTGACAAGCACACCCTGAGCAAGAAGGAGCTGAAGGAGCTGATCCAGA  
432  
Sbjct 591 CCGGCAGGGAGGGTGACAAGCACACCCTGAGCAAGAAGGAGCTGAAGGAGCTGATCCAGA  
650  
Query 433 AGGAGCTCACCATTGGCTCGAAGCTGCAGGATGCTGAAATTGCAAGGCTGATGGAAGACT  
492  
Sbjct 651 AGGAGCTCACCATTGGCTCGAAGCTGCAGGATGCTGAAATTGCAAGGCTGATGGAAGACT  
710  
Query 493 TGGACCGAACAAGGACCAGGAGGTGAACTTCCAGGAGTATGTC 536  
Sbjct 711 TGGACCGAACAAGGACCAGGAGGTGAACTTCCAGGAGTATGTC 754

**S100A6 NCBI Reference Sequence: NM\_014624.3**

CTGCGCAGATGAGGGGAGACTCGTCACCAGGCGTGCAGTGGGCACTGCTGGGCTCCCCATCCCGTCCTA  
ACCCGGAACAGCCCCGGGCAGGAGGCGTGAAAGTCGAGGGGTAAACCGCAATGTGCGTTGTGTAAGC  
CACGGCGCAGGGTGGGGCGGGCGGGACTTGGGCGGGCGGGTGGGCTTGGCCGAGCTGGCCTCCGGGG  
CACCGACCGCTATAAGGCCAGTCGGACTGCGACACAGCCATCCCCTCGACCGCTCGCGTCGCATTTGGC  
CGCCTCCCTACCGCTCCAAGCCCAGCCCTCAGCCATGGCATGCCCCCTGGATCAGGCCATTGGCCTCCTC  
GTGGCCATCTTCCACAAGTACTCCGGCAGGGAGGGTGACAAGCACACCCTGAGCAAGAAGGAGCTGAAGG  
AGCTGATCCAGAAGGAGCTCACCATTGGCTCGAAGCTGCAGGATGCTGAAATTGCAAGGCTGATGGAAGA  
CTTGGACCGAACAAGGACCAGGAGGTGAACTTCCAGGAGTATGTCACCTTCCTGGGGGCCTTGGCTTTG  
ATCTACAATGAAGCCCTCAAGGGCTGAAAATAAATAGGGAAGATGGAGACACCCTCTGGGGGTCTCTCT  
GAGTCAAATCCAGTGGTGGGTAATTGTACAATAAATTTTTTTGGTCAAATTT

CDS-315...587

### Figure 7-3: Sequence of M53 fragment of NM IIA

Forward and reverse primers were used for M53 DNA plasmid synthesis by PCR amplification using Hmyo3B as a templet.

#### PQE-30 Sequence:

T5 Promoter sequence:

5' TCATAAAAAATTTATTTGCTTTGTGAGCGGATAACAATTATAATA 3'

CTCGAGAAA TCATAAAAAATTTATTTGCTTTGTGAGCGGATAACAATTATAATA GATTCAATTGTGAGCGGA  
TAACAATTTACACAGAATTCATTAAGAGGAGAAAATTA ACTATGAGAGGATCG CATCACCATCACCATCAC  
GGATCC GCATGCGAGCTCGGTACCCCGGGTCGACCTGCAGCCAAGCTT AATTAGCTGAGCTTGGACTCCTG  
TTGATAGATCCAGTAATGACCTCAGA ACTCCATCTGGATTTGTT CAGAACGCTCGGTTGCCGCCGGGCGTTT  
TTTATTGGTGAGAAATCCAAGCTAGCTTGGCGAGATTTT CAGGAGCTAAGGAAGCTAAAATGGAGAAAAAAA  
TCACTGGATATAACCACCGTTGATATATCCAATGGCATCGTAAAGAACATTTT GAGGCATTT CAGTCAGTTG  
CTCAATGTACCTATAACCAGACCGTTCAGCTGGATATTACGGCCTTTTT AAAGACCGTAAAGAAAAATAAGC  
ACAAGTTTTATCCGGCCTTTATT CACATTCTTGCCCGCCTGATGAATGCTCATCCGGAATTT CGTATGGCAAT  
GAAAGACGGTGAGCTGGT GATATGGGATAGTGTTCACCTTGTACACCGTTTT CCATGAGCAA ACTGAAA  
CGTTTTCATCGCTCTGGAGTGAATACCACGACGATTTCCGGCAGTTTCTACACATATATT CGCAAGATGTGG  
CGTGTACGGTGAAAACCTGGCCTATTTCCCTAAAGGGTTTATTGAGAATATGTTTTT CGTCTCAGCCAATCC  
CTGGGTGAGTTTACCAGTTTTGATTTAAACGTGGCCAATATGGACA ACTTCTTCGCCCCGTTTTTACCATG  
GGCAAATATTATACGCAAGGCGACAAGGTGCTGATGCCGCTGGCGATT CAGGTT CATCATGCCGTTTGTGA  
TGGCTCCATGTCGGCAGAATGCTTAATGAATTACAACAGTACTGCGATGAGTGGCAGGGCGGGGCGTAAT  
TTTTTAAAGGCAGTTATTGGTGCCCTTAAACGCCTGGGGTAATGACTCTTAGCTTGAGGCATCAAATAAAA  
CGAAAGGCTCAGTCGAAAGACTGGGCCTTTCTGTTTTATCTGTTGTTTGTGCGGTGAACGCTCTCCTGAGTAGG  
ACAAATCCGCCCTTAGAGCTGCCTCGCGCTTTCCGGTGATGACGGTGAAAACCTCTGACACATGCAGCTCC  
CGGAGACGGTCACAGCTTGTCTGTAAGCGGATGCCGGGAGCAGACAAGCCCGTCAGGGCGCGTCAGCGG  
GTGTTGGCGGGTGTGCGGGGCGCAGCCATGACCCAGTCACGTAGCGATAGCGGAGTGTATACTGGCTTAAC  
TATGCGGCATCAGAGCAGATTG TACTGAGAGTGCACCATATGCGGTGTGAAATACCGCACAGATGCGTAA  
GGAGAAAATACCGCATCAGGCGCTTCTCCGCTTCTCGCTCACTGACTCGCTGCGCTCGGTGTTCCGGCTGC  
GGCGAGCGGTATCAGCTCACTCAAAGGCGGTAATACGGTTATCCACAGAATCAGGGGATAACGCAGGAAA  
GAACATGTGAGCAAAAGGCCAGCAAAAGGCCAGGAACCGTAAAAAGGCCGCTTGTGCGCTTTTTCCAT  
AGGCTCCGCCCCCTGACGAGCATCACA AAAATCGACGCTCAAGTCAGAGGTGGCGAAACCCGACAGGAC  
TATAAAGATAACCAGGCGTTTCCCCTGGAAGCTCCCTCGTGCCTCTCCTGTTCCGACCCTGCCGTTACCGG  
ATACCTGTCCGCTTTCTCCCTTCGGGAAGCGTGGCGCTTTCTCATAGCTCACGCTGTAGGTATCTCAGTTCCG  
GTGTAGGTGTTCCGCTCCAAGCTGGGCTGTGTGCACGAACCCCGTT CAGCCCAGCCGCTGCGCTTATCC  
GGTAACTATCGTCTT GAGTCCAACCCGTAAGACACGACTTATCGCCACTGGCAGCAGCCACTGGTAACAG  
GATTAGCAGAGCGAGGTATGTAGGCGGTGCTACAGAGTTCTTGAAGTGGTGGCCTAACTACGGCTACTACTA  
GAAGGACAGTATTTGGTATCTGCGCTCTGCTGAAGCCAGTTACCTTCGGAAAAAGAGTTGGTAGCTCTTGA

TCCGGCAAACAAACCACCGCTGGTAGCGGTGGTTTTTTTTGTTTGCAAGCAGCAGATTACGCGCAGAAAAAA  
AGGATCTCAAGAAGATCCTTTGATCTTTTCTACGGGGTCTGACGCTCAGTGGAACGAAAACCTCACGTTAAG  
GGATTTTGGTCATGAGATTATCAAAAAGGATCTTACCTAGATCCTTTTAAATTAATAAATGAAGTTTTAAATC  
AATCTAAAGTATATATGAGTAACTTGGTCTGACAGTTACCAATGCTTAATCAGTGAGGCACCTATCTCAGC  
GATCTGTCTATTTGTTTCATCCATAGTTGCCTGACTCCCCGTCGTGTAGATAACTACGATACGGGAGGGCTT  
ACCATCTGGCCCCAGTGCTGCAATGATACCGCGAGACCCACGCTCACCGGCTCCAGATTTATCAGCAATAAA  
CCAGCCAGCCGGAAGGGCCGAGCGCAGAAGTGGTCCTGCAACTTTATCCGCCTCCATCCAGTCTATTAATT  
GTTGCCGGAAGCTAGAGTAAGTAGTTGCCAGTTAATAGTTTGCGCAACGTTGTTGCCATTGCTACAGGC  
ATCGTGGTGTACGCTCGTCGTTTGGTATGGCTTCATTAGCTCCGGTTCCAACGATCAAGGCGAGTTACA  
TGATCCCCATGTTGTGCAAAAAGCGGTTAGCTCCTTCGGTCTCCGATCGTTGTCAGAAGTAAGTTGGCC  
GCAGTGTATCACTCATGGTTATGGCAGCACTGCATAATTCTTACTGTCATGCCATCCGTAAGATGCTTTT  
CTGTGACTGGTGAGTACTCAACCAAGTCATTCTGAGAATAGTGTATGCGGCGACCGAGTTGCTCTTGCCCG  
GCGTCAATACGGGATAATACCGCGCCACATAGCAGAACTTTAAAAGTGCTCATCATTGGAAAACGTTCTTCG  
GGGCGAAAACCTCTCAAGGATCTTACCGCTGTTGAGATCCAGTTCGATGTAACCCACTCGTGCACCCAACTGA  
TCTTCAGCATCTTTTACTTTACCAGCGTTTCTGGGTGAGCAAAAACAGGAAGGCAAAATGCCGCAAAAAG  
GGAATAAGGGCGACACGGAAATGTTGAATACTCATACTCTTCTTTTCAATATTATTGAAGCATTATCAG  
GGTTATTGTCTCATGAGCGGATACATATTTGAATGTATTTAGAAAAATAAACAAATAGGGGTTCCGCGCACA  
TTTCCCCGAAAAGTGCCACCTGACGTCTAAGAAACCATTATTATCATGACATTAACCTATAAAAATAGGCGT  
ATCACGAGGCCCTTTCGTCTTCAC

**Figure 7-4: Schamatic represtative of PQE-30 Sequence:**

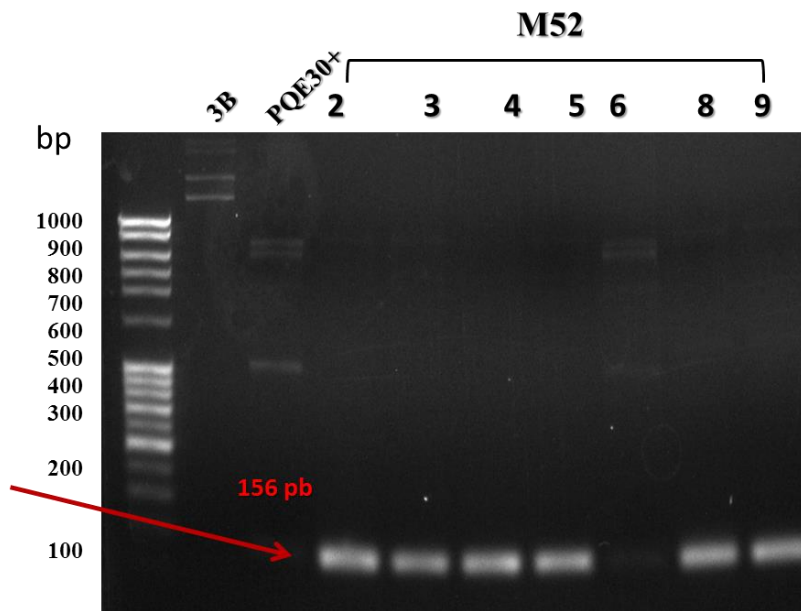


**Figure 7-5: Analysis of M53 plasmid DNA by gel agaros electrophoresis.**

Plasmid DNA from the selected clones was isolated and digested by BamHI and HindIII enzymes and analysed.0.5µg was loaded on 1.5%TBA agarose gel and visualised using ethidium bromide.The bands of approximately 159 pb represents M53 which is consistent with predicted size of this insertion.

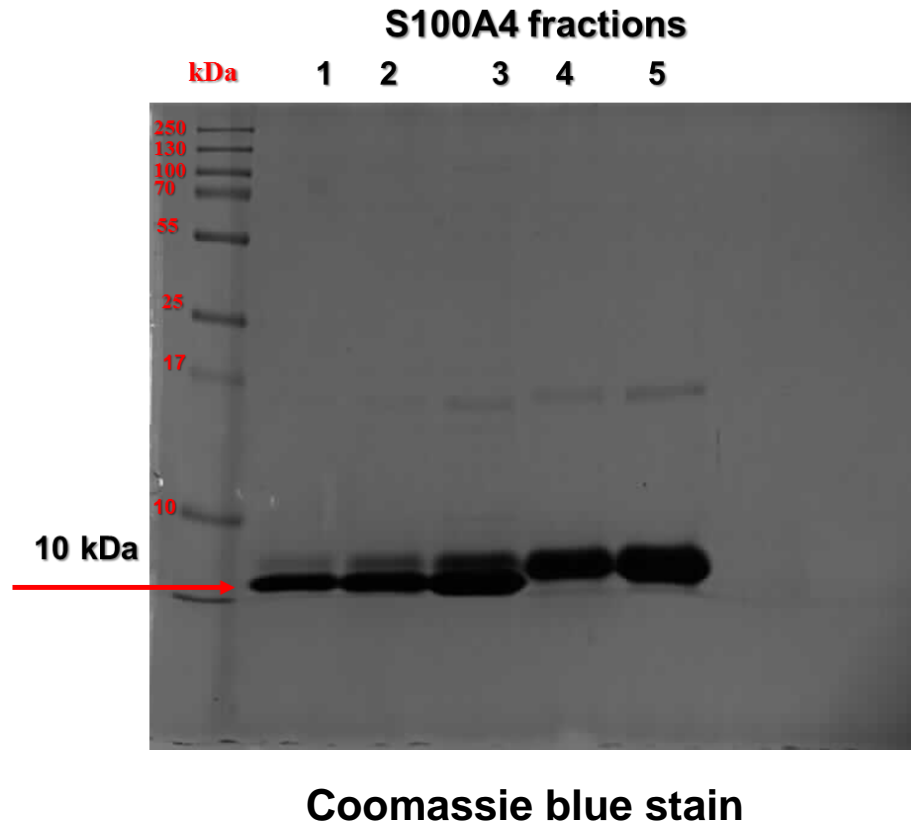


**Figure 7-6: Isolation of S100A4 proteins purified under native condition.**

To test the presence of S100A4 proteins, eluted fractions of S100A4 proteins under native conditions were resolved on 15% SDS-PAGE. The gel was then stained with Coomassie blue.

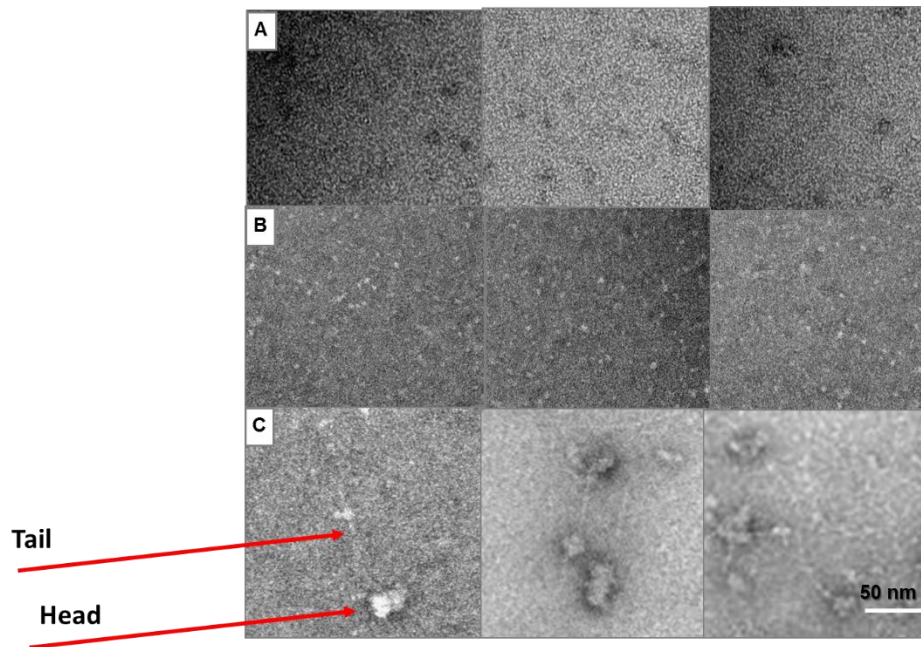


**Figure 7-7: Myosin IIA exists in monomers in high salt buffer.**

A- Myosin buffer control (500 mM NaCl, 1 mM DTT, 25mM Tris, 47.6 mM glycine, 0.25 mM CaCl<sub>2</sub>, and pH7.5). B- Isolated S100A4 protein C- GFP-myosin IIA molecules extracted from A431/ZEB2-WT cells in high salt buffer by using GFP-Trap®-A bead and negatively stained. Scale bar = 200 nm. Scale bar = 50 nm.

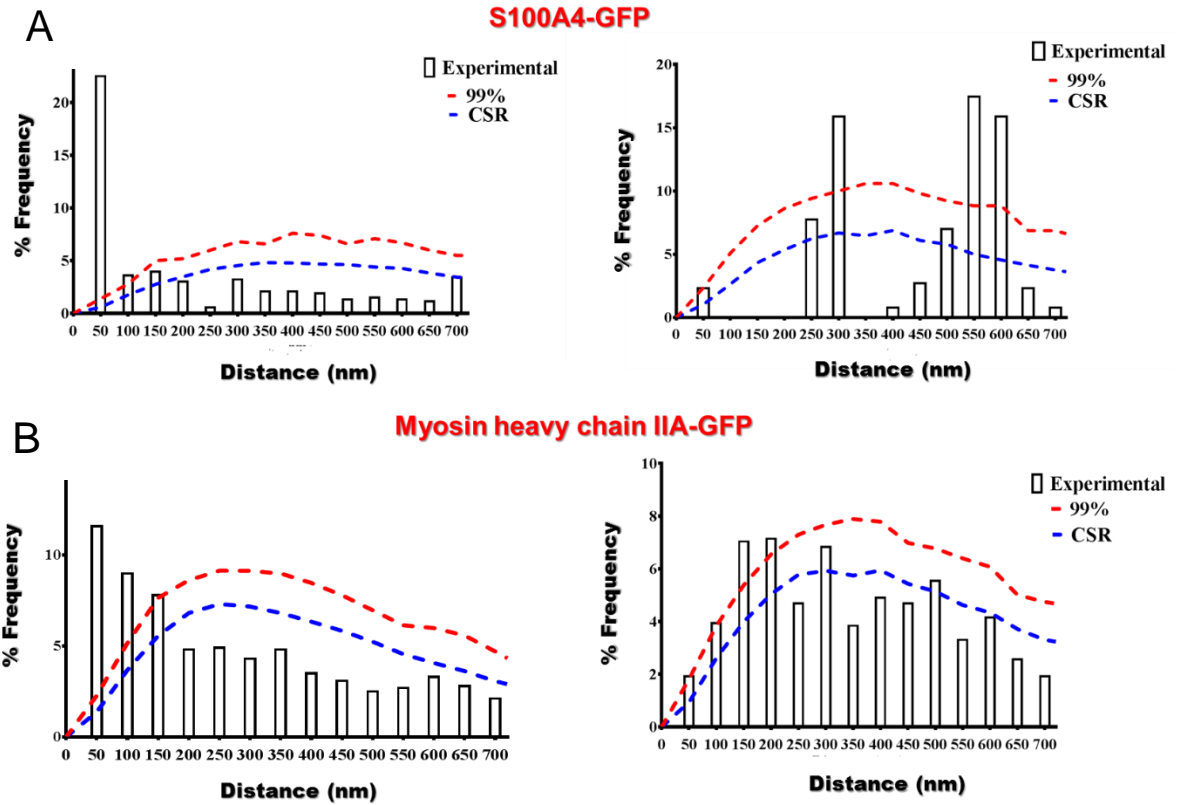


**Figure 7-8: S100A4 interacts only with 10S myosin monomer in S1943E cells.**

Resin embedded sections of Dox treated siControl transfected S1943E cells and siS1004 transfected S1943E cells were immunolabelled for GFP and S100A4 (A) or MHC IIA and GFP (B) and visualised using 30 and 15 nm gold-conjugated secondary antibodies, respectively. A-The Nearest-neighbour co-localisation analysis shows one statistically significant peak at 50 nm in siControl cells, while three significant peaks at 300 nm, 550 nm and 600 nm. B-The Nearest-neighbour co-localisation analysis shows two statistically significant peaks at 50 nm and 100 nm in siControl cells, whereas two statistically significant peaks at 150 nm and 200 nm in siS100A4 cells. Blue dashed line reflects random distribution between small particles (15nm) and large particles (30 nm) (CSR). 99% confidence interval (CI). These cells represent the analysis of 1750 images of three independent experiments.

## References

- ALVES, C. C., ROSIVATZ, E., SCHOTT, C., HOLLWECK, R., BECKER, I., SARBIA, M., CARNEIRO, F. & BECKER, K. F. 2007. Slug is overexpressed in gastric carcinomas and may act synergistically with SIP1 and Snail in the down- regulation of E- cadherin. *The Journal of pathology*, 211, 507-515.
- BADYAL, S. K., BASRAN, J., BHANJI, N., KIM, J. H., CHAVDA, A. P., JUNG, H. S., CRAIG, R., ELLIOTT, P. R., IRVINE, A. F. & BARSUKOV, I. L. 2011. Mechanism of the Ca<sup>2+</sup>-dependent interaction between S100A4 and tail fragments of nonmuscle myosin heavy chain IIA. *Journal of molecular biology*, 405, 1004-1026.
- BAI, H., QIAN, J.-L. & HAN, B.-H. 2014. S100A4 is an independent prognostic factor for patients with lung cancer: a meta-analysis. *Genetic testing and molecular biomarkers*, 18, 371-374.
- BAO, L., ODELL, A. F., STEPHEN, S. L., WHEATCROFT, S. B., WALKER, J. H. & PONNAMBALAM, S. 2012. The S100A6 calcium- binding protein regulates endothelial cell- cycle progression and senescence. *FEBS journal*, 279, 4576-4588.
- BARBAZAN, J., DUNKEL, Y., LI, H., NITSCHKE, U., JANSSEN, K.-P., MESSER, K. & GHOSH, P. 2016. Prognostic impact of modulators of g proteins in circulating tumor cells from patients with metastatic colorectal Cancer. *Scientific reports*, 6.
- BARRACLOUGH, R. 1998. Calcium-binding protein S100A4 in health and disease. *Biochimica et Biophysica Acta (BBA)-Molecular Cell Research*, 1448, 190-199.
- BARROS, C. S., PHELPS, C. B. & BRAND, A. H. 2003. Drosophila nonmuscle myosin II promotes the asymmetric segregation of cell fate determinants by cortical exclusion rather than active transport. *Developmental cell*, 5, 829-840.
- BEACH, J. R. & EGELHOFF, T. T. 2009. Myosin II recruitment during cytokinesis independent of centralspindlin-mediated phosphorylation. *J Biol Chem*, 284, 27377-83.
- BEACH, J. R., HUSSEY, G. S., MILLER, T. E., CHAUDHURY, A., PATEL, P., MONSLOW, J., ZHENG, Q., KERI, R. A., REIZES, O. & BRESNICK, A. R. 2011a. Myosin II isoform switching mediates invasiveness after TGF- $\beta$ -induced epithelial–mesenchymal transition. *Proceedings of the National Academy of Sciences*, 108, 17991-17996.
- BEACH, J. R., LICATE, L. S., CRISH, J. F. & EGELHOFF, T. T. 2011b. Analysis of the role of Ser1/Ser2/Thr9 phosphorylation on myosin II assembly and function in live cells. *BMC Cell Biol*, 12, 52.
- BEACH, J. R., SHAO, L., REMMERT, K., LI, D., BETZIG, E. & HAMMER, J. A. 2014. Nonmuscle myosin II isoforms coassemble in living cells. *Current Biology*, 24, 1160-1166.
- BELTRAN, M., PUIG, I., PEÑA, C., GARCÍA, J. M., ÁLVAREZ, A. B., PEÑA, R., BONILLA, F. & DE HERREROS, A. G. 2008. A natural antisense transcript regulates Zeb2/Sip1 gene expression during Snail1-induced epithelial–mesenchymal transition. *Genes & development*, 22, 756-769.

- BETAPUDI, V. 2014. Life without double-headed non-muscle myosin II motor proteins. *Front Chem*, 2, 45.
- BETAPUDI, V., GOKULRANGAN, G., CHANCE, M. R. & EGELHOFF, T. T. 2011. A proteomic study of myosin II motor proteins during tumor cell migration. *Journal of molecular biology*, 407, 673-686.
- BILLINGTON, C. K., OJO, O. O., PENN, R. B. & ITO, S. 2013a. cAMP regulation of airway smooth muscle function. *Pulmonary pharmacology & therapeutics*, 26, 112-120.
- BILLINGTON, N., WANG, A., MAO, J., ADELSTEIN, R. S. & SELLERS, J. R. 2013b. Characterization of three full-length human nonmuscle myosin II paralogs. *J Biol Chem*, 288, 33398-410.
- BIRI-KOVÁCS, B., KISS, B., VADÁSZI, H., GÓGL, G., PÁLFY, G., TÖRÖK, G., HOMOLYA, L., BODOR, A. & NYITRAY, L. 2017. Ezrin interacts with S100A4 via both its N-and C-terminal domains. *PLoS one*, 12, e0177489.
- BISHOP, A. L. & ALAN, H. 2000. Rho GTPases and their effector proteins. *Biochemical Journal*, 348, 241-255.
- BÖNI, R., BURG, G., DOGUOGLU, A., ILG, E., SCHÄFER, B., MÜLLER, B. & HEIZMANN, C. 1997. Immunohistochemical localization of the Ca<sup>2+</sup> binding S100 proteins in normal human skin and melanocytic lesions. *British Journal of Dermatology*, 137, 39-43.
- BOOM, A., POCHET, R., AUTHELET, M., PRADIER, L., BORGHGRAEF, P., VAN LEUVEN, F., HEIZMANN, C. W. & BRION, J.-P. 2004. Astrocytic calcium/zinc binding protein S100A6 over expression in Alzheimer's disease and in PS1/APP transgenic mice models. *Biochimica et Biophysica Acta (BBA)-Molecular Cell Research*, 1742, 161-168.
- BORNHORST, J. A. & FALKE, J. J. 2000. Purification of proteins using polyhistidine affinity tags. *Methods Enzymol*, 326, 245-54.
- BOWERS, R. R., MANEVICH, Y., TOWNSEND, D. M. & TEW, K. D. 2012. Sulfiredoxin redox-sensitive interaction with S100A4 and non-muscle myosin IIA regulates cancer cell motility. *Biochemistry*, 51, 7740.
- BRECKENRIDGE, M. T., DULYANINOVA, N. G. & EGELHOFF, T. T. 2009. Multiple regulatory steps control mammalian nonmuscle myosin II assembly in live cells. *Molecular biology of the cell*, 20, 338-347.
- BREEN, E. C. & TANG, K. 2003. Calcyclin (S100A6) regulates pulmonary fibroblast proliferation, morphology, and cytoskeletal organization in vitro. *Journal of cellular biochemistry*, 88, 848-854.
- BRESNICK, A. R., WEBER, D. J. & ZIMMER, D. B. 2015. S100 proteins in cancer. *Nature reviews Cancer*, 15, 96-109.
- BRONSERT, P., KOHLER, I., TIMME, S., KIEFER, S., WERNER, M., SCHILLING, O., VASHIST, Y., MAKOWIEC, F., BRABLETZ, T., HOPT, U. T., BAUSCH, D., KULEMANN, B., KECK, T. & WELLNER, U. F. 2014. Prognostic significance of

Zinc finger E-box binding homeobox 1 (ZEB1) expression in cancer cells and cancer-associated fibroblasts in pancreatic head cancer. *Surgery*, 156, 97-108.

- BURGESS, S. A., WALKER, M. L., THIRUMURUGAN, K., TRINICK, J. & KNIGHT, P. J. 2004. Use of negative stain and single-particle image processing to explore dynamic properties of flexible macromolecules. *Journal of structural biology*, 147, 247-258.
- BURGESS, S. A., YU, S., WALKER, M. L., HAWKINS, R. J., CHALOVICH, J. M. & KNIGHT, P. J. 2007. Structures of smooth muscle myosin and heavy meromyosin in the folded, shutdown state. *Journal of molecular biology*, 372, 1165-1178.
- CAI, Y., BIAIS, N., GIANNONE, G., TANASE, M., JIANG, G., HOFMAN, J. M., WIGGINS, C. H., SILBERZAN, P., BUGUIN, A., LADOUX, B. & SHEETZ, M. P. 2006. Nonmuscle myosin IIA-dependent force inhibits cell spreading and drives F-actin flow. *Biophys J*, 91, 3907-20.
- CAMBY, I., NAGY, N., LOPES, M. B., SCHÄFER, B. W., MAURAGE, C. A., RUCHOUX, M. M., MURMANN, P., POCHE, R., HEIZMANN, C. W. & BROTTI, J. 1999. Supratentorial pilocytic astrocytomas, astrocytomas, anaplastic astrocytomas and glioblastomas are characterized by a differential expression of S100 proteins. *Brain pathology*, 9, 1-19.
- CHAABANE, C., HEIZMANN, C. W. & BOCHATON-PIALLAT, M.-L. 2015. Extracellular S100A4 induces smooth muscle cell phenotypic transition mediated by RAGE. *Biochimica et Biophysica Acta (BBA)-Molecular Cell Research*, 1853, 2144-2157.
- CHAFFER, C. L. & WEINBERG, R. A. 2011. A perspective on cancer cell metastasis. *Science*, 331, 1559-1564.
- CHEN, H.-L., FERNIG, D. G., RUDLAND, P. S., SPARKS, A., WILKINSON, M. C. & BARRACLOUGH, R. 2001. Binding to intracellular targets of the metastasis-inducing protein, S100A4 (p9Ka). *Biochemical and biophysical research communications*, 286, 1212-1217.
- CHEN, H., XU, C., JIN, Q. & LIU, Z. 2014a. S100 protein family in human cancer. *Am J Cancer Res*, 4, 89-115.
- CHEN, H., XU, C. & LIU, Z. 2014b. S100 protein family in human cancer. *American journal of cancer research*, 4.
- CHEN, M. 2016. *S100A4 regulation and function*.
- CHEN, X., LIU, X., LANG, H., ZHANG, S., LUO, Y. & ZHANG, J. 2015. S100 Calcium-Binding Protein A6 Promotes Epithelial-Mesenchymal Transition through  $\beta$ -Catenin in Pancreatic Cancer Cell Line. *PloS one*, 10, e0121319.
- CHEONG, K. A., NOH, M., KIM, C. H. & LEE, A. Y. 2014. S100B as a potential biomarker for the detection of cytotoxicity of melanocytes. *Exp Dermatol*, 23, 165-71.
- CHO, Y.-E., AHN, D.-S., MORGAN, K. G. & LEE, Y.-H. 2011. Enhanced contractility and myosin phosphorylation induced by Ca<sup>2+</sup>-independent MLCK activity in hypertensive rats. *Cardiovascular research*, 91, 162-170.

- CITI, S., CROSS, R. A., BAGSHAW, C. R. & KENDRICK-JONES, J. 1989. Parallel modulation of brush border myosin conformation and enzyme activity induced by monoclonal antibodies. *The Journal of cell biology*, 109, 549-556.
- CLARK, K., LANGESLAG, M., FIGDOR, C. G. & VAN LEEUWEN, F. N. 2007. Myosin II and mechanotransduction: a balancing act. *Trends in cell biology*, 17, 178-186.
- COMIJN, J., BERX, G., VERMASSEN, P., VERSCHUEREN, K., VAN GRUNSVEN, L., BRUYNEEL, E., MAREEL, M., HUYLEBROECK, D. & VAN ROY, F. 2001. The two-handed E box binding zinc finger protein SIP1 downregulates E-cadherin and induces invasion. *Molecular cell*, 7, 1267-1278.
- CONTI, M. A. & ADELSTEIN, R. S. 2008. Nonmuscle myosin II moves in new directions. *Journal of cell science*, 121, 11-18.
- CONTOS, J. J., ISHII, I. & CHUN, J. 2000. Lysophosphatidic acid receptors. *Mol Pharmacol*, 58, 1188-96.
- COOLS-LARTIGUE, J., SPICER, J., MCDONALD, B., GOWING, S., CHOW, S., GIANNIAS, B., BOURDEAU, F., KUBES, P. & FERRI, L. 2013. Neutrophil extracellular traps sequester circulating tumor cells and promote metastasis. *The Journal of clinical investigation*, 123, 3446-3458.
- CRNOGORAC- JURCEVIC, T., MISSIAGLIA, E., BLAVERI, E., GANGESWARAN, R., JONES, M., TERRIS, B., COSTELLO, E., NEOPTOLEMOS, J. P. & LEMOINE, N. R. 2003. Molecular alterations in pancreatic carcinoma: expression profiling shows that dysregulated expression of S100 genes is highly prevalent. *The Journal of pathology*, 201, 63-74.
- CROSS, R., JACKSON, A., CITI, S., KENDRICK-JONES, J. & BAGSHAW, C. 1988. Active site trapping of nucleotide by smooth and non-muscle myosins. *Journal of molecular biology*, 203, 173-181.
- DAVIES, B. R., O'DONNELL, M., DURKAN, G. C., RUDLAND, P. S., BARRACLOUGH, R., NEAL, D. E. & KILIAN MELLON, J. 2002. Expression of S100A4 protein is associated with metastasis and reduced survival in human bladder cancer. *The Journal of pathology*, 196, 292-299.
- DAVIS, J. S., HASSANZADEH, S., WINITSKY, S., LIN, H., SATORIUS, C., VEMURI, R., ALETRAS, A. H., WEN, H. & EPSTEIN, N. D. 2001. The overall pattern of cardiac contraction depends on a spatial gradient of myosin regulatory light chain phosphorylation. *Cell*, 107, 631-641.
- DE PETRIS, L., ORRE, L. M., KANTER, L., PERNEMALM, M., KOYI, H., LEWENSOHN, R. & LEHTIÖ, J. 2009. Tumor expression of S100A6 correlates with survival of patients with stage I non-small-cell lung cancer. *Lung Cancer*, 63, 410-417.
- DE SILVA RUDLAND, S., MARTIN, L., ROSHANLALL, C., WINSTANLEY, J., LEINSTER, S., PLATT-HIGGINS, A., CARROLL, J., WEST, C., BARRACLOUGH, R. & RUDLAND, P. 2006. Association of S100A4 and osteopontin with specific prognostic factors and survival of patients with minimally invasive breast cancer. *Clinical Cancer Research*, 12, 1192-1200.

- DE SILVA RUDLAND, S., PLATT-HIGGINS, A., WINSTANLEY, J. H., JONES, N. J., BARRACLOUGH, R., WEST, C., CARROLL, J. & RUDLAND, P. S. 2011. Statistical association of basal cell keratins with metastasis-inducing proteins in a prognostically unfavorable group of sporadic breast cancers. *The American journal of pathology*, 179, 1061-1072.
- DEL VALLE, M., HARWIN, S., MAESTRO, A., MURCIA, A. & VEGA, J. 1998. Immunohistochemical analysis of mechanoreceptors in the human posterior cruciate ligament: a demonstration of its proprioceptive role and clinical relevance. *The Journal of arthroplasty*, 13, 916-922.
- DENARDO, D. G., ANDREU, P. & COUSSENS, L. M. 2010. Interactions between lymphocytes and myeloid cells regulate pro-versus anti-tumor immunity. *Cancer and Metastasis Reviews*, 29, 309-316.
- DERYNCK, R., AKHURST, R. J. & BALMAIN, A. 2001. TGF- $\beta$  signaling in tumor suppression and cancer progression. *Nature genetics*, 29, 117-129.
- DMYTRIYEVA, O., PANKRATOVA, S., OWCZAREK, S., SONN, K., SOROKA, V., RIDLEY, C. M., MARSOLAIS, A., LOPEZ-HOYOS, M., AMBARTSUMIAN, N. & LUKANIDIN, E. 2012. The metastasis-promoting S100A4 protein confers neuroprotection in brain injury. *Nature communications*, 3, 1197.
- DONATO, R. 2001. S100: a multigenic family of calcium-modulated proteins of the EF-hand type with intracellular and extracellular functional roles. *Int J Biochem Cell Biol*, 33, 637-68.
- DONATO, R., R CANNON, B., SORCI, G., RIUZZI, F., HSU, K., J WEBER, D. & L GECZY, C. 2013. Functions of S100 proteins. *Current molecular medicine*, 13, 24-57.
- DOTAN, E., COHEN, S. J., ALPAUGH, K. R. & MEROPOL, N. J. 2009. Circulating tumor cells: evolving evidence and future challenges. *Oncologist*, 14, 1070-82.
- DU, M., WANG, G., ISMAIL, T. M., GROSS, S., FERNIG, D. G., BARRACLOUGH, R. & RUDLAND, P. S. 2012. S100P dissociates myosin IIA filaments and focal adhesion sites to reduce cell adhesion and enhance cell migration. *Journal of Biological Chemistry*, 287, 15330-15344.
- DUAN, L., WU, R., ZOU, Z., WANG, H., YE, L., LI, H., YUAN, S., LI, X., ZHA, H. & SUN, H. 2014. S100A6 stimulates proliferation and migration of colorectal carcinoma cells through activation of the MAPK pathways. *International journal of oncology*, 44, 781-790.
- DULYANINOVA, N. G. & BRESNICK, A. R. 2013. The heavy chain has its day: regulation of myosin-II assembly. *Bioarchitecture*, 3, 77-85.
- DULYANINOVA, N. G., HOUSE, R. P., BETAPUDI, V. & BRESNICK, A. R. 2007. Myosin-IIA heavy-chain phosphorylation regulates the motility of MDA-MB-231 carcinoma cells. *Mol Biol Cell*, 18, 3144-55.

- DULYANINOVA, N. G., MALASHKEVICH, V. N., ALMO, S. C. & BRESNICK, A. R. 2005. Regulation of myosin-IIA assembly and Mts1 binding by heavy chain phosphorylation. *Biochemistry*, 44, 6867-6876.
- DUTTA, K., COX, C. J., HUANG, H., BASAVAPPA, R. & PASCAL, S. M. 2002. Calcium coordination studies of the metastatic Mts1 protein. *Biochemistry*, 41, 4239-4245.
- ECKERT, R. L., BROOME, A.-M., RUSE, M., ROBINSON, N., RYAN, D. & LEE, K. 2004. S100 proteins in the epidermis. *Journal of Investigative Dermatology*, 123, 23-33.
- ECKHOUTE, J., CARROLL, J. S., GEISTLINGER, T. R., TORRES-ARZAYUS, M. I. & BROWN, M. 2006. A cell-type-specific transcriptional network required for estrogen regulation of cyclin D1 and cell cycle progression in breast cancer. *Genes & development*, 20, 2513-2526.
- EGELHOFF, T. T., LEE, R. J. & SPUDICH, J. A. 1993. Dictyostelium myosin heavy chain phosphorylation sites regulate myosin filament assembly and localization in vivo. *Cell*, 75, 363-371.
- ELLIOTT, P. R., IRVINE, A. F., JUNG, H. S., TOZAWA, K., PASTOK, M. W., PICONE, R., BADIYAL, S. K., BASRAN, J., RUDLAND, P. S. & BARRACLOUGH, R. 2012. Asymmetric mode of Ca<sup>2+</sup>-S100A4 interaction with nonmuscle myosin IIA generates nanomolar affinity required for filament remodeling. *Structure*, 20, 654-666.
- ELLIS, A. L., WANG, Z., YU, X. & MERTZ, J. E. 2010. Either ZEB1 or ZEB2/SIP1 can play a central role in regulating the Epstein-Barr virus latent-lytic switch in a cell-type-specific manner. *Journal of virology*, 84, 6139-6152.
- ELLIS, E. F., WILLOUGHBY, K. A., SPARKS, S. A. & CHEN, T. 2007. S100B protein is released from rat neonatal neurons, astrocytes, and microglia by in vitro trauma and anti-S100 increases trauma-induced delayed neuronal injury and negates the protective effect of exogenous S100B on neurons. *Journal of neurochemistry*, 101, 1463-1470.
- ESPINOZA-FONSECA, L. M., COLSON, B. A. & THOMAS, D. D. 2014. Effects of pseudophosphorylation mutants on the structural dynamics of smooth muscle myosin regulatory light chain. *Molecular BioSystems*, 10, 2693-2698.
- FABRIS, L., CADAMURO, M., MOSERLE, L., DZIURA, J., CONG, X., SAMBADO, L., NARDO, G., SONZOGNI, A., COLLEDAN, M. & FURLANETTO, A. 2011. Nuclear expression of S100A4 calcium-binding protein increases cholangiocarcinoma invasiveness and metastasization. *Hepatology*, 54, 890-899.
- FARIED, A., FARIED, L. S., USMAN, N., KATO, H. & KUWANO, H. 2007. Clinical and prognostic significance of RhoA and RhoC gene expression in esophageal squamous cell carcinoma. *Annals of surgical oncology*, 14, 3593-3601.
- FERNANDEZ-FERNANDEZ, M. R., RUTHERFORD, T. J. & FERSHT, A. R. 2008. Members of the S100 family bind p53 in two distinct ways. *Protein Sci*, 17, 1663-70.

- FERNANDEZ- FERNANDEZ, M. R., RUTHERFORD, T. J. & FERSHT, A. R. 2008. Members of the S100 family bind p53 in two distinct ways. *Protein Science*, 17, 1663-1670.
- FILIPEK, A., MICHOWSKI, W. & KUZNICKI, J. 2008. Involvement of S100A6 (calcyclin) and its binding partners in intracellular signaling pathways. *Advances in enzyme regulation*, 48, 225-239.
- FISCHER, K. R., DURRANS, A., LEE, S., SHENG, J., LI, F., WONG, S. T., CHOI, H., EL RAYES, T., RYU, S. & TROEGER, J. 2015. Epithelial-to-mesenchymal transition is not required for lung metastasis but contributes to chemoresistance. *Nature*, 527, 472-476.
- FODDE, R. & BRABLETZ, T. 2007. Wnt/ $\beta$ -catenin signaling in cancer stemness and malignant behavior. *Current opinion in cell biology*, 19, 150-158.
- FONT-BURGADA, J., SUN, B. & KARIN, M. 2016. Obesity and cancer: the oil that feeds the flame. *Cell metabolism*, 23, 48-62.
- FORD, H. L., SILVER, D. L., KACHAR, B., SELLERS, J. R. & ZAIN, S. B. 1997. Effect of Mts1 on the structure and activity of nonmuscle myosin II. *Biochemistry*, 36, 16321-16327.
- FUNAHASHI, J.-I., SEKIDO, R., MURAI, K., KAMACHI, Y. & KONDOH, H. 1993. Delta-crystallin enhancer binding protein delta EF1 is a zinc finger-homeodomain protein implicated in postgastrulation embryogenesis. *Development*, 119, 433-446.
- GARBUGLIA, M., VERZINI, M., HOFMANN, A., HUBER, R. & DONATO, R. 2000. S100A1 and S100B interactions with annexins. *Biochimica et Biophysica Acta (BBA)-Molecular Cell Research*, 1498, 192-206.
- GAYNOR, R., IRIE, R., MORTON, D., HERSCHMAN, H., JONES, P. & COCHRAN, A. 1981. S100 protein: a marker for human malignant melanomas? *The lancet*, 317, 869-871.
- GIARD, D. J., AARONSON, S. A., TODARO, G. J., ARNSTEIN, P., KERSEY, J. H., DOSIK, H. & PARKS, W. P. 1973. In Vitro Cultivation of Human Tumors: Establishment of Cell Lines Derived From a Series of Solid Tumors 2. *Journal of the National Cancer Institute*, 51, 1417-1423.
- GINGRAS, A. R., BASRAN, J., PRESCOTT, A., KRIAJEVSKA, M., BAGSHAW, C. R. & BARSUKOV, I. L. 2008. Crystal structure of the Ca<sup>2+</sup>- form and Ca<sup>2+</sup>- binding kinetics of metastasis- associated protein, S100A4. *FEBS letters*, 582, 1651-1656.
- GOLITSINA, N., KORDOWSKA, J., WANG, C.-L. & LEHRER, S. 1996. Ca<sup>2+</sup>-dependent binding of calyculin to muscle tropomyosin. *Biochemical and biophysical research communications*, 220, 360-365.
- GONZALEZ- MARTINEZ, T., PEREZ- PIÑERA, P., DÍAZ- ESNAL, B. & VEGA, J. 2003. S- 100 proteins in the human peripheral nervous system. *Microscopy research and technique*, 60, 633-638.

- GRIFFITHS, G. & LUCOCQ, J. M. 2014. Antibodies for immunolabeling by light and electron microscopy: not for the faint hearted. *Histochemistry and cell biology*, 142, 347-360.
- GRIGORIAN, M., ANDRESEN, S., TULCHINSKY, E., KRIAJEVSKA, M., CARLBERG, C., KRUSE, C., COHN, M., AMBARTSUMIAN, N., CHRISTENSEN, A. & SELIVANOVA, G. 2001. Tumor Suppressor p53 Protein Is a New Target for the Metastasis-associated Mts1/S100A4 Protein FUNCTIONAL CONSEQUENCES OF THEIR INTERACTION. *Journal of Biological Chemistry*, 276, 22699-22708.
- GROSS, S. R., SIN, C. G. T., BARRACLOUGH, R. & RUDLAND, P. S. 2014. Joining S100 proteins and migration: for better or for worse, in sickness and in health. *Cellular and molecular life sciences*, 71, 1551-1579.
- GRUM-SCHWENSEN, B., KLINGELHÖFER, J., GRIGORIAN, M., ALMHOLT, K., NIELSEN, B. S., LUKANIDIN, E. & AMBARTSUMIAN, N. 2010. Lung metastasis fails in MMTV-PyMT oncomice lacking S100A4 due to a T-cell deficiency in primary tumors. *Cancer research*, 70, 936-947.
- GUPTA, M., SHEPPARD, B. C., CORLESS, C. L., MACDONELL, K. R., BLANKE, C. D. & BILLINGSLEY, K. G. 2006. Outcome following surgical therapy for gastrointestinal stromal tumors. *Journal of gastrointestinal surgery*, 10, 1099-1105.
- GUPTA, S., HUSSAIN, T., MACLENNAN, G. T., FU, P., PATEL, J. & MUKHTAR, H. 2003. Differential expression of S100A2 and S100A4 during progression of human prostate adenocarcinoma. *Journal of Clinical Oncology*, 21, 106-112.
- GUSEV, K., ACKERMANN, G. E., HEIZMANN, C. W. & NIGGLI, E. 2009. Ca<sup>2+</sup> signaling in mouse cardiomyocytes with ablated S100A1 protein. *General physiology and biophysics*, 28, 371-383.
- HALL, R. A. 2004. Studying protein-protein interactions via blot overlay or Far Western blot. *Protein-protein interactions: methods and applications*, 167-174.
- HANAHAH, D. & WEINBERG, R. A. 2000. The hallmarks of cancer. *cell*, 100, 57-70.
- HANAHAH, D. & WEINBERG, R. A. 2011. Hallmarks of cancer: the next generation. *cell*, 144, 646-674.
- HANNA, A. & SHEVDE, L. A. 2016. Hedgehog signaling: modulation of cancer properties and tumor microenvironment. *Molecular cancer*, 15, 24.
- HARRIS, M. A., YANG, H., LOW, B. E., MUKHERJE, J., GUHA, A., BRONSON, R. T., SHULTZ, L. D., ISRAEL, M. A. & YUN, K. 2008. Cancer stem cells are enriched in the side population cells in a mouse model of glioma. *Cancer research*, 68, 10051-10059.
- HARRIS, T. J. & TEPASS, U. 2010. Adherens junctions: from molecules to morphogenesis. *Nature reviews Molecular cell biology*, 11, 502-514.
- HAYS, T., D'AGATI, V. D., GARELLEK, J. A., WARREN, T., TRUBIN, M. E., HYINK, D. P., HE, J. C. & KLOTMAN, P. E. 2012. Glomerular MYH9 expression is reduced by HIV-1. *AIDS (London, England)*, 26, 797.

- HEATH, K. E., CAMPOS-BARROS, A., TOREN, A., ROZENFELD-GRANOT, G., CARLSSON, L. E., SAVIGE, J., DENISON, J. C., GREGORY, M. C., WHITE, J. G. & BARKER, D. F. 2001. Nonmuscle myosin heavy chain IIA mutations define a spectrum of autosomal dominant macrothrombocytopenias: May-Hegglin anomaly and Fechtner, Sebastian, Epstein, and Alport-like syndromes. *The American Journal of Human Genetics*, 69, 1033-1045.
- HEISSLER, S. M. & MANSTEIN, D. J. 2013a. Nonmuscle myosin-2: mix and match. *Cell Mol Life Sci*, 70, 1-21.
- HEISSLER, S. M. & MANSTEIN, D. J. 2013b. Nonmuscle myosin-2: mix and match. *Cellular and Molecular Life Sciences*, 70, 1-21.
- HEMANDAS, A., SALTO- TELLEZ, M., MARICAR, S., LEONG, A. & LEOW, C. 2006. Metastasis- associated protein S100A4—a potential prognostic marker for colorectal cancer. *Journal of surgical oncology*, 93, 498-503.
- HEO, S. C., JEON, E. S., LEE, I. H., KIM, H. S., KIM, M. B. & KIM, J. H. 2011. Tumor necrosis factor- $\alpha$ -activated human adipose tissue-derived mesenchymal stem cells accelerate cutaneous wound healing through paracrine mechanisms. *Journal of Investigative Dermatology*, 131, 1559-1567.
- HERNANDEZ-OCHOA, E. O., PROSSER, B. L., WRIGHT, N. T., CONTRERAS, M., WEBER, D. J. & SCHNEIDER, M. F. 2009. Augmentation of Cav1 channel current and action potential duration after uptake of S100A1 in sympathetic ganglion neurons. *Am J Physiol Cell Physiol*, 297, C955-70.
- HERNÁNDEZ-OCHOA, E. O., PROSSER, B. L., WRIGHT, N. T., CONTRERAS, M., WEBER, D. J. & SCHNEIDER, M. F. 2009. Augmentation of Ca v 1 channel current and action potential duration after uptake of S100A1 in sympathetic ganglion neurons. *American Journal of Physiology-Cell Physiology*, 297, C955-C970.
- HODGE, R. G. & RIDLEY, A. J. 2016. Regulating Rho GTPases and their regulators. *Nature Reviews Molecular Cell Biology*.
- HOROWITZ, A., TRYBUS, K. M., BOWMAN, D. S. & FAY, F. S. 1994. Antibodies probe for folded monomeric myosin in relaxed and contracted smooth muscle. *The Journal of cell biology*, 126, 1195-1200.
- HOYAUX, D., ALAO, J., FUCHS, J., KISS, R., KELLER, B., HEIZMANN, C. W., POCHET, R. & FRERMANN, D. 2000. S100A6, a calcium-and zinc-binding protein, is overexpressed in SOD1 mutant mice, a model for amyotrophic lateral sclerosis. *Biochimica et Biophysica Acta (BBA)-Molecular Cell Research*, 1498, 264-272.
- HUANG, L.-Y., XU, Y., CAI, G.-X., GUAN, Z.-Q., SHENG, W.-Q., LU, H.-F., XIE, L.-Q., LU, H.-J. & CAI, S.-J. 2011. S100A4 over-expression underlies lymph node metastasis and poor prognosis in colorectal cancer. *World J Gastroenterol*, 17, 69-78.
- HUANG, S., ZHENG, J., HUANG, Y., SONG, L., YIN, Y., OU, D., HE, S., CHEN, X. & OUYANG, X. 2016. Impact of S100A4 expression on clinicopathological characteristics and prognosis in pancreatic cancer: a meta-analysis. *Disease markers*, 2016.

- IKEBE, M., IKEBE, R., KAMISOYAMA, H., REARDON, S., SCHWONEK, J. P., SANDERS, C. R. & MATSUURA, M. 1994. Function of the NH<sub>2</sub>-terminal domain of the regulatory light chain on the regulation of smooth muscle myosin. *Journal of Biological Chemistry*, 269, 28173-28180.
- IMAMICHI, Y., KÖNIG, A., GRESS, T. & MENKE, A. 2007. Collagen type I-induced Smad-interacting protein 1 expression downregulates E-cadherin in pancreatic cancer. *Oncogene*, 26, 2381-2385.
- INFANTE, E. & RIDLEY, A. J. 2013. Roles of Rho GTPases in leucocyte and leukaemia cell transendothelial migration. *Phil. Trans. R. Soc. B*, 368, 20130013.
- IRVINE, A. F. 2012. *Characterising the Interaction between Metastasis-associated Protein S100A4 and Non-muscle Myosin IIA in vitro and in vivo*. University of Leicester.
- ISMAIL, M. F., EL BOGHADADY, N. A., SHABAYEK, M. I., AWIDA, H. A. & ABOZEED, H. 2016. Evaluation and screening of mRNA S100A genes as serological biomarkers in different stages of bladder cancer in Egypt. *Tumor Biology*, 37, 4621-4631.
- ISMAIL, T. M., FERNIG, D. G., RUDLAND, P. S., TERRY, C. J., WANG, G. & BARRACLOUGH, R. 2008. The basic C-terminal amino acids of calcium-binding protein S100A4 promote metastasis. *Carcinogenesis*, 29, 2259-66.
- ITOH, K. & ADELSTEIN, R. S. 1995. Neuronal cell expression of inserted isoforms of vertebrate nonmuscle myosin heavy chain II-B. *Journal of Biological Chemistry*, 270, 14533-14540.
- JAFFE, A. B. & HALL, A. 2005. Rho GTPases: biochemistry and biology. *Annu. Rev. Cell Dev. Biol.*, 21, 247-269.
- JORDÀ, M., OLMEDA, D., VINYALS, A., VALERO, E., CUBILLO, E., LLORENS, A., CANO, A. & FABRA, À. 2005. Upregulation of MMP-9 in MDCK epithelial cell line in response to expression of the Snail transcription factor. *J Cell Sci*, 118, 3371-3385.
- JOYCE, J. A. & POLLARD, J. W. 2009. Microenvironmental regulation of metastasis. *Nature Reviews Cancer*, 9, 239-252.
- JUANES-GARCÍA, A., LLORENTE-GONZÁLEZ, C. & VICENTE-MANZANARES, M. 2016. Molecular control of non-muscle myosin II assembly. *Oncotarget*, 7, 5092.
- JUNG, H. S., BILLINGTON, N., THIRUMURUGAN, K., SALZAMEDA, B., CREMO, C. R., CHALOVICH, J. M., CHANTLER, P. D. & KNIGHT, P. J. 2011. Role of the tail in the regulated state of myosin 2. *Journal of molecular biology*, 408, 863-878.
- JUNG, H. S., KOMATSU, S., IKEBE, M. & CRAIG, R. 2008. Head-head and head-tail interaction: a general mechanism for switching off myosin II activity in cells. *Molecular biology of the cell*, 19, 3234-3242.
- KALLURI, R. & WEINBERG, R. A. 2009. The basics of epithelial-mesenchymal transition. *The Journal of clinical investigation*, 119, 1420-1428.
- KAMAI, T., YAMANISHI, T., SHIRATAKI, H., TAKAGI, K., ASAMI, H., ITO, Y. & YOSHIDA, K.-I. 2004. Overexpression of RhoA, Rac1, and Cdc42 GTPases is

- associated with progression in testicular cancer. *Clinical cancer research*, 10, 4799-4805.
- KANEKO-KAWANO, T., TAKASU, F., NAOKI, H., SAKUMURA, Y., ISHII, S., UEBA, T., EIYAMA, A., OKADA, A., KAWANO, Y. & SUZUKI, K. 2012. Dynamic regulation of myosin light chain phosphorylation by Rho-kinase. *PLoS one*, 7, e39269.
- KANG, Y. G., JUNG, C. K., LEE, A., KANG, W. K., OH, S. T. & KANG, C. S. 2012. Prognostic significance of S100A4 mRNA and protein expression in colorectal cancer. *Journal of surgical oncology*, 105, 119-124.
- KANLAYA, R. & THONGBOONKERD, V. 2016. Unraveling epigenetic regulation of epithelial mesenchymal transition. *Translational Cancer Research*, 5, S1177-S1180.
- KATOH, K., KANO, Y. & NODA, Y. 2011. Rho-associated kinase-dependent contraction of stress fibres and the organization of focal adhesions. *Journal of the Royal Society Interface*, 8, 305-311.
- KATOH, M. & KATOH, M. 2009. Integrative genomic analyses of ZEB2: Transcriptional regulation of ZEB2 based on SMADs, ETS1, HIF1alpha, POU/OCT, and NF-kappaB. *Int J Oncol*, 34, 1737-42.
- KATSUNO, Y., LAMOUILLE, S. & DERYNCK, R. 2013. TGF- $\beta$  signaling and epithelial-mesenchymal transition in cancer progression. *Current opinion in oncology*, 25, 76-84.
- KENDRICK-JONES, J., SMITH, R. C., CRAIG, R. & CITI, S. 1987. Polymerization of vertebrate non-muscle and smooth muscle myosins. *Journal of molecular biology*, 198, 241-252.
- KENGYEL, A., WOLF, W. A., CHISHOLM, R. L. & SELLERS, J. R. 2010. Nonmuscle myosin IIA with a GFP fused to the N-terminus of the regulatory light chain is regulated normally. *Journal of muscle research and cell motility*, 31, 163-170.
- KHAMIS, Z. I., SAHAB, Z. J. & SANG, Q.-X. A. 2012. Active roles of tumor stroma in breast cancer metastasis. *International journal of breast cancer*, 2012.
- KIBOKU, T., KATOH, T., NAKAMURA, A., KITAMURA, A., KINJO, M., MURAKAMI, Y. & TAKAHASHI, M. 2013. Nonmuscle myosin II folds into a 10S form via two portions of tail for dynamic subcellular localization. *Genes Cells*, 18, 90-109.
- KIKUCHI, N., HORIUCHI, A., OSADA, R., IMAI, T., WANG, C., CHEN, X. & KONISHI, I. 2006. Nuclear expression of S100A4 is associated with aggressive behavior of epithelial ovarian carcinoma: an important autocrine/paracrine factor in tumor progression. *Cancer science*, 97, 1061-1069.
- KIM, E. J. & HELFMAN, D. M. 2003. Characterization of the metastasis-associated protein, S100A4. Roles of calcium binding and dimerization in cellular localization and interaction with myosin. *J Biol Chem*, 278, 30063-73.
- KIM, J. H. & PARK, J. 2014. Prognostic significance of heme oxygenase-1, S100 calcium-binding protein A4, and syndecan-1 expression in primary non-muscle-invasive bladder cancer. *Human pathology*, 45, 1830-1838.

- KIMPLE, M. E., BRILL, A. L. & PASKER, R. L. 2013. Overview of affinity tags for protein purification. *Current protocols in protein science*, 9.9. 1-9.9. 23.
- KIMURA, K., ENDO, Y., YONEMURA, Y., HEIZMANN, C., SCHAFER, B., WATANABE, Y. & SASAKI, T. 2000. Clinical significance of S100A4 and E-cadherin-related adhesion molecules in non-small cell lung cancer. *International journal of oncology*, 16, 1125-1156.
- KISS, A. N., DANIS, W. M. & CAVUSGIL, S. T. 2012. International entrepreneurship research in emerging economies: A critical review and research agenda. *Journal of Business Venturing*, 27, 266-290.
- KISS, B. 2014. *NOVEL PERSPECTIVES IN THE STRUCTURAL BIOLOGY OF S100 PROTEINS*. Eötvös Loránd University.
- KISS, B., KALMAR, L., NYITRAY, L. & PAL, G. 2016. Structural determinants governing S100A4-induced isoform-selective disassembly of nonmuscle myosin II filaments. *Febs j*, 283, 2164-80.
- KLEIN, C. A. 2009. Parallel progression of primary tumours and metastases. *Nature Reviews Cancer*, 9, 302-312.
- KOMATSU, K., KOBUNE-FUJIWARA, Y., ANDOH, A., ISHIGURO, S., HUNAI, H., SUZUKI, N., KAMEYAMA, M., MURATA, K., MIYOSHI, J. & AKEDO, H. 2000. Increased expression of S100A6 at the invading fronts of the primary lesion and liver metastasis in patients with colorectal adenocarcinoma. *British journal of cancer*, 83, 769.
- KORPAL, M., LEE, E. S., HU, G. & KANG, Y. 2008. The miR-200 family inhibits epithelial-mesenchymal transition and cancer cell migration by direct targeting of E-cadherin transcriptional repressors ZEB1 and ZEB2. *Journal of Biological Chemistry*, 283, 14910-14914.
- KRAEMER, A. M., SARAIVA, L. R. & KORSCHING, S. I. 2008. Structural and functional diversification in the teleost S100 family of calcium-binding proteins. *BMC evolutionary biology*, 8, 48.
- KRAUSE, M., UKKONEN, K., HAATAJA, T., RUOTTINEN, M., GLUMOFF, T., NEUBAUER, A., NEUBAUER, P. & VASALA, A. 2010. A novel fed-batch based cultivation method provides high cell-density and improves yield of soluble recombinant proteins in shaken cultures. *Microb Cell Fact*, 9, 11.
- KRIAJEVSKA, M. 1998. Metastasis-associated Mts1 (S100A4) Protein Modulates Protein Kinase C Phosphorylation of the Heavy Chain of Nonmuscle Myosin. *Journal of Biological Chemistry*, 273, 9852-9856.
- KRIAJEVSKA, M., BRONSTEIN, I. B., SCOTT, D. J., TARABYKINA, S., FISCHER-LARSEN, M., ISSINGER, O.-G. & LUKANIDIN, E. 2000. Metastasis-associated protein Mts1 (S100A4) inhibits CK2-mediated phosphorylation and self-assembly of the heavy chain of nonmuscle myosin. *Biochimica et Biophysica Acta (BBA)-Molecular Cell Research*, 1498, 252-263.

- KRIAJEVSKA, M., FISCHER-LARSEN, M., MOERTZ, E., VORM, O., TULCHINSKY, E., GRIGORIAN, M., AMBARTSUMIAN, N. & LUKANIDIN, E. 2002. Liprin  $\beta$ 1, a member of the family of LAR transmembrane tyrosine phosphatase-interacting proteins, is a new target for the metastasis-associated protein S100A4 (Mts1). *Journal of Biological Chemistry*, 277, 5229-5235.
- KRIAJEVSKA, M., TARABYKINA, S., BRONSTEIN, I., MAITLAND, N., LOMONOSOV, M., HANSEN, K., GEORGIEV, G. & LUKANIDIN, E. 1998. Metastasis-associated Mts1 (S100A4) protein modulates protein kinase C phosphorylation of the heavy chain of nonmuscle myosin. *Journal of Biological Chemistry*, 273, 9852-9856.
- KRIAJEVSKA, M. V., CARDENAS, M. N., GRIGORIAN, M. S., AMBARTSUMIAN, N. S., GEORGIEV, G. P. & LUKANIDIN, E. M. 1994. Non-muscle myosin heavy chain as a possible target for protein encoded by metastasis-related mts-1 gene. *J Biol Chem*, 269, 19679-82.
- KUŹNICKI, J., KORDOWSKA, J., PUZIANOWSKA, M. & WOŹNIEWICZ, B. 1992. Calcyclin as a marker of human epithelial cells and fibroblasts. *Experimental cell research*, 200, 425-430.
- KWAK, J. M., LEE, H. J., KIM, S. H., KIM, H. K., MOK, Y. J., PARK, Y. T., CHOI, J. S. & MOON, H. Y. 2010. Expression of protein S100A4 is a predictor of recurrence in colorectal cancer. *World J Gastroenterol*, 16, 3897-3904.
- LE HIR, M., HEGYI, I., CUENI-LOFFING, D., LOFFING, J. & KAISLING, B. 2005. Characterization of renal interstitial fibroblast-specific protein 1/S100A4-positive cells in healthy and inflamed rodent kidneys. *Histochemistry and cell biology*, 123, 335-346.
- LE, K., LI, C.-C., YE, G., MOSS, J. & VAUGHAN, M. 2013. Arf guanine nucleotide-exchange factors BIG1 and BIG2 regulate nonmuscle myosin IIA activity by anchoring myosin phosphatase complex. *Proceedings of the National Academy of Sciences*, 110, E3162-E3170.
- LECLERC, E., FRITZ, G., VETTER, S. W. & HEIZMANN, C. W. 2009. Binding of S100 proteins to RAGE: an update. *Biochimica et Biophysica Acta (BBA)-Molecular Cell Research*, 1793, 993-1007.
- LECLERC, E. & VETTER, S. W. 2015. The role of S100 proteins and their receptor RAGE in pancreatic cancer. *Biochim Biophys Acta*, 1852, 2706-11.
- LEE, S. H., KIM, H., HWANG, J.-H., SHIN, E., LEE, H. S., HWANG, D. W., CHO, J. Y., YOON, Y.-S., HAN, H.-S. & CHA, B. H. 2014. CD24 and S100A4 expression in resectable pancreatic cancers with earlier disease recurrence and poor survival. *Pancreas*, 43, 380-388.
- LEE, W.-Y., SU, W.-C., LIN, P.-W., GUO, H.-R., CHANG, T.-W. & CHEN, H. H. 2004. Expression of S100A4 and Met: potential predictors for metastasis and survival in early-stage breast cancer. *Oncology*, 66, 429-438.
- LEHMANN, W., MOSSMANN, D., KLEEMANN, J., MOCK, K., MEISINGER, C., BRUMMER, T., HERR, R., BRABLETZ, S., STEMLER, M. P. & BRABLETZ,

- T. 2016. ZEB1 turns into a transcriptional activator by interacting with YAP1 in aggressive cancer types. *Nat Commun*, 7, 10498.
- LEŚNIAK, W., SZCZEPAŃSKA, A. & KUŹNICKI, J. 2005. Calcyclin (S100A6) expression is stimulated by agents evoking oxidative stress via the antioxidant response element. *Biochimica et Biophysica Acta (BBA)-Molecular Cell Research*, 1744, 29-37.
- LI, Y., BROWN, J. H., RESHETNIKOVA, L. & BLAZSEK, A. 2003a. Visualization of an unstable coiled coil from the scallop myosin rod. *Nature*, 424, 341.
- LI, Z.-H. & BRESNICK, A. R. 2006. The S100A4 metastasis factor regulates cellular motility via a direct interaction with myosin-IIA. *Cancer research*, 66, 5173-5180.
- LI, Z.-H., DULYANINOVA, N. G., HOUSE, R. P., ALMO, S. C. & BRESNICK, A. R. 2010. S100A4 regulates macrophage chemotaxis. *Molecular biology of the cell*, 21, 2598-2610.
- LI, Z., TANG, M., LING, B., LIU, S., ZHENG, Y., NIE, C., YUAN, Z., ZHOU, L., GUO, G. & TONG, A. 2014. Increased expression of S100A6 promotes cell proliferation and migration in human hepatocellular carcinoma. *Journal of Molecular Medicine*, 92, 291-303.
- LI, Z. H., SPEKTOR, A., VARLAMOVA, O. & BRESNICK, A. R. 2003b. Mts1 regulates the assembly of nonmuscle myosin-IIA. *Biochemistry*, 42, 14258-66.
- LIAO, J. K., SETO, M. & NOMA, K. 2007. Rho kinase (ROCK) inhibitors. *J Cardiovasc Pharmacol*, 50, 17-24.
- LIM, S. H., BECKER, T. M., CHUA, W., NG, W. L., DE SOUZA, P. & SPRING, K. J. 2014. Circulating tumour cells and the epithelial mesenchymal transition in colorectal cancer. *J Clin Pathol*.
- LING, Z. & LI, R. 2013. Clinicopathological and prognostic value of S100A4 expression in gastric cancer: a meta-analysis.
- LISTER, I., ROBERTS, R., SCHMITZ, S., WALKER, M., TRINICK, J., VEIGEL, C., BUSS, F. & KENDRICK-JONES, J. 2004. Myosin VI: a multifunctional motor. Portland Press Limited.
- LIU, J. C. Y., ROTTLE, J., WANG, L., ZHANG, J., PASCOE, C. D., LAN, B., NORRIS, B. A., HERRERA, A. M., PARÉ, P. D. & SEOW, C. Y. 2013a. Myosin filaments in smooth muscle cells do not have a constant length. *The Journal of physiology*, 591, 5867-5878.
- LIU, X., BILLINGTON, N., SHU, S., YU, S.-H., PISZCZEK, G., SELLERS, J. R. & KORN, E. D. 2017. Effect of ATP and regulatory light-chain phosphorylation on the polymerization of mammalian nonmuscle myosin II. *Proceedings of the National Academy of Sciences*, 114, E6516-E6525.
- LIU, Y.-N., YIN, J., ABOU-KHEIR, W., HYNES, P., CASEY, O., FANG, L., YI, M., STEPHENS, R., SENG, V. & SHEPPARD-TILLMAN, H. 2013b. MiR-1 and miR-200 inhibit EMT via Slug-dependent and tumorigenesis via Slug-independent mechanisms. *Oncogene*, 32, 296-306.

- LIU, Y., TANG, W., WANG, J., XIE, L., LI, T., HE, Y., QIN, X. & LI, S. 2013c. Clinicopathological and prognostic significance of S100A4 overexpression in colorectal cancer: a meta-analysis. *Diagnostic pathology*, 8, 181.
- LOGOTHETIS, C. J. & LIN, S.-H. 2005. Osteoblasts in prostate cancer metastasis to bone. *Nature Reviews Cancer*, 5, 21-28.
- LOKMAN, N. A., WEEN, M. P., OEHLER, M. K. & RICCIARDELLI, C. 2011. The role of annexin A2 in tumorigenesis and cancer progression. *Cancer Microenvironment*, 4, 199-208.
- LOOSEN, S. H., BENZ, F., NIEDEGGEN, J., SCHMEDING, M., SCHÜLLER, F., KOCH, A., VUCUR, M., TACKE, F., TRAUTWEIN, C. & RODERBURG, C. 2016. Serum levels of S100A6 are unaltered in patients with resectable cholangiocarcinoma. *Clinical and translational medicine*, 5, 39.
- LU, Y., LU, J., LI, X., ZHU, H., FAN, X., ZHU, S., WANG, Y., GUO, Q., WANG, L., HUANG, Y., ZHU, M. & WANG, Z. 2014. MiR-200a inhibits epithelial-mesenchymal transition of pancreatic cancer stem cell. *BMC Cancer*, 14, 85.
- LUO, X., SHARFF, K. A., CHEN, J., HE, T.-C. & LUU, H. H. 2008. S100A6 expression and function in human osteosarcoma. *Clinical orthopaedics and related research*, 466, 2060-2070.
- MA, X. & ADELSTEIN, R. S. 2014. The role of vertebrate nonmuscle Myosin II in development and human disease. *Bioarchitecture*, 4, 88-102.
- MAELANDSMO, G. M., FLOERENES, V. A., MELLINGSAETER, T., HOVIG, E., KERBEL, R. S. & FODSTAD, Ø. 1997. Differential expression patterns of S100A2, S100A4, and S100A6 during progression of human malignant melanoma. *International journal of cancer*, 74, 464-469.
- MÆLANDSMO, G. M., FLØRENES, V. A., NGUYEN, M. T., FLATMARK, K. & DAVIDSON, B. 2009. Different expression and clinical role of S100A4 in serous ovarian carcinoma at different anatomic sites. *Tumor Biology*, 30, 15-25.
- MALASHKEVICH, V. N., DULYANINOVA, N. G., RAMAGOPAL, U. A., LIRIANO, M. A., VARNEY, K. M., KNIGHT, D., BRENOWITZ, M., WEBER, D. J., ALMO, S. C. & BRESNICK, A. R. 2010. Phenothiazines inhibit S100A4 function by inducing protein oligomerization. *Proceedings of the National Academy of Sciences*, 107, 8605-8610.
- MALASHKEVICH, V. N., VARNEY, K. M., GARRETT, S. C., WILDER, P. T., KNIGHT, D., CHARPENTIER, T. H., RAMAGOPAL, U. A., ALMO, S. C., WEBER, D. J. & BRESNICK, A. R. 2008. Structure of Ca<sup>2+</sup>-bound S100A4 and its interaction with peptides derived from nonmuscle myosin-IIA. *Biochemistry*, 47, 5111.
- MALY, I. P. & NITSCH, C. 2007. SDS disc electrophoresis of proteins in homogeneous, low- concentrated polyacrylamide gels. *Electrophoresis*, 28, 1508-1513.
- MANDINOVA, A., ATAR, D., SCHAFER, B., SPIESS, M., AEBI, U. & HEIZMANN, C. W. 1998. Distinct subcellular localization of calcium binding S100 proteins in human

- smooth muscle cells and their relocation in response to rises in intracellular calcium. *Journal of cell science*, 111, 2043-2054.
- MARENHOLZ, I., LOVERING, R. C. & HEIZMANN, C. W. 2006. An update of the S100 nomenclature. *Biochimica et Biophysica Acta (BBA)-Molecular Cell Research*, 1763, 1282-1283.
- MATSUMOTO, K., IRIE, A., SATOH, T., ISHII, J., IWABUCHI, K., IWAMURA, M., EGAWA, S. & BABA, S. 2007. Expression of S100A2 and S100A4 predicts for disease progression and patient survival in bladder cancer. *Urology*, 70, 602-607.
- MATSUMURA, F. & HARTSHORNE, D. J. 2008. Myosin phosphatase target subunit: Many roles in cell function. *Biochemical and biophysical research communications*, 369, 149-156.
- MCKIERNAN, E., MCDERMOTT, E. W., EVOY, D., CROWN, J. & DUFFY, M. J. 2011. The role of S100 genes in breast cancer progression. *Tumor Biology*, 32, 441-450.
- MEJLVANG, J., KRIAJEVSKA, M., VANDEWALLE, C., CHERNOVA, T., SAYAN, A. E., BERX, G., MELLON, J. K. & TULCHINSKY, E. 2007. Direct repression of cyclin D1 by SIP1 attenuates cell cycle progression in cells undergoing an epithelial mesenchymal transition. *Molecular biology of the cell*, 18, 4615-4624.
- MELLE, C., ERNST, G., SCHIMMEL, B., BLEUL, A. & VON EGGELING, F. 2008. Colon-derived liver metastasis, colorectal carcinoma, and hepatocellular carcinoma can be discriminated by the Ca<sup>2+</sup>-binding proteins S100A6 and S100A11. *PloS one*, 3, e3767.
- MELO, R. C., MORGAN, E., MONAHAN-EARLEY, R., DVORAK, A. M. & WELLER, P. F. 2014. Pre-embedding immunogold labeling to optimize protein localization at subcellular compartments and membrane microdomains of leukocytes. *Nature protocols*, 9, 2382-2394.
- MILTON, D. L., SCHNECK, A. N., ZIECH, D. A., BA, M., FACEMYER, K. C., HALAYKO, A. J., BAKER, J. E., GERTHOFFER, W. T. & CREMO, C. R. 2011. Direct evidence for functional smooth muscle myosin II in the 10S self-inhibited monomeric conformation in airway smooth muscle cells. *Proceedings of the National Academy of Sciences*, 108, 1421-1426.
- MIN, H. S., CHOE, G., KIM, S.-W., PARK, Y. J., PARK, D. J., YOUN, Y.-K., PARK, S. H., CHO, B. Y. & PARK, S. Y. 2008. S100A4 expression is associated with lymph node metastasis in papillary microcarcinoma of the thyroid. *Modern Pathology*, 21, 748-755.
- MIYAZAKI, N., ABE, Y., OIDA, Y., SUEMIZU, H., NISHI, M., YAMAZAKI, H., IWASAKI, M., INOUE, H., UYAMA, Y. & NAKAMURA, M. 2006. Poor outcome of patients with pulmonary adenocarcinoma showing decreased E-cadherin combined with increased S100A4 expression. *International journal of oncology*, 28, 1369-1374.
- MIYOSHI, A., KITAJIMA, Y., SUMI, K., SATO, K., HAGIWARA, A., KOGA, Y. & MIYAZAKI, K. 2004. Snail and SIP1 increase cancer invasion by upregulating MMP family in hepatocellular carcinoma cells. *British journal of cancer*, 90, 1265-1273.

- MOORE, B. W. 1965. A soluble protein characteristic of the nervous system. *Biochemical and biophysical research communications*, 19, 739-744.
- MORAVKOVA, P., KOHOUTOVA, D., REJCHRT, S., CYRANY, J. & BURES, J. 2016. Role of S100 proteins in colorectal carcinogenesis. *Gastroenterology research and practice*, 2016.
- MUELLER, B. K., MACK, H. & TEUSCH, N. 2005. Rho kinase, a promising drug target for neurological disorders. *Nature reviews Drug discovery*, 4, 387-398.
- MURAKAMI, N., CHAUHAN, V. P. & ELZINGA, M. 1998. Two nonmuscle myosin II heavy chain isoforms expressed in rabbit brains: filament forming properties, the effects of phosphorylation by protein kinase C and casein kinase II, and location of the phosphorylation sites. *Biochemistry*, 37, 1989-2003.
- MURTEY, M. D. 2016. Immunogold techniques in electron microscopy. *Modern Electron Microscopy in Physical and Life Sciences*. InTech.
- NATARAJAN, J., HUNTER, K., MUTALIK, V. S. & RADHAKRISHNAN, R. 2014. Overexpression of S100A4 as a biomarker of metastasis and recurrence in oral squamous cell carcinoma. *Journal of Applied Oral Science*, 22, 426-433.
- NEDJADI, T., KITTERINGHAM, N., CAMPBELL, F., JENKINS, R., PARK, B., NAVARRO, P., ASHCROFT, F., TEPIKIN, A., NEOPTOLEMOS, J. & COSTELLO, E. 2009. S100A6 binds to annexin 2 in pancreatic cancer cells and promotes pancreatic cancer cell motility. *British journal of cancer*, 101, 1145-1154.
- NGUYEN, D. X., BOS, P. D. & MASSAGUÉ, J. 2009. Metastasis: from dissemination to organ-specific colonization. *Nature Reviews Cancer*, 9, 274-284.
- NISHI, M., MATSUMOTO, K., KOBAYASHI, M., YANAGITA, K., MATSUMOTO, T., NAGASHIO, R., ISHII, D., FUJITA, T., SATO, Y. & IWAMURA, M. 2014. Serum expression of S100A6 is a potential detection marker in patients with urothelial carcinoma in the urinary bladder. *Biomedical research*, 35, 351-356.
- OIDA, Y., YAMAZAKI, H., TOBITA, K., MUKAI, M., OHTANI, Y., MIYAZAKI, N., ABE, Y., IMAIZUMI, T., MAKUUCHI, H. & UEYAMA, Y. 2006. Increased S100A4 expression combined with decreased E-cadherin expression predicts a poor outcome of patients with pancreatic cancer. *Oncology reports*, 16, 457-464.
- ORLOV, I., SCHERTEL, A., ZUBER, G., KLAHOLZ, B., DRILLIEN, R., WEISS, E., SCHULTZ, P. & SPEHNER, D. 2015. Live cell immunogold labelling of RNA polymerase II. *Scientific reports*, 5, 8324.
- ORRE, L. M., PERNEMALM, M., LENGQVIST, J., LEWENSOHN, R. & LEHTIÖ, J. 2007. Up-regulation, modification, and translocation of S100A6 induced by exposure to ionizing radiation revealed by proteomics profiling. *Molecular & Cellular Proteomics*, 6, 2122-2131.
- OSTENDORP, T., LECLERC, E., GALICHET, A., KOCH, M., DEMLING, N., WEIGLE, B., HEIZMANN, C. W., KRONECK, P. M. & FRITZ, G. 2007. Structural and functional insights into RAGE activation by multimeric S100B. *The EMBO journal*, 26, 3868-3878.

- ÖSTERREICHER, C. H., PENZ-ÖSTERREICHER, M., GRIVENNIKOV, S. I., GUMA, M., KOLTSOVA, E. K., DATZ, C., SASIK, R., HARDIMAN, G., KARIN, M. & BRENNER, D. A. 2011. Fibroblast-specific protein 1 identifies an inflammatory subpopulation of macrophages in the liver. *Proceedings of the National Academy of Sciences*, 108, 308-313.
- PACHMAYR, E., TREESE, C. & STEIN, U. 2017. Underlying mechanisms for distant metastasis-molecular biology. *Visceral Medicine*, 33, 11-20.
- PARK, I., HAN, C., JIN, S., LEE, B., CHOI, H., KWON, J. T., KIM, D., KIM, J., LIFIRSU, E. & PARK, W. J. 2011. Myosin regulatory light chains are required to maintain the stability of myosin II and cellular integrity. *Biochemical Journal*, 434, 171-180.
- PATEL, J., MCLEOD, L. E., VRIES, R. G., FLYNN, A., WANG, X. & PROUD, C. G. 2002. Cellular stresses profoundly inhibit protein synthesis and modulate the states of phosphorylation of multiple translation factors. *The FEBS Journal*, 269, 3076-3085.
- PATHURI, P., VOGLEY, L. & LUECKE, H. 2008. Crystal structure of metastasis-associated protein S100A4 in the active calcium-bound form. *Journal of molecular biology*, 383, 62-77.
- PAVLOVA, N. N. & THOMPSON, C. B. 2016. The emerging hallmarks of cancer metabolism. *Cell metabolism*, 23, 27-47.
- PEDERSEN, K., NESLAND, J., FODSTAD, Ø. & MAELANDSMO, G. 2002. Expression of S100A4, E-cadherin,  $\alpha$ - and  $\beta$ -catenin in breast cancer biopsies. *British journal of cancer*, 87, 1281-1286.
- PHILIMONENKO, A. A., JANACEK, J. & HOZAK, P. 2000. Statistical evaluation of colocalization patterns in immunogold labeling experiments. *J Struct Biol*, 132, 201-10.
- PIKOR, L., THU, K., VUCIC, E. & LAM, W. 2013. The detection and implication of genome instability in cancer. *Cancer and Metastasis Reviews*, 32, 341-352.
- PLATT- HIGGINS, A. M., RENSHAW, C. A., WEST, C. R., WINSTANLEY, J. H., DE SILVA RUDLAND, S., BARRACLOUGH, R. & RUDLAND, P. S. 2000. Comparison of the metastasis- inducing protein S100A4 (p9ka) with other prognostic markers in human breast cancer. *International journal of cancer*, 89, 198-208.
- PORTER, A. P., PAPAIOANNOU, A. & MALLIRI, A. 2016. Deregulation of Rho GTPases in cancer. *Small GTPases*, 7, 123-38.
- POSTIGO, A. A. & DEAN, D. C. 1999. ZEB represses transcription through interaction with the corepressor CtBP. *Proceedings of the National Academy of Sciences*, 96, 6683-6688.
- POSTIGO, A. A., DEPP, J. L., TAYLOR, J. J. & KROLL, K. L. 2003. Regulation of Smad signaling through a differential recruitment of coactivators and corepressors by ZEB proteins. *The EMBO journal*, 22, 2453-2462.
- PRIOR, I. A., PARTON, R. G. & HANCOCK, J. F. 2003. Observing cell surface signaling domains using electron microscopy. *Sci Stoke*, 2003.

- QI, S., SONG, Y., PENG, Y., WANG, H., LONG, H., YU, X., LI, Z., FANG, L., WU, A. & LUO, W. 2012. ZEB2 mediates multiple pathways regulating cell proliferation, migration, invasion, and apoptosis in glioma. *PLoS one*, 7, e38842.
- QUAIL, D. F. & JOYCE, J. A. 2013. Microenvironmental regulation of tumor progression and metastasis. *Nature medicine*, 19, 1423-1437.
- RAAB, M., SWIFT, J., DINGAL, P. D. P., SHAH, P., SHIN, J.-W. & DISCHER, D. E. 2012. Crawling from soft to stiff matrix polarizes the cytoskeleton and phosphoregulates myosin-II heavy chain. *J Cell Biol*, 199, 669-683.
- RAFTOPOULOU, M. & HALL, A. 2004. Cell migration: Rho GTPases lead the way. *Developmental biology*, 265, 23-32.
- RAI, V., THOMAS, D. G., BEACH, J. R. & EGELHOFF, T. T. 2017. Myosin IIA Heavy Chain Phosphorylation Mediates Adhesion Maturation and Protrusion in 3D. *Journal of Biological Chemistry*, jbc. M116. 733402.
- RAMAGOPAL, U. A., DULYANINOVA, N. G., VARNEY, K. M., WILDER, P. T., NALLAMSETTY, S., BRENOWITZ, M., WEBER, D. J., ALMO, S. C. & BRESNICK, A. R. 2013. Structure of the S100A4/myosin-IIA complex. *BMC structural biology*, 13, 31-31.
- RAVASI, T., HSU, K., GOYETTE, J., SCHRODER, K., YANG, Z., RAHIMI, F., MIRANDA, L. P., ALEWOOD, P. F., HUME, D. A. & GECZY, C. 2004. Probing the S100 protein family through genomic and functional analysis. *Genomics*, 84, 10-22.
- RAYMENT, I. & ALLINGHAM, J. 2007. Myosin Motors: The Chemical Restraints Imposed by ATP. *Controlled Nanoscale Motion*. Springer.
- REHMAN, I., CROSS, S., AZZOUZI, A., CATTO, J., DELOULME, J., LARRE, S., CHAMPIGNEUILLE, J., FROMONT, G., CUSSENOT, O. & HAMDY, F. 2004. S100A6 (Calcyclin) is a prostate basal cell marker absent in prostate cancer and its precursors. *British journal of cancer*, 91, 739-744.
- REHMAN, I., CROSS, S. S., CATTO, J. W., LEIBLICH, A., MUKHERJEE, A., AZZOUZI, A. R., LEUNG, H. Y. & HAMDY, F. C. 2005. Promoter hyper- methylation of calcium binding proteins S100A6 and S100A2 in human prostate cancer. *The Prostate*, 65, 322-330.
- RICKETSON, D., JOHNSTON, C. A. & PREHODA, K. E. 2010. Multiple tail domain interactions stabilize nonmuscle myosin II bipolar filaments. *Proceedings of the National Academy of Sciences*, 107, 20964-20969.
- RIDLEY, A. J. 2015. Rho GTPase signalling in cell migration. *Current opinion in cell biology*, 36, 103-112.
- RIZZO, P., OSIPO, C., FOREMAN, K., GOLDE, T., OSBORNE, B. & MIELE, L. 2008. Rational targeting of Notch signaling in cancer. *Oncogene*, 27, 5124-5131.
- RONEN, D., ROSENBERG, M. M., SHALEV, D. E., ROSENBERG, M., ROTEM, S., FRIEDLER, A. & RAVID, S. 2010. The positively charged region of the myosin IIC

- non-helical tailpiece promotes filament assembly. *Journal of Biological Chemistry*, 285, 7079-7086.
- ROSENFELD, S. S. & RENER, B. 1994. The GPQ-rich segment of Dictyostelium myosin IB contains an actin binding site. *Biochemistry*, 33, 2322-2328.
- RUDLAND, P. S., PLATT-HIGGINS, A., RENSHAW, C., WEST, C. R., WINSTANLEY, J. H., ROBERTSON, L. & BARRACLOUGH, R. 2000. Prognostic significance of the metastasis-inducing protein S100A4 (p9Ka) in human breast cancer. *Cancer research*, 60, 1595-1603.
- RUSAKOV, D. A., DAVIES, H. A., STEWART, M. G. & SCHACHNER, M. 1995. Clustering and co-localization of immunogold double labelled neural cell adhesion molecule isoforms in chick forebrain. *Neuroscience letters*, 183, 50-53.
- RYAN, G. W. & BERNARD, H. R. 2003. Techniques to identify themes. *Field methods*, 15, 85-109.
- S DATTA, R., GUTTERIDGE, A., SWANTON, C., MALEY, C. C. & GRAHAM, T. A. 2013. Modelling the evolution of genetic instability during tumour progression. *Evolutionary applications*, 6, 20-33.
- SAKURADA, K., SETO, M. & SASAKI, Y. 1998. Dynamics of myosin light chain phosphorylation at Ser 19 and Thr 18/Ser 19 in smooth muscle cells in culture. *American Journal of Physiology-Cell Physiology*, 274, C1563-C1572.
- SALAMA, I., MALONE, P., MIHAIMEED, F. & JONES, J. 2008. A review of the S100 proteins in cancer. *European Journal of Surgical Oncology (EJSO)*, 34, 357-364.
- SALEEM, M., KWEON, M.-H., JOHNSON, J. J., ADHAMI, V. M., ELCHEVA, I., KHAN, N., HAFEEZ, B. B., BHAT, K. M., SARFARAZ, S. & REAGAN-SHAW, S. 2006. S100A4 accelerates tumorigenesis and invasion of human prostate cancer through the transcriptional regulation of matrix metalloproteinase 9. *Proceedings of the National Academy of Sciences*, 103, 14825-14830.
- SAMBROOK, J., FRITSCH, E. & MANIATIS, T. 2001. Molecular cloning: a laboratory manual, 144.
- SANTAMARIA-KISIEL, L., RINTALA-DEMPSEY, A. C. & SHAW, G. S. 2006. Calcium-dependent and-independent interactions of the S100 protein family. *Biochemical Journal*, 396, 201-214.
- SAVOIA, A. & PECCI, A. 2015. MYH9-related disorders.
- SAYAN, A. E., GRIFFITHS, T. R., PAL, R., BROWNE, G. J., RUDDICK, A., YAGCI, T., EDWARDS, R., MAYER, N. J., QAZI, H. & GOYAL, S. 2009. SIP1 protein protects cells from DNA damage-induced apoptosis and has independent prognostic value in bladder cancer. *Proceedings of the National Academy of Sciences*, 106, 14884-14889.
- SCHMIDT-HANSEN, B., KLINGELHÖFER, J., GRUM-SCHWENSEN, B., CHRISTENSEN, A., ANDRESEN, S., KRUSE, C., HANSEN, T., AMBARTSUMIAN, N., LUKANIDIN, E. & GRIGORIAN, M. 2004. Functional significance of metastasis-inducing S100A4 (Mts1) in tumor-stroma interplay. *Journal of Biological Chemistry*, 279, 24498-24504.

- SCHNEIDER, M., HANSEN, J. L. & SHEIKH, S. P. 2008. S100A4: a common mediator of epithelial–mesenchymal transition, fibrosis and regeneration in diseases? *Journal of molecular medicine*, 86, 507-522.
- SCHNEIDER, M., KOSTIN, S., STRØM, C. C., APLIN, M., LYNGBÆK, S., THEILADE, J., GRIGORIAN, M., ANDERSEN, C. B., LUKANIDIN, E. & LERCHE HANSEN, J. 2007. S100A4 is upregulated in injured myocardium and promotes growth and survival of cardiac myocytes. *Cardiovascular research*, 75, 40-50.
- SCHOUTEN, L. J., RUTTEN, J., HUVENEERS, H. A. & TWIJNSTRA, A. 2002. Incidence of brain metastases in a cohort of patients with carcinoma of the breast, colon, kidney, and lung and melanoma. *Cancer*, 94, 2698-2705.
- SCHRAMEK, D., SENDOEL, A., SEGAL, J. P., BERONJA, S., HELLER, E., ORISTIAN, D., REVA, B. & FUCHS, E. 2014. Direct in vivo RNAi screen unveils myosin IIa as a tumor suppressor of squamous cell carcinomas. *Science*, 343, 309-313.
- SEDAGHAT, F. & NOTOPOULOS, A. 2008. S100 protein family and its application in clinical practice. *Hippokratia*, 12, 198-204.
- SELLERS, J. R. 2000. Myosins: a diverse superfamily. *Biochimica et Biophysica Acta (BBA)-Molecular Cell Research*, 1496, 3-22.
- SELLERS, J. R. & KNIGHT, P. J. 2007. Folding and regulation in myosins II and V. *Journal of muscle research and cell motility*, 28, 363-370.
- SERRANO-GOMEZ, S. J., MAZIVEYI, M. & ALAHARI, S. K. 2016. Regulation of epithelial-mesenchymal transition through epigenetic and post-translational modifications. *Molecular cancer*, 15, 18.
- SHIMAMOTO, S., TAKATA, M., TOKUDA, M., OOHIRA, F., TOKUMITSU, H. & KOBAYASHI, R. 2008. Interactions of S100A2 and S100A6 with the tetratricopeptide repeat proteins, Hsp90/Hsp70-organizing protein and kinesin light chain. *Journal of Biological Chemistry*, 283, 28246-28258.
- SIMONS, M., WANG, M., MCBRIDE, O., KAWAMOTO, S., YAMAKAWA, K., GDULA, D., ADELSTEIN, R. S. & WEIR, L. 1991. Human nonmuscle myosin heavy chains are encoded by two genes located on different chromosomes. *Circulation research*, 69, 530-539.
- SLEEMAN, J. P. & THIERY, J. P. 2011. SnapShot: The epithelial-mesenchymal transition. *Cell*, 145, 162-162. e1.
- SON, H. & MOON, A. 2010. Epithelial-mesenchymal transition and cell invasion. *Toxicological research*, 26, 245.
- SRINIVASAN, S., WANG, F., GLAVAS, S., OTT, A., HOFMANN, F., AKTORIES, K., KALMAN, D. & BOURNE, H. R. 2003. Rac and Cdc42 play distinct roles in regulating PI (3, 4, 5) P3 and polarity during neutrophil chemotaxis. *J Cell Biol*, 160, 375-385.
- STANGEL, I., NATHANSON, D. & HSU, C. 1987. Shear strength of the composite bond to etched porcelain. *Journal of Dental Research*, 66, 1460-1465.

- STARY, M., PASTEINER, W., SUMMER, A., HRDINA, A., EGER, A. & WEITZER, G. 2005. Parietal endoderm secreted SPARC promotes early cardiomyogenesis in vitro. *Experimental cell research*, 310, 331-343.
- STEEG, P. S. 2006. Tumor metastasis: mechanistic insights and clinical challenges. *Nature medicine*, 12, 895.
- STREICHER, W. W., LOPEZ, M. M. & MAKHATADZE, G. I. 2010. Modulation of quaternary structure of S100 proteins by calcium ions. *Biophysical chemistry*, 151, 181-186.
- STŘÍŽ, I. & TREBICHA VSKÝ, I. 2004. Calprotectin—a pleiotropic molecule in acute and chronic inflammation. *Physiol Res*, 53, 245-253.
- SUDO, T. & HIDAKA, H. 1998. Regulation of calyculin (S100A6) binding by alternative splicing in the N-terminal regulatory domain of annexin XI isoforms. *Journal of Biological Chemistry*, 273, 6351-6357.
- SUGAI, T., YAMADA, N., EIZUKA, M., SUGIMOTO, R., UESUGI, N., OSAKABE, M., ISHIDA, K., OTSUKA, K., SASAKI, A. & MATSUMOTO, T. 2017. Vascular Invasion and Stromal S100A4 Expression at the Invasive Front of Colorectal Cancer are Novel Determinants and Tumor Prognostic Markers. *Journal of Cancer*, 8, 1552-1561.
- SUZUKI, H., ONISHI, H., TAKAHASHI, K. & WATANABE, S. 1978. Structure and function of chicken gizzard myosin. *The Journal of Biochemistry*, 84, 1529-1542.
- TAHARA, S., NOJIMA, S., OHSHIMA, K., HORI, Y., KURASHIGE, M., WADA, N., IKEDA, J. I. & MORII, E. 2016. S100A4 accelerates the proliferation and invasion of endometrioid carcinoma and is associated with the “MELF” pattern. *Cancer Science*, 107, 1345-1352.
- TAKENAGA, K., NAKAMURA, Y. & SAKIYAMA, S. 1997. Expression of antisense RNA to S100A4 gene encoding an S100-related calcium-binding protein suppresses metastatic potential of high-metastatic Lewis lung carcinoma cells. *Oncogene*, 14, 331-337.
- TARABYKINA, S., L GRIFFITHS, T., TULCHINSKY, E., MELLON, J., BRONSTEIN, I. & KRIAJEVSKA, M. 2007. Metastasis-associated protein S100A4: spotlight on its role in cell migration. *Current cancer drug targets*, 7, 217-228.
- TARABYKINA, S., SCOTT, D. J., HERZYK, P., HILL, T. J., TAME, J. R., KRIAJEVSKA, M., LAFITTE, D., DERRICK, P. J., DODSON, G. G. & MAITLAND, N. J. 2001. The dimerization interface of the metastasis-associated protein S100A4 (Mts1) in vivo and in vitro studies. *Journal of Biological Chemistry*, 276, 24212-24222.
- TERPE, K. 2003. Overview of tag protein fusions: from molecular and biochemical fundamentals to commercial systems. *Applied microbiology and biotechnology*, 60, 523-533.
- THIERY, J. P., ACLOQUE, H., HUANG, R. Y. & NIETO, M. A. 2009. Epithelial-mesenchymal transitions in development and disease. *Cell*, 139, 871-90.

- TRYBUS, K. M. 1994. Role of myosin light chains. *Journal of Muscle Research & Cell Motility*, 15, 587-594.
- TRYBUS, K. M., HUIATT, T. W. & LOWEY, S. 1982. A bent monomeric conformation of myosin from smooth muscle. *Proceedings of the National Academy of Sciences*, 79, 6151-6155.
- TSUKAMOTO, N., EGAWA, S., AKADA, M., ABE, K., SAIKI, Y., KANEKO, N., YOKOYAMA, S., SHIMA, K., YAMAMURA, A. & MOTOI, F. 2013. The expression of S100A4 in human pancreatic cancer is associated with invasion. *Pancreas*, 42, 1027-1033.
- VALASTYAN, S. & WEINBERG, R. A. 2011. Tumor metastasis: molecular insights and evolving paradigms. *Cell*, 147, 275-292.
- VAN DE GRAAF, S. F., HOENDEROP, J. G., GKIKI, D., LAMERS, D., PRENEN, J., RESCHER, U., GERKE, V., STAUB, O., NILIUS, B. & BINDELS, R. J. 2003a. Functional expression of the epithelial Ca<sup>2+</sup> channels (TRPV5 and TRPV6) requires association of the S100A10–annexin 2 complex. *The EMBO journal*, 22, 1478-1487.
- VAN DE GRAAF, S. F., HOENDEROP, J. G., GKIKI, D., LAMERS, D., PRENEN, J., RESCHER, U., GERKE, V., STAUB, O., NILIUS, B. & BINDELS, R. J. 2003b. Functional expression of the epithelial Ca(2+) channels (TRPV5 and TRPV6) requires association of the S100A10-annexin 2 complex. *EMBO J*, 22, 1478-87.
- VAN DE PUTTE, T., MARUHASHI, M., FRANCIS, A., NELLES, L., KONDOH, H., HUYLEBROECK, D. & HIGASHI, Y. 2003. Mice lacking Zfhx1b, the gene that codes for Smad-interacting protein-1, reveal a role for multiple neural crest cell defects in the etiology of Hirschsprung disease–mental retardation syndrome. *The American Journal of Human Genetics*, 72, 465-470.
- VAN DIECK, J., FERNANDEZ-FERNANDEZ, M. R., VEPRINTSEV, D. B. & FERSHT, A. R. 2009. Modulation of the oligomerization state of p53 by differential binding of proteins of the S100 family to p53 monomers and tetramers. *Journal of Biological Chemistry*, 284, 13804-13811.
- VAN GRUNSVEN, L. A., TAELEMAN, V., MICHIELS, C., OPDECAMP, K., HUYLEBROECK, D. & BELLEFROID, E. J. 2006.  $\delta$ EF1 and SIP1 are differentially expressed and have overlapping activities during *Xenopus* embryogenesis. *Developmental dynamics*, 235, 1491-1500.
- VAN ZIJL, F., KRUPITZA, G. & MIKULITS, W. 2011. Initial steps of metastasis: cell invasion and endothelial transmigration. *Mutation Research/Reviews in Mutation Research*, 728, 23-34.
- VANDEWALLE, C., COMIJN, J., DE CRAENE, B., VERMASSEN, P., BRUYNEEL, E., ANDERSEN, H., TULCHINSKY, E., VAN ROY, F. & BERX, G. 2005. SIP1/ZEB2 induces EMT by repressing genes of different epithelial cell–cell junctions. *Nucleic acids research*, 33, 6566-6578.
- VANDEWALLE, C., VAN ROY, F. & BERX, G. 2009. The role of the ZEB family of transcription factors in development and disease. *Cell Mol Life Sci*, 66, 773-87.

- VASQUEZ, C. G., HEISLER, S. M., BILLINGTON, N., SELLERS, J. R. & MARTIN, A. C. 2016. Drosophila non-muscle myosin II motor activity determines the rate of tissue folding. *eLife*, 5, e20828.
- VERSCHUEREN, K., REMACLE, J. E., COLLART, C., KRAFT, H., BAKER, B. S., TYLZANOWSKI, P., NELLES, L., WUYTENS, G., SU, M.-T. & BODMER, R. 1999. SIP1, a novel zinc finger/homeodomain repressor, interacts with Smad proteins and binds to 5'-CACCT sequences in candidate target genes. *Journal of Biological Chemistry*, 274, 20489-20498.
- VICENTE-MANZANARES, M. 2013. Cell migration: cooperation between myosin II isoforms in durotaxis. *Current Biology*, 23, R28-R29.
- VICENTE-MANZANARES, M., MA, X., ADELSTEIN, R. S. & HORWITZ, A. R. 2009. Non-muscle myosin II takes centre stage in cell adhesion and migration. *Nature reviews Molecular cell biology*, 10, 778-790.
- VIMALACHANDRAN, D., GREENHALF, W., THOMPSON, C., LÜTTGES, J., PRIME, W., CAMPBELL, F., DODSON, A., WATSON, R., CRNOGORAC-JURCEVIC, T. & LEMOINE, N. 2005. High nuclear S100A6 (Calcyclin) is significantly associated with poor survival in pancreatic cancer patients. *Cancer research*, 65, 3218-3225.
- VISWANATHAN, A. N., DEAVERS, M. T., JHINGRAN, A., RAMIREZ, P. T., LEVENBACK, C. & EIFEL, P. J. 2004. Small cell neuroendocrine carcinoma of the cervix: outcome and patterns of recurrence. *Gynecologic oncology*, 93, 27-33.
- WALSH, M. P. 2011. Vascular smooth muscle myosin light chain diphosphorylation: mechanism, function, and pathological implications. *IUBMB life*, 63, 987-1000.
- WANG, A., MA, X., CONTI, M. A. & ADELSTEIN, R. S. 2011. Distinct and redundant roles of the non-muscle myosin II isoforms and functional domains. *Biochem Soc Trans*, 39, 1131-5.
- WANG, J., CHEN, X., ZHOU, Z., LI, J. & SUN, H. 2013. The Inhibitory Effect of 3 beta - Hydroxy-12-oleanen-27-oic Acid on Growth and Motility of Human Hepatoma HepG2 Cells through JNK and Akt Signaling Pathway. *Evid Based Complement Alternat Med*, 2013, 685159.
- WANG, X.-H., ZHANG, L.-H., ZHONG, X.-Y., XING, X.-F., LIU, Y.-Q., NIU, Z.-J., PENG, Y., DU, H., ZHANG, G.-G. & HU, Y. 2010a. S100A6 overexpression is associated with poor prognosis and is epigenetically up-regulated in gastric cancer. *The American journal of pathology*, 177, 586-597.
- WANG, Y.-Y., YE, Z.-Y., ZHAO, Z.-S., TAO, H.-Q. & CHU, Y.-Q. 2010b. High-level expression of S100A4 correlates with lymph node metastasis and poor prognosis in patients with gastric cancer. *Annals of surgical oncology*, 17, 89-97.
- WARD, W. W. & SWIATEK, G. 2009. Protein Purification. *Current Analytical Chemistry*, 5, 85-105.
- WATANABE, T., HOSOYA, H. & YONEMURA, S. 2007. Regulation of myosin II dynamics by phosphorylation and dephosphorylation of its light chain in epithelial cells. *Mol Biol Cell*, 18, 605-16.

- WETERMAN, M. A., STOOPEN, G. M., VAN MUIJEN, G. N., KUZNICKI, J., RUITER, D. J. & BLOEMERS, H. P. 1992. Expression of calyculin in human melanoma cell lines correlates with metastatic behavior in nude mice. *Cancer Res*, 52, 1291-6.
- WETTING, H. L., HADLER-OLSEN, E., MAGNUSSEN, S., RIKARDBSEN, O., STEIGEN, S. E., SUNDKVIST, E., LOENNECHEN, T., KANAPATHIPPILLAI, P., KILDALSEN, H. & WINBERG, J.-O. 2011. S100A4 expression in xenograft tumors of human carcinoma cell lines is induced by the tumor microenvironment. *The American journal of pathology*, 178, 2389-2396.
- YAN, X. L., JIA, Y. L., CHEN, L., ZENG, Q., ZHOU, J. N., FU, C. J., CHEN, H. X., YUAN, H. F., LI, Z. W. & SHI, L. 2013. Hepatocellular carcinoma- associated mesenchymal stem cells promote hepatocarcinoma progression: Role of the S100A4- miR155-SOCS1- MMP9 axis. *Hepatology*, 57, 2274-2286.
- YANG, H., ZHAO, K., YU, Q., WANG, X., SONG, Y. & LI, R. 2012. Evaluation of plasma and tissue S100A4 protein and mRNA levels as potential markers of metastasis and prognosis in clear cell renal cell carcinoma. *Journal of International Medical Research*, 40, 475-485.
- YILMAZ, M. & CHRISTOFORI, G. 2009. EMT, the cytoskeleton, and cancer cell invasion. *Cancer and Metastasis Reviews*, 28, 15-33.
- YUEN, S. L., OGUT, O. & BROZOVICH, F. V. 2009. Nonmuscle myosin is regulated during smooth muscle contraction. *American Journal of Physiology-Heart and Circulatory Physiology*, 297, H191-H199.
- ZAKARIA, R., PLATT-HIGGINS, A., RATHI, N., CROOKS, D., BRODBELT, A., CHAVREDAKIS, E., LAWSON, D., JENKINSON, M. D. & RUDLAND, P. S. 2016. Metastasis-inducing proteins are widely expressed in human brain metastases and associated with intracranial progression and radiation response. *British journal of cancer*.
- ZHANG, J., ZHANG, D., JIAO, X. & DONG, Q. 2013. S100A4 regulates migration and invasion in hepatocellular carcinoma HepG2 cells via NF- $\kappa$ B-dependent MMP-9 signal. *Eur Rev Med Pharmacol Sci*, 17, 2372-2382.
- ZHANG, S., WANG, G., LIU, D., BAO, Z., FERNIG, D. G., RUDLAND, P. S. & BARRACLOUGH, R. 2005. The C-terminal region of S100A4 is important for its metastasis-inducing properties. *Oncogene*, 24, 4401-4411.
- ZHANG, W. & GUNST, S. J. 2016. Serine Phosphorylation Of Non-Muscle Myosin II Heavy Chain Regulates The Contraction Of Airway Smooth Muscle (ASM) By Regulating The Assembly Of Adhesion Junction Signaling Complexes. A29. *INFLAMMATION AND MECHANISMS OF AIRWAY SMOOTH MUSCLE CONTRACTION*. Am Thoracic Soc.
- ZHOU, P. 2004. Determining protein half-lives. *Signal Transduction Protocols*, 67-77.
- ZIMMER, D. B. & WEBER, D. J. 2010. The calcium-dependent interaction of S100B with its protein targets. *Cardiovascular psychiatry and neurology*, 2010.

ZIMMER, D. B., WRIGHT SADOSKY, P. & WEBER, D. J. 2003. Molecular mechanisms of S100- target protein interactions. *Microscopy research and technique*, 60, 552-559.

<http://www.nature.com/nprot/journal/v7/n9/full/nprot.2012.096.html>

<http://www.western-blot.us/western-blot-protocol/wet-western-blot>

<http://www.mobyle.pasteur.fr/cgi-bin/portal.py/>

[http://www.ebiotrade.com/buyf/productsf/qiagen/qiaexpress\\_protein\\_purification\\_system.htm](http://www.ebiotrade.com/buyf/productsf/qiagen/qiaexpress_protein_purification_system.htm)